



Ph.D. Thesis

MULTISCALE ASSESSMENT OF CONSTRUCTION AND DEMOLITION WASTE AGGREGATES STABILIZATION THROUGH ALKALINE ACTIVATION

March 2019

Luca Tefa

POLITECNICO DI TORINO

Ph.D. Program in Civil and Environmental Engineering





Doctoral School
Doctoral Program in Civil and Environmental Engineering
(31st Cycle)

Multiscale assessment of construction and demolition waste aggregates stabilization through alkaline activation

LUCA TEFA

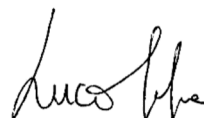
Supervisor
prof. Marco Bassani

Doctoral Examination Committee:

prof. Dimitrios Goulias, University of Maryland (US)
prof. José Ramón Jiménez, University of Cordoba (ES)
prof. Salvatore Damiano Cafiso, University of Catania (IT)
prof. Claudio Ferone, University of Napoli Parthenope (IT)
prof. Paola Palmero, Politecnico di Torino (IT)

This thesis is submitted in partial fulfilment of the requirements for the degree of Doctor of Philosophy.

I hereby declare that, the contents and organisation of this dissertation constitute my own original work and do not compromise in any way the rights of third parties, including those relating to the security of personal data.



.....
Luca Tefa

Turin, March 11th, 2019

ABSTRACT

Recycled aggregates from construction and demolition waste (CDW) are a viable alternative to natural granular materials (NGM) in the formation of unbound layers of low to medium trafficked roads. Several methods to improve the mechanical and durability properties of CDW aggregates through stabilization techniques have been proposed. The recent use of alternative and more sustainable binders (i.e. alkali-activated by-products) in place of traditional ones (i.e. ordinary Portland cement, OPC) has been attracting interest in the scientific community. With the aims of (1) promoting the adoption of CDW aggregates and (2) avoiding the use of cementitious products, this research investigates the alkaline activation (AA) of fine particles of recycled aggregates as a new stabilization method for whole CDW mixtures. The laboratory investigation adopted a multiscale approach. At the smallest scale, the alkali-reactivity of fine particles ($d < 0.125$ mm) of the individual constituents present in CDW (concrete, asphalt, ceramics, natural aggregates, and undivided fraction) was evaluated. The larger scale assessment aimed at verifying the mechanical and durability properties of CDW aggregates in their typical particle size distribution stabilized as per the AA of their fines. An alkaline solution (AS) of sodium hydroxide and sodium silicate was prepared in different concentrations and employed to trigger the AA process.

A preliminary chemical analysis of CDW fines detected the presence of aluminosilicates needed for the AA process. The adequate compression and flexural strength values achieved by specimens made from alkali-activated CDW fines and cured for 28 days at room temperature demonstrated the effective reactivity of these precursors.

At the larger scale, cylindrical specimens of CDW aggregates were compacted with AS (in different concentrations) in place of water. Resilient modulus (RM), unconfined compressive strength (UCS), and indirect tensile strength (ITS) were measured after different curing times (7, 28, and 60 days) at room temperature. The results obtained showed that the AS concentration played a key role in strength and stiffness development. The mechanical properties of CDW aggregates compacted with the undiluted AS (AS-100%) were considerably higher than those of mixtures containing the half diluted AS (AS-50%) and water only (AS-0%). RM, UCS, and ITS of CDW-AS-100% mixtures were comparable to (1) those of an OPC-stabilized NGM studied for comparison purposes and (2) to mechanical properties of CDW aggregates and NGM stabilized with both ordinary and alternative binders available in literature.

The occurrence of AA in CDW-AS-100% mixtures apparently responsible for the formation of bonds between coarser grains was confirmed by microstructural observations performed through field emission scanning electron microscopy, coupled with the elemental analysis of the energy dispersive spectroscopy.

Durability tests carried out on compacted and cured CDW-AS-100% and NGM-OPC mixtures revealed, as expected, that recycled aggregates are more susceptible to freeze/thaw (F/T) degradation than stabilized natural aggregates. Mechanical properties decreased with an increment in F/T cycles. However, after 12 F/T cycles, the RM was greater than the highest values measured in a previous research on similar unbound CDW materials.

Leaching tests confirmed the environmental compatibility of investigated materials according to the European Council Decision 2003/33/EC.

The investigated stabilization technique is consistent with the most common practices in road constructions and promotes the use of CDW aggregates also in applications with higher mechanical requirements (i.e. road bases and subbases). The reuse of waste materials otherwise destined for landfill sites and the exclusion of environmentally harmful binders meet the demand for sustainability increasingly pursued in civil infrastructures.

ACKNOWLEDGMENTS

I would like to acknowledge my supervisor, prof. Marco Bassani, for his continuous support and guidance during the entire Doctoral Program. His experience, brilliant thoughts, and valuable advices were fundamental to the success of the research presented in this document. I also would like to express my gratitude to prof. Paola Palmero who made available the Chemistry Laboratory of the Department of Applied Science and Technology and thoroughly revised the manuscript. Her contribution was very helpful in the development of the experimental investigation.

I would like to thank the Director of the Road Materials Laboratory of Department of Environment, Land and Infrastructure Engineering, prof. Ezio Santagata, for giving me the opportunity to develop my research with advanced equipment and expert technicians.

Important thanks go also to prof. Dimitrios Goulias (University of Maryland, US) and prof. José Ramón Jiménez (University of Cordoba, ES), who carefully revised the thesis providing useful comments to improve the final manuscript.

I am very grateful to my colleagues of the Department of Environment, Land, and Infrastructure Engineering, who helped my research with their experiences and inspiring discussions. Special thanks go to Lorenzo, who shared with me these three years of PhD Program, for his support and sincere friendship.

I am truly thankful to all students and engineers who helped in performing extensive laboratory tests: Federica Arcidiacono, Cristiano Bertello, Davide Guglielmo, Cristina Minchillo, Martina Ridolfo, Rommy Lourdes Rojas Gil, Maria Jose Rojas Medrano, Antonio Russo, and Alessandro Tarabba. This research could have never been completed without their contribution to the experimental work.

Finally, I would like to express my sincere gratitude to my family, my friends and my love Elisa.

LIST OF CONTENTS

ABSTRACT	VII
ACKNOWLEDGMENTS.....	IX
LIST OF CONTENTS	XI
LIST OF PUBLICATIONS.....	XV
NOTATION LIST	XVII
1. INTRODUCTION.....	1
1.1 Previous and current research	3
1.2 Aims and objectives.....	3
1.3 Structure of the thesis	5
2. BACKGROUND.....	7
2.1 Definition and quantification of CDW.....	7
2.2 Waste policy in European Union	8
2.2.1 Waste framework directive 2008/98/EC.....	9
2.2.2 Waste legislation in Italy	10
2.3 Recycling of CDW.....	11
2.4 From waste to resource	13
2.4.1 End of waste (EoW).....	13
2.4.2 EoW for recycled aggregates from CDW	14
2.4.3 CDW aggregates production process.....	15
2.4.4 Life cycle assessment of CDW aggregates	17
2.5 Uses of recycled aggregates from CDW	21
2.5.1 Recycling of CDW aggregate in concrete.....	21
2.5.2 Recycling of CDW in geotechnical applications	22
2.5.3 Recycling of CDW in road applications	24

2.6 Alkali-activation processes	35
2.6.1 Advantages in using alkali-activated binders.....	37
2.7 Alkali-activation of CDW fines	39
3. EXPERIMENTAL PROGRAM	43
3.1 Research objective	43
3.2 Experimental plan	44
3.2.1 Alkali-activation of CDW fines	45
3.2.2 Stabilization of CDW aggregates with AA of fines.....	48
3.2.3 Durability of stabilized CDW-AS mixtures.....	49
4. MATERIALS	53
4.1 CDW aggregates	53
4.2 Fines from CDW aggregates.....	54
4.3 Alkaline solution.....	56
4.4 Cement-stabilized natural material	59
5. METHODS.....	61
5.1 Alkali-activation of CDW fines	61
5.1.1 Physical-chemical characterization of fines.....	61
5.1.2 Specimens preparation and curing	67
5.1.3 Viscosity measurement	68
5.1.4 Mechanical properties of hardened products	69
5.1.5 Environmental assessment.....	73
5.2 Stabilization of CDW aggregates with AA of fines.....	74
5.2.1 Physical and mechanical characterization of aggregates	75
5.2.2 Proctor compaction test	78
5.2.3 Compaction of specimens	80
5.2.4 Mechanical properties of stabilized mixtures	82
5.2.5 FESEM and EDS analysis	88
5.3 Durability of stabilized CDW-AS mixtures.....	90
5.3.1 Compaction and curing of specimens	90

5.3.2	Simulation of freeze and thaw degradation.....	91
5.4	Environmental compatibility of CDW-AS mixtures.....	93
6.	RESULTS AND DISCUSSION.....	95
6.1	Alkali-activation of CDW fines.....	95
6.1.1	Physical characterization of fines	95
6.1.2	Chemical-mineralogical characterization of fines	98
6.1.3	Viscosity of fresh mixtures	105
6.1.4	Strength of hardened specimens	108
6.1.5	Environmental assessment.....	122
6.2	Stabilization of CDW aggregates with AA of fines.....	128
6.2.1	Preliminary characterization of aggregates.....	128
6.2.2	Compaction properties of mixtures.....	132
6.2.3	Resilient behaviour	138
6.2.4	Strengths	147
6.2.5	FESEM and EDS analysis	152
6.3	Durability of stabilized CDW-AS mixtures.....	156
6.3.1	Compaction properties of mixtures.....	156
6.3.2	Effect of F/T degradation on mechanical properties.....	158
6.4	Environmental compatibility of CDW-AS mixtures.....	174
7.	CONCLUSIONS.....	177
7.1	Key findings.....	177
7.1.1	Alkali-activation of CDW fines	178
7.1.2	Stabilization of CDW aggregates.....	179
7.1.3	Durability of AA-CDW mixtures	181
7.2	Final considerations and future perspectives	182
8.	REFERENCES	185
	ANNEXES.....	215
A.	Small scale investigation (Exp. A).....	216
A.1.	Brookfield viscosity.....	216

A.2. Flexural strength tests	217
A.3. Compressive strength tests.....	223
B. Exp. B1	229
B.1. Particle size distribution.....	229
B.2. Resilient modulus results	230
B.3. Stress-strain curves of UCS test.....	231
B.4. EDS analysis output.....	241
C. Exp. B2	249
C.1. Resilient modulus results	249
C.2. Stress-strain curves of UCS test.....	252

LIST OF PUBLICATIONS

The work of this thesis is based on the following publications:

- Bassani, Tefa, Russo, Palmero (2019). Alkali-activation of recycled construction and demolition waste aggregate with no added binder. *Construction and Building Materials*, 20
- Bassani, Tefa, Palmero (2018). The alkali-activation of construction and demolition waste components for stabilization purposes. In *6th International Conference on Sustainable Solid Waste Management*. Naxos, Greece, June 13th - 16th 2018
- Bassani, Tefa (2018). Compaction and freeze-thaw degradation assessment of recycled aggregates from unseparated construction and demolition waste. *Construction and Building Materials*, 160
- Bassani, Riviera, Tefa (2017). Short and long-term effects of cement kiln dust stabilization of construction and demolition waste. *Journal of Materials in Civil Engineering*, 29(5)
- Bassani, Riviera, Lillo, Tefa (2016). Use of Cement Kiln Dust to Stabilize Construction and Demolition Waste for Pavement Applications. In *95th TRB Annual Meeting*, Washington, D.C., January 10th - 14th 2016

NOTATION LIST

Acronyms and abbreviations

AA	Alkaline Activation
AS	Alkaline Solution
BFS	Blast Furnace Slag
BT	Bricks and Tiles
C-A-S-H	Calcium-Alumina-Silicate-Hydrate
CBR	California Bearing Ratio
CCR	Calcium Carbide Residue
CDW	Construction and Demolition Waste
CDW_{meas}	Mixed CDW sample
CED	Cumulative Energy Demand
CG	Crushed Glass
CKD	Cement Kiln Dust
C-S-H	Calcium-Silicate-Hydrate
DGABC	Dense-Graded Aggregate Base Coarse
EDS	Energy Dispersive Spectroscopy
EoW	End of Waste
EPA	Environmental Protection Agency
ES	Ecological Scarcity
EU	European Union
EU-28	European Union consisting in 28 Member States
FI	Flakiness Index
F/T	Freeze and Thaw
FA	Fly Ash
FBCBA	Fluidized Bed Combustion Bottom Ash
FESEM	Field Emission Scanning Electron Microscopy
FI	Flakiness Index
FWD	Falling Weight Deflectometer
GC	Gyratory Compaction
GDP	Gross Domestic Product
GPP	Green Public Procurement
GSC	Gyratory Shear Compactor
GWP	Global Warming Potential
IMP	Impurities
ISPRA	Istituto Superiore per la Protezione e la Ricerca Ambientale

ITS	Indirect Tensile Strength
l/s	liquid/solid
LA	Los Angeles
LBA	Lignite Bottom Ash
LCA	Life Cycle Assessment
LCFS	Low Calcium Ferronickel Slag
LVDT	Linear Variable Differential Transformers
LWD	Light-Weight Deflectometer
MDD	Maximum Dry Density
MEPDG	Mechanistic Empirical Pavement Design Guide
ML	Mass Loss
NA	Natural Aggregates
N-A-S-H	Sodium-Alumina-Silicate-Hydrate
NCHRP	National Cooperative Highway Research Program
NGM	Natural Granular Materials
NVA	Natural Virgin Aggregates
NWPP	National Waste Prevention Programme
OMC	Optimum Moisture Content
OPC	Ordinary Portland Cement
RA	Reclaimed Asphalt
RC	Recycled Concrete
RCA	Recycled Concrete Aggregates
RCS	Reservoir Clay Sediment
RH	Relative Humidity
RLT	Repeated Load Triaxial
RM	Resilient Modulus
RMA	Recycled Mixed Aggregates
RMCA	Recycled Mixed Ceramic Aggregates
RSG	Road Surface Gravel
SEM	Scanning Electron Microscopy
SM	Stone Mud
UCS	Unconfined Compression Strength
UND1	Undivided CDW fraction 1
UND2	Undivided CDW fraction 2
US	United States
VM	Vulcanic Mud
WR	Waste Rock
WTS	Water Treatment Sludge
XRD	X-Ray Diffraction
XRF	X-Ray Fluorescence

Main symbols

Φ	Friction angle (°)
$(m_w)_i$	Mass of wet material for the formation of the layer i (kg)
Al	Aluminium
Al_2O_3	Aluminium oxide
C_1	Self-compaction (%)
$C_{1,avg}$	Average value of self-compaction (%)
C_{100}	Degree of compaction after 100 gyrations (%)
$C_{100,avg}$	Average value of final degree of compaction (%)
$CaCO_3$	Calcite
CaO	Calcium oxide
Cl ⁻	Chlorides
C_n	Degree of compaction at gyration n (%)
$C_{n,i}$	Degree of compaction of layer i at gyration n (%)
CO_2	Carbon Dioxide
d_{50}	Diameter corresponding to 50% of frequency (mm)
d_{90}	Diameter corresponding to 90% of frequency (mm)
Δw_{AS}	AS loss (%)
e	Void index
$\epsilon_{1,r}$	Recoverable deformation in vertical direction (mm/mm)
ϵ_c	Compressive strain (%)
$\epsilon_c(\sigma_{c,max})$	Compressive strain at failure (%)
ϵ_f	Flexural strain at midpoint (%)
$\epsilon_f(\sigma_{f,max})$	Flexural strain at midpoint during failure (%)
ϵ_p	Permanent deformation (mm/mm)
$E_{S,c}$	Compressive secant modulus (MPa)
$E_{T,c}$	Compressive tangent modulus (MPa)
$E_{T,f}$	Flexural tangent modulus (MPa)
F	Fluorides
$\gamma_{b,fine}$	Bulk density of fines (kg/m ³)
γ_d	Dry density (kg/m ³)
$\gamma_{d,max}$	Maximum dry density (kg/m ³)
γ_p	Particle density of CDW and NGM materials (kg/m ³)
$\gamma_{p,fine}$	Particle density of fines (kg/m ³)
γ_{wet}	Wet density (kg/m ³)
η	Viscosity of fresh pastes (cP)
ITS	Indirect tensile strength (MPa)
K	Potassium
k_g	Workability
$k_{g,avg}$	Average value of workability
LA	Los Angeles coefficient (%)

LA_{8F/T}	Los Angeles coefficient after 8 F/T cycles (%)
M	Generic alkaline metal
ML	Mass loss (%)
n	Number of gyrations at the GSC
Na	Sodium
Na₂O	Sodium oxide
Na₂SiO₃	Sodium silicate
NaOH	Sodium hydroxide
NO₃⁻	Nitrates
v_r	Rigden void content (%)
p(CDW_{pred})	Predicted parameter (p = LA or LA _{8F/T} or ML)
p_a	Atmospheric pressure (MPa)
θ	Bulk Stress (kPa)
R²	Determination coefficient
R²_{adj}	Adjusted determination coefficient
RM	Resilient modulus (MPa)
S	Degree of saturation (%)
σ₁	Vertical stress (kPa)
σ₃	Confining pressure (kPa)
σ_c	Compressive stress (MPa)
σ_{c,max}	Compressive strength (MPa)
σ_d	Deviatoric stress (kPa)
S_e	Standard error of the estimate
S_e/S_y	Standard error ratio
σ_f	Flexural stress (MPa)
σ_{f,max}	Flexural strength (MPa)
Si	Silicon
SiO₂	Silicon dioxide (silica)
σ_{max}(UND2_{meas})	Measured compression strength of UND2 (MPa)
σ_{max}(UND2_{pred})	Estimated compression strength of UND2 (MPa)
SO₄²⁻	Sulphates
S_y	Standard deviation of measures
T_c	Compressive toughness (kPa·mm/mm)
T_f	Flexural toughness (kPa·mm/mm)
τ_{oct}	Octahedral shear stress (kPa)
UCS	Unconfined compression strength (MPa)
v	Void content (%)
w_a	Water absorption (%)
w_{AS}	AS content (%)
w_{AS,opt}	Optimum content of AS (%)
w_{AS,real}	Real AS (%)

w_w	Moisture content (%)
$w_{w,opt}$	Optimum moisture content (%)

1.INTRODUCTION

The industrial development of modern society is undoubtedly the driving force behind current economic and social growth. The European Builders Confederation estimates that the construction sector accounts for one tenth of the gross domestic product (GDP) of the European Union [1]. On the other hand, construction industry has always been perceived as the main cause of environmental degradation [2], in terms of (1) energy and non-renewable resources consumption, (2) gas emissions, (3) waste generation, and (4) noise pollution [3], [4]. Following the introduction of the “sustainable development” concept by the World Commission on Environment and Development [5] in the late 1980s, a framework of priorities in building design and construction industries has evolved [6]. The application of the sustainability concept led to a new paradigm (Figure 1.1) in which (1) the minimization of resources consumed, (2) the reduction in environmentally harmful activities and (3) the human health protection became the criteria of vital importance [7], [8].

Accordingly, the efficient use of material is considered one of the greatest challenges for the sustainable construction approach [9]. In this context, the two major problems are related to the excessive consumption of natural resources and the high levels of waste generated [10].

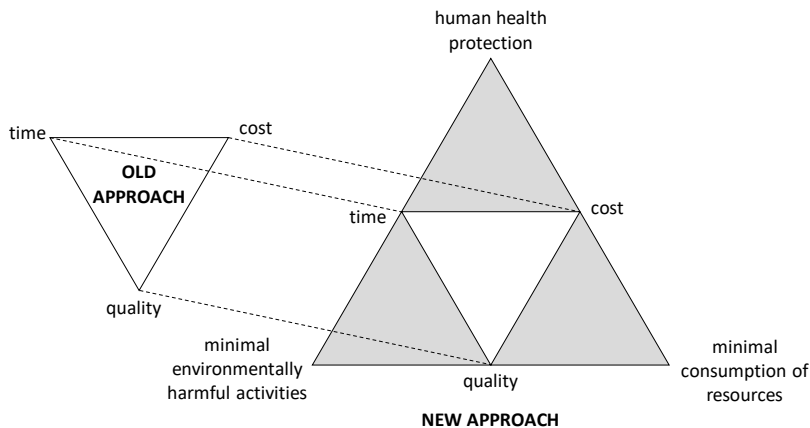


Figure 1.1 - Evolution of paradigm after the introduction of sustainable development in construction sector [11]

Kylili and Fokaides [12] reported that more than 50% of extracted materials in the European Union (EU) are employed in building and civil infrastructures. Meanwhile, one third of the total waste generated in the EU is produced by the construction industry, with the resultant landfill operations having a severe impact on the environment [13], [14]. The reuse of construction and demolition waste (CDW) is universally regarded a viable way to reduce the depletion of natural resources and the growing deposition of same in landfill sites [15]. In recent decades, the use of recycled materials in substitution for primary resources has been emphasized worldwide, in compliance with the circular economy model strongly promoted by the policies of several States [16]. According to this development approach, resources are repeatedly used at their highest utility and value in a closed loop of a restorative and regenerative system (Figure 1.2) [17], [18].

CDW derives from demolitions, micro-demolitions, and renovation operations of buildings and civil infrastructures. It is composed of a variety of materials such as concrete, ceramics, soils, asphalt, and occasionally metals, wood, glass, and other materials normally used in civil constructions. When this waste is crushed and adequately treated for the removal of impurities, it becomes a recycled aggregate consistent with the end of waste (EoW) concept.

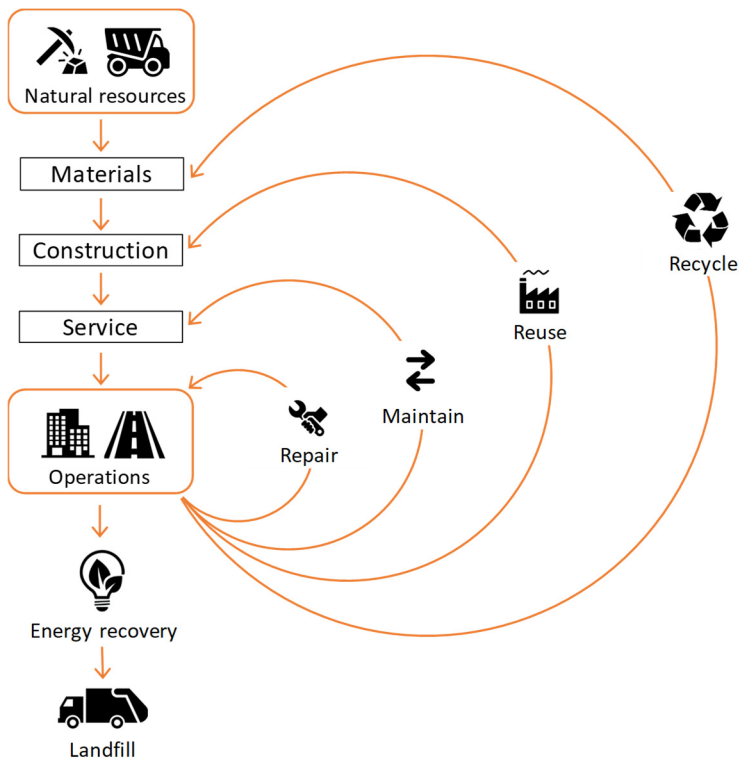


Figure 1.2 - Circular economy principle in the construction value chain

1.1 Previous and current research

Despite several studies pointing out that CDW materials can be satisfactorily used as recycled aggregates in concrete production [19], in the last twenty years, CDW aggregates have mainly been employed as granular material for unbound layers of low- to medium-trafficked roads [20]. More recently, in line with the EU Directive 2008/98/EC [21], which imposed a minimum recycling rate of CDW equal to 70% by 2020, there were several attempts to increase and extend the use of this recycled material. For instance, some case studies showed that CDW aggregates can be successfully used in unpaved rural roads [22], while other experimental investigations demonstrated the feasibility of using CDW aggregates in subgrade layers of pavements and in road embankments [23]. To improve performances and meet the requirements of base and subbase layers of road pavements, some authors proposed the stabilization of CDW aggregates with both ordinary [24], [25] and alternative [26] binders. Among alternative binders, alkali-activated materials are of increasing interest even for stabilization purposes, especially those derived from industrial by-products [27], [28]. When used as stabilizers for road granular materials, alkali-activated binders led to adequate mechanical performances [28]. The alkaline activation (AA) process involves chemical reactions between aluminosilicate-rich materials and alkaline silicates in strongly basic conditions. The final product is a material characterized by a strong binding attitude and excellent mechanical properties. Of particular interest are some investigations which recognized the feasibility of employing CDW powders as precursors for the AA process [29], [30], especially after a curing at moderately high temperatures (60÷80°C).

1.2 Aims and objectives

The present research investigates the stabilization of CDW aggregates without the addition of any binders, but taking advantage of the AA of fine particles normally present in these materials. The laboratory investigation evaluated the AA of CDW fines as a stabilization method for coarser particles prior to their use in base and subbase layers of road pavements. This method would also support the use of CDW materials in applications which require superior mechanical properties without the consumption of non-renewable resources (i.e. natural aggregates). Meanwhile, an improvement in the recycling rate and an increase in the market value of these waste flows are desirable. Therefore, certain environmental benefits can be claimed, of which (1) the reduction in waste material disposed of in landfills, and (2) the reduction in the use of cementitious products are the most relevant.

To meet these objectives, the laboratory investigation adopted the multiscale approach reported in Figure 1.3.

The smaller scale evaluated the alkali-reactivity of fine particles only ($d < 0.125$ mm). These particles were analysed separately depending on their origin: recycled concrete (RC), reclaimed asphalt (RA), bricks and tiles (BT), natural aggregates (NA), and two undivided fractions (UND1 and UND2). Preliminary chemical analyses were carried out to verify the presence of aluminosilicates necessary for the AA process. The development of mechanical strength of prismatic specimens cured without thermal treatments was considered the pivotal factor when assessing the AA effectiveness.

The larger scale investigation involved an evaluation of the performances of undivided CDW aggregates in their complete particle size distribution ($0\div 25$ mm) stabilized as per the alkali-activation of their own fines. Two different laboratory experiments were set up at this scale.

The first aimed at verifying the feasibility and the effectiveness of the stabilization method depending on the concentration and quantity of the chemical activator employed to trigger the AA reactions. Cylindrical specimens of CDW were compacted with an alkaline solution (in lieu of water) and cured at room temperature. Their mechanical properties, in terms of stiffness (resilient modulus) and strength (unconfined compression strength and indirect tensile strength) were measured after 7, 28, and 60 days of curing.

The objective of the second experiment was to assess the durability of alkali-activated CDW aggregates when subjected to freezing and thawing (F/T) degradation. In this case, the mechanical properties of cylindrical specimens exposed to 4, 8 and 12 F/T cycles from -18°C to $+25^{\circ}\text{C}$ were compared to those obtained with undisturbed material. Moreover, a natural granular material typically used in road-works was stabilized with ordinary Portland cement and subjected to the same degradation process for comparison purposes.

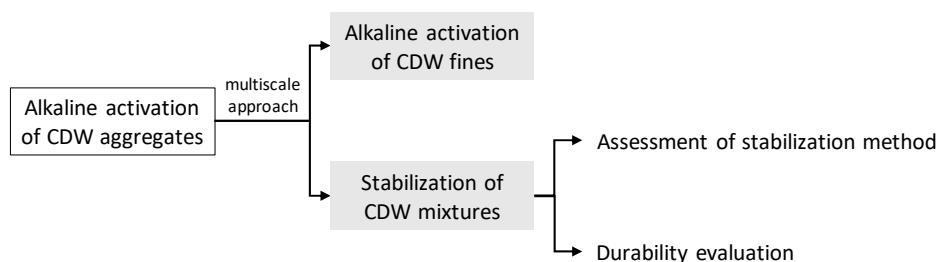


Figure 1.3 - Scheme of multiscale investigation

1.3 Structure of the thesis

This manuscript is divided into seven chapters. The opening chapter contains a general introduction presenting the problem statement together with a background summary of CDW research.

Chapter 2 provides a description of the waste policy framework in the EU and Italy, as well as an explanation of the EoW concept applied to CDW materials. It includes a comprehensive literature review of the most important contributions concerning the use of CDW aggregates in concrete, geotechnical, and road applications. Finally, a theoretical background of the AA process is provided, as well as the main findings on the alkali-reactivity of CDW powders.

Chapter 3 introduces the experimental program and the objectives of the research. For each experiment, variables, motivation, gaps in knowledge and lists of tests are reported.

The materials used in the experimental investigation are presented in Chapter 4, while methodological approaches are described in Chapter 5. The latter includes (1) the reference standards followed for laboratory tests, (2) a description of testing equipment and procedures, and (3) the methods of data acquisition and results treatment.

Chapter 6 reports and discusses the results of the experimental investigation, with specific emphasis on a comparison with literature data for similar materials. In addition to the description of observed phenomena, the analysis of results provides a comprehensive explanation for mechanical behaviour taking both physical and chemical properties into account. With the aim of supporting the discussion, some microstructure observations are also reported and commented on.

Lastly, Chapter 7 contains the conclusions, in which key findings are presented, as well as possible future developments of the work illustrated in this thesis.

2.BACKGROUND

2.1 Definition and quantification of CDW

The residual material generated during construction, renovation and demolition of buildings and civil infrastructures (roads, bridges, channels, etc.) is identified with construction and demolition waste (CDW). More precisely, the “CDW” term designates:

- waste arising from total or partial demolition of buildings and civil structures;
- debris produced during construction or renovation of buildings and infrastructures;
- soils and rocks arising from land levelling operations, excavations, foundations construction and other general civil works;
- waste generated during road maintenance activities [31].

CDW includes bulky materials like concrete, asphalt, bricks, ceramics, plaster, glass, gypsum, metals, plastics, wood, excavated soil, and natural rocks. Examples of CDW components and relative origins are provided by the US Environmental Protection Agency (EPA) [32] and are listed in Table 2.1. Particles of concrete, asphalt, ceramic and natural material are considered as constituents, since they are mostly present in CDW [33], while glass, metal, plastic, and wood are usually indicated as impurities [34], [35].

The statistical office of the European Union (Eurostat) estimated, for 2014, an annual production of 2.5 billion of tonnes of waste including all economic activities and households (from EU-28).

Table 2.1 - Materials present in CDW [32]

Material	Content examples
Concrete	Foundation, columns, slabs, driveways
Asphalt	Sidewalks, roads
Ceramic	Bricks, tiles, roof tiles, masonry, sanitary ware
Natural material	Excavations, tunnel muck, stone processing
Glass	Windows, mirrors, lights
Metals	Pipes, rebar, wiring, framings
Plastic	Pipes, packaging, sidings
Wood	Framing lumber, wood flooring
Miscellaneous	Carpeting, fixtures, insulations, wallpaper

Almost one third of this number includes CDW (868 million of tonnes) and another third is attributed to mining and quarrying activities (703 million of tonnes) [36]. According to estimates of EPA, in the same year, an amount of 534 million of CDW was generated in US [37].

In Italy, referring to the data published by the *Istituto Superiore per la Protezione e la Ricerca Ambientale* (ISPRA), the amount of CDW produced in 2014 exceeded 50 million of tonnes [38].

2.2 Waste policy in European Union

The European Union (EU) waste policy, diffused through Directives and Regulations, is included in several Environment Action Programmes [39]. The 7th Environment Action Programme [40] is currently heading the EU in “becoming a smart, sustainable and inclusive economy by 2020 with a set of policies and actions aimed at making it a low-carbon and resource-efficient economy”. It aims at protecting and preserving the natural capital of the EU, safeguarding the citizens from environmental-related risks, and supporting the economic growth through policies based on the reduction of (1) resources consumption and (2) carbon emissions. The Programme focuses on turning waste into resource as the main key for a circular economy development.

In the past 30 years of environmental action plans and framework legislation and, currently, with 7th Environment Action Programme, the EU waste policy aspires to protect the environment through the minimization of impacts generated by human activities. Its pursuit is implemented by a series of principles which regulate the waste management [41]:

- waste hierarchy (categorization from the most to the least preferred procedures to treat waste that cannot be prevented in its generation);
- self-sufficiency at Community (integrated network of waste disposal facilities between Member States);
- best available techniques with limited costs (limitation of emissions from installations);
- proximity (disposition of waste as close as possible to the source);
- precautionary principle (anticipation of potential problem connected to waste production) [42];
- producer responsibility (inclusion of economic operators and products manufacturers in the life-cycle approach);
- polluter pays (taxation for waste generation);

- life-cycle thinking (evaluation of environmental impacts of the entire life of a product or good).

In this context, the EU fixed several priorities for ensuring an adequate network of safe waste disposal and recovery facilities, for (1) reducing some categories of waste streams, (2) defeating the illegal waste disposal, and (3) instilling in Member States a transition to a circular economy with a reduction of waste and its harmfulness.

2.2.1 Waste framework directive 2008/98/EC

The current EU waste management practices are regulated by the latest version of European Commission's Waste Framework, the Directive 2008/98/EC [21]. It sets out the basic concepts and definitions for adequately managing waste in relation to the objectives of the European Waste Strategy. Firstly, the Directive 2008/98/EC provides a definition of waste as “any substance or object which the holder discards or intends or is required to discard”, as well as, the criteria to identify a by-product, i.e. “any substance or object, resulting from a production process, the primary aim of which is not the production of that item” [21].

The “waste hierarchy” (Article 4) is the most representative principle enforced in the Directive, since it indicates a priority organization in the waste management approach. The EU strategy aims primarily at preventing the generation of waste (Figure 2.1), also involving new clean technologies that generate lower amounts of waste at the end of processes. When it is not possible, the reuse and recycling of waste is strongly recommended. Reuse is preferred to the recycling, since it is better to use repetitively objects and goods without transforming them.

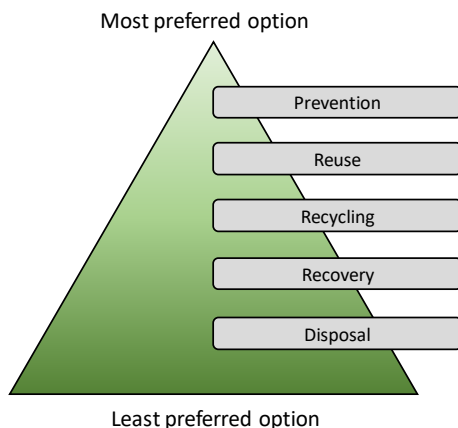


Figure 2.1 - Waste hierarchy

Differently, recycling, which refers to the process of producing raw materials from waste (e.g. glass, aluminium) implies energy consuming operations. The recovery of energy includes the incineration of waste and the combustion of alternative fuels derived from landfill gases. The least option is the safe disposal, which includes landfilling and incineration without energy recovery [43].

2.2.2 Waste legislation in Italy

The Legislative Decree No 152/2006 (Environmental Protection Code) [44] is the reference Italian law in terms of environmental regulation. Its main objective is the enhancement of the quality of life by the preservation of environment and the rational exploitation of natural resources. This law regulates (1) the environmental impact assessment, (2) the soil conservation and water protection, (3) the waste management, (4) the reduction of pollution, and (5) the compensation requirements due to environmental offenses. The Environmental Protection Code was updated in 2010 through the Legislative Decree No 205/2010 [45], with the aim of implementing the new principles included in the European Directive 2008/98/EC.

In 2013, the Italian Minister for the Environment introduced the first National Waste Prevention Programme (NWPP) [46]. It established a series of objectives to dissociate the economic growth and the environmentally harmful activities related to the waste generation. According to the European Directive 2008/98/EC, the main purpose of NWPP is the waste prevention through the reduction by 2020 of:

- 5% of urban solid waste for each unit of gross domestic product (GDP);
- 5% of non-hazardous waste for each GDP unit;
- 10% of hazardous waste for each GDP unit.

Furthermore, the NWPP introduced a series of general measures that can significantly contribute to the success of the prevention policy, such as (1) the sustainability of production processes, (2) the citizens' awareness of the issue, (3) the fiscal regulation, and (4) the implementation of Green Public Procurement (GPP) for public administrations.

Finally, the National Stability Law [47] of 2014 introduced new environmental regulations, which were later included in the Law No 221/2015 [48]. It is a comprehensive legislation for promoting the Green Economy and reduce the use of natural resources. Its main objective consists in the integration of different aspects of environmental framework and green economy, encouraging the reuse of resources with incentives for virtuous management.

2.3 Recycling of CDW

The recycling rate of total waste produced in the EU-28 is considerably variable between Member States, as shown in Figure 2.2. Italy, Belgium, Iceland, Denmark, Latvia, and Portugal have very high recycling rate (higher than 55% of total waste produced), while in other States (Romania, Serbia, Bulgaria, Montenegro, Macedonia) waste is almost completely disposed into landfill sites (with a landfilling rate higher the 90%). Figure 2.3 indicates that the average rate in the EU-28 of landfilled waste is estimated as the 47.4% of produced waste. A similar percentage is referred to the recycled waste (46.4%), that includes also the backfilled waste. Only the 4.7% and the 1.5% of waste is managed with incineration, and energy recovery operations respectively. Similar numbers are valid for CDW, that constitutes a predominant percentage of the total waste generated in Europe.

In the past, landfilling was the most common and cheapest method of solid waste disposal. It caused several negative consequences on the environment and human health in terms of gas and leachate generation [49]. Accordingly, the disposal of CDW in landfill can have severe consequences, since it can contain hazardous and non-inert components (e.g. plastic, wood, bitumen, paints residues, etc.). These materials release pollutants over time, which may be transported over long distances by air and water [35].

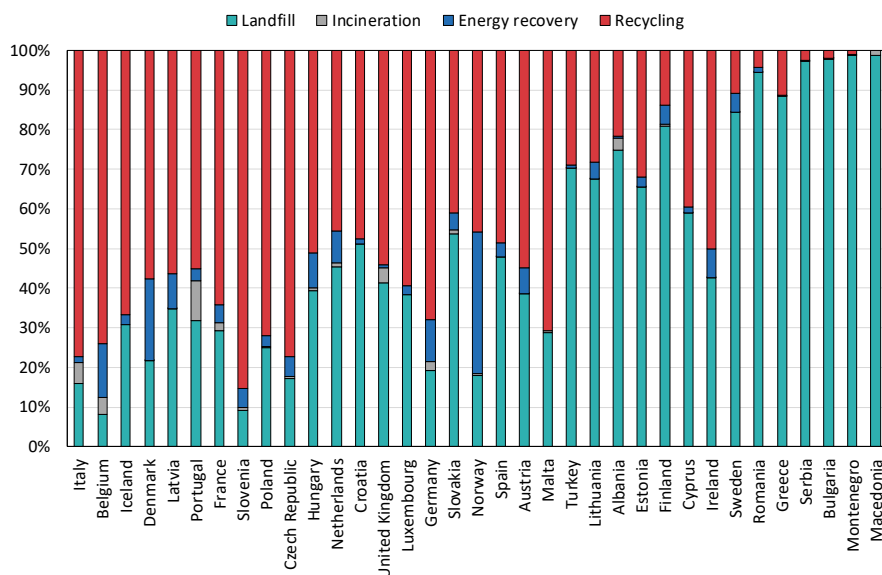


Figure 2.2 - Percentage distribution of waste management in the EU-28, year 2014 (data from Eurostat, [36])

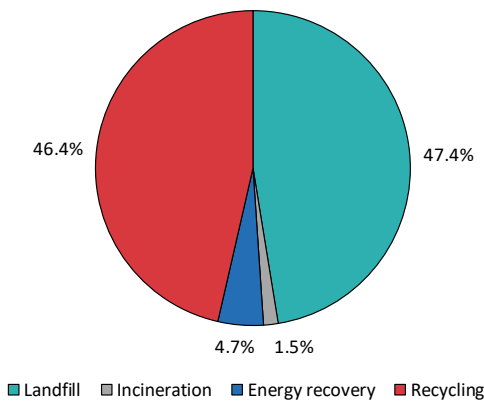


Figure 2.3 - Waste treatment method in the EU-28 for 2014 (data from Eurostat, [36])

Moreover, due to large volumes of CDW generated worldwide, its disposal in landfill sites occupies wide areas, gradually reducing the landfilling available space [13]. However, this waste treatment is still an economic way for CDW, especially in rural contexts where (1) there are free areas suitable for landfilling operations, (2) the CDW production is low, and (3) natural aggregates are usually cheaper [50], [51]. According to Duran et al. [52], the low recycling rate of CDW is still due to purely economic issues and the trend can be reversed only if: (1) the landfilling becomes more expensive than recycling, and (2) primary natural aggregates are more priced than those recycled from CDW. In addition, the generalized belief of a lower quality and limited properties of CDW recycled aggregates with respect to natural ones does not encourage the recycling [4].

Several EU Member States are adopting countermeasures for making landfilling unattractive and favouring recycling. The taxation of landfilling operations has the purpose of increasing the costs of CDW disposal and make it less competitive in comparison to other treatments, such as recycling. However, Garbarino and Blengini [51] pointed out that, in certain countries, the effectiveness of taxation can be controversial since tends to increase the risk of illegal waste disposal. To contrast this drawback, some stakeholders are trying to increase the CDW recycling rate by means of incentives to directly subsidize recycling plants [53].

In these contexts, the taxation of resource extraction is considered an effective practice to discourage the use of primary natural material. Accordingly, this action contributes to the reduction of primary aggregates demand and promote the use of recycled resources [54].

With the aim of reducing the users' distrust of recycled materials, the GPP policy can effectively promote their use. The GPP imposes to authorities and municipalities the adoption of products or services with reduced harmfulness on environment and human health [55], [56]. This approach favours the market of recycled products and guarantees a sustainable and resource-efficient economy [57], [58]. At the same time, the GPP policy should be supported by additional decisions which make possible its complete application. For instance, despite the Ministerial Decree No 203/2003 of the Italian Ministry of the Environment [59] imposing the partial adoption of recycled aggregates in infrastructures funded with public investments, many public authorities incurred in several implementation difficulties caused by the lack of these recycled materials in the price lists and in the contract specifications [60].

2.4 From waste to resource

Waste generated from construction and demolition of buildings and civil infrastructures, and from maintenance works is a relevant portion in waste streams in the EU. Fractions derived from concrete, bricks and other construction materials are suitable to be crushed and transformed into an alternative aggregate for unbound, stabilized and bound pavement layers, in partial and/or total substitution of virgin material [61]. The conversion from waste to resource requires an adequate regulation to guarantee a high level of protection towards environmental and health consequences. This concept was introduced in the Directive 2008/98/EC [21] with the aim of providing technical and environmental criteria to (1) promote the reuse of materials and products with guaranteed properties and (2) increase the users' confidence in these materials and products. The methods and requirements for reclassifying a generic waste into a new product are indicated in the so-called End of Waste (EoW) concept.

2.4.1 End of waste (EoW)

The EoW concept establishes the conditions for which a certain waste ceases to be such and becomes a product or a secondary raw material. The article 6 of the Directive 2008/98/EC [21] states that a waste material undergone to recovery operations (including recycling) can be considered a secondary raw material or a product, and it ceases to be regulated by waste legislation if it complies with the following conditions:

- the material or object is commonly used for specific purposes;
- there is an existing market or demand for that product or material;

- its use is lawful and the substance or object fulfils the technical requirements for its recovery;
- the use of recovered product does not produce environmental or human health harmful consequences.

According to the Joint Research Centre [62], waste streams that are suitable for EoW assessment are divided into three main categories:

1. streams in line with the EoW principles and considered priority materials due to their known composition and low potential risk for environmental and health damage. Materials of this category are considered highly valuable and there is a consolidated market in the EU. This category can be further split into:
 - a. streams used as feedstock in industrial processes, with controlled environmental impacts by industrial permits (e.g. metal scrap of iron and steel, aluminium, copper, zinc, lead and tin, paper, plastic, textiles, glass);
 - b. streams used in applications that imply direct exposure to the environment and require further assessment including limit values of pollutant content (e.g. CDW aggregates, ashes, slag, and biodegradable waste materials);
2. streams that may be in line with the EoW criteria, but it is not well defined their management in Europe (e.g. solid fuels, wood, oil, tyres, and solvents);
3. streams not appropriate for EoW classification, like precious metals.

The EoW status is reached through the fulfilment of different criteria in the whole recovery process, which include (1) the characterization of input material, (2) the recovery processing, (3) the quality assessment of recovered product, and (4) the product application [61].

2.4.2 EoW for recycled aggregates from CDW

Aggregates are granular materials employed in the construction sector to manufacture (1) ready-mixed concrete, (2) precast concrete, (3) and road layers (e.g. asphalt, stabilized and unbound granular material for bases, subbases, subgrades, and in backfilling operations). Aggregates of mineral origin (sand, gravel, crushed rock) are classified as *natural aggregates*. Aggregates are also generated from secondary materials of industrial process and are called *secondary aggregates* (slags, ashes) or from materials previously used in buildings and infrastructures and then transformed into *recycled aggregates* (CDW aggregates).

Wastes derived from construction and demolition activities become recycled aggregates when they comply with technical and environmental requirements. During the demolition phase, it is necessary to remove some hazardous materials (i.e. asbestos,

hydrocarbons, mineral wool, tar, mercury, etc.) and other substances that can create negative consequences on the environment (wood, plastics, gypsum, glass, metals, paper, rubber). The quality of CDW aggregates is evaluated according to (1) technical specifications related to construction materials and (2) environmental requirements of national regulations. The first quality condition guarantees the performance of the aggregate for its specific application. The European standards listed in Table 2.2 [63] specify the requirements of aggregates on the basis of their potential application. The environmental criteria to obtain the EoW status evaluate the potential risk of the inclusion of environmentally harmful substances in CDW aggregates. This environmental assessment is based on the determination of leaching pollutants from recycled aggregates. The acceptance limits depend on the final destination of the aggregate and are, generally, set by each Member State [64]. In Italy, the Ministerial Decree of 5th February 1998 [65] establishes the procedures for recovering non-hazardous waste and fixes the acceptance limits of leaching tests to be performed on recovered material.

Table 2.2 – European standards on aggregates for engineering purposes

EU standard	Context
EN 13242 [66]	Aggregates for civil works and road construction
EN 13043 [67]	Aggregates for bituminous mixtures
EN 13450 [68]	Aggregates for railway ballast
EN 12620 [69]	Aggregates for cement concrete
EN 13055 [70]	Lightweight aggregates
EN 13139 [71]	Aggregates for mortar
EN 13383-1 [72]	Aggregates for use as armourstone

2.4.3 CDW aggregates production process

The variety of CDW and the resulting quality of derived recycled aggregates depends on the adopted demolition methodology. To facilitate the employment of CDW in new construction materials, the selective demolition is strongly promoted in lieu of conventional one [73]. In conventional demolition activities, a building or an infrastructure is demolished with explosives, wrecking balls, hydraulic crushers and bulldozers. The resulting waste is a mixture of concrete, plastic, metals, ceramics, tiles, bricks, and wood. In selective demolition, specialized workers operate with light mechanical tools, which allow to separate demolished materials. This procedure is usually more expensive and time-consuming than the conventional demolition, but produces selected and cleaner waste (with a higher economic value) and higher rates of recovery [74]. In both cases, the removal of hazardous materials is a preliminary

operation during the transformation from waste to aggregates. Occasional contaminants should be adequately treated according to specific regulations.

The CDW is transformed into recycled aggregates in management plants, traditionally classified in three levels [31], as reported in Figure 2.4. Mobile plants of *level 1* provide crushing and sieving operations and constitute a simple technology usually employed in construction sites where also some demolition activities can take place. *Level 2* facilities are mobile or fixed management plants with higher capacity of *level 1* and include metal separation after crushing and sieving operations. In countries where the CDW management is considered a primary issue, *level 3* plants are prevailing. In addition to crushing and sieving operations, a more selective identification and separation of impurities through hand sorting and high pressure washings is carried out in *level 3* plants [75].

Management plants can receive CDW in clean components (e.g. concrete, bituminous mixture) or in mixed condition. After an initial identification and separation of large contaminants by means of cranes and diggers, debris are reduced of dimensions through crushing operations. Depending on the final product to be obtained, three types of crushers can be employed: jaw crusher (Figure 2.5.a), impact crusher (Figure 2.5.b) and cone crusher (Figure 2.5.c).

The first consists of a plate which moves toward a fixed base and produces compressive actions that crush and reduce the dimensions of particles. This type of crushing, widely employed for CDW, generates flaky aggregates with low content of fines (<10%). In impact crusher facilities, rotating hammers crush particles and reduce size by impact actions. In this crushing system, the amount of produced fine is greater with respect of jaw crusher but it is possible to produce aggregates of smaller particles size [76]. The crushing action of a cone crusher is achieved by the movement of a conical mantle which rotates eccentrically with respect to the main shaft and compresses particles into an external conic wall. With this type of crusher, it is possible to obtain a wider particle size distribution with respect to the two previous systems and a limited amount of fine [77]. After crushing, CDW particles are subjected to an additional separation process aimed at removing unwanted materials (residuals of metals, plastics, paper). There are several procedures suitable for the removal of one or more contaminants: hand sorting, magnetic separation, and gravimetric separation [78]. At the end, aggregates are sieved into different size fractions (based on market requests) and stored in heaps. During crushing and sieving operations, huge quantities of dusts are produced, thus the management plants usually adopt technique and technologies for reducing the level of dusts in work environment [79]. The two most common applications are suction hoods for air cleaning and wet spray systems for dust prevention.

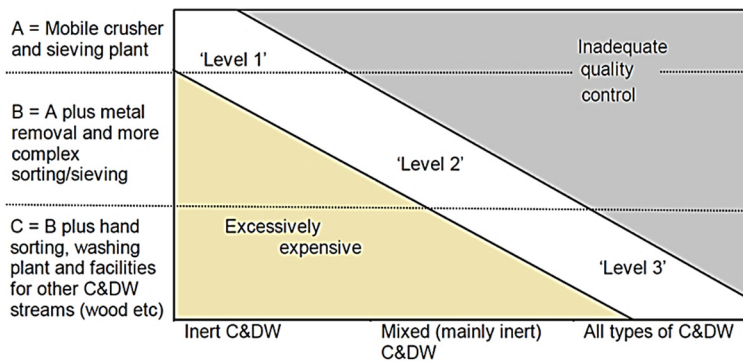


Figure 2.4 - CDW facilities according to Symonds Group [31]

The technological research on new and more efficient crushing and recycling plants deals with several aspects: technical [34], [80], [81], economic [82], [83], [84], [53], and environmental [85], [86]. From the technical point of view, researches and practices are exploring more advanced sorting systems to obtain recycled aggregates of superior quality [87], [88]. The economic and environmental perspective is currently evaluated with life cycle assessment methodologies [89], [90], [91].

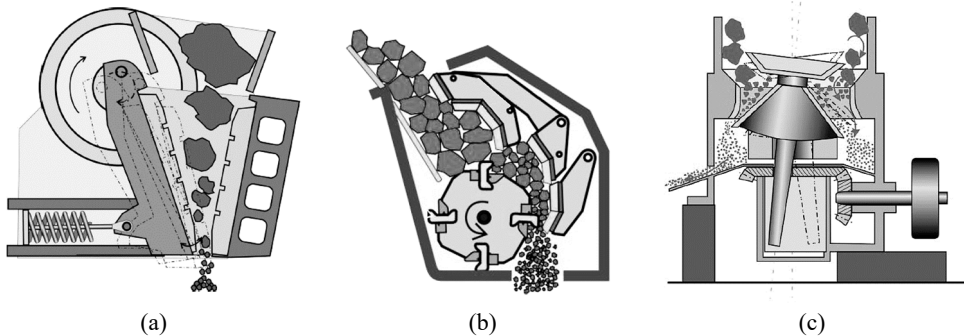


Figure 2.5 - Types of crusher in CDW management plants. (a) Jaw crusher, (b) impact crusher, (c) cone crusher [79]

2.4.4 Life cycle assessment of CDW aggregates

As previously described, CDW becomes a resource when it is converted into recycled aggregate and enters in the supply chain of construction sector. Although numerous researches and practices demonstrated the feasibility in producing aggregates from CDW and using them for building and infrastructure sectors, they can be effectively considered an alternative to non-renewable resources if their environmental and economic

sustainability is verified. This kind of evaluation takes into account the entire life cycle of a material and its application (Figure 2.6) by means of the life cycle assessment (LCA) method [92].

The ISO 14044 [93] defines the LCA methodology as the “compilation and evaluation of the inputs, outputs and the potential environmental impacts of a product system throughout its life cycle”. The LCA approach is worldwide adopted for comprehensively comparing the environmental impacts of different scenarios and to support the decision making [94], [95]. In the context of the production of recycled aggregates, Hossain et al. [96] compared the environmental consequences caused by the production of CDW and natural aggregates. The output of LCA revealed that the production of recycled coarse CDW aggregates reduces of 65% the greenhouse gas emission and of 58% the non-renewable energy consumption with respect of quarrying and processing operations of natural aggregates. A similar result was found by Simion et al. [97], who used the LCA approach to compare the environmental impact of the recycling process of CDW.

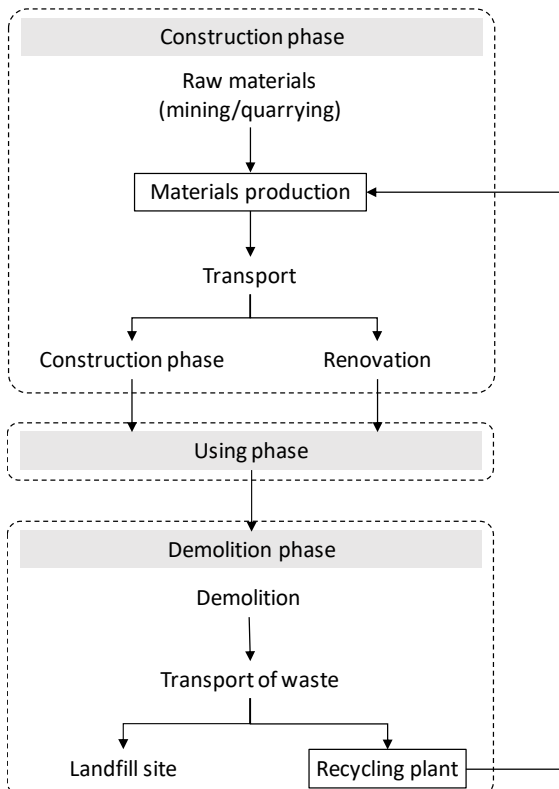


Figure 2.6 - Life cycle approach for a civil infrastructure or a building [92]

Ghanbari et al. [98] demonstrated that the production of CDW in Iran reduces drastically the energy consumption, the CO₂ emissions and the total annual cost in comparison to the extraction and crushing of natural aggregates. The North Italy case-study presented by Blengini [99] evidenced that the recycling of demolished materials can compensate part of energy consumed for quarrying and transporting virgin aggregates. The recycling of lithoid materials allows to decrease of 19% the gross energy requirement and of 10% the global warming potential (GWP). Balaguera et al. [100] endorsed the LCA as the method for quantifying the impacts derived from the use of traditional and alternative materials in road constructions. The author claimed that the use of waste materials in roads decreases both the energy consumption and the GWP since the disposal in landfills is avoided. Chowdhury et al. [101] pointed out that the use of recycled concrete pavement waste is attractive only if the transportation distance is lower than a quarter of that of natural aggregates, since its production process causes higher energy consumption, GWP and acidification potential in comparison with natural aggregates. The transport of material is considered a key factor for discriminating the environmental benefits in using CDW materials for road construction by many authors. For instance, the LCA analysis carried out by Rosado et al. [102] revealed that the use of unselected CDW aggregates in base and subbase layers of road pavements is environmentally advantageous if the distance between construction and production site is up to 20 km longer than that of natural aggregates. The authors identified in the handling and transportation the most impacting stages in the process of recycling and using CDW aggregates. Accordingly, Penteado and Rosado [103] corroborated that the recycling of CDW is effectively beneficial when the sorting stage takes place at construction site, avoiding the transport of unwanted materials to the recycling plant. They suggested that the maximum distance between the demolition site and the recycling plant should be lower than 30 km, since the most environmentally harmful processes are related to fuel consumption and transport. Butera et al. [104] carried out a comparative LCA analysis between two scenarios: (1) the utilisation of 1 tonne of CDW aggregates in road subbases construction and (2) the disposal of the same quantity in a mineral landfill. Considering as main environmental indicators the GWP and the abiotic resource depletion, they demonstrated that the reuse of CDW in road constructions avoids the environmentally harmful activities related to the quarrying of virgin materials. Furthermore, they indicated that around 30% and 40÷50% of all impacts are caused by crushing operations and transportation respectively, in line with the study of Mroueh et al. [105] and Marinković et al. [106]. Based on the results of an LCA analysis, Parajuli et al. [107] recommended to use RC aggregates in low trafficked roads (e.g. access and feeder roads) and virgin aggregates in strategic infrastructures (e.g. highways). Gschösser et al. [108] carried out an LCA of recycled and primary aggregates for construction of roads in Switzerland. The authors concluded that the use of cement-stabilized CDW aggregates

in the formation of subbase layers generally reduces the environmental-related impacts in comparison to cement-stabilized natural aggregates. Moreover, they indicated that the production at site decreases the considered impact categories in comparison to at-plant mixing (Table 2.3).

Specific LCA studies on the production of cement concrete revealed that the environmental benefits in using recycled aggregates (typically from RC) in substitution of natural ones are limited. For instance, Yazdanbakhsh et al. [109] pointed out that the production of concrete with natural aggregates led to similar environmental impacts of concrete production with RC, since the larger distance between natural quarries and mixing plants is compensated by the greater quantity of cement required in case of RC usage. Ding et al. [110] evaluated the environmentally harmful consequences when 50% and 100% of RC aggregates are substituted to natural ones in cement concrete production. The authors concluded that only limited environmental benefits derived from the use of recycled aggregates, since cement is regarded the largest contributor to all impact categories in both cases of concrete with natural and recycled aggregates. Knoeri et al. [111] compared the production of conventional concrete with concrete including CDW aggregates, identifying as the main advantage of the second option the avoidance of waste landfilling. The research of Colangelo et al. [112] demonstrated that the use of cement concrete with 100% of CDW as coarse aggregate reduced all the considered impact categories in comparison to a conventional concrete.

Table 2.3 - LCA results of different mixing method (at plant, with central mixing at site, and in-situ mixing) and aggregates origin (from CDW and virgin) analysed by Gschösser et al. [108]

Impact category	Mixing at plant		Central mixing method at site		In-situ direct mixing	
	NVA ⁴	CDW	NVA ⁴	CDW	NVA ⁴	CDW
GWP ¹ (kg CO ₂ -eq./m ³)	75	70	67	62	64	58
CED ² (MJ-eq./m ³)	599	476	474	352	420	298
ES ³ (1000 Pt/m ³)	114	49	105	39	100	35

Notes: ⁽¹⁾ GWP = Global Warming Potential

⁽²⁾ CED = Cumulative Energy Demand (non-renewable)

⁽³⁾ ES = Ecological Scarcity method (defined in eco-points Pt per unit)

⁽⁴⁾ NVA = Natural virgin aggregates

2.5 Uses of recycled aggregates from CDW

From the literature review of Section 2.4.4 it emerges that recycling of CDW undoubtedly involves several benefits towards the environment, of which (1) the reduction of the amount of disposal waste and (2) the prevention of the exploitation of non-renewable raw materials are the most important.

Despite the recycling of CDW implying significant environmental benefits, there is still a strong diffidence in using secondary materials derived from this waste stream. Yuan and Shen [113] identified as a key barrier in the recycling of CDW the extra-costs of recycling process in comparison to natural materials, especially in regions where the price of primary natural resources is too low (i.e. recycled materials are not competitive) [114]. In some countries, the main reason of the poor implementation of CDW aggregates in civil sector is associated to the restrictiveness of design rules and the lack of adequate standards [115]. In addition, Cardoso et al. [23] ascribed to (1) the bad quality of CDW aggregates, (2) the large availability of natural materials and (3) their consolidated experience, the potential disadvantages that encourage users in employing primary raw materials instead of recycled resources. According to Silva et al. [116], the scepticism in using CDW aggregates comes from the poor knowledge of their performances and from the uncertainty related their environmentally harmful consequences. Notwithstanding, CDW aggregates were introduced in the construction sector more than twenty years ago [114]. Their most common use is actually in the formation of unbound layers for road constructions [20], although numerous experimental investigations supported their employment in a variety of other applications [23], [117].

2.5.1 Recycling of CDW aggregate in concrete

Cement concrete is one of the most used material in construction sector. Several experimental investigations claimed the feasibility of substituting natural aggregates with selected CDW aggregates derived from crushed recycled concrete (RC) in new concretes for structural and non-structural applications. They commonly concluded that no significant effects on compressive strength are noticeable up to a rate of substitution equal to 25÷30% [118], [119], [120], [121]. Sagoe-Crentsil et al. [122] compared the results of 28-day cured compressive and splitting tensile strengths of specimens containing 100% of RC aggregates and those made of conventional (basalt) aggregates, observing negligible differences.

Aggregates recycled from demolished concrete represents only the 15% of the total CDW generated [123], thus most of studies tried to evaluate fresh and hardened

properties of cement concrete containing mixed CDW aggregates (i.e. including concrete, ceramics, and other material). The inclusion of these materials tends to reduce the workability of fresh mixtures, due to the higher water absorption in comparison with virgin aggregates [124], [125], [126]. Mas et al. [127] draw a comparison between conventional concrete and alternative concrete containing 25% of CDW aggregates, recognizing a decrease in strength of 15% on the second one. Generally, an increase of recycled aggregates from CDW in substitution of natural ones leads to a reduction of the mechanical properties of hardened concrete [128], [129], [130]. Moreover, the durability tends to reduce due to the presence of CDW aggregates [131]. Bravo et al. [131] concluded that the use of CDW aggregates is highly detrimental in concrete, since their presence increases the carbonation depth.

Generalizing, the literature on the use of CDW aggregates in concrete production suggests that it is possible to partially substitute natural aggregates with recycled ones with a limited reduction of strengths and durability. Nevertheless, these weaknesses can be contrasted employing a good quality recycled material.

2.5.2 Recycling of CDW in geotechnical applications

Recycled granular materials from CDW can be employed to substitute natural aggregates in different geotechnical applications, mainly as a backfilling material. Santos and Vilar [132] presented a first attempt of using CDW materials for backfilling geosynthetic structures. They compared the behaviour of recycled materials with a typical sand and a sandy soil. The results of direct shear tests revealed a greater friction angle for CDW materials ($\Phi = 42^\circ$) in comparison with the sand ($\Phi = 32^\circ$) and the sandy soil ($\Phi = 33^\circ$). The pull-out tests showed that the mechanical strength of the CDW material is higher than that measured on sand specimens and lower than that of the sandy soil. The viability of using CDW as backfilling material for geosynthetic reinforced walls was studied also in larger scale applications [133], finding similar properties to those of a geosynthetic wall containing granular material of natural origin. The research concluded that huge costs saving may be possible if using recycled CDW backfilling materials in place of more expensive traditional ones.

Aqil et al. [134] demonstrated that RC aggregates behave as a high quality backfill material if adequately compacted. In well-compacted state, RC specimens showed a compressive strength and a pre-peak stiffness comparable to those of a well graded gravelly soil. A great number of studies [135], [136], [137], [138] investigated the interface shear strength properties of reinforced geogrids containing CDW aggregates, demonstrating their feasibility to be employed as alternative backfilling materials in geosynthetic-reinforced structures. Specifically, the two experimental investigations

carried out by Arulrajah et al. [135], [136] investigated the interface shear strength of CDW materials divided into RC, ceramic materials (i.e. bricks and tiles, BT), and reclaimed asphalt (RA) components using a large-scale direct shear test apparatus. They found that reinforced geogrids containing RC aggregates with particle size in the range $0.075\div 19$ mm were characterized by the highest interface peak and residual shear strength properties, while those containing RA aggregates showed the lowest ones. However, they concluded that all three CDW constituent (RC, BT, RA) met the requirements of peak and residual shear strength for aggregates to be used in civil engineering applications. The studies of Vieira and Pereira [137] and Vieira et al. [138] compared shear strengths and pull-out interaction coefficients of fine-grained CDW aggregates ($0\div 10$ mm) with those reported for typical natural soils. The feasibility of using CDW materials in geotechnical applications was also verified in environmental terms in order to protect groundwater from possible contaminants. The values of leaching tests of CDW materials were below the limitations imposed by the European Council Decision 2003/33/EC [139] for inert materials, with exception of sulphate and total dissolved solids. The two investigations pointed out that properly selected and compacted CDW materials can be employed as backfills in geosynthetic reinforced structures.

Despite recycled aggregates from CDW showing acceptable shear strength for several geotechnical applications, Sivakumar et al. [140] argued about the durability to the repeated loading which can cause particle crushing. The authors showed that shear strengths were comparable between RC, BT, and crushed basalt (employed for comparison purposes) specimens, but after 8 cycles of loading, CDW exhibited a marked reduction of the peak friction angle (from 43° to 38° for RC, and from 43° to 37° for BT) in comparison to the reduction from 47° to 45° of the basalt.

Rahman et al. [141] evaluated the suitability of using CDW aggregates as alternative backfilling materials in pipelines trenches, by determining the geotechnical properties of RC, BT, and RA separately. They observed that friction angle ranges from 51° of RC to 58° of RA, while the cohesion was equal to 66 kPa for RC, 60 kPa for BT, and 45 kPa for RA. They concluded that the shear strength properties of RC and BT are equivalent or superior to those of natural quarry materials used for pipe backfilling.

CDW granular materials have been also studied as gabion filling material by Nawagamuwa et al. [142], who simulated the gabion behaviour containing RC, BT, plaster, and pebbled separately. They recognized that only particles derived from RC can be sustainably reused as a gabion fill material, while the others did not satisfy the requirements of compressive strength and durability.

2.5.3 Recycling of CDW in road applications

The most common use of recycled aggregates from CDW is certainly in road applications [20], since the construction of a road infrastructure involves large volumes of granular materials. All layers of a road pavement structure (Figure 2.7) are made of granular materials. In bottom layers (i.e. the subgrade and the subbase), aggregates are in unbound conditions. In the upper layers (i.e. the base), higher quality aggregates are required due to the greater stresses transferred from the traffic loads. In these cases, granular materials are often stabilized with the addition of cementitious binders for improving bearing capacity and durability. Surface layers, which are directly in contact with traffic loads, are made of asphalt mixtures (flexible pavement) or concrete (rigid pavement), both largely composed by aggregates [143]. Likewise, road embankments are made of compacted granular materials and soil

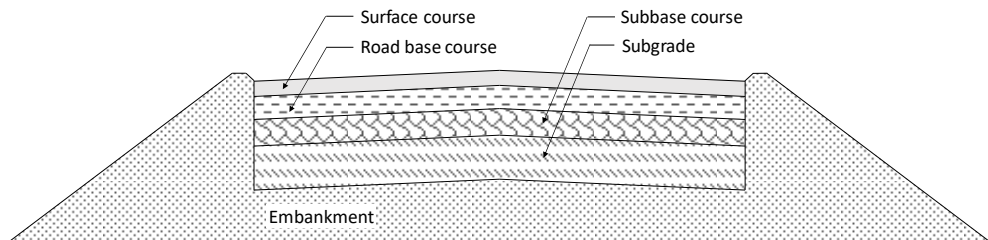


Figure 2.7 - Cross section of a typical road pavement structure [144]

Unbound applications

Concerning the use of mixed recycled materials from CDW in place of natural granular materials in embankment structures, Cristelo et al. [145] reported that the mechanical behaviour of specimens compacted at the 95% of the Modified Proctor test and 7% of water was consistent with that of a natural soil. Moreover, results of leaching revealed that CDW aggregates behave like inert materials according to the European Council Decision 2003/33/EC, demonstrating the fully feasibility of employing these materials. Sangiorgi et al. [146] verified the in-situ behaviour of a road embankment comparing different mixtures of CDW aggregates by mean of light-weight deflectometer (LWD) measurements. The results pointed out that (1) the stiffness increased with the increment of roller passes, (2) the stiffest layer was that containing 50% of RC and 50% of RA, and (3) the stiffness tended to increase over time due to the self-cementing properties of RC components included in the CDW materials.

The phenomenon of self-cementing of RC particles was also investigated by Arm [147] and Poon et al. [148], who attributed to traces of un-hydrated cement adhering to RC

particles the main cause of their behaviour. More specifically, Arm [147] studied the self-cementing phenomenon both at the laboratory scale through resilient modulus (RM) results and at the field scale through falling weight deflectometer (FWD) measurements, concluding that the increments were largely higher in the case of back-calculated moduli from FWD than in case of RM tests. From chemical analyses and unconfined compression strength (UCS) results, Poon et al. [148] recognized that the two most active size fractions were those containing particles with dimensions lower than 0.15 mm and in the range 0.3÷0.6 mm. Similarly, Vegas et al. [149] carried out a pre-normative research to investigate the properties of mixed CDW aggregates for unbound pavement layers. They measured that, after 90 days of soaking, the California bearing ratio (CBR) was higher than that recorded on samples soaked for 4 days. The authors attributed to the residual pozzolanic reactions induced by concrete and ceramic materials the large improvement of the bearing capacity.

The use of recycled aggregates in unbound layers of road pavements has been studied since several decades ago. In 1991, O'Mahony and Milligan [150] reported the possibility of using of RC and mixed CDW aggregates in road subbases. CBR and compaction tests revealed similar results between RC and natural aggregates and lower performance of mixed CDW aggregates. However, these results were higher than the limitations imposed by the British highway works specifications [151]. The National Cooperative Highway Research Program (NCHRP) Synthesis 199 [152] reported that, in 1994, several States of US were studying the feasibility of using demolition debris as aggregates in roads construction. For example, the Connecticut Department of Transportation successfully employed CDW as aggregates for subbase layers. The research report of Goulias et al. [153] indicated some recommendations for using RC and RA as aggregates for road bases. For instance, RA content in recycled base layers should not exceed 25÷50% by weight to guarantee adequate strengths and avoid excessive permeant deformations. In case of RC materials, angular and cubical grains were declared preferred in the production of recycled aggregates for road bases. The experimental investigation of Bennert et al. [154] compared the performance of CDW mixtures containing RC and RA aggregates with that of a dense-graded aggregate base coarse (DGABC). They found the highest RM values for 100% RC and 100% RA mixtures and the lowest one for specimens made of natural aggregates (Table 2.4). Conversely, the RA material tended to accumulate excessive rates of permanent deformations, leading the authors to conclude that the mixture made of 25% of RA and 75% of RC was the good compromise to obtain a recycled granular material with approximately the same RM and permanent deformation properties of a natural one commonly used in bases and subbases layers.

Table 2.4 - Results of RM and permanent strain of CDW and DGABC mixtures investigated by Bennert et al. [154]

Mixture	RM ($\theta=344.7$ kPa) (MPa)	Permanent strain (mm/mm)
100% DGABC	179.5	0.0067709
75% DGABC, 25% RA	234.2	0.0071812
50% DGABC, 50% RA	279.5	0.0198218
25% DGABC, 75% RA	280.9	0.0252393
100% RA	360.9	0.0562942
75% DGABC, 25% RC	201.5	0.0059426
50% DGABC, 50% RC	321.8	0.0052879
25% DGABC, 75% RC	325.6	0.0044802
100% RC	375.9	0.0038648

The resilient response of different RC aggregates was discussed by Nataatmadja and Tan [155]. Repeated load triaxial (RLT) tests displayed RM values depending on the compressive strength of the original concrete, and on the flakiness index (FI) and Los Angeles (LA) coefficient of RC aggregates. However, the resilient response of RC materials was found similar to that of natural aggregates used for comparison purposes. Molenaar and van Niekerk [156] found that also gradation, composition, and compaction have an influence on the resilient behaviour and the resistance to permanent deformation of mixtures made up of recycled CDW aggregates. They identified in the degree of compaction the most important factor, and pointed out that a higher compaction produces specimens with (1) higher cohesion, (2) greater RM, and (3) lower permanent deformations. Correspondingly, da Conceição Leite et al. [157] suggested that compaction could promote crushing and breakdown of CDW particles, leading to a better densification of the CDW aggregate. As a consequence, an improvement of (1) the bearing capacity, (2) the RM and (3) the resistance to permanent deformation have been highlighted. Their results outlined that CBR increased from 73% to 117% when the compaction effort passed from the standard to the modified Proctor level. Figure 2.8 reports the evolution of RM with bulk stress (θ) depending on compaction energy obtained by da Conceição Leite et al. [157].

Several authors [158], [159], [160], [161] used RLT tests to estimate the stiffness of compacted CDW mixtures. All these studies compared the resilient and permanent strain behaviour between recycled aggregates from CDW and natural granular materials (NGM), claiming a good mechanical response of recycled aggregates. Arulrajah et al. [158] reported that RC, BT, and waste rock (WR) performed satisfactorily at 70% of the optimum moisture content (OMC) and generally better than a NGM investigated for comparison purposes.

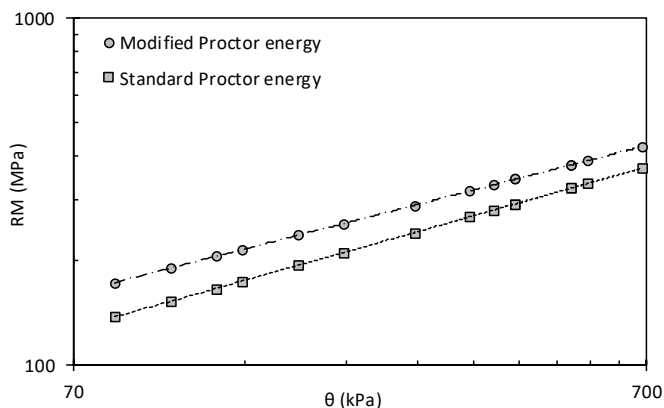


Figure 2.8 -RM results of CDW depending on the compaction energy [157]

Bozyurt et al. [159] recorded average values of RM (for $\theta = 208$ kPa) equal to 540, 620, and 690 MPa for NGM, RC, and RA respectively. In terms of average plastic deformations, RC showed values of 0.7%, RA of 1.4% and natural aggregates of 1.6%. Permanent deformation behaviour of CDW mixtures has been extensively investigated by Cerni et al. [162], who highlighted that, at optimum moisture condition, CDW specimens showed cohesive behaviour, since they are less sensitive to confining pressure and axial stress than natural material. Authors attributed this attitude to (1) the cohesive behaviour of CDW materials and to (2) the production of fines during compaction, which ensured a good permanent deformation resistance. The blends of RC and RA examined by Arulrajah et al. [163] exhibited the negative effects of increment of water content, which caused an increase of permanent strains and a reduction of the RM. Moreover, authors stated that the content of RA must be limited to 15% to meet the requirements for using these granular materials in pavement subbase layer.

According to Dong & Huang [164], who investigated the viscoelastic properties of RA aggregates for pavement base applications, RA mixtures (0÷19 mm) exhibited higher RM than natural crushed limestone and gravel mixtures tested for comparison purposes. However, RA aggregates accumulated more permanent deformations than natural ones, thus suggesting the authors to discourage the use of 100% RA aggregates as unbound material for pavement bases.

A lot of research was carried out on the behaviour of recycled aggregates derived from crushed concrete [19], [155]. Ayan et al. [165] studied the degradation of RC aggregates, pointing out that the compaction process tends to significantly modify the particle size distribution due to the presence of mortar which is crushed and detached from the aggregate. Very high LA coefficients were recorded on RC aggregates investigated by Rustom et al. [166] ranging from 42% to 49%, but CBR values exceeded values of 180%

making the authors to conclude that RC aggregates can be considered a good alternative to natural aggregates for road constructions. According to Park et al. [167], RC aggregates can be also used as base and subbase materials for supporting rigid pavements, since deflections measured by means of FWD apparatus were comparable between two layers made of RC aggregates and NGM mixtures. Figure 2.9 summarizes the values of modulus of subgrade reaction estimated from FWD measurements on RC aggregates and NGM layers obtained by Park et al. [167]. Recycled crushed glass (CG) waste was also considered by several authors for using in road works [168], [169], [170]. Wartman et al. [168] investigated the characteristics of CG aggregates as materials for embankments and road applications. Mixtures of CG aggregates in size fraction 0÷10 mm were characterized by an OMC of 10.5% and a maximum dry density (MDD) of 1825 kg/m³ obtained with modified Proctor compaction test, while the direct shear friction angles varied from 47 and 62° (with normal stresses in the range 0÷200 kPa). Disfani et al. [170] suggested that the properties of CG aggregates depend on the particles size, since medium (0÷10 mm) and fine (0÷5 mm) sized CG aggregates showed similar geotechnical properties of natural aggregates, while coarse particles (0÷20 mm) was unsuitable for road applications.

Numerous experiences demonstrated the good mechanical performances of CDW aggregates both in unbound layers of paved roads (bases and subbases) [171], [172], [173], [174], [175], [176] and in unpaved rural roads [177], [22], [178]. Of particular interest are the results of Herrador et al. [171] and Neves et al. [173], which indicated the satisfactory behaviour of unbound bases containing CDW materials in terms of deflections measured as per the FWD method. Recently, Távira et al. [176] evaluated the in-situ performances of low quality CDW mixed with excavated soil to build an experimental road in Spain. Their results underlined the higher bearing capacity of road sections containing recycled aggregates compared to those made up of natural materials.

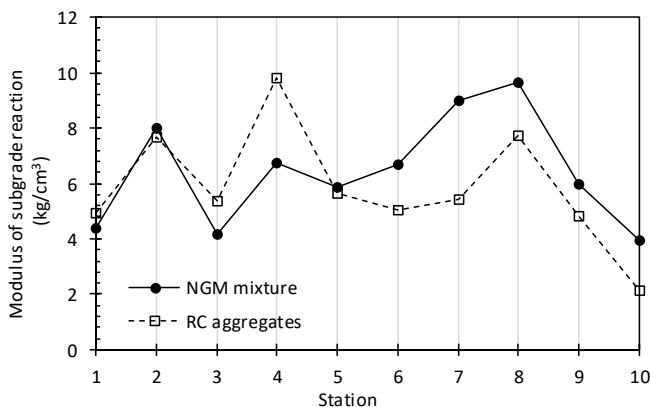


Figure 2.9 - Comparison between modulus of subgrade reaction derived from FWD measurements on RC aggregates and NGM layers [167]

Jiménez et al. [22] investigated the mechanical and the environmental behaviour of two sections of an unpaved road built with structural layers of different materials. The first section (Figure 2.10.a) was made up entirely of recycled aggregates (RC materials in the surface layer and mixed CDW in the base course), while the reference section included a surface layer made up of NGM and a base layer with mixed CDW materials (Figure 2.10.b). All materials were found of good quality, meeting the requirements of leaching tests, except for soluble salt. The authors reported that both sections showed excellent bearing capacity, which was maintained during the following two years. The FWD tests evidenced slightly higher deflections in section made of RC aggregates than the reference one. In a similar investigation, the same authors [177] compared the results of plate bearing tests and FWD tests of two sections (Figure 2.11) of another unpaved road. The first section consisted in a base course containing NGM and a surface layer made of unselected CDW aggregates (Figure 2.11.a), while the second one was completely built with NGM (Figure 2.11.b). The authors found that the Young modulus of section containing mixed recycled aggregates increased by 27% over time, while the same decreased by 23% in the reference section (Figure 2.11.b). FWD tests confirmed that deflections were slightly lower in the section containing CDW materials in the surface layer than those exhibited by the section build entirely with NGM. In terms of environmental properties, CDW aggregates did not meet the limit of sulphur compounds (in line with results of Vegas et al. [179]). Similarly to previous studies, Del Rey et al. [178] showed that non-selected CDW aggregates can be used for unpaved road construction built over expansive clays subgrades.

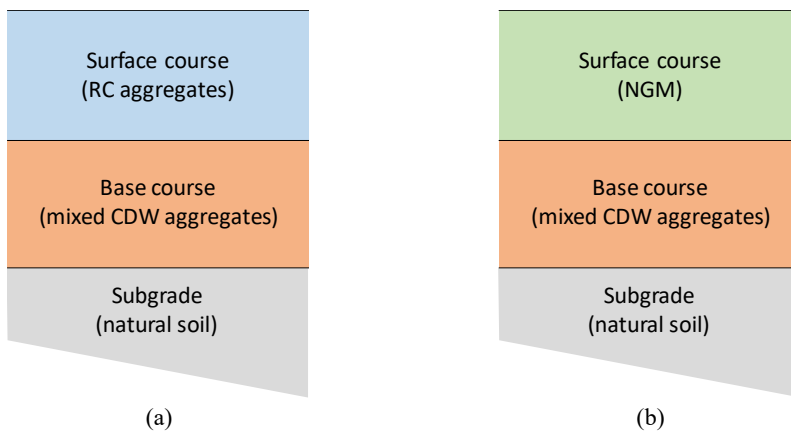


Figure 2.10 - Scheme of unpaved rural road sections of Jiménez et al. [22]: (a) surface course made of RC aggregates and base course of CDW, (b) surface course made of NGM and base course made of CDW

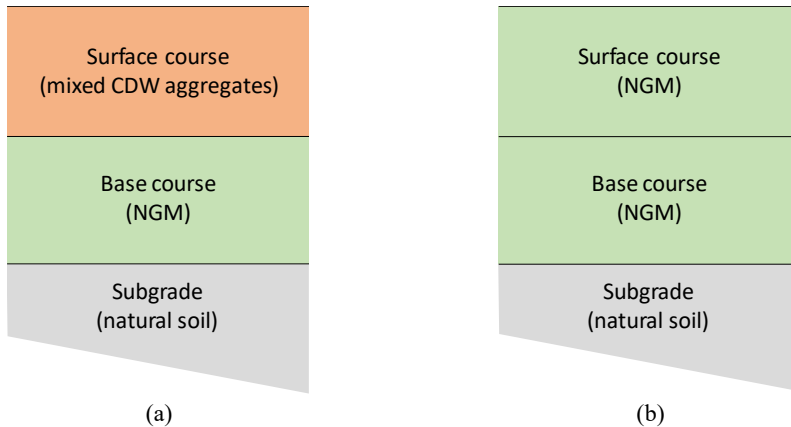


Figure 2.11 - Scheme of unpaved rural road sections of Jiménez et al. [177]: (a) surface course made of unselected CDW aggregates and base course of NGM, (b) section built entirely with NGM

Technical literature revealed that CDW can be satisfactorily employed in the formation of unbound layers of road pavements. These recycled materials, both in unselected condition (mixed CDW) or in separated constituents (RC, RA, BT), exhibited comparable properties of those of natural origin. On the other hand, the significant heterogeneity in composition led several authors in measuring high variability of mechanical and environmental performances both in laboratory and in-field investigations [23], [180], [181], [182], [183], [184].

Stabilized applications

The pavement structure of highly trafficked roads usually requires the presence of layers with higher strength, stiffness, and durability [185]. This is the case of the semi-rigid (Figure 2.12.a) and the inverted semi-rigid (Figure 2.12.b) pavement configurations, in which the base layer and the subbase layer, respectively, are built with cement-stabilized granular materials to improve mechanical properties and guarantee an adequate durability of the whole pavement [20].

Pasetto [186] demonstrated that the properties of layers containing unselected CDW materials can be improved by adding 3÷5% (in mass of aggregates) of cement. Gobieanandh and Jayakody [187] analysed the CBR of cement treated aggregates mixtures with different amount of CDW aggregates instead of natural ones. They pointed out that the addition of 5% of ordinary Portland cement (OPC) drastically increases the bearing capacity of all mixtures in comparison to the untreated specimens. On the other hand, the increment of CDW rate into the mixtures causes a decrease of CBR (Figure 2.13).

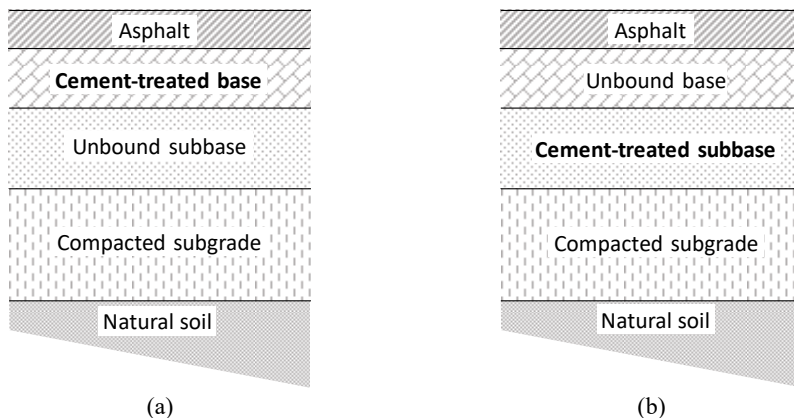


Figure 2.12 - Scheme of (a) semi-rigid and (b) inverted semi-rigid pavement

Vice versa, in the cement treated mixtures of soils and CDW aggregates investigated by Reis et al. [188], an increment of the amount of recycled aggregates from 0% to 50% in mass of mixtures ensured an increase of compressive strength, which reached 2.8 MPa after 7 days of curing. To evaluate the mechanical properties of mixed CDW aggregates stabilized with OPC for road base layers, Del Rey et al. [25], carried out a laboratory investigation on 0÷8 mm size aggregates. Their results suggested that fine grained recycled aggregates can satisfactorily be employed in road bases, since specimens containing 3% of OPC reached values of UCS in the ranges 2.6÷3.4 MPa and 3.4÷4.4 MPa after 7 and 28 days of curing respectively.

The comparison between the addition of OPC in mixtures containing RC and BT aggregates and in those made up of NGM revealed comparable, and sometimes, better performances of recycled aggregates.

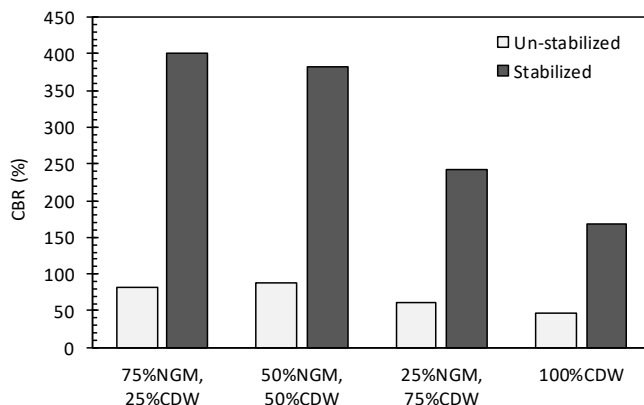


Figure 2.13 - CBR results on un-stabilized and stabilized mixture of CDW and NGM [187]

For example, Xuan et al. [189] studied the performance of a cement-treated granular mixture of BT and RC, observing that UCS and indirect tensile strength (ITS) increased linearly with an increment of cement content, curing time, and degree of compaction. Disfani et al. [190] highlighted that mixture containing 50% of RC and 50% of BT stabilized with 3% (in mass) of OPC exhibited similar RM to cement-stabilized quarry aggregates, as well as the fatigue life evaluated as per the flexural beam configuration. Agrela et al. [191] built an experimental road section in Spain to demonstrate the potentiality of using cement-treated recycled aggregates of RC and BT in place of natural ones for the subbase construction. Back-calculated moduli from FWD testing confirmed the better behaviour of mixtures containing recycled aggregates. A similar in-field investigation was carried out by Pérez et al. [192], who monitored a road section consisting in the base layer made up of cement-stabilized RC aggregates. The authors showed that the recycled material has a slightly lower modulus (from FWD tests) than that measured on the stabilized NGM base layer built for comparison purposes.

The feasibility of using individually cement-stabilized RC, RA, and BT materials for base and subbase layer of road pavement have been investigated by different authors [193], [194], [24], [195], [196], [197]. Of particular interest is the laboratory investigation of Mohammadinia et al. [24], who demonstrated that the stabilization with OPC improved significantly the mechanical properties of RC, RA, and BT aggregates. Figure 2.14 shows the evolution of RM in function of θ , for un-stabilized and cement-stabilized RC, RA, and BT aggregates (cured for 7 days). With the aim of avoiding the use of OPC, several authors tried to stabilize recycled aggregates with alternative binders, such as cement kiln dust (CKD) and fly ash (FA). In 2003, Taha [198] found that RA aggregates with the addition of 15% in mass of CKD are an appropriate alternative to NGM for road bases and subbases construction.

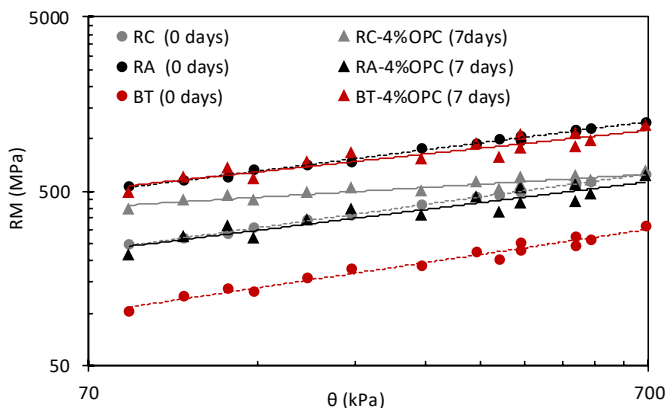


Figure 2.14 - RM results of un-stabilized and stabilized RC, RA, and BT aggregates investigated by Mohammadinia et al. [24]

More recently, Bassani et al. [26] compared the short- and long-term mechanical properties of unselected CDW granular material stabilized with CKD and those stabilized with OPC. They observed similar results in terms of RM and UCS, with the best performances exhibited by specimens containing 10% of CKD. They also noticed a huge enhancement of the mechanical properties with curing time, as shown in Figure 2.15.

Arulrajah et al. [199] obtained encouraging results from their experimental investigation on blends of CKD and FA for stabilizing recycled aggregates. Camargo et al. [200] determined at the laboratory scale the strength and stiffness of two different types of recycled aggregates (RA and road surface gravel, RSG) stabilized with FA. The author claimed that the addition of FA increased both the CBR and the UCS. Moreover, after 5 cycles of freeze and thaw (F/T) degradation, only small reductions of RM were recorded: 15% for RA aggregates, and only 5% for specimens containing RSG. Investigating the same materials (RA aggregates and FA), Hoy et al. [201] tried to improve the performances of the binder (FA) through its alkaline activation (AA).

The process of AA involves chemical reactions between precursors (normally aluminosilicate powders) and activators (alkaline liquids), which induce strength development over time [202], [203]. In the experimental investigation of Hoy et al. [201], the precursor was the FA, while the activator was a liquid solution of sodium silicate and sodium hydroxide. They compared the same mixtures containing RA aggregates and FA as a binder, adding in one case the chemical activator and, in the other case, only water. The highest values of UCS were achieved with the alkali-activated FA.

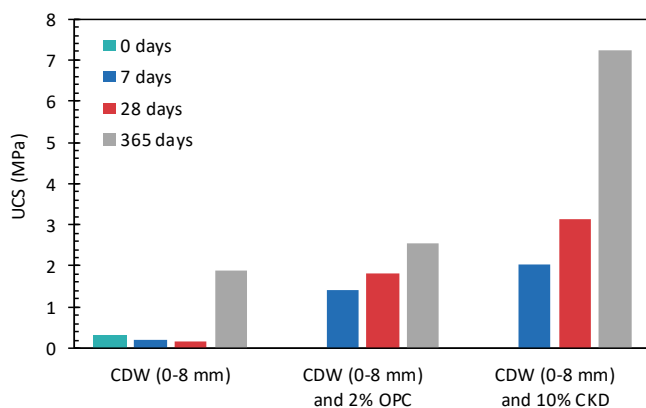


Figure 2.15 - UCS results for different curing time of CDW aggregates stabilized with OPC and CKD by Bassani et al. [26]

In an analogous research [204], the same authors attributed to the formation of calcium-alumina-silicate-hydrate (C-A-S-H) products the increment of strength due to the alkali-activation of FA. These species were generated from the reaction of the calcium and the magnesium contained in RA aggregates and the silica and the alumina in FA. Moreover, they found that the leaching of heavy metals from the alkali-activated RA-FA mixtures was lower than that measured on non-activated mixtures.

Very recently, Cristelo et al. [28] published the strength results of specimens containing CDW materials treated with alkali-activated FA. They attributed the better mechanical response of recycled aggregates in comparison to the natural ones to the fact that CDW aggregates promoted the formation of C-A-S-H gel in the early stages of AA process with the coexistence of sodium-alumina-silicate-hydrate (N-A-S-H) gel induced by the presence of FA. They concluded that CDW acted not only as aggregates, but it also contributed to the total volume of amorphous material available for the AA. Alkali-activated FA was also employed as stabilizing agent of RC, RA, and BT aggregates by Mohammadinia et al. [205]. FA was added in different percentages (4, 8, 16%) and activated by an aqueous solution of sodium silicate and sodium hydroxide. The results highlighted that RC and RA aggregates performed satisfactory as pavement subbase materials if treated with 8% and 16% of alkali-activated FA and cured at 40°C. The curing temperature was found to have a key role in the AA process, since the heat treatment increased the reaction kinetic and, consequently, the stiffness and strength of stabilized specimens. In another laboratory investigation, Mohammadinia et al. [27] demonstrated that recycled aggregates from RC, RA, and BT treated with alkali-activated FA and blast furnace slag (BFS) improved strength and stiffness without specific thermal treatments. The highest increment of UCS was observed on RC samples, followed by RA and BT specimens. The best resilient response was recognized on RA specimens. Among the two precursors (FA and BFS), the higher compressive strength was achieved with the addition of alkali-activated BFS. To understand the potentiality of different precursors, Arulrajah et al. [206] tried to alkali-activate calcium carbide residue (CCR), FA, and BFS for stabilizing RC and BT materials. Firstly, they observed a marked increment of strength and stiffness of stabilized specimens in comparison to the non-stabilized ones. Secondly, they reported that the AA of BFS induced the highest compressive strength, followed by CCR and FA after 7 days of curing at 40°C. Finally, the authors pointed out that the combination of these precursors did not enhance the mechanical properties. The addition of alkali-activated FA has also been proposed by Vitale et al. [207] to stabilize clayey soils. The authors observed that the high reactivity of FA promoted the precipitation of new mineralogical phases forming networks characterized by cementitious properties. As a result, an overall improvement of mechanical properties comparable to that induced by OPC was noticed.

2.6 Alkali-activation processes

The alkali-activation technology is scientifically known from more than 70 years [208]. Since 1940, when Purdon [209] proposed the AA of BFS as alternative to the traditional cement, the international research about alkali-activated binders has continued for decades. In the 50s, Glukhovsky experimented the alkali-activation of clays, feldspars, and slags containing silica and alumina [210], [211], while in 1979, Davidovits coined the term “geopolymer” [212] to indicate a material originated by the inorganic polycondensation of aluminosilicates present in this material induced during the AA [213]. Alkali-activated binders gained interest in civil engineering when, in 1994, Wastiels et al. [214] showed that alkali-activated FA binders exhibited higher strengths than OPC, extending their potential employment also in structural applications.

The mechanisms of alkali-activation depends both on the nature of precursor [215] and on the type of liquid activator [216], [217], [218]. The chemistry of the AA process is still discussed in the scientific community [219], [220]. According to Liew et al. [221], the mechanism is characterized by simultaneous steps reported in following list and schematically depicted in Figure 2.16:

- (a) dissolution of aluminosilicates in the alkaline medium; in this step, the release of aluminate and silicate species occurs; amorphous and semi-crystalline phases are completely solubilized in the alkaline medium, while well-crystallized phases tend to be activated only superficially [213], [222];
- (b) to restore the equilibrium, released ions and silicate contained in the activating solution reorganize and interact to form small coagulated structures [223];
- (c) as the chemical reaction continues, some oligomers (small number of monomers) condensate in the aqueous medium to form large networks; these intermediate products have been distinguished in two gel stages: gel 1 (characterized by high Al content), which transforms into gel 2 (characterized by the presence of high content of Si);
- (d) after the intermediate gelation steps, the system continues the polycondensation process and the three-dimensional aluminosilicate network grows up until the hardening and solid-state transformation.

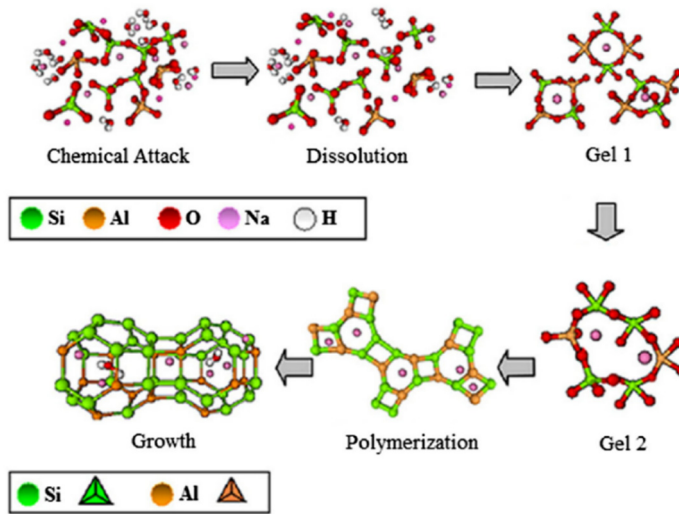
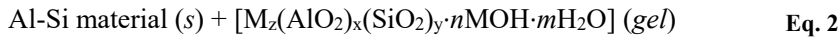
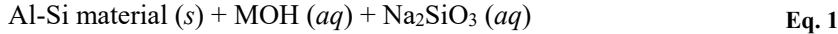


Figure 2.16 - Conceptual model for alkali-activation mechanism [221]

Xu and Van Deventer [224] formulated the chemical reactions between aluminosilicates oxides and silicates during the alkali-activation process as follows:



Eq. 1 expresses the dissolution of aluminosilicate materials into a MOH (M=generic alkaline metal, usually Na or K) and Na_2SiO_3 alkaline solution (AS). The transportation and the formation of a gel phase derived from the polycondensation of Al and Si ions is explained by Eq. 2. As last, the formation of geopolymers with amorphous structure is showed by Eq. 3 [225]. Wang et al. [226] explained that both the precursor and the liquid activator affect the AA process. The properties of aluminosilicates have an effect on the dissolution stage, while the AS affects the recombination of aluminosilicate in the reacting system and the polycondensation stage.

After the main mechanisms of AA were introduced, at first, by Glukhovsky and, afterwards, by Davidovits, a wide range of materials have been tried to be alkali-activated. According to Pacheco-Torgal et al. [227] any material composed of silicon and aluminium oxides can react in alkaline conditions: from natural raw materials, such as kaolinitic clays [228], [229], metakaolin [230], [231], clay sediments

[232], [233], and stone muds [234], to industrial by-products, such as BFS [235], [236], FA [237], [238], combination of BFS and FA [239], [240], CKD [241], silica fume [242], and lignite bottom ash [243].

2.6.1 Advantages in using alkali-activated binders

A wide variety of alternatives to OPC have been explored over the years, since its production process is considered energy-consuming and environmentally harmful [244]. Recent studies have estimated that the production of OPC generates around 5% of the total volume of carbon dioxide (CO₂) emissions [245], [246]. The ACI-ITG-10R report [244] asserts that the main motivations of using alternative cements are related to the reduction of costs and the environmentally harmful consequences, and the need of specific properties which cannot be obtained with OPC. For instance, the use of calcium aluminate cement (cement with high content of calcium and aluminium oxides and low content of silica) guarantees a remarkable resistance to chemical attack when compared to OPC [247]. The interest in this type of cement is also related to the lowering CO₂ emissions associated with its production [248]; however, its cost is significantly higher than OPC due the shortage of alumina resources in nature [249], [250]. Similarly, calcium sulfo-aluminate and calcium sulfo-aluminate belite cements are considered more sustainable than OPC, due to the lower CO₂ emission associated to their manufacturing [251]. Magnesium-based cements can also be considered alternative to OPC with interesting engineering properties (rapid setting, early-stage strength, high durability) and lower CO₂ emissions deriving from its production [252], [253], [254]. Juenger et al. [220] added to the list of alternative binders the super-sulphated cements due to their low heat of hydration and good resistance to chemical attacks [255]. Since this type of cement is composed mainly by BFS and calcium sulphate and very low quantity of OPC (used as activator), it is considered more sustainable than OPC [256],[257]. Table 2.5 shows a list of alternative binders highlighting the advantages and drawbacks for each.

In addition to the development of novel and resource-efficient cements reported in Table 2.5, several attempts were also made in order to replace Portland clinker with supplementary by-products materials [258], [259]: municipal waste incinerator ash [260], [261], pulverized waste concrete [262], silica fume [249], BFS, FA, and ceramic waste [263]. The LCA analysis on cement concrete production carried out by Flower and Sanjayan [264] demonstrated that the addition of BFS and FA as supplementary materials in cement binders decreases of 22% and 14%, respectively, the CO₂ emission in comparison to OPC.

Table 2.5 - Comparison of alternatives to OPC (adapted from Juenger et al. [220])

Alternative	Advantages	Drawbacks
OPC	<ul style="list-style-type: none"> ▪ long history ▪ low price ▪ standard composition 	<ul style="list-style-type: none"> ▪ energy-intensive production ▪ high CO₂ emissions ▪ low durability in aggressive environments
Calcium aluminate cement	<ul style="list-style-type: none"> ▪ low CO₂ emissions ▪ rapid strength ▪ good resistance to chemical attacks 	<ul style="list-style-type: none"> ▪ high costs ▪ strength loss during time
Calcium sulfo-aluminate cement	<ul style="list-style-type: none"> ▪ low CO₂ emissions ▪ rapid strength ▪ capability of waste encapsulation [265] 	<ul style="list-style-type: none"> ▪ difficulties in controlling the dimensional stability ▪ unproved durability
Magnesium-based cements	<ul style="list-style-type: none"> ▪ low CO₂ emissions [266] ▪ rapid strength ▪ good water resistance 	<ul style="list-style-type: none"> ▪ absence of industrial manufacturing process ▪ strength reduction in moist environment [254]
Super-sulphated cements	<ul style="list-style-type: none"> ▪ contain partially waste materials ▪ low heat of hydration ▪ good resistance to chemical attacks [255] 	<ul style="list-style-type: none"> ▪ low strength development ▪ hardening process strongly dependent on temperature [267]
AA-binders	<ul style="list-style-type: none"> ▪ contain 100% waste materials ▪ low CO₂ emissions ▪ excellent strengths ▪ good fire resistance ▪ good resistance to chemical attacks ▪ immobilization of hazardous waste ▪ extensive research and development 	<ul style="list-style-type: none"> ▪ use of chemical activators (whom production causes CO₂ emissions) ▪ fluctuations in precursors chemistry [268] ▪ thermal treatments to reach the highest strengths ▪ high costs

Among alternative cements, alkali-activated binders have the advantage of being constituted by 100% of waste or by-product materials, allowing a larger reduction of greenhouse emissions [269], [270]. Several studies indicated that the AA of BFS or FA have the potential to reduce from 30 to 80% the CO₂ emission when compared to OPC [271], [272], [273]. It is worth mentioning that the discussion is still open, since the production of the chemical activators of the AA process is recognized the most critical aspect in the LCA analysis of geopolymetric materials [274], [275], [276], [277]. Recently, Turner and Collins [278] estimated that the CO₂ footprint of a FA-based geopolymer concrete is only 9% lower than that of traditional concrete with OPC. As

indicated in Section 2.4.4, the CO₂ emissions depend on several factors (i.e. source of raw materials, manufacturing processes, energy, and transportation consumptions) which may explain the huge differences in the previously-mentioned values.

In addition to the environmental benefits, alkali-activated binders have several properties that make them much more attractive than the previously-mentioned alternative cements [279]. For example, Van Deventer et al. [271] pointed out that the majority of magnesium-based cement exhibited both technical and economic limitations with respect to alkali-activated binders. A number of experimental investigations confirmed that the AA of wastes or by-products produces binders characterized by excellent strengths [280], [281], low permeability, good resistance to fire and chemical attack [282], better carbonation resistance, lower hydration heat [283], and lower shrinkage [284] in comparison to OPC. Finally, some indicated that alkali-activated binders have also the capability in immobilizing toxic substances [285].

Although alkali-activated binders have many advantages over OPC and other alternative cementitious products, it is worth mentioning that Burris et al. [268] identified in (1) the fluctuation of precursor chemistry and in (2) the necessity of thermal treatment for achieving the highest values of strength [286] the two main disadvantages of these alternatives. Moreover, Pacheco-Torgal et al. [287] denoted that the high cost of alkali-activated binders remains a drawback over OPC. Provis [288] pointed out that alkali-activated materials are more expensive than OPC if precursors such as FA and BFS are purchased at the same cost of OPC. Vice versa, with locally sourced materials (such as CDW, stone muds, etc.) and low dosage of chemical activators, the AA can be cost-competitive.

2.7 Alkali-activation of CDW fines

More recently, fine particles (or powders) of CDW gained a certain interest as precursors for alkali-activated binders. Most of research focalized on the activation of cementitious and ceramic particles with a thermal curing for improving the properties of the final products. Komnitsas et al. [30] induced the alkali-activation of powders of RC and BT evaluating the effect of different synthesis conditions such as the curing temperature and the molarity of activator (NaOH). Higher compressive strengths (more than 50 MPa) have been recorded on specimens of BT cured for 7 days at 80°C (Figure 2.17.b). Conversely, a low alkali-reactivity was attributed to RC specimens since they reached compressive strength lower than 15 MPa (Figure 2.17.a). The greater mechanical properties of BT component were ascribed to the higher content of Al₂O₃ in comparison to RC. No significant improvement of strength was observed when passing from 80°C

to 90°C of curing temperature. Comparable values of strength were achieved by alkali-activated ceramic waste studied by Sun et al. [289]. In their investigation, the compressive strength of pastes with a liquid/solid (l/s) ratio of 0.4 and cured for 28 days at 60°C exceeded 50 MPa, demonstrating the potentiality of this waste as alternative material for geopolymerization processes. The potential use of ceramic waste, such as BT, was deepened in the two studies of Reig et al. [290], [291]. Mechanical tests on mortars containing alkali-activated ceramic waste as binder and cured for 7 days at 65°C revealed compressive strengths variable from 22 to 41 MPa. Similarly, the experimental investigation of Robayo-Salazar et al. [292] focalized on the development of alternative binders from the AA of BT waste. The authors demonstrated that the addition of Na_2SiO_3 to NaOH in the AS composition is fundamental for the development of high compressive strengths. Moreover, they found that the final strength is strongly related to the elemental composition of the precursor (in particular the $\text{SiO}_2/\text{Al}_2\text{O}_3$ ratio) and the molar ratio $\text{Na}_2\text{O}/\text{SiO}_2$, as reported in bar diagrams of Figure 2.18.

Table 2.6 reports compressive strength results obtained by Allahverdi and Kani [293] on 28-day cured blends of alkali-activated BT and RC powders cured at room temperature in function of Na_2O concentration (in weight of dry binder). The authors argued that the higher reactivity of BT specimens is due to the greater content of aluminosilicates in these components, which led to higher compressive strengths. Similar observations were pointed out by Pathak et al. [294], who detected a greater dissolution of aluminosilicate species under alkaline conditions of BT compared to RC by means of calorimetric measures.

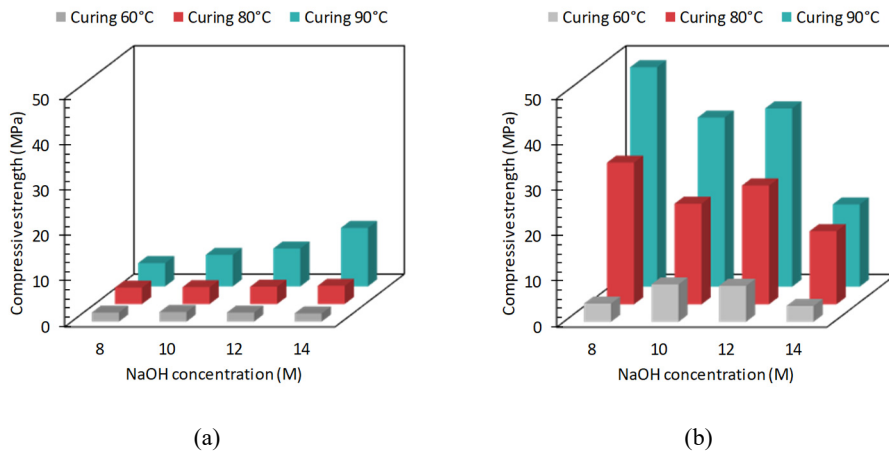


Figure 2.17 - 7-day compression strengths of (a) RC and (b) BT powders depending on NaOH concentration and curing temperature from Komnitsas et al. [30]

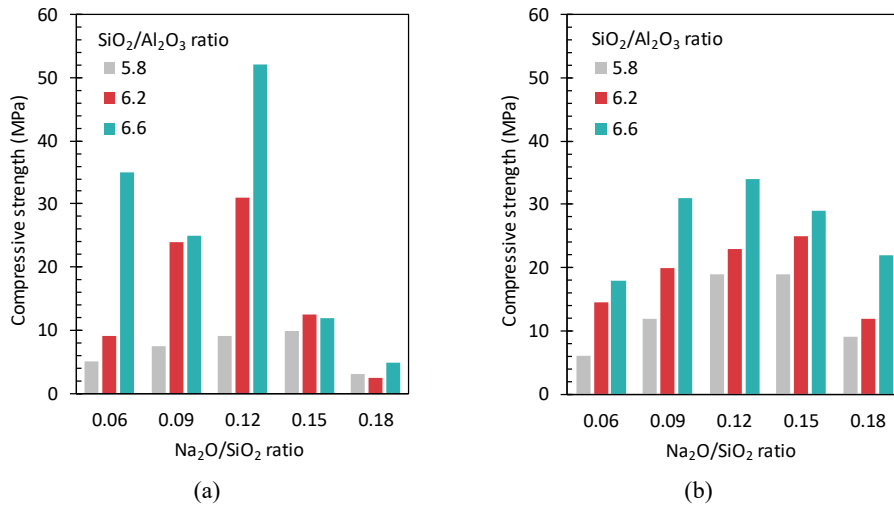


Figure 2.18 - 28-day compression strengths of alkali-activated BT depending on $\text{SiO}_2/\text{Al}_2\text{O}_3$ and $\text{Na}_2\text{O}/\text{SiO}_2$ from Robayo-Salazar et al. [292]: (a) curing at room temperature, (b) treatment at 70 °C for 24 hours

Table 2.6 - Results of compressive strength (in MPa) recorded by Allahverdi and Kani [293] on alkali-activated mixtures of BT and RC cured for 28 days in function of Na_2O concentration

Mixture	Na_2O concentration (%wt)		
	6	7	8
40% BT, 60% RC	10.0	12.0	16.5
50% BT, 50% RC	12.5	13.8	18.5
60% BT, 40% RC	13.8	27.5	28.5
80% BT, 20% RC	17.0	30.0	33.0
100% BT	22.5	33.8	40.0

Jha and Tuladhar [295] demonstrated the benefit of increasing curing time from 5 to 15 days (at 40°C) for the development of strengths of RC-based geopolymers. They also suggested that the best results were achieved with a concentration of sodium hydroxide of 5 M and with a ratio between sodium silicate and RC equal to 0.5. Also Paya et al. [296] studied the AA of RC. They recognized the enhancement of thermal treatment at 65°C in comparison to a curing at room temperature, obtaining good mechanical strengths after 3 days, despite the low content of SiO_2 and Al_2O_3 element in the starting raw material.

In some studies, CDW fines have been added in blends with other materials. For example, Zaharaki et al. [297] prepared cubic specimens by mixing powders of BT, RC, ferronickel slag and red mud with a chemical activator of sodium silicate and sodium

hydroxide. After 24 hours of curing at 80°C and 7 days at room temperature, compressive strength results demonstrated that the molarity of sodium hydroxide has a key role in the reactivity of mixtures, as well as the molar ratio of oxides contained in the initial paste. They noticed that the addition of 10 M sodium hydroxide produced the highest compressive strengths for each mixture. Moreover, they concluded that the higher $\text{SiO}_2/\text{Al}_2\text{O}_3$ ratio, the greater the strength, due to the formation of strong Si-O-Al and Si-O-Si bonds. Similarly, Komnitsas [298] analysed the effect on compressive strength of cured samples caused by the AS molarity and the percentage of each precursor material (marine sediments, BT, and RC). He concluded that the strength development can be enhanced adequately mixing starting precursors to adjust the chemical composition of the blend. The investigation confirmed that, independently of the molarity of the AS, mixtures containing mainly RC were characterized by lower compressive strength than those containing mainly BT. The author attributed this behaviour to the shortage of SiO_2 and Al_2O_3 and prevalence of CaO in RC material. Ahmari et al. [299] obtained geopolymeric binders from blends of pulverized RC aggregates and FA. They recommended the addition of RC up to 50% since it increased the compressive strengths. Similarly, Zedan et al. [300] replaced BFS with different percentages of BT and RC fines for producing alkali-activated pastes. At long curing times, pastes including BT exhibited higher mechanical strengths than those with RC, due to the better dissolution of aluminosilicates in BT, which led to a more complete geopolymerization reaction.

3. EXPERIMENTAL PROGRAM

The analysis of literature put in evidence the encouraging results arising from the use of CDW aggregates in substitution of natural ones for civil applications. Recycled granular materials have been already used in the formation of unbound layers of pavements and in road embankments. Several authors also tried to improve their mechanical properties with the addition of both traditional and alternative binders. The growing interest in recycled aggregates from CDW is driven by (1) the recent implementation of stringent European regulations on the disposal of waste from construction and demolition activities [19] and (2) the target of increasing up to 70% the reuse of non-hazardous CDW (by 2020) imposed by the European Commission [21].

However, there is still a strong disparity between the progress of the research and the effective application of CDW materials in real (full-scale) applications. In the Italian context, the employment of CDW granular materials is limited due to the lack of specific regulations able in promoting their use in road constructions. Moreover, the innate distrust of recycled aggregates in comparison to traditional material of natural origin, as documented in Section 2.4.4, contributes in limiting the extensive adoption of these materials.

This Chapter introduces the objectives of the investigation and illustrates the experimental plan designed to meet these objectives. The investigation was arranged into a multiscale approach. Key aspects emerged from technical literature and gaps in knowledge are extensively discussed for each experimental stage, as well as the explanation of the investigated variables and the testing methods.

3.1 Research objective

The experimental investigation originates from the general objective of valorising and promoting the use of CDW aggregates in unbound and stabilized layers (i.e. subbases and bases) of road pavements. It will lead to a significant increment of the recycling rate of this waste stream, with direct environmental and economic benefits [301]. To extend as much as possible the use of CDW materials, a large number of experimental investigations proposed their stabilization with traditional and alternative binders. The addition of small quantities of these binders guarantees an increment of structural

characteristic of base and subbase layers [302], allowing the use of CDW aggregates also in applications which require superior mechanical properties [24], [26], [199].

This research is based on the laboratory characterization of CDW granular materials stabilized without the addition of any binders. The investigation deals with the improvement of mechanical and durability properties of CDW materials by the alkaline activation (AA) of finer particles normally present in these mixtures. The study aims to demonstrate that CDW aggregates can be stabilized through the addition of an alkaline solution (AS). This stabilization method does not feature in scientific literature and practical applications. As reported in Section 2.6.1, among the broader availability of alternative binders over Portland cement [244], the AA of waste materials is considered the most attractive in terms of environmental protection and mechanical properties [279]. The experimental research carried out (and described in this document) is an absolute novelty in the field of stabilization technologies for road constructions. The improvement of the mechanical properties of granular materials (both virgin and recycled) of unbound layers of road pavements has always been achieved through the addition of bitumen, lime, or cementitious binders (i.e. Portland cement) into the mixtures [303]. More recently, some investigations demonstrated that the mechanical and durability properties of recycled aggregates can be improved adding alkali-activated reactive by-products rich of aluminosilicates (i.e., fly-ash and blast furnace slag) [201], [28], [27], [206]. In this investigation, the stabilization occurred without the addition of any binder, but taking advantage of the AA of aluminosilicates in finer particles of CDW materials. With the addition of an AS in place of water, these particles tend to react and develop a binding phase, which stabilize the whole recycled aggregates mixture.

3.2 Experimental plan

The laboratory investigation adopted the multiscale approach shown in Figure 3.1. At the smaller scale, the experimental plan (Exp. A) involved the assessment of the alkali-reactivity of fine particles only ($d < 0.125$ mm). At the larger scale, the research was mainly focused on the investigation of stabilized CDW mixtures in their complete particle size distribution through the AA of smaller fractions. Two different experiments were designed and set up at this level of investigation. The first one (Exp. B1) was dedicated to the assessment of alkali-activation of fines as a stabilization method for CDW aggregates. The improvement of strength and stiffness due to the AA of fines was compared to mixtures of CDW aggregates compacted with water only.

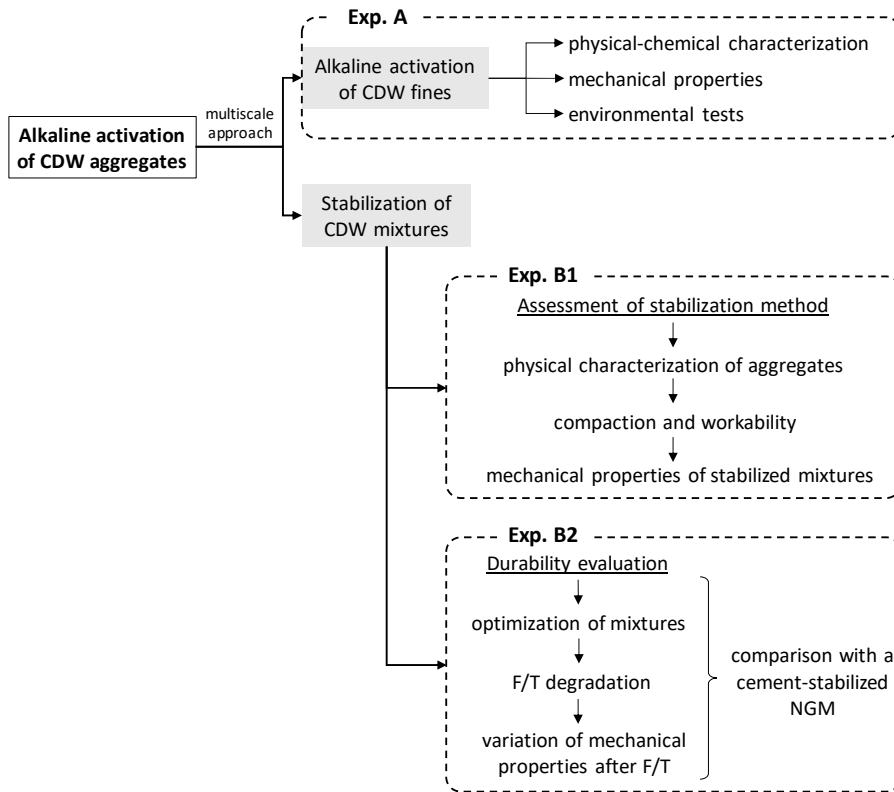


Figure 3.1 - Organization of the multiscale experimental plan

In the second experiment (Exp. B2), the durability of optimized CDW-AS mixtures subjected to freezing and thawing (F/T) degradation was evaluated. In this experimental stage, also a typical natural granular material (NGM) stabilized with ordinary Portland cement (OPC) was employed as top-quality reference material for comparison purposes.

3.2.1 Alkali-activation of CDW fines

In a mixture of granular material, finer particles are the most reactive and sensitive to water and can act like a binder for the coarser ones. They occupy the volume left by coarser grains and, in presence of water, they promote the formation of menisci that bind particles together, thus creating an internal (apparent) cohesion [304]. Small particles also exhibit a higher amount of specific surface where physical interactions and chemical reactions can take place.

In this investigation, the study of the alkali-reactivity of fine particles (with representative diameters $d < 0.125$ mm) was considered preparatory to the experiments at a larger scale. The maximum size of particles (0.125 mm) was selected in agreement with most of the geopolymer-oriented studies [30], [289], [293], [297]. Current research suggests that the AA of aluminosilicate-rich precursors is becoming a consolidated and popular practice to develop alternative binders [305]. By-products rich of Al and Si, such as FA and BFS, were found excellent materials for producing alkali-activated binders. The temperature of curing, and the composition and the alkalinity of the activating solution are fundamental parameters for a significant strength development. In literature, several investigations already proved that CDW constituents, in particular cementitious and ceramics, are characterized by a relevant alkali-activation potential. Moreover, the greatest part of literature explored the effectiveness of AA of CDW powders when subjected to thermal treatments (Section 2.7).

The Exp. A had the objective of evaluating the alkali-reactivity of CDW constituents: recycled concrete (RC), reclaimed asphalt (RA), ceramic elements (i.e., bricks and tiles, BT), and natural aggregates mixed with excavated soil (NA). Differently from other studies, the alkali-activation of powders was induced at room temperature, to simulate the actual condition of materials in real applications. This investigation (Exp. A) aimed at verifying if the addition of an alkaline solution (AS) is able to activate CDW powders and produce new materials with significant mechanical strengths. In this way, alkali-activated fines could act as a binding phase in mixtures containing also coarser CDW aggregates. In addition to the four main constituents (RC, RA, BT, NA), two other fractions were investigated and labelled as UND1 and UND2. The first one was simply obtained by sieving the CDW granular material at 0.125 mm, while the second was reconstructed from particles of the four constituents in equal proportion (25% RC, 25% RA, 25% BT, 25% NA).

Specimens were produced mixing solid particles (with 50% of $d < 0.063$ mm, and 50% of $0.063 < d < 0.125$ mm) with the liquid activator. Three different liquid/solid (l/s) ratios were considered to evaluate the effects of this parameter on the strength development of each constituent. The l/s ratio varied from 0.4, 0.5, and 0.6, in line with most of literature [298], [306]. The AS always plays a fundamental role in AA processes [294], [307], [308], [309], thus its concentration was included in the list of variables (Table 3.1). In Exp. A, the AS was employed in both undiluted and diluted form, with concentrations of 100% (undiluted), 75%, and 50%. Additional details concerning AS are provided in Section 4.3.

Table 3.1 summarises all the variables of the experimental plan related to the alkali-activation of CDW fines (Exp. A), while Table 3.2 lists the tests carried out in this experimental stage.

Table 3.1 - Variables in the experimental plan related to the alkali-activation of CDW fines (Exp. A)

Variable	Value	Description
Constituent	6	RC, RA, BT, NA, UND1, UND2
l/s ratio	3	0.4, 0.5, 0.6
AS concentration	3	100%, 75%, 50%
Size distribution	1	50% of $d < 0.063$ mm and 50% of $0.063 < d < 0.125$ mm
Curing	1	28 days

This experimental stage (Exp. A) involved a preliminary characterization of raw powders derived for CDW. The chemical analysis of fines was carried out by means of x-ray diffraction (XRD) and x-ray fluorescence (XRF) tests. This step was fundamental for identifying crystalline phases and chemical elements in each constituent. In addition, a physical characterization of fine particles was carried out. Although all mixtures were replicated with fixed proportions of passing at 0.125 mm and 0.063 mm, a laser granulometry on the two fractions was carried out to find out if the particle size distribution could have influenced the reactivity potential of CDW components [30], [310], [311], [312]. Rigden voids and particle densities provided other information on density and void content in the compacted state of powders.

The consistency of fresh pastes (mixtures of powders and AS) influenced the workability and the casting phase, thus the viscosity of fresh mixtures was measured for each combination of variables. The effectiveness of AA was read in terms of mechanical properties of hardened products [222]. Compression and 3-point flexural strength tests allowed to recognize and measure the effect of each variable on the final products. Mechanical tests ascertained the most reactive constituent and how the l/s ratio and the AS concentration affected this reactivity (and the development of strength as well).

Measurements of pH and leaching test were carried out on both raw fines and re-pulverized hardened products, for assessing the eventual environmentally harmful consequences of these materials and how the AA had influenced the leaching of several heavy metals.

Table 3.2 - Tests for the assessment of AA of fines only (Exp. A)

Sample	Investigated property	Test
Powders	Physical	Granulometry, density, Rigden voids
	Chemical	XRD, XRF
	Environmental	pH, leaching test
Fresh mixtures	Workability	Viscosity
Hardened mixtures	Mechanical	Compression, flexural strength
	Environmental	pH, leaching test

3.2.2 Stabilization of CDW aggregates with AA of fines

Literature review of Section 2.5.3 evidenced that recycled aggregates from CDW can be used for road applications both in un-stabilized and stabilized conditions. Several stabilization techniques have been proposed, from the traditional addition of OPC to the inclusion of alternative binders, such as cement kiln dust (CKD) and FA. FA- and BFS-based geopolymers have already been employed for the stabilization of recycled aggregates [201], [28], [27], [206]. In previous studies, the improvement of mechanical and durability properties was achieved by adding aluminosilicates-rich by-products to CDW mixtures. Differently, the experimental study presented in this thesis (Exp. B1) involved the stabilization of CDW aggregates without the addition of any specific binder. This experimental stage aimed at assessing the mechanical properties of CDW granular materials stabilized through the binding phase originated by the AA of the smallest particles normally included in these mixtures.

Table 3.3 lists the variables considered for the design of Exp. B1. Three different moisture contents (w_w) were taken into account, corresponding to the optimum value ($w_{w,opt}$) and the two variations of $\pm 2\%$ around it ($w_{w,opt}-2\%$ and $w_{w,opt}+2\%$), to evaluate the evolution of the mechanical properties due to small water content variations. This is a recurrent approach for granular materials in road applications, since it allows to quantify the effects of water content variations that typically occur in real-scale constructions. The water content (w_w) was intended as the real amount of H_2O in the mixture, while the AS content (w_{AS}) was the content of the added AS. Since the AS is basically an aqueous dissolution of salts, it contains a certain amount of H_2O depending on its concentration (Section 4.3). In Exp. B1, the w_w was considered as a controlling variable.

The concentration of the AS was found to strongly affect the development of mechanical strength during the Exp. A, thus it was included in the list of variables of Exp. B1. In this case, three AS concentrations, equal to 100%, 50% and 0%, were selected. The latter percentage represents a liquid phase containing only water. Pure water (AS-0%) was used to compact non-stabilized mixtures for comparison purposes. The mechanical properties of CDW-AS mixtures were evaluated after 7, 28, and 60 days corresponding to short, standard and long periods of curing.

Table 3.3 - Variables of the experimental plan on the stabilization of CDW aggregates with AA of their fines (Exp. B1)

Variable	Value	Description
Material	1	CDW
Water content	3	$w_{w,opt}-2\%$, $w_{w,opt}$, $w_{w,opt}+2\%$
AS concentration	3	100%, 50%, 0%
Curing	3	7, 28, 60 days

The experimental plan of Exp. B1 involved preliminary tests on loose particles, compaction and workability tests, and mechanical properties assessment of compacted and cured specimens (Table 3.4). A preliminary analysis of physical properties of loose aggregates was carried out to evaluate their composition, particle density and water absorption. The composition, defined as the percentage of each constituent (RC, RA, BT, NA) in an undivided CDW sample, is considered a fundamental parameter [156], [157]. Los Angeles (LA) and F/T tests on loose particles were carried out for assessing the durability properties in terms of fragmentation and frost actions degradation of CDW materials, according to the current Italian technical specifications [313]. A Proctor compaction study was performed to define the optimal amount of liquid phase (both in terms of w_w and w_{AS}). This value was then used for compacting cylindrical specimens by means of the gyratory shear compactor (GSC). Resilient modulus (RM), unconfined compression strength (UCS) and indirect tensile strength (ITS) tests allowed (1) to verify the effectiveness of proposed stabilization technique and (2) to evaluate the effect of each variable on the mechanical properties of CDW-AS mixtures. Lastly, some fragments of broken specimens were submitted to field emission scanning electron microscopy (FESEM) and energy dispersive spectroscopy (EDS) analyses to examine the microstructure and the morphology of alkali-activated products.

Table 3.4 - Experimental plan related to the stabilization of CDW aggregates with AA of their fines (Exp. B1)

Sample	Investigated property	Test
Loose aggregates	Physical	Composition, particle density, water absorption
	Durability	LA test, F/T degradation cycles
Fresh mixtures	Compaction	Proctor test
	Workability	Gyratory shear compaction (GSC)
Cured specimens	Mechanical	RM, UCS, ITS
	Microstructure	FESEM, EDS

3.2.3 Durability of stabilized CDW-AS mixtures

The Exp. B2 dealt with the assessment of the durability of stabilized CDW aggregates as per the technique investigated in Exp. B1. A certain level of distrust in the use of recycled aggregates can arise from the lack of results about the durability of these materials over time. Furthermore, results of preliminary qualification tests (i.e. Los Angeles and F/T resistance) carried out in Exp. B1 revealed that CDW aggregates were more susceptible to degradation phenomena than natural ones. This latter aspect can contribute in increasing the reticence of operators in considering these materials [314]. With the aim of bridging this gap, the Exp. B2 involved the study of the degradation

caused by F/T actions through more simulative testing conditions than traditional ones (developed for conventional materials). It is worth highlighting that:

- (a) traditional tests were originally developed for investigating natural aggregates with the aim of classifying and selecting the most suitable one for a specific application;
- (b) the degradation in loose conditions (i.e. Los Angeles and micro-Deval tests) is not representative of real (compacted) field conditions;
- (c) traditional degradation tests do not provide fundamental engineering parameters such as stiffness and strength.

In this study, the effect of F/T degradation was explored on materials in compacted condition with their optimal moisture content (or AS content in this specific case), consistently with some published researches [315], [316], [317], [318]. This procedure simulates the physical state of materials when located in subgrades, subbases, and bases of road pavement structures. Furthermore, the influence of F/T degradation on compacted mixtures was assessed in terms of variation of the mechanical properties (RM, UCS, ITS) compared to those exhibited by non-degraded specimens. This approach provided a more reliable magnitude of changes in the structural response of these materials.

Exp. B2 involved also the comparison between the proposed stabilization methodology (AA of fine particles of CDW) and the traditional stabilization of a NGM with OPC. The latter solution represents a conventional stabilization approach employed in subbase and base pavement layers in which higher stiffness, strength, and durability are required [319].

Table 3.5 lists the variables of Exp. B2. As mentioned, two different materials were considered: recycled aggregates stabilized with AS-100% (CDW-AS-100%) and a NGM stabilized with 3% in mass of OPC (NGM-OPC). In this experiment, the AS concentration and content were fixed. The degradation exposure was applied to cured specimens in order to simulate the real-scale conditions.

Table 3.5 - Variables of Exp. B2

Variable	Value	Description
Material	2	CDW-AS-100%, NGM-OPC
AS content	1	w_{opt}^1
AS concentration	1	100%
Curing	3	7, 28, 45 ² , 60 ² days
Degradation severity	4	0, 4, 8, 12 F/T cycles

Notes: ⁽¹⁾ for CDW-AS-100% it is a $w_{AS,opt}$, while for NGM-OPC it is a $w_{w,opt}$
⁽²⁾ these curing times were considered only for CDW-AS-100%

NGM-OPC mixtures were cured for 7 and 28 days, while in case of alkali-activated CDW mixtures the curing continued to 45 and 60 days, in addition to 7 and 28 days. The additional curing time for CDW-AS-100% mixtures was taken into consideration due to the slow AA reaction kinetic at room temperature [320], [321], [322]. The detrimental action of F/T was applied for three different severity levels (4, 8, and 12 F/T cycles) in addition to the reference condition, i.e. the non-degraded specimens, labelled with 0 F/T cycles in Table 3.5.

The list of tests performed during Exp. B2 is provided in Table 3.6. It includes the compaction as per the GSC method, the F/T degradation, and the tests adopted for mechanical characterization of mixtures.

In addition, some pH and leaching tests were envisaged to investigate environmental properties of stabilized mixtures. pH and leaching tests were carried out both on CDW-AS-100% and NGM-OPC specimens cured for 28 days and not subjected to degradation (0 F/T). An additional environmental test was performed on loose CDW aggregates.

Table 3.6 - Experimental plan involving the durability of both recycled and natural aggregates stabilized mixtures (Exp. B2)

Sample	Investigated property	Test
Loose aggregates	Environmental	pH, leaching test
Fresh mixtures	Workability	Gyratory shear compaction (GSC)
	Durability	F/T cycles on compacted specimens
Cured specimens	Mechanical	RM, UCS, ITS
	Environmental	pH, leaching test

4. MATERIALS

Granular materials (both recycled and natural) employed in the investigation were collected in Cavit S.p.A plant in the Turin metropolitan area (North West of Italy). The recycling plant treats waste materials derived mainly from demolitions of civil infrastructures, micro-demolitions of buildings, and renovation works. After the ascertainment of the absence of hazardous substances into the incoming material, the waste is converted into aggregates by impact crushers in dry conditions. Sprinklers nebulize water to limit the amount of dust in the atmosphere. Electromagnetic and pneumatic devices clean the material from metallic and light (plastics, papers, etc.) impurities. CDW aggregates are, then, sieved and stored in two size fractions $0\div 8$ mm and $0\div 40$ mm.

The CDW material was collected according to the EN 932-1 [323], taking samples from different points of the pile. A total of 800 kg of material (considering both size fractions) was collected in plastic bags and stored at the *Road Materials Laboratory* of Politecnico di Torino. Before any test or treatment, the CDW material was dried in a fan-assisted oven at 105°C for 24 hours for removing the residual moisture according to the EN ISO 17892-1 [324].

4.1 CDW aggregates

The coarse fraction ($0\div 40$ mm) was preliminarily sieved to remove particles greater than 25 mm, which are too large for preparing cylindrical specimens of 100 mm in diameter. A preliminary sieve analysis was performed as per the EN 933-1 [325] on samples of the two collected size fractions. Results showed that both grading distributions were outside the limitation of the Italian technical specification of the Ministry of Infrastructures and Transports [313] (Figure 4.1). For this reason and in order to preclude any effect of gradation, all specimens were prepared on the basis of the same reference gradation curve (Figure 4.1). The average of the two limits indicated by the Italian specification [313] was considered the reference particle size distribution of the aggregates employed to prepare specimens in both Exp. B1 and Exp. B2. Hence, the CDW material was preliminarily divided into different size classes by sieving operations. The required

material for each specimen was selected from each size fraction and combined according to the proportions listed in Table 4.1.

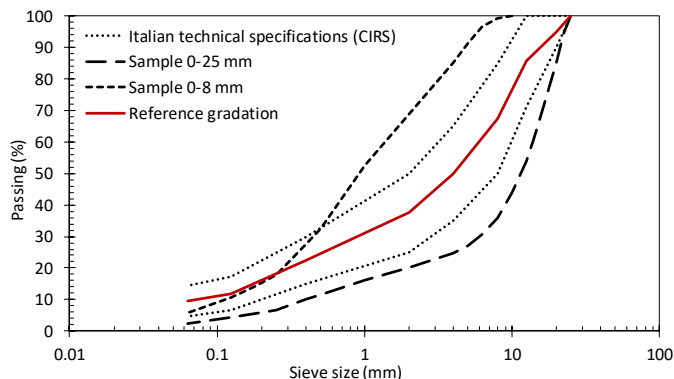


Figure 4.1 - Particle size distribution of 0÷8 mm and 0÷25 mm collected CDW aggregates

Table 4.1 - Proportions of size classes according to the reference gradation curve

Sieve size (mm)	Passing (%)
25	100
20	95.0
12.5	85.6
8	67.5
4	50.0
2	37.5
0.4	22.5
0.125	11.9
0.063	9.5

4.2 Fines from CDW aggregates

A portion of collected samples was used to produce fine particles for Exp. A (smaller scale of investigation). The material was preliminary divided into the four main components depending on the origin of each particle (Figure 4.2): recycled concrete (RC), reclaimed asphalt (RA), bricks and tiles (BT), and natural aggregates and soils (NA). Coarse particles were then crushed and ground in a rotatory drum to obtain fine powders. The produced fines were separated in two size fractions ($0.063 \text{ mm} < d < 0.125 \text{ mm}$ and $d < 0.063 \text{ mm}$) and used as precursors for the alkaline activation (AA) process. The particle size of raw powders is an important aspect of the

AA phenomenon. Finest fractions, due to the higher surface area, are more reactive, thus are characterized by a stronger binding capacity and a higher strength of alkali-activated products [30], [326], [327].

The UND1 samples (in the two fractions) were obtained by sieving at 0.125 mm and at 0.063 mm the original 0÷8 mm material without separating the constituents. The UND1 component represented the real fine fraction of an undivided CDW mixture. This sample contained unknown combination of RC, RA, BT, NA, natural clayey soil and some unidentifiable particles. Due to the essentially unknown composition of UND1, and additional sample, identified as UND2, was obtained combining RC, RA, BT, and NA in equal proportion (25 % in weight of each constituent). Figure 4.3 illustrates some pictures of the raw powders employed in Exp. A



Figure 4.2 - Pictures of CDW aggregates separated in: (a) RC, (b) RA, (c) BT, and (d) NA



Figure 4.3 - Pictures of raw CDW constituents: (a) RC, (b) RA, (c) BT, (d) NA, (e) UND1, and (f) UND2

4.3 Alkaline solution

The chemical activator employed for triggering the AA of CDW fines was a mixture of sodium hydroxide (NaOH) and sodium silicate (Na_2SiO_3) [328], [233], [329]. The NaOH, provided in solid form (flakes), was firstly dissolved in distilled water to form an aqueous solution containing 50% in weight of NaOH and 50% of distilled water, with a final concentration of 25 M (Figure 4.4).



Figure 4.4 - Pictures of (a) NaOH flakes and (b) their dissolution in distilled water

The Na_2SiO_3 , already in liquid form, was characterized by a content in weight of 8.4% of Na_2O , 27.6% of SiO_2 ($\text{SiO}_2/\text{Na}_2\text{O}$ molar ratio equal to 3.4) and 64.0% of H_2O (concentration of Na_2SiO_3 equal to 36%). The alkaline solution (AS) was prepared mixing sodium hydroxide and sodium silicate in a 1:4 mass ratio by means of magnetic stirrers [330].

During the investigation, the AS was employed both in diluted and undiluted form, to explore the effects of a dilution of the activator on the alkali-reactivity of CDW fines. Specifically, the AS was prepared in three different concentrations (Table 4.2): 100% (totally concentrated solution, without the addition of water), 75% (dilution of the totally concentrated solution with the addition of 25% in mass of water), and 50% (AS containing 50% of totally concentrated solution and 50% of additional water, in mass). In case of stabilization of CDW aggregates with the AA of their fines (Exp. B1), the reference mixture containing only water was labelled with AS-0%. Table 4.2 provides also the values of the density at 25°C of the AS for the different concentrations.

The increase of the AS concentration is reflected in an increment of viscosity. At 23°C, the viscosity of the AS-100% was found equal to 64.0 cP (for an angular speed of 40 rpm). This value is considerably higher than the viscosity of water (0.9 cP) at the same temperature indicated by the ISO/TR 3666 [331]. These results are consistent with the measurements of Yang et al. [332], who determined the static viscosity of a sodium silicate solution in the same proportions of SiO_2 and Na_2O of AS-100%, finding a viscosity 78 times higher than that characterizing distilled water (70.3 cP for sodium silicate versus 0.9 cP of distilled water at 25°C). The viscosity of the AS influenced the workability of mixtures, both in case of pastes and alkali-activated CDW aggregates and will be discussed later on.

Table 4.2 - Concentration of AS, with labelling indications and density values

AS concentration	Label	AS content (%)	Additional water content (%)	Density (g/cm ³)
100%	AS-100%	100	0	1.45
75% ⁽¹⁾	AS-75%	75	25	1.29
50%	AS-50%	50	50	1.18
0% ⁽²⁾	AS-0%	0	100	1.00

Notes: ⁽¹⁾ used only in case of AA of fines (Exp. A)

⁽²⁾ adopted as the reference in Exp. B1 (stabilization of CDW with AA)

Figure 4.5 illustrates the proportions between constituents included in the AS depending on the concentration. Diagrams put in evidence that the concentration of the NaOH in the whole AS decreased to 4, 3.5, and 1.5 M for AS-100%, AS-75%, and AS-50% respectively.

Due to the heat generated during the mixing phase, the AS was left to cool down at room temperature for some hours before using it in the preparation of specimens. The AS had the dual function of (1) creating the alkaline environment for triggering the chemical reaction of aluminosilicates and (2) providing enough workability in both cases of pastes made of CDW fines and mixtures containing CDW aggregates.

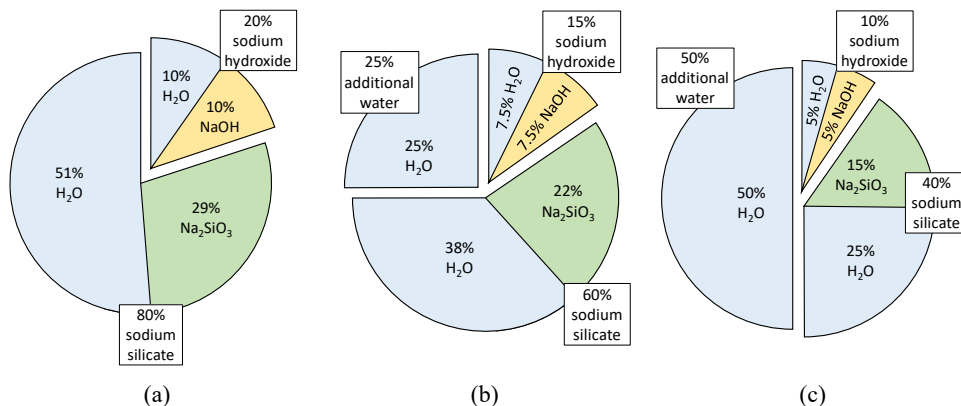


Figure 4.5 - Proportion of components in the AS with different concentration: (a) AS-100%, (b) AS-75%, (c) AS-50%

4.4 Cement-stabilized natural material

As mentioned in Section 3.2.3, a cement-stabilized natural material was employed as reference for the assessment of the durability properties of CDW-AS-100% mixtures. Ordinary Portland cement (OPC) is an effective stabilizing agent for granular materials and it is considered a top-quality materials for road bases and subbases, which require high bearing capacity and durability [333]. Cement is usually added in a quantity ranging between 2 and 4% of the dry weight of aggregates, while the optimum water content is in the range 6÷8% [302], [334].

In Exp. B2, a mixture of quarry materials and earthwork soils was used for preparing cement-stabilized specimens. Natural aggregates were collected in Cavit S.p.A plant (the same company where CDW aggregates were sampled), adopting the procedures of EN 932-1 [323] and EN ISO 17892-1 [324] for material sampling and drying, respectively. All particles with dimensions greater than 25 mm were discarded through sieving operations directly at the plant. Collected samples of natural granular material (NGM) contained mainly rounded grains with more regular shape than CDW aggregates.

To avoid differences in the particle size distribution between CDW and natural aggregates, the reference grading curve of the Italian specification [313] was employed also for preparing all NGM-OPC specimens. For this reason, aggregates were initially divided into size classes finer than 25, 22.4, 12.5, 8, 4, 2, 0.4, and 0.063 mm (Table 4.1) by sieving operations.

The OPC employed as binder was classified as CEM-I 42.5 R and included 95÷100% of clinker according to the EN 197-1 [335]. It was supplied by Buzzi Unicem and its chemical and physical characteristics are listed in Table 4.3 and Table 4.4 respectively.

Table 4.3 - Chemical composition of OPC (CEM-I 42.5 R)

Element	Mass (%)
SiO ₂	17.0
Al ₂ O ₃	3.68
CaO	59.5
CO ₂	10.8
Fe ₂ O ₃	2.95
MgO	1.50
SO ₃	3.38
K ₂ O	1.02
MnO	0.08
SrO	0.03
ZrO ₂	0.008

Table 4.4 - Physical properties of the binder OPC (CEM-I 42.5 R)

Property	Value
Loss on ignition	< 5.0%
Specific surface	3700 cm ² /g
Initial setting time	110 min
Volumetric stability	< 10 mm
Compressive strength (2 days)	26.0 MPa
Compressive strength (28 days)	48.0 MPa

Chemical properties, determined through the x-ray fluorescence analysis (Section 5.1.1), revealed the abundance of CaO and SiO₂ elements. Physical and mechanical properties, included in Table 4.4 and declared by the supplier, indicate the compliance of the binder with the standard requirements associated to this type cement (CEM-I 42.5 R).

5. METHODS

The experimental methods adopted in the investigation are presented here. The Chapter is divided in three main sections according to the experimental plan reported in Chapter 3. Each experiment stage is described in terms of methodology, procedures and reference standards. An essential explanation of equipment, data acquisition, and analysis of results is also provided.

5.1 Alkali-activation of CDW fines

The assessment of the alkali-reactivity of fine particles of CDW was preparatory for the stabilization of the whole mixture (coarse and fine particles) through the AA technique. Experimental methods described in this Section refer to the Exp. A and include all tests carried out to characterize fine fractions ($d < 0.125$ mm) of CDW aggregates. Physical and chemical properties of these fines allowed to evaluate their potential reactivity in alkaline environments. They included the analysis of particle size distribution, density, chemical composition, and mineralogical structure. In this section, preparation of specimens and curing are also explained, as well as, the procedures for viscosity determination of fresh mixtures and for mechanical testing of hardened products.

5.1.1 Physical-chemical characterization of fines

Physical and chemical properties of fines may explain how these particles can interact each other and how can react in alkaline conditions. The particle size distribution affects many properties of both fresh and hardened products [30], [310], [311], [312]. It gives information on the specific area of particles which directly reflects the surface potential reactivity in the chemical process of AA. Particle and bulk densities are fundamental properties since provide information on the packing of particles during mixing and casting stages. The chemical analysis, carried out by means of x-ray diffraction (XRD) and x-ray fluorescence (XRF) tests aims at identifying the presence of aluminosilicate elements which are a requirement to develop chemical reactions of AA.

Laser granulometry

The grain size distribution of fines particles with dimension lower than 0.125 mm was carried out through the particle size analyser apparatus (Fristch Analysette 22). The laser granulometry technique is based on the principle of light scattering due to the collision with a particle. Essentially, when a group of particles is illuminated by a laser beam, the latter is diffracted and the diffraction pattern is read by a detector (Figure 5.1). The particle diameter is related to the angular variation in intensity of light, thus the particle size distribution of sample is obtained by an integral measurement of diffraction patterns generated by each particle [336]. The result is expressed as the cumulated frequency (in volume) in function of particle size.

Each constituent of CDW (RC, RA, BT, NA, UND1, and UND2) in the two size fractions ($0.063 < d < 0.125$ mm, and $d < 0.063$ mm) was subjected to the laser granulometry analysis. To avoid aggregation of particles, few grams of powder were dispersed in water, and this suspension was stirred and scanned in the laser particle analyser.

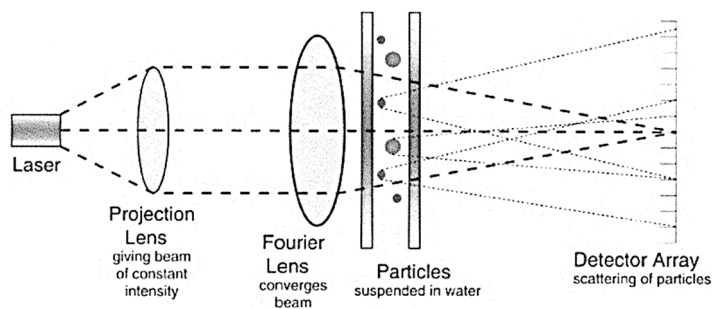


Figure 5.1 - Schematic diagram of a laser particle size analyser [337]

Density and Rigden voids

The density is a characteristic propriety of each material. Monolithic materials are characterized by a unique value of density defined as the ratio between mass and volume, while different densities can be defined in case of granular materials. In this investigation, two different densities of CDW powders were measured: the particle ($\gamma_{p,\text{fine}}$) and the bulk density ($\gamma_{b,\text{fine}}$). The first is the mass of particles over the effective volume of these particles, while the second is the mass of compacted particles (in a dry process) in a known volume.

The volume of granular particles was determined through to the pycnometer method according to the EN 1097-7 [338]. The $\gamma_{p,\text{fine}}$ (in kg/m^3) was evaluated with Eq. 4, in which m_1 is the mass of the empty pycnometer and the stopper (in grams), m_2 is the mass of the pycnometer containing the powder sample and the stopper (in grams), m_3 is the

mass of the pycnometer containing the sample, the water, and the stopper (in grams), V is the volume of the pycnometer (in mm^3), and $\gamma_{w,25^\circ\text{C}}$ is the density of water at 25°C used during test (in kg/m^3).

$$\gamma_{p,\text{fine}} = \frac{m_2 - m_1}{V - \left(\frac{m_3 - m_2}{\gamma_{w,25^\circ\text{C}} \cdot 10^{-6}} \right)} \cdot 10^6 \quad \text{Eq. 4}$$

The $\gamma_{b,\text{fine}}$ was measured with the Rigden apparatus, used also for the determination of Rigden void content (v_r). This test provides a measure of the filler ability to retain bitumen [339]. In this investigation, Rigden apparatus was used to:

- measure the void content in the compacted structure of dry powders to relate indirectly with the mineralogical nature, angularity, and texture of particles [302];
- determine the $\gamma_{b,\text{fine}}$ according to a standardized procedure.

According to the EN 1097-4 [340], 10 grams of dry powder of each constituent were placed in the Rigden apparatus (Figure 5.2) and compacted by applying 100 blows of the dropping mould from a height of 100 mm. After compaction, the height of compacted sample was recoded and the Rigden voids (v_r) were estimated with Eq. 5:

$$v_r = \left(1 - \frac{4 \cdot 10^6 \cdot m_c}{\alpha^2 \cdot \pi \cdot h \cdot \gamma_{p,\text{fine}}} \right) \cdot 100 \quad \text{Eq. 5}$$

In Eq. 5, v_r is in percentage (%), m_c is the mass of compacted specimen (in grams), α is the internal diameter of the mould (in mm), h is the height of sample at the end of compaction (in mm), and $\gamma_{p,\text{fine}}$ is the particle density of the powder obtained with the pycnometer method, in kg/m^3 .

The bulk density of fines ($\gamma_{b,\text{fine}}$), in kg/m^3 , is the ratio between the mass m_c (in grams) and the volume (in mm^3) at the end of compaction, as reported in Eq. 6.

$$\gamma_{b,\text{fine}} = \left(\frac{4 \cdot m_c}{\alpha^2 \cdot \pi \cdot h} \right) \cdot 10^6 \quad \text{Eq. 6}$$

The particle density, the dry bulk density, and the Rigden voids were determined for both size fractions (powders passing at 0.063 mm and in the range 0.063÷0.125 mm) of RC, RA, BT, NA, and UND1 fines. In case of UND2, these parameters were estimated as the weighted average of the values obtained on four constituents included.

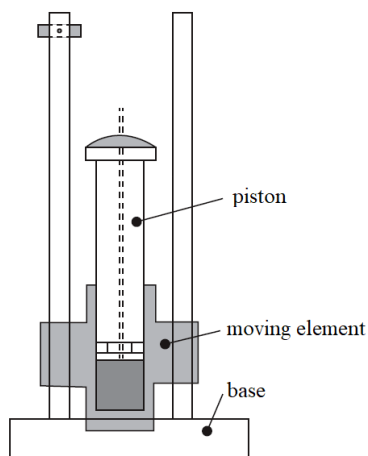


Figure 5.2 - Rigden apparatus [302]

X-ray diffraction

X-ray diffraction (XRD) analysis is a non-destructive technique used for the qualitative and semi-quantitative identification of crystalline phases of solid materials [341]. It is based on the principle of interference between monochromatic x-rays and crystalline lattices of the material. In fact, the x-ray wavelength is comparable to the spacing between crystalline planes, thus when an x-ray interacts with the crystalline lattice of the sample, it is diffracted according to Bragg's law [342].

$$n \cdot \lambda = 2 \cdot d \cdot \sin(\theta)$$

Eq. 7

The Eq. 7 states that the diffraction angle of the incidental ray (θ) is directly proportional to the wavelength of the incident ray (λ) multiplied for a positive integer (n), and inversely proportional to the interplanar distance of the crystal (d). The schematic representation of the diffraction of x-rays by a crystal according to Bragg's law is reported in Figure 5.3.

In a powdered material, crystals have a random orientation, thus the sample is scanned by different angles, changing the inclination of the incident x-ray. In this way, all possible diffraction directions of the crystalline lattice are detected and counted to obtain a diffraction spectrum. The output pattern reports a series of peaks of different intensities in correspondence of different angles, as the example of Figure 5.4. The distance between crystals, which is a unique characteristic of each mineral, is obtained by converting the angle and the intensity of diffracted ray.

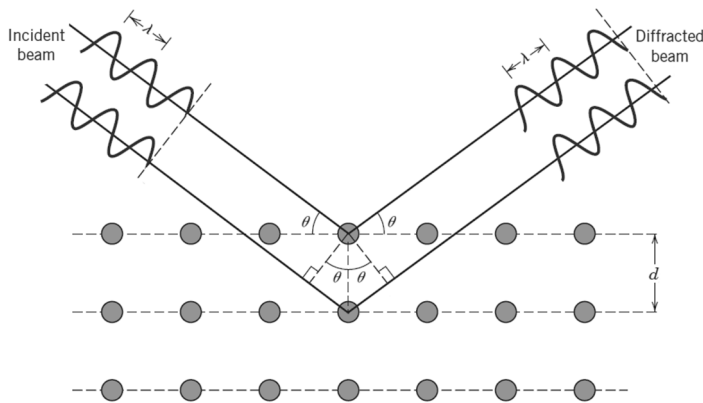


Figure 5.3 - Diffraction of x-rays by a crystal according to Bragg's law [343]

The identification of the crystalline phases of the specimen is carried out by the matching of the output spectrum with standard reference patterns, published and uploaded by the International Centre for Diffraction Data [344].

The XRD analysis was performed on each constituent of CDW (RC, RA, BT, NA, and UND1) with the aim of identifying the main crystalline phases and detecting the presence of aluminosilicates, which are necessary for the development of the alkali-activation reactions. The testing specimens, composed of few grams of particles smaller than 0.063 mm, were scanned by the Philips PW 1710 diffractometer in the angle (2θ) range $5 \div 70^\circ$.

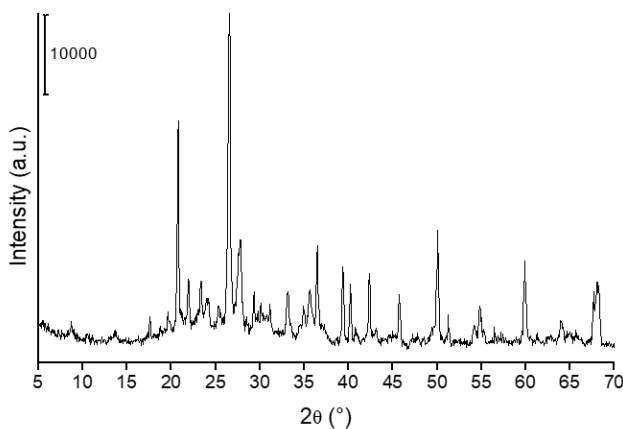


Figure 5.4 - Example of XRD output pattern (BT specimen)

Additionally, a semi-quantitative phase analysis was carried out to determine the abundance of crystalline phases in each sample. This procedure is based on the relative intensity of peaks of a particular spectrum in relation to the global output spectrum [344]. It was carried out considering the Reference Intensity Ratio (RIR) provided in the standard reference patterns [345]. In case of UND2, the semi-quantitative results were calculated as the weighted average of values obtained on RC, RA, BT, and NA fines.

X-ray fluorescence

X-ray fluorescence (XRF) analysis is another non-destructive test to characterize materials from a chemical point of view. It identifies and quantifies each element having an atomic number greater than the oxygen [342]. The XRF technique is based on the emission of “secondary” radiations from individual atoms when they are excited by an external source of energy. In this test, the sample is irradiated by a high energy x-ray beam interacting with the atomic structure of the material and displacing electrons from their orbits. The atom counterbalances the instability moving down electrons from the higher orbital to the lower one, in which the vacancy has occurred (Figure 5.5). In this movement toward the nucleus, the electron loses an amount of energy determined by the distance between orbitals, which is a unique property of each element. This energy is released in form of photons and the phenomenon is called fluorescence or “secondary” radiation emission [346]. There are two different types of XRF equipment: wavelength dispersive spectrometer and energy dispersive spectrometer, which differ substantially in the x-ray detection system. The first one collects and discriminates characteristic wavelengths generated from the specimen according to the Bragg’s law (Eq. 7), the second uses a photon detector to identify and quantify the characteristic x-ray photons on the basis of their energy [347].

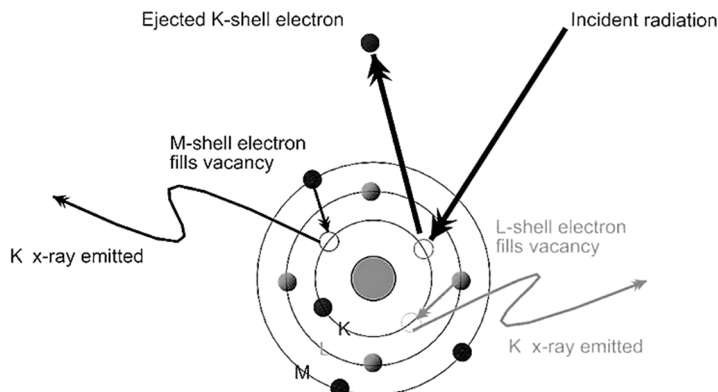


Figure 5.5 - Scheme of fluorescence phenomenon (www.bruker.com)

In this investigation, CDW fine fractions (separated in the constituents RC, RA, BT, NA, UND1, and UND2) were characterized by a wavelength dispersive spectrometer (Rigaku ZSX 100E) to detect chemical elements and their abundance, with the aim of verifying the presence of minerals required for the development of the alkali-activation process.

5.1.2 Specimens preparation and curing

Specimens for mechanical characterization were prepared by mixing CDW powders with the alkaline solution (AS). Each constituent (RC, RA, BT, NA, UND1, and UND2) was mechanically mixed adding progressively the liquid phase until the mixture reached the required workability to be casted. The solid phase was constituted by 50% in weight of particles with dimension lower than 0.063 mm and another 50% in the size fraction 0.063÷0.125 mm. The AS had the dual role of chemical activator and liquid phase to provide workability to mixtures. Three different liquid/solid (l/s) ratios were considered in the investigation (0.4, 0.5, and 0.6) as indicated in Section 3.2.1. The fresh mixtures were casted in plastic prismatic moulds of 80 mm in length, 20 mm in width, and 20 mm in height, previously sprinkled with a form-release agent for facilitating the demoulding operation. Specimens were cured in a hermetic chamber at room temperature (25°C) and at a relative humidity (RH) higher than 90% (Figure 5.6). After 24 hours of curing, specimens were demoulded and continued their curing in humid conditions (at 25°C) until the 28th day. Some specimens, especially those containing more liquid phase (i.e. those with l/s = 0.6), were kept in the moulds for more time due to their slower hardening.

Table 5.1 summarizes the proportions in mass of solid phase (fine particles differentiated in the two size fractions), sodium hydroxide, sodium silicate and water employed in the preparation of each mixture depending on the AS concentration and l/s ratio. A total of 270 samples have been produced, resulting from six constituents, three AS concentrations, three l/s ratios (Table 3.1), and five replicates for each mixture.



Figure 5.6 - Pictures of casting (a) and curing (b) phase of specimens of pastes

Table 5.1 - Mix-design of pastes for each AS concentration and l/s ratio

AS concentration	Component	Percentage in mass (%)		
		l/s = 0.6	l/s = 0.5	l/s = 0.4
100%	fines (d<0.063 mm)	31.3	33.3	35.7
	fines (0.063÷0.125 mm)	31.3	33.3	35.7
	sodium hydroxide (NaOH)	7.5	6.7	5.7
	sodium silicate (Na ₂ SiO ₃)	30.0	26.7	22.9
	water (H ₂ O)	0.0	0.0	0.0
75%	fines (d<0.063 mm)	31.3	33.3	35.7
	fines (0.063÷0.125 mm)	31.3	33.3	35.7
	sodium hydroxide (NaOH)	5.6	5.0	4.3
	sodium silicate (Na ₂ SiO ₃)	22.5	20.0	17.1
	water (H ₂ O)	9.4	8.3	7.1
50%	fines (d<0.063 mm)	31.3	33.3	35.7
	fines (0.063÷0.125 mm)	31.3	33.3	35.7
	sodium hydroxide (NaOH)	3.8	3.3	2.9
	sodium silicate (Na ₂ SiO ₃)	15.0	13.3	11.4
	water (H ₂ O)	18.8	16.7	14.3

5.1.3 Viscosity measurement

The viscosity (η) is the ratio between the applied shear stress (τ) and the shear rate (dy/dt), as indicated in Eq. 8 [302].

$$\eta = \frac{\tau}{dy/dt} \quad \text{Eq. 8}$$

The viscosity of fresh mixtures was measured by means of a rotating Brookfield viscometer. The device applies a rotation speed to a spindle immersed in the sample and measures the torque necessary to overcome the viscous resistance exhibited by the material. By changing the dimension of the spindle and the rotation speed, a wider range of viscosities was appreciated [348]. For this reason, results reported in Section 6.1.3 are shown in function of rotational speed (in rpm).

The viscosity was considered as a parameter of the consistency of fresh pastes during the mixing stage. It provided information on the easiness of casting and compacting the mixtures into the moulds. Depending on the consistency of fresh mixtures a different procedure was adopted for transferring pastes into the mould. Powders mixed with AS-100% and low l/s ratios were not fluid at all, thus the fresh material was carefully

placed into the moulds in several layers and adequately compacted. In some cases, especially with $l/s = 0.4$ and AS-100%, the viscosity cannot be even determined since its values were outside the reading ranges of the viscometer equipment. A different approach was adopted for more fluid pastes, which were directly poured into the plastic moulds.

5.1.4 Mechanical properties of hardened products

The effectiveness of alkaline activation of fine particles of CDW was assessed by measuring the compressive and flexural strength of hardened specimens after 28 days of curing at room temperature. The comparison between mechanical results indicated (1) the most reactive constituent and (2) the effect of the l/s ratio and the AS concentration on the development of strength.

For both tests an electro-pneumatic testing machine (MTM Zwick/Roell static press) equipped with a 50 kN load cell (Figure 5.7) was employed. A constant strain rate of 0.25 mm/min and 0.50 mm/min in flexural and compressive configuration, respectively, was applied during tests. After a preload of 5 N for flexural and 10 N for compressive test, both load and vertical displacement were recorded at a frequency of 10 Hz.

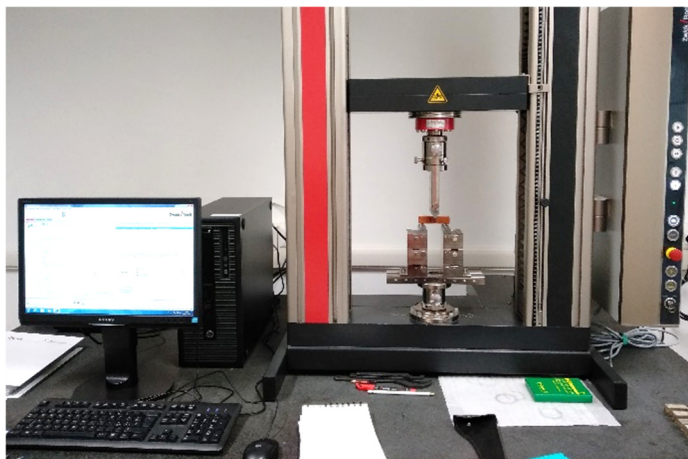


Figure 5.7 - Zwick/Roell testing machine in flexural test configuration

Flexural strength

Flexural strength is a measure of the capability of material to withstand bending forces. In 3-point bending configuration, the upper part of the testing beam (concave face) is in compression state, while tensile stresses occur in the bottom part (convex face). Ceramic materials (as those tested in this investigation) cannot support high tensile stresses, thus

they fail due to the tensile stress of bottom face. For this reason, the maximum tensile stress which exists at the bottom face before failure is usually considered the flexural strength of material [343].

Flexural strength of hardened prismatic specimens was measured in the 3-point bending configuration, according to the scheme reported in Figure 5.8. The load (F) was converted into flexural stress (σ_f) taking into account the configuration geometry and the inertia of cross section, as indicated in Eq. 9.

$$\sigma_f = \frac{3 \cdot F \cdot L}{2 \cdot b \cdot h^2} \quad \text{Eq. 9}$$

In Eq. 9, L is the bottom span (distance between the two bottom supports), while b and h represent the width and the height, respectively, of the cross section of testing specimen. The maximum value of σ_f before failure was considered the flexural strength ($\sigma_{f,\max}$) of the material.

During the test, the displacement at midpoint of the beam was recorded and converted into strain as per the Eq. 10:

$$\varepsilon_f = \frac{6 \cdot \delta \cdot h}{L^2} \cdot 100 \quad \text{Eq. 10}$$

where ε_f is the strain of the beam at midpoint in percentage, δ is the displacement at midpoint, h is the height of cross section, and L is the bottom span.

Before the beam starts to adequately support the load, it exhibits an accommodation phase due to the imperfect geometry of the specimen and, consequently, the imperfect contact between supports and beam itself. For this reason, the initial part of stress-strain curve was corrected and properly linearized for each specimen, as depicted in Figure 5.9.

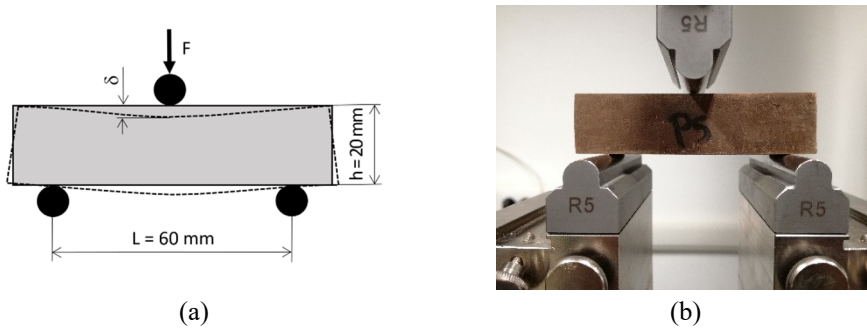


Figure 5.8 - Flexural strength test configuration: (a) scheme, and (b) picture

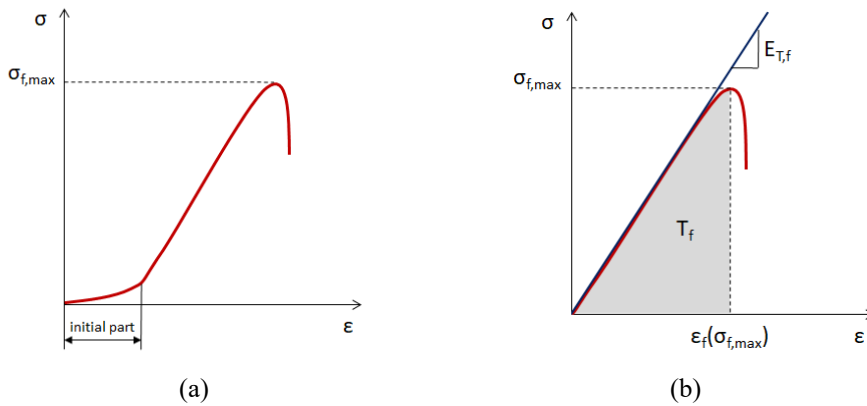


Figure 5.9 - Stress-strain curvilinear relationship during flexural test: (a) raw curve, and (b) corrected curve with the indication of mechanical parameters

The parameters considered for the evaluation of the mechanical properties of prismatic specimens subjected to the flexural strength test are indicated in Figure 5.9 and listed here:

- maximum tensile stress of bottom surface $\sigma_{f,max}$, indicated as flexural strength;
- strain at maximum stress level $\epsilon_f(\sigma_{f,max})$;
- tangent modulus $E_{T,f}$ which is the slope of the tangent segment of the stress-strain curve at the origin [349];
- toughness T_f , which indicates the required energy to break the specimen [349], i.e. the area under the stress-strain curve up to the maximum stress point ($\sigma_{f,max}$).

Compressive strength

Compressive strength test is one of the simplest and most common test for measuring the mechanical performance of a material. During the compression test, it is possible to estimate the maximum amount of compressive load supported before failure.

In this investigation, the two residual parts of the beam derived from flexural test were employed for compressive strength measurement as indicated in the EN 196-1 [350]. The compression load is provided by the plates of the testing machine, which press the specimen up to the failure. A compression device adapter has been employed for applying the load exactly on the surfaces of an ideal cubic specimen of 20 mm side. Figure 5.10 shows a scheme of compression configuration and a picture of compression device adapter. Thanks to the load and displacement recorded during test, the stress-strain curvilinear relationship of the specimen was obtained.

The compressive stress (σ_c) is estimated from the applied load (F) read by the load cell, as indicated in Eq. 11:

$$\sigma_c = \frac{F}{b \cdot d} \quad \text{Eq. 11}$$

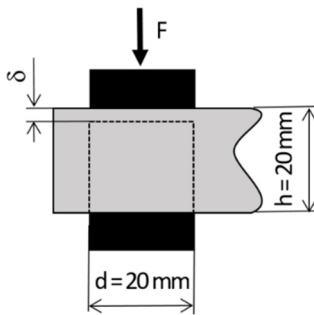
The displacement (δ), detected by the crosshead transducer was converted into compressive strain (ε_c) as suggested in Eq. 12:

$$\varepsilon_c = \frac{\delta}{h} \cdot 100 \quad \text{Eq. 12}$$

The parameters b , d , and h of Eq. 11 and Eq. 12 are the width, the length, and the height of the specimen, respectively.

Identically to flexural test, the raw stress-strain curve was corrected to eliminate the effects of the accommodation of specimen to the testing heads (Figure 5.11). Based on corrected stress-strain curvilinear relationship, the following parameters were taken into account in the analysis of results:

- the maximum stress $\sigma_{c,\max}$ before failure (compressive strength);
- the strain at maximum stress level $\varepsilon_c(\sigma_{c,\max})$;
- the tangent modulus $E_{T,c}$;
- the secant modulus $E_{S,c}$, which is the slope of the segment drawn from the origin to the maximum stress point $\sigma_{c,\max}$ [349];
- the toughness T_c of specimen before failure, i.e. the area under the stress-strain curve up to the maximum stress point.



(a)



(b)

Figure 5.10 - Compression test configuration: (a) scheme, and (b) picture

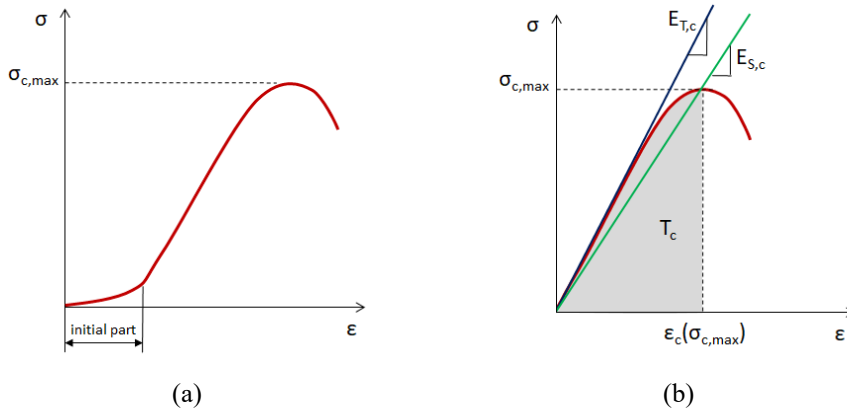


Figure 5.11 - Stress-strain curvilinear relationship during compression test: (a) raw curve, and (b) corrected curve with the indication of mechanical parameters

5.1.5 Environmental assessment

In road constructions, rainwater can infiltrate in base and subbase layers due to pavement damages [351]. CDW aggregates can contain traces of pollutants (anions and heavy metals), which may be dissolved into the percolating water and can contaminate the underlying layers and the groundwater [101], [352]. For this reason, it is important to identify and quantify any released hazardous pollutants through leaching tests. Furthermore, as specified in Section 2.4.2, the EoW concept for converting CDW into recycled aggregates for road applications requires an analytical assessment of pollutants leaching. The environmental compatibility of CDW aggregates was evaluated by comparing the concentrations of pollutants resulting from the leaching processes and the limitations imposed by European and National regulations. The standard EN 12457-2 [353] describes the procedures for determining the leaching of soluble substances from a solid matrix to an aqueous phase.

In this investigation, leaching tests were carried out both on raw fines and alkali-activated final products with the aim of (1) estimating the environmental compatibility of unreacted and alkali-activated products and (2) comparing the leaching before and after the AA process. Raw powders of RC, RA, BT, NA, and UND1 were subjected to leaching test in the same particle size distribution used to prepare specimens, i.e. 50% of passing at 0.063 mm and 50% in the fraction 0.063÷0.125 mm (Section 5.1.2). For limiting the number of tests, only hardened specimens with an AS concentration of 100% and a l/s ratio equal to 0.5 were submitted to leaching test. According to EN 12457-2 [353], hardened products were reduced in particles smaller than 4 mm with a jaw crusher. The testing portion (around 90 g) was mixed with the

leaching agent (distilled water) in proportion 1:10 (i.e. solid liquid ratio equal to 10) for 24 hours. The sample was filtered and the eluate was analysed with a ionic chromatograph and a mass spectrometer to determine the concentration of anions and heavy metals, respectively [20]. Meanwhile, the pH was measured on the same eluate. Results were compared with the limits indicated by the Ministerial Decree of 5th February 1998 [65] and the Council Decision 2003/33/EC [139], reported in Table 5.2.

Table 5.2 - Acceptance criteria for landfilling waste

Parameter	Unit of measurement	Italian Decree 05/02/1998	European Council Decision 2003/33/EC	
		EoW	Inert waste	Non-hazardous waste
Cyanides	(µg/l)	50	-	-
Chlorides	(mg/l)	100	800	15000
Fluorides	(mg/l)	1.5	10	150
Nitrates	(mg/l)	50	-	-
Sulphates	(mg/l)	250	1000	20000
Arsenic	(µg/l)	50	500	2000
Barium	(mg/l)	1	20	100
Beryllium	(µg/l)	10	-	-
Cadmium	(µg/l)	5	40	1000
Cobalt	(µg/l)	250	-	-
Tot. chromium	(µg/l)	50	500	10000
Mercury	(µg/l)	1	10	200
Nickel	(µg/l)	10	400	10000
Lead	(µg/l)	50	500	10000
Copper	(mg/l)	0.05	2	50
Selenium	(µg/l)	10	100	500
Vanadium	(µg/l)	250	-	-
Zinc	(mg/l)	3	4	50
Asbestos	(mg/l)	30	-	-
pH	(-)	5.5÷12	-	-

5.2 Stabilization of CDW aggregates with AA of fines

After the evaluation of the alkali-reactivity of fine particles of CDW, the investigation evolved in the wider scale of stabilization of recycled aggregates as per the AA method (Exp. B1). This research stage involved both the evaluation of physical properties of loose aggregates and mechanical tests on compacted specimens.

This section provides a description of testing methods adopted for characterizing CDW aggregates in their complete particle size distribution and stabilized with the addition of the AS. According to the testing program, the procedures for the determination of density, composition, resistance to fragmentation, and F/T degradation of CDW aggregates are illustrated here. Afterwards, experimental methodologies for compaction and stabilization of aggregates are described, as well as, the methods for measuring mechanical performances of cured specimens.

5.2.1 Physical and mechanical characterization of aggregates

Composition

Due to the heterogeneity of CDW materials [20], [314], the knowledge of the amount of particles of concrete, asphalt, bricks and other constituents is fundamental to categorize the material according to the classification proposed by Jiménez [20] and synthesized in the Table 5.3. The composition of recycled aggregates from CDW depends basically on the waste delivered to the treatment plant [314], [354].

The composition in terms of percentage of constituents was determined on a representative sample of 20.0 kg. The compositional analysis was performed on the 10÷14 mm size fraction by visually identifying the origin of each particle. According to the main constituents of CDW materials, four classes were considered: RC, RA, BT, and NA. The composition percentage of each class was calculated by dividing the mass of that class with the total mass of the investigated sample.

Table 5.3 - Classification of CDW according to Jiménez [20]

RCA ¹	RMA ²	RMCA ³	Unclassified CDW
RC+NA≥90%	RC+RA+NA≥70%	RC+RA+NA≤70%	-
BT≤10%	BT≤30%	BT≥30%	-
RA≤5%	RA≤15%	RA≤15%	-
IMP ⁴ ≤1.7%	IMP ⁴ ≤3.0%	IMP ⁴ ≤3.0%	IMP ⁴ ≥3.0%

Notes: ⁽¹⁾ Recycled concrete aggregates

⁽²⁾ Recycled mixed aggregates

⁽³⁾ Recycled mixed ceramic aggregates

⁽⁴⁾ Impurities such as floating particles, gypsum, wood, glass, plastic, metals

Density and water absorption

The density and water absorption of CDW aggregates were determined according to the EN 1097-6 [355]. The particle density (γ_p) is the ratio between mass and volume (evaluated with the pycnometer method). The following Eq. 13 was adopted for the estimation of γ_p in kg/m³:

$$\gamma_p = \frac{m_2 - m_1}{V - \left(\frac{m_3 - m_2}{\gamma_{w, \text{test}} \cdot 10^{-6}} \right)} \cdot 10^6 \quad \text{Eq. 13}$$

where,

- m_1 is the mass of the pycnometer and the stopper (in grams);
- m_2 is the mass of the pycnometer containing the aggregates and the stopper (in grams);
- m_3 is the mass of the pycnometer containing the sample, the water and the stopper (in grams);
- V indicates the volume of the pycnometer (in mm³);
- $\gamma_{w, \text{test}}$ is the density of water at testing temperature (in kg/m³).

The particle density was determined for separated components (RC, RA, BT, and NA) and undivided materials (CDW_{meas}). In the first case, grains were in the size 10÷14 mm, while the undivided sample was reconstructed according to the size distribution indicated in Section 4.1. The water absorption was measured only on coarse aggregates (10÷14 mm) of RC, RA, BT, and NA. This parameter is usually considered pivotal in the mix-design of concrete [19], while less importance is given to it when the aggregate is used as granular material for road pavement. However, it provides some evidences, which can be useful for justifying the F/T resistance of aggregates. The water absorption was determined according to the procedure reported in the EN 1097-6 [355], through the difference between the mass of saturated surface-dry aggregates (m_{SSD}) and the mass of dry aggregates (m_D). Eq. 14 reports the formulation for determining the percentage of water absorption (w_a).

$$w_a = \frac{m_{SSD} - m_D}{m_D} \cdot 100 \quad \text{Eq. 14}$$

Resistance to fragmentation

The mechanical quality of coarse aggregates is traditionally evaluated through the fragmentation resistance. The laboratory test simulates, through the Los Angeles (LA) apparatus, the degradation actions of impact and abrasion which aggregates experience

during mixing and implementation stages [302]. The Los Angeles degradation test was performed on 10÷14 mm aggregates separated in RC, RA, BT, NA. An additional sample containing all constituents in the proportions reported in Section 6.2.1 was investigated as well. Before the test, samples were washed to remove residual fine particles, dried at 105°C for 24 h and, finally, cooled down to room temperature. According to the EN 1097-2 [356], the testing samples of 5.0 kg were subjected to degradation actions generated by 500 rotations of LA drum and 11 spherical steel balls added. The resistance to fragmentation was expressed by the LA coefficient (in %) as reported in the following Eq. 15, in which m_0 is the initial mass of the sample, and $m_{1.6\text{mm}}$ is the mass retained on the 1.6 mm sieve after test.

$$LA = \frac{m_0 - m_{1.6\text{mm}}}{m_0} \cdot 100 \quad \text{Eq. 15}$$

For comparison purposes, LA coefficient was determined also on a sample of natural granular material (NGM) in the same size range 10÷14 mm.

Resistance to freezing and thawing actions

When temperatures below zero are expected, the resistance of aggregates to freezing and thawing (F/T) actions is usually evaluated [23]. Granular materials subjected to F/T cycles experience the negative effects of volume increment caused by the freezing of water in the mixtures. This volume expansion creates internal stresses that, if repeated in time, may lead to the breakdown of grains. Several factors can affect the F/T resistance, such as the strength of particles, the number of permeable pores, and their dimensions [23]. According to the EN 1397-1 [357], the frost degradation is reproduced at laboratory scale on saturated specimens of loose particles submitted to 10 F/T cycles.

The detrimental effect of F/T cycles can be evaluated in terms of mass loss (ML) according to Eq. 16, in which m_0 is the mass of initial sample and $m_{5\text{mm}}$ is the mass retained on the 5.0 mm sieve after test.

$$ML = \frac{m_0 - m_{5\text{mm}}}{m_0} \cdot 100 \quad \text{Eq. 16}$$

In the present investigation, samples of different constituents (RC, RA, BT, NA) and an undivided sample (CDW_{meas}) in the size distribution 10÷14 mm, underwent to 8 thermal cycles from +25°C to -18°C. Contrary to the EN 1367-1 [357], each F/T cycle lasted 48 hours instead of 24 hours due to the impossibility of following the cooling path imposed by the standard and maintaining at least 4 hours the sample at -18°C in a 24-hour cycle. The temperature was monitored through a thermal sensor placed in the bucket containing

the aggregate to check its evolution during time. The progression of temperature with the F/T cycles is reported in Figure 5.12. After the application of 8 F/T cycles, the ML was determined. Moreover, all samples were submitted to Los Angeles test for determining the LA coefficient after the thermal degradation ($LA_{8F/T}$). The variation of this parameter before and after the F/T treatment provided additional information on the effect of frost actions on the strength of grains.

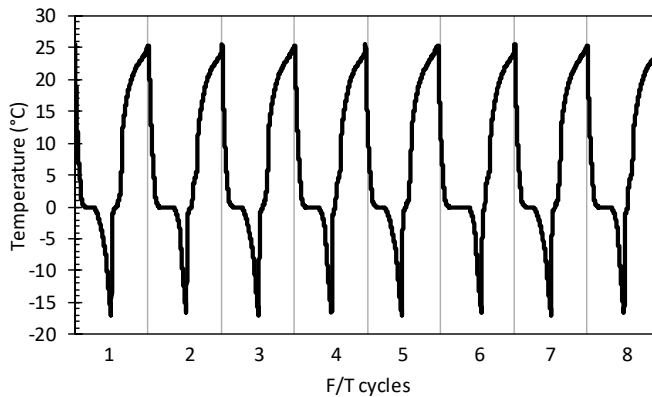


Figure 5.12 - Example of measured temperature evolution during 8 F/T cycles

5.2.2 Proctor compaction test

The compaction of unbound granular materials is the simplest way for improving their bearing capacity. It is reached through the physical densification of particles by an applied force that facilitates the removal of air voids in the material [358]. The addition of water lubricates particles and promotes their rearrangement into a denser structure. Although impact compaction has been demonstrated to be not appropriate for granular materials, Proctor compaction is frequently used to estimate the optimum moisture content ($w_{w,opt}$) and the maximum dry density ($\gamma_{d,max}$) [23], [359]. In Exp. B1, the compaction analysis was performed as per the Proctor method, according to EN 13286-2 [360].

Considering that the AS was added to the CDW material as liquid phase in place of water, two different liquid contents were defined:

- the AS content (w_{AS}), which is the amount of the AS added to the mixture;
- the moisture content (w_w), which is the effective quantity of H_2O in the mixture.

The amount of H_2O in the AS depends upon its concentration (Section 4.3). In case of totally concentrated solution (AS-100%), 61% of total mass was water, while the content

of H₂O increased to 80% in the 50% concentrated solution (AS-50%). Both w_{AS} and w_w were taken into account for data analysis, but only the w_w was considered as controlling variable during Proctor test. Conversely, w_{AS} was taken into account in the estimation of dry density (γ_d) since it reasonably represents the real amount of liquid phase which affects effectively the packing of particles during compaction. The γ_d was derived from the wet density (γ_{wet}) as indicated in following Eq. 17:

$$\gamma_d = \frac{\gamma_{wet}}{\left(\frac{w_{AS}}{100} + 1 \right)} \quad \text{Eq. 17}$$

The Proctor test, as per the EN 13286-2 [360], requires to compact a specimen into a mould of given dimensions with the impact action of a free-falling hammer. When the same compaction process is repeated for five different w_w , the relationship between the dry density and the amount of water or liquid phase is obtained. According to the modified Proctor compaction mode, specimens were compacted into 5 layers with 56 blows of the 4.5 kg hammer falling from a height of 0.457 m (Figure 5.13).

The Proctor test was performed on mixtures of CDW aggregates and AS. Considering that the viscosity of the liquid activator (Section 4.3) could affect the material compaction, a specific Proctor study was carried out for each AS concentration (100%, 50%, 0%). As mentioned in Section 4.1, specimens destined to mechanical tests were prepared with the same particle size distribution (Figure 4.1) to exclude any effect of this variable in data analysis. Accordingly, all specimens compacted with the Proctor method were reconstructed considering the same reference distribution.

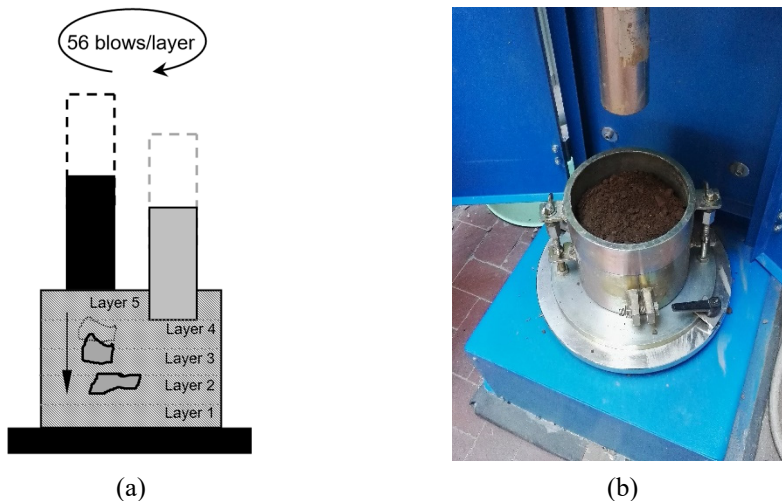


Figure 5.13 - Proctor compaction method: (a) scheme, and (b) picture

5.2.3 Compaction of specimens

Mechanical tests were carried out on specimens of different dimensions. In case of resilient modulus (RM) and unconfined compression strength (UCS) tests, slim specimens of 100 mm in diameter and 200 mm in height were produced, while squat cylinder of 100 mm in diameter and 100 mm in height were prepared for investigating the indirect tensile strength (ITS). In both cases, specimens were compacted by means of the gyratory shear compactor (GSC). This compaction method was found more simulative of field compaction by rollers [361]. GSC was successfully used alternatively to Proctor procedure for compacting specimens of both unbound and stabilized granular materials [362], [363], [364], [365].

In the present investigation, CDW-AS mixtures were subjected to a vertical pressure of 600 kPa and a shear stress induced by the rotation of mould around an axis inclined by 1.25° with respect to the vertical. The revolution speed was set equal to 0.5 gyration per second, as indicated in the scheme of Figure 5.14. Cylindrical specimens were compacted into four (in case of cylinders of 200 mm in height) or two (cylinders of 100 mm in height) layers of equal thickness. The amount of loose wet material (dry granular material mixed with the liquid phase) introduced into the mould was estimated according to Eq. 18:

$$(m_w)_i = V \cdot \gamma_{d,targ} \cdot \left(1 + \frac{w_{AS}}{100}\right) \cdot \frac{h_{f,i}}{h_{tot}} \quad \text{Eq. 18}$$

where, the mass of wet material for the formation of the layer i is indicated with $(m_w)_i$, V is the final volume of the cylindrical specimens ($1.57 \cdot 10^{-3} \text{ m}^3$ for specimens with height 200 mm and $0.79 \cdot 10^{-3} \text{ m}^3$ in case of specimens with height equal to 100 mm), $\gamma_{d,targ}$ is the target dry density of material, w_{AS} is the amount of liquid phase in the sample, $h_{f,i}$ represents the expected height of layer i after its compaction (fixed equal to 50 mm), and h_{tot} is the final height of sample (200 mm or 100 mm depending on the test).

During compaction, the evolution of height of the layer i was recorded to determine the degree of compaction $C_{n,i}$ at each gyration n :

$$C_{n,i} = 100 \cdot \frac{\gamma_{d,i} \cdot h_{f,i}}{\gamma_p \cdot h_{n,i}} \quad \text{Eq. 19}$$

In Eq. 19, $\gamma_{d,i}$ is the dry density of the i layer at the end of its compaction [366], $h_{f,i}$ represents the final height of the layer i , γ_p is the particle density determined as per the pycnometer method (Section 5.2.1), and $h_{n,i}$ is the height of the layer i at a generic (n) gyration.

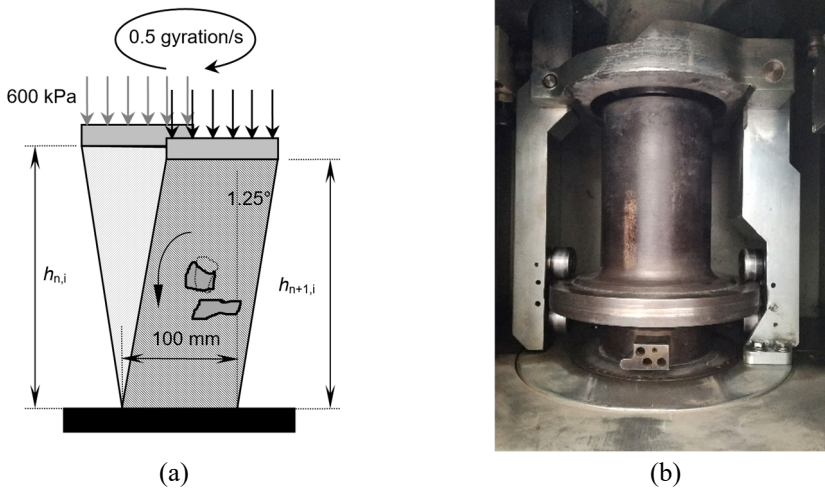


Figure 5.14 - Compaction of specimens as per the gyratory method: (a) scheme, and (b) picture

The evolution of C_n in function of the logarithm of the number of gyration is linear, as shown in Figure 5.15 and Eq. 20. The degree of compaction at the first gyration is the self-compaction (C_1), while the slope of the compaction line indicates the propensity of the material to be compacted, and it is generally known as workability (k_g). The average of the four or two C_1 and k_g values corresponding to each layer, was considered as the self-compaction and workability of the entire sample.

$$C_n = C_1 + k_g \cdot \log(n) \quad \text{Eq. 20}$$

After compaction, specimens were demoulded from the GSC mould, placed into a splitting plastic container and wrapper in a cellophane film to prevent any moisture loss. The curing phase took place in a chamber at room temperature ($20 \pm 25^\circ\text{C}$) and at a RH always higher than 90%.

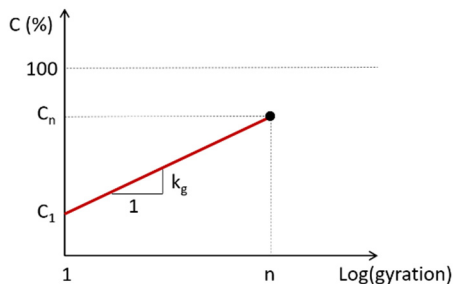


Figure 5.15 - Compaction curve as a result of gyratory compaction

5.2.4 Mechanical properties of stabilized mixtures

Table 5.1 summarizes the number of specimens submitted to each mechanical test of Exp. B1, considering different AS concentrations, curing times, and water contents.

Table 5.4 - Synthesis of tests performed during Exp. B1

AS concentration	Curing	Water content	Specimen 200 x 100 mm		Specimen 100 x 100 mm
			RLT	UCS ¹	ITS
AS-0%	7 days	W _{w,opt} -2%	1	2	2
		W _{w,opt}	1	2	2
		W _{w,opt} +2%	1	2	2
	28 days	W _{w,opt} -2%	1	2	2
		W _{w,opt}	1	2	2
		W _{w,opt} +2%	1	2	2
	60 days	W _{w,opt} -2%	1	2	2
		W _{w,opt}	1	2	2
		W _{w,opt} +2%	1	2	2
AS-50%	7 days	W _{w,opt} -2%	1	2	2
		W _{w,opt}	1	2	2
		W _{w,opt} +2%	1	2	2
	28 days	W _{w,opt} -2%	1	2	2
		W _{w,opt}	1	2	2
		W _{w,opt} +2%	1	2	2
	60 days	W _{w,opt} -2%	1	2	2
		W _{w,opt}	1	2	2
		W _{w,opt} +2%	1	2	2
AS-100%	7 days	W _{w,opt} -2%	1	2	2
		W _{w,opt}	1	2	2
		W _{w,opt} +2%	1	2	2
	28 days	W _{w,opt} -2%	1	2	2
		W _{w,opt}	1	2	2
		W _{w,opt} +2%	1	2	2
	60 days	W _{w,opt} -2%	1	2	2
		W _{w,opt}	1	2	2
		W _{w,opt} +2%	1	2	2

Note: ⁽¹⁾ one of the two specimens submitted to UCS test was previously subjected to RLT test

Repeated load triaxial (RLT) test is regarded the most representative configuration of the stress state induced by traffic loading on the material [358]. Strength tests, in UCS and ITS configurations, provide values of maximum stress that the material can support before failure. They are less simulative of the typical in-field stress conditions of base and subbase layers of road pavements. However, these parameters allow to compare the behaviour of different mixtures in relation to literature results.

Repeated load triaxial test

RTL tests on compacted granular materials were carried out for determining the resilient modulus (RM). This parameter is fundamental in the design of road pavements, since it indicates the (non-linear) elastic behaviour of unbound and/or stabilized layers. The RM is the ratio between the applied replicated deviator stress (σ_d) and the resilient (or recoverable) strain in the principal direction ($\epsilon_{1,r}$) [367]:

$$RM = \frac{\sigma_d}{\epsilon_{1,r}} = \frac{\sigma_1 - \sigma_3}{\epsilon_{1,r}} \quad \text{Eq. 21}$$

The deviatoric stress (σ_d) in Eq. 21 is the difference between the major principal stress (σ_1) and the minor principal stress (σ_3).

Under dynamic loads, granular materials exhibit an elastoplastic response. In the first loading cycles, some permanent strains (ϵ_p) occur due to the slipping of particles and changes in density. After a great number of repetitions, ϵ_p reaches a constant value and the deformation is completely recoverable [143]. Figure 5.16 shows the stress and strain response in time during the RM test.

The RLT test was performed by means of a servo-pneumatic testing machine (Cooper NU-10) equipped with a triaxial cell able to accommodate specimens of 100 mm in diameter and 200 mm in height. Figure 5.17 reports the scheme of the loading configuration during RLT test and a picture of the testing apparatus. The axial load was provided by a servo-pneumatic actuator capable of applying repeated cycles of haversine-shaped pulses. The applied load was checked by a 10-kN loading cell located between the actuator and the triaxial chamber. Compressed air was pumped into the triaxial cell to provide the confining pressure. The axial strain was measured by two linear variable differential transformers (LVDT), fixed to opposite sides of the piston rod outside the triaxial chamber.

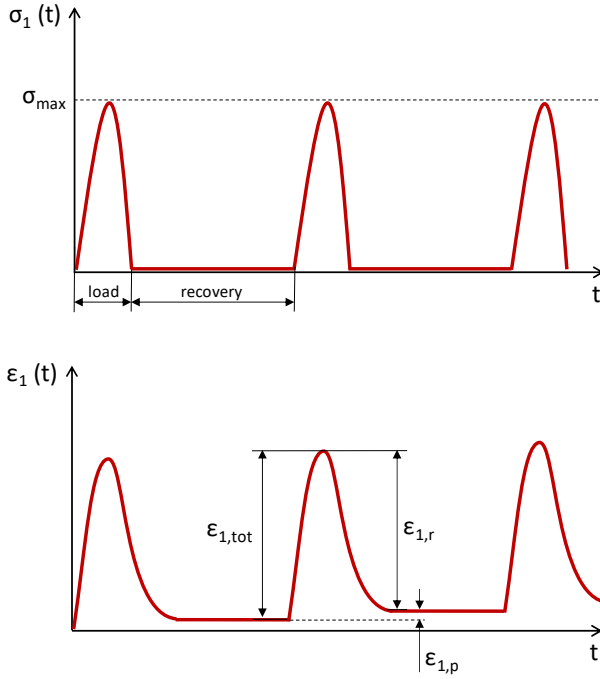
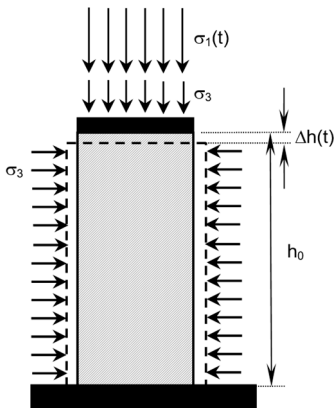


Figure 5.16 - Stress and strain response in time during RM test ($\epsilon_{1,p}$ indicates the vertical permanent strain)



(a)



(b)

Figure 5.17 - RLT test. In (a), testing configuration is shown in which $\sigma_1(t)$ is the principal stress in function of time, σ_3 is the confining pressure, h_0 is the initial height of specimen, and $\Delta h(t)$ is the recoverable displacement variable with time. In (b), a picture of the triaxial apparatus and servo-pneumatic testing machine is reported

Since the RM is strongly dependent on the stress state [368], the AASHTO T-307 standard [369] envisages to perform the RLT test according to fifteen loading sequences, with an increasing deviatoric and confining stress level. For each sequence, the specimen was subjected to 100 loading pulses (characterized by a total duration of 1 second, in which there are 0.1 s of haversine load pulse and 0.9 s of resting time) and only the last five were recoded and employed for the RM estimation. RLT tests were carried out following the base/subbase testing protocol suggested by AASHTO T-307 [369] and applying a preconditioning sequence of 500 loading pulses (characterized by a maximum axial stress and a confining pressure of 103.4 kPa) before the start of the first loading sequence. The purpose of the preconditioning sequence was (1) the settlement of the specimen and (2) the minimization of any misalignment between the sample and the loading plates.

The RM values of the fifteen loading sequences were fitted with the generalized stress-dependent non-linear model of the Mechanistic Empirical Pavement Design Guide (MEPDG) [370]:

$$RM = k_1 \cdot p_a \cdot \left(\frac{\theta}{p_a} \right)^{k_2} \cdot \left(\frac{\tau_{oct}}{p_a} + 1 \right)^{k_3} \quad \text{Eq. 22}$$

In Eq. 22, θ is the first invariant (i.e. the sum of the three principal stresses, Eq. 23), τ_{oct} is the octahedral shear stress (Eq. 24), p_a indicates the values of the atmospheric pressure (equal to 0.10133 MPa) used to normalize the equation, while k_1 , k_2 , and k_3 are the calibration factors which characterize each material.

$$\theta = \sigma_1 + \sigma_2 + \sigma_3 \quad \text{Eq. 23}$$

$$\tau_{oct} = \frac{1}{3} \cdot \sqrt{(\sigma_1 - \sigma_2)^2 + (\sigma_1 - \sigma_3)^2 + (\sigma_2 - \sigma_3)^2} \quad \text{Eq. 24}$$

Regression parameters were obtained through the least square method, minimizing the differences between measured and estimated data. The quality of modelling was assessed taking into account the standard error ratio (S_e/S_y) and the adjusted determination coefficient (R^2_{adj}).

S_e is the standard error of the estimate determined as:

$$S_e = \sqrt{\frac{\sum_{i=1}^n (y_i - x_i)^2}{n - p}} \quad \text{Eq. 25}$$

while S_y is the standard deviation of measures:

$$S_y = \sqrt{\frac{\sum_{i=1}^n (y_i - \bar{y})^2}{n-1}} \quad \text{Eq. 26}$$

In Eq. 25 and Eq. 26, y_i and x_i indicate the measured and predicted values, \bar{y} is the mean of measured values, while n and p are the number of observations and the number of parameters respectively.

The R^2_{adj} was estimated as follows (Eq. 27):

$$R^2_{\text{adj}} = 1 - (S_e/S_y)^2 \quad \text{Eq. 27}$$

A good accuracy of the prediction model is characterized by small values of S_e/S_y and values of R^2_{adj} close to the unity [371], [372].

Unconfined compression strength test

The unconfined compression strength (UCS) test is a simple and fast testing method for determining the maximum stress of a material before failure. In this test, a slim cylindrical specimen (100 mm in diameter and 200 mm in height) is progressively compressed between two loading plates (Figure 5.18.a). The specimen is free to deform radially since there is not lateral confinement. The maximum stress before failure is the UCS, which is estimated with Eq. 28 (F_{max} is the maximum applied load, and D indicates the diameter of specimen).

$$\text{UCS} = \frac{4 \cdot F_{\text{max}}}{\pi \cdot D^2} \quad \text{Eq. 28}$$

The UCS test was performed by means of an electro-pneumatic loading machine (Tecnotest T-052/E), equipped with a 50-kN loading cell (Figure 5.18.b). For each test, the displacement rate was maintained constant in time and equal to 0.50 mm per minute.



(a)

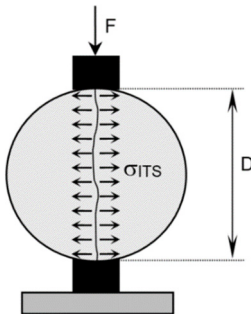


(b)

Figure 5.18 - UCS test: (a) scheme of testing configuration, (b) picture of the testing machine

Indirect tensile strength test

The indirect tensile strength (ITS) test is commonly carried out for determining the tensile properties of stabilized materials [373]. The tensile stress is generated by a load which compresses a cylindrical specimen along its vertical diametrical plane (Figure 5.19.a). This configuration induces a tensile stress perpendicularly to the direction of load application until the failure of specimen [374].



(a)



(b)

Figure 5.19 - ITS test: (a) scheme of testing configuration, (b) picture of the ITS device

The ITS is obtained from the failure load according to the Eq. 29 [375], in which F_{\max} is the maximum load supported from the specimen, while h and D represent the height and the diameter of the cylindrical specimen.

$$ITS = \frac{2 \cdot F_{\max}}{\pi \cdot h \cdot D} \quad \text{Eq. 29}$$

The ITS test was performed with the same loading machine employed in UCS tests, equipped with a specific device able to apply the load as shown in Figure 5.19. Also in this case, the testing machine applied a constant rate of displacement equal to 0.50 mm per minute to each specimen.

5.2.5 FESEM and EDS analysis

Scanning electron microscopy (SEM) is widely used for investigating the microstructure of materials [376]. SEM analysis takes advantages of the principle of “secondary” electron emission explained in Section 5.1.1. A finely focused electron beam is swept in a raster across the surface of the sample to create the image pixel by pixel. As a consequence of electron bombardment, secondary electrons are emitted with intensities, wavelengths, and directions depending on the surface topography [377]. These electrons as well as backscattered electrons are collected by detectors which convert signals into images. The variation of emitted signals from one location to another generates contrast in the image resulting in the microscopic morphology of the sample [378]. The field emission scanning electron microscopy (FESEM) is an evolution of the traditional SEM. The two substantial differences between these techniques are the electron generation method and the detectors system. Thanks to an extremely focused and low-energy electron beam and to in-lens detectors, the final resolution of FESEM is considerably higher than the SEM [379].

After mechanical tests, small fragments of 60-day cured broken specimens were submitted to FESEM analysis, with the aim of observing their microstructure and morphology. Microscopic observations were carried out on two set of specimens

- those containing $w_{w,opt}$ and the three different AS concentrations;
- those containing AS-100% the two variations of w_w , ($w_{w,opt}-2\%$, and $w_{w,opt}+2\%$).

The first set provided information on the compactness of the structure and the presence of porosity [380] as a consequence of the AS concentration, while the second allowed to appreciate differences in the microstructure topography due to different amount of binding phase (induced by the different quantity of AS).

In order to ensure electrical conductivity, fragments were fixed to a stub with carbon-conductive tab. Moreover, they were exposed to a chromium metallization to create a conductive thin film coating indispensable for electron microscopy testing.

During the observation of particles of CDW-AS-100% mixtures, some energy-dispersive spectroscopy (EDS) analyses were also performed, directing the electrons beam towards both portions of aggregates and surrounding coatings. The EDS analysis coupled with FESEM provided the elemental composition of a specific zone in the investigated sample. EDS technique is analogous to the XRF analysis (Section 5.1.1): (1) a localized point of the sample is bombarded with a focused beam of electrons, (2) some electrons are ejected from excited atoms, (3) the movement of electrons from higher orbitals fills vacancies just created, (5) to balance the energy between two states, an x-ray radiation is emitted (called “secondary” radiation), (5) energy of secondary radiation (characteristic of each element) is collected from a detector, which identifies and quantifies the chemical composition of the examined portion of the sample [376].

The EDS analysis coupled with FESEM observation had the objective of associating a chemical analysis to the microstructural characterization. Accordingly, the chemical demonstration of geopolymerization occurrence could be provided by the difference between the stoichiometry of coated and uncoated portions of the observed sample. Figure 5.20 shows a picture of the Oxford instruments-Zeiss FESEM equipment employed in the microstructure analysis and a screenshot of the vacuum chamber containing the sample.



(a)



(b)

Figure 5.20 - EDS-FESEM analysis: (a) picture of the electron microscope, (b) picture of vacuum chamber containing the sample

5.3 Durability of stabilized CDW-AS mixtures

As mentioned in Section 3.2.3, the sensitivity to degradation of granular materials for road applications is commonly evaluated through Los Angeles and freeze and thaw (F/T) tests on loose materials. In these cases, the degradation is assessed through the comparison of LA and F/T indexes with those obtained on materials of proven behaviour in the field. These tests do not reproduce or simulate field state conditions and weathering processes. The results are used for granular material qualification and acceptance, in agreement with international, and Italian as well, technical specifications [313].

Hence, when simulative conditions are considered as a focus point of the investigation, granular materials need to be evaluated in typical compacted and partially saturated states like those occurring in the field. The objective of Exp. B2 was the assessment of F/T degradation on compacted specimens of CDW aggregates stabilized with the addition of AS-100%. The detrimental effect of frost action was evaluated in terms of variation of resilient behaviour and mechanical strengths (UCS and ITS) in comparison to reference specimens which were not submitted to F/T cycles. The same degradation process was applied to a NGM stabilized with 3% of OPC for comparison purposes. This section provides detailed information concerning (1) the optimization of CDW mixtures in terms of quantity of AS and (2) the simulation of F/T degradation at laboratory scale.

5.3.1 Compaction and curing of specimens

In contrast to the approach adopted in the Exp. B1, the compaction study in Exp. B2 did not involve the Proctor test. The gyratory compaction method was considered for estimating the optimal quantity of liquid phase to add in the CDW aggregate mixture. The optimal value of AS content ($w_{AS,opt}$) was selected in order to (1) improve the workability (k_g) and (2) reach the highest dry density (γ_d). It is worth remembering that the AS had the dual role of triggering the alkali-activation process of the finest CDW particles and providing enough workability for mixture compaction.

Six specimens were compacted by means of the GSC at the same energy (corresponding to 100 gyrations and 600 kPa of vertical stress), but varying the AS content (w_{AS}) from 8.0 to 13.0%. In Exp. B2, no distinction between the water content (w_w) and the AS content (w_{AS}) was considered since exclusively the totally concentrated AS (AS-100%) was employed. The $w_{AS,opt}$ was estimated through the analysis of the evolution of compaction parameters (C_1 , k_g , C_{100}) and dry density as a function of w_{AS} .

In case of NGM, the percentage of OPC was fixed at 3% on the basis of literature data [302], [334], while the optimal water content ($w_{w,opt}$) was estimated as per the GSC method, compacting three specimens with 6.0%, 6.5%, and 7.0% of water.

After the estimation of the optimal content of AS for CDW aggregates and water for NGM, all cylindrical specimens were compacted according to the GSC procedure already described in Section 5.2.3. In line with Exp. B1, all specimens were prepared considering the same reference gradation curve (Section 4.1) Specimens of 100 mm in diameter and 200 mm in height were produced for RLT and UCS tests, while cylinders of 100 mm in diameter and 100 mm in height were compacted for ITS characterization.

5.3.2 Simulation of freeze and thaw degradation

The detrimental F/T action was simulated by exposing specimens at several cycles of temperature from -18°C to $+25^{\circ}\text{C}$. Each cycle lasted for 48 hours in agreement with the procedure adopted in the preliminary assessment of F/T degradation on loose aggregates in the size fraction $10\div 14$ mm (Section 5.2.1). Three different degradation severity levels were applied: low, medium, and high, corresponding to 4, 8, and 12 F/T cycles, respectively.

The effect of F/T cycles was evaluated after different curing periods, since both alkali-activated and cement-stabilized materials developed mechanical properties over time. This approach is consistent with the experimental investigation of Khoury and Zaman [316] concerning the durability of cement-stabilized aggregates. In case of CDW-AS-100% mixtures, the degradation was applied after 7, 28, 45, and 60 days of curing, according to the scheme of Figure 5.21. For NGM-OPC mixtures, the reference curing times were set equal to 7 and 28 days. After curing, performed at room temperature and $\text{RH} > 90\%$, specimens were placed in a thermal cabin for the F/T exposure.

After compaction, specimens were placed in plastic containers and wrapped with a cellophane film to prevent any moisture exchanges with the environment during curing (Figure 5.22.a) and thermal treatment (Figure 5.22.b).

Two replicates of each testing configuration were considered for UCS and ITS tests analogously to Exp. B1. A total of 64 specimens of CDW aggregates stabilized with AS-100% and 32 specimens of cement-stabilized NGM were prepared for this investigation stage. The effect of F/T degradation was evaluated in terms of variation of strength (UCS and ITS) and stiffness (RM) in comparison with the corresponding values showed by specimens not exposed to the degradation process (indicated as 0 F/T).

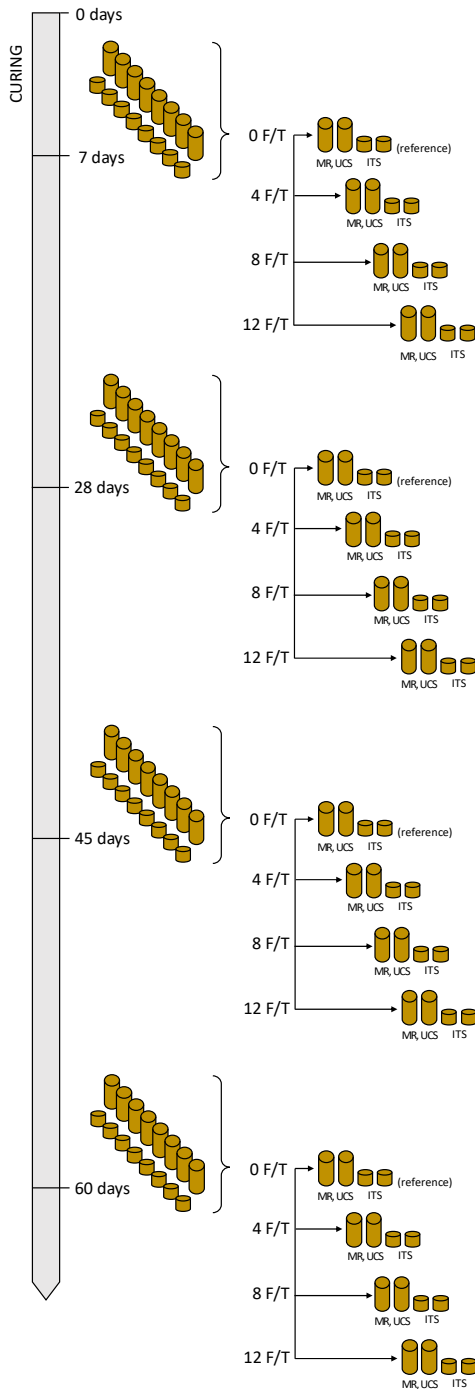


Figure 5.21 - Scheme of testing plan for F/T degradation assessment phase

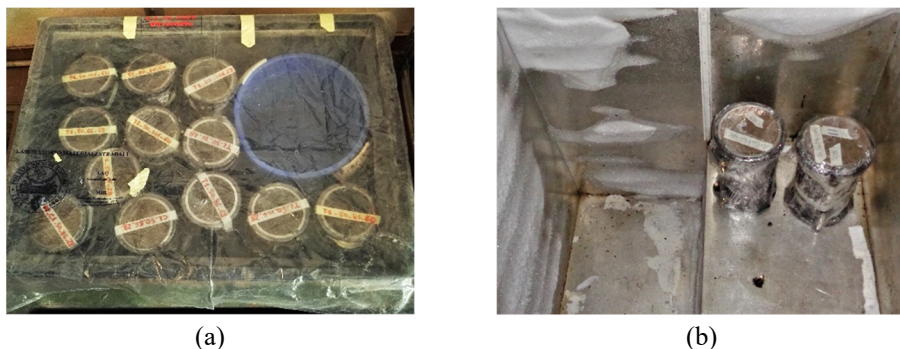


Figure 5.22 - Curing and F/T degradation phases: (a) specimens placed in a curing chamber at room temperature, (b) specimens exposed to freezing

5.4 Environmental compatibility of CDW-AS mixtures

When CDW materials are used as aggregates in road constructions, it is necessary to evaluate their environmental compatibility in terms of pollutants leaching. National and European laws fix the limits of concentrations for these pollutants. Leaching test was performed according to the EN 12457-2 [353] and consistently with the methodology adopted on CDW powders (Exp. A). Samples were collected from broken cylindrical specimens after UCS and ITS tests. The testing portions were preliminary grinded in particles with dimension lower than 4 mm and, successively, submitted to the leaching test.

This test consists in mixing the sample with distilled water in proportion 1:10 for 24 hours and quantifying the concentration of anions and cations released in the eluate. The environmental compatibility was performed on samples of CDW-AS-100% and NGM-OPC mixtures after 28 days of curing and not exposed to F/T. An additional leaching test performed on raw (non-compacted) CDW aggregates allowed to evaluate the effects of AA process on the pollutants leaching behaviour. For these three samples, the concentrations of pollutants in the eluates were compared with the acceptance limits of the Ministerial Decree of 5th February 1998 [65] and the Council Decision 2003/33/EC [139], previously reported in Table 5.2.

6. RESULTS AND DISCUSSION

Results of the experimental investigation are presented and discussed in this Chapter. This is divided in three main sections (Exp. A, Exp. B1, and Exp. B2) according to the experimental program described in Chapter 3. All results obtained from more than one repetition are grouped and averaged. For each experiment, the measured parameters have been extensively compared with literature.

6.1 Alkali-activation of CDW fines

The results of the alkali-reactivity of powders derived from CDW are reported here. The experimental investigation dealt with (1) the preliminary physical and chemical characterization of raw powders, (2) the measurement of viscosity of fresh mixtures containing powders and AS, and (3) the flexural and compressive strengths of cured specimens. Lastly, the results of leaching tests are reported and discussed as well.

6.1.1 Physical characterization of fines

The physical analysis of CDW fines, differentiated into the constituents RC, RA, BT, NA, UND1, and UND2, involved the determination of particles size distribution, density and Rigden voids. Figure 6.1 and Figure 6.2 illustrate the particle size distribution curves of the two grain classes $0.063 < d < 0.125$ mm and $d < 0.063$ mm, respectively. All fines, in the fraction $0.063 \div 0.125$ mm, had a similar particle size distribution. The mean diameter of the distribution, expressed by the particle size corresponding to 50% of cumulative frequency (d_{50}), was around 0.100 mm. A marked increment of cumulative frequency after 0.063 mm is noticeable, proving the goodness of the sieving operations carried out for all CDW constituents.

In the finer size fraction ($d < 0.063$ mm), differences between the gradation of each constituent are more evident. Considering the value of d_{50} , UND1, RC, and NA constituents were characterized by the smallest particle size (around 0.018 mm), followed by BT (0.022 mm), and UND2 (0.024 mm). RA showed a clearly coarser size distribution in the whole investigated dimensional range, with a value of d_{50} equal to

0.036 mm. It suggests that the milling process was less effective probably due to the presence of the bitumen film which partially contrasted the grinding action. It is also worth noting the progressive reduction of particle sizes corresponding to 90% of cumulative frequency (d_{90}) from the larger particles of RA to the finer of RC and UND1 constituents.

In Figure 6.3, the grain size distributions of fines with $d < 0.125$ mm are reported. They were obtained combining the results of the two different size fractions previously described. Similar considerations can be pointed out, with the finer gradation shown by UND1, RC, and NA constituents.

Table 6.1 reports the values of particle density ($\gamma_{p,\text{fine}}$), bulk density ($\gamma_{b,\text{fine}}$) and Rigden voids (v_r) of CDW fines separated in the two size fractions ($0.063 < d < 0.125$ mm and $d < 0.063$ mm). The values of $\gamma_{p,\text{fine}}$ were obtained by the average of two pycnometer measurements.

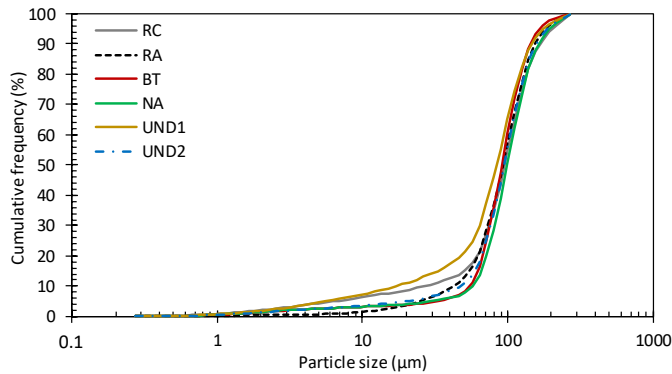


Figure 6.1 - Particle size distribution of CDW fines in the fraction 0.063-0.125 mm

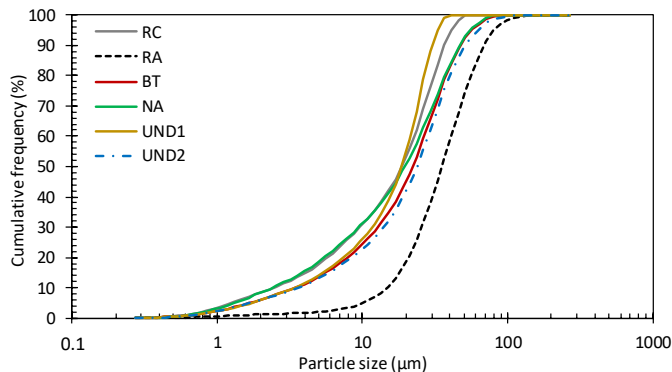


Figure 6.2 - Particle size distribution of CDW fines with $d < 0.063$ mm

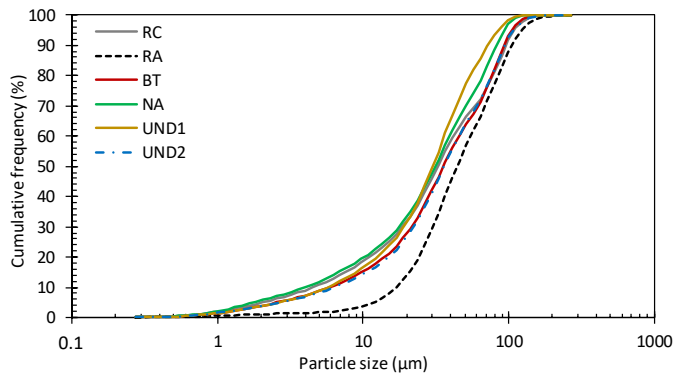


Figure 6.3 - Particle size distribution of CDW fines with $d < 0.125$ mm

Generally, $\gamma_{p,\text{fine}}$ resulted slightly higher for the finest fraction, with the exception of RC and UND1 samples. BT and NA powders were characterized by the highest values of particle density, while the lowest one was exhibited by RA. The bulk density and the Rigden voids provided indications on the propensity of packing of the grains. The values of $\gamma_{b,\text{fine}}$ were in the range $1940 \div 2025 \text{ kg/m}^3$, while Rigden porosity was around 26% for all constituents, with the exception of RA sample. The latter constituent was characterized by a lower value of v_r (15.2% in the $0.063 \div 0.125$ mm fraction and 20.0% in the finer fraction) due to the presence of viscoelastic particles of bitumen which tended to partially close voids during compaction. The greater values of voids recorded in RC, BT, NA, UND1, and UND2 samples, could be explained by the higher quantities of very fine particles, which left a higher volume of small spaces between grains.

Table 6.1 - Particle density ($\gamma_{p,\text{fine}}$), bulk density ($\gamma_{b,\text{fine}}$) and Rigden voids (v_r) of CDW fines separated in constituents and size fractions

Constituent	Particle size	$\gamma_{p,\text{fine}}$ (kg/m ³)	$\gamma_{b,\text{fine}}$ (kg/m ³)	v_r (%)
RC	0.063 ÷ 0.125	2687	1953	27.3
	<0.063	2580	1945	24.6
RA	0.063 ÷ 0.125	2347	1990	15.2
	<0.063	2424	1940	20.0
BT	0.063 ÷ 0.125	2722	1946	28.5
	<0.063	2763	2010	27.3
NA	0.063 ÷ 0.125	2710	2025	25.3
	<0.063	2726	1987	27.1
UND1	0.063 ÷ 0.125	2673	1963	26.5
	<0.063	2640	1963	25.6
UND2	0.063 ÷ 0.125	2617	1979	24.1
	<0.063	2623	1970	24.7

6.1.2 Chemical-mineralogical characterization of fines

The indexed XRD patterns of the investigated constituents are depicted from Figure 6.4 to Figure 6.8. Firstly, it is worth noting that all samples were well crystallized, with very limited presence of amorphous phases. Quartz phase was detected in all analysed samples. It exhibits the main peak (lattice plan 101 and 2θ equal to 26.65°) with a predominant intensity in comparison to other phases. Calcite was also commonly present in all samples, with the highest peaks in RC constituent. It is due (1) to the presence of residual cement paste adhering to aggregate [381] and (2) to carbonation phenomena in the demolished concrete [382], [383]. In RC (Figure 6.4) some magnesium- and silicate-rich phases were also detected, such as enstatite, lizardite, and clinochlore minerals [384]. Traces of gypsum were also found in RC, since this material is sometimes added to cement for regulating the early-stage hydration reactions [385]. Enstatite and clinochlore phases were present in RA and NA constituents as well (Figure 6.5 and Figure 6.7 respectively). In addition to quartz and calcite, RA sample contained serpentine- (antigorite), cyclosilicate- (cordierite), inosilicate- (diopside) and mica-group (muscovite) minerals. Figure 6.6 shows the output pattern of BT sample. Also in this case quartz and calcite were steadily present. Additional aluminosilicate phases were identified in albite (feldspar mineral) and muscovite, in agreement with the results of Angulo et al. [386] and Pacheco-Torgal and Jalali [387]. In BT powders, also hematite and cristobalite minerals were found, both typically present in ceramic materials [30], [387], [388]. Hematite is the primary cause of the characteristic red colour of bricks and tiles.

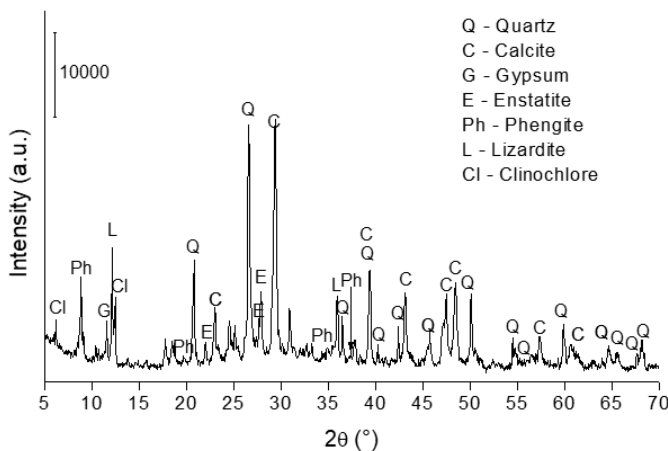


Figure 6.4 - XRD output pattern of RC

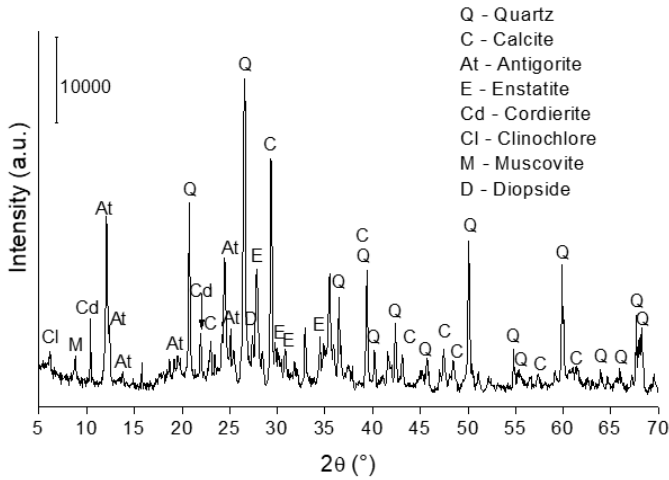


Figure 6.5 - XRD output pattern of RA

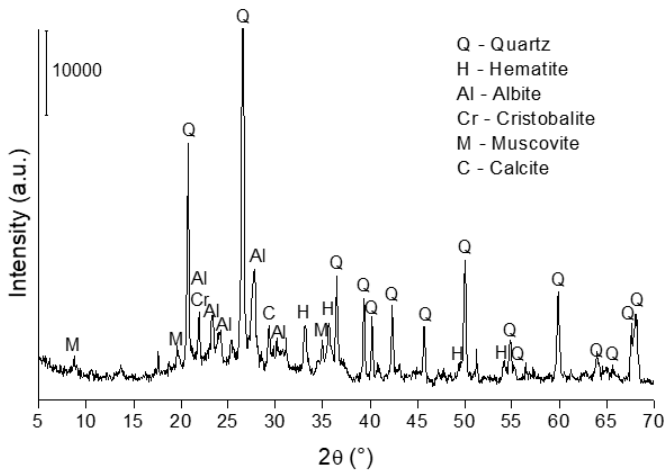


Figure 6.6 - XRD output pattern of BT

In NA samples, typical minerals of West Alpine region were recognized through the indexing of XRD results (albite, lizardite, clinocllore). Detectable amount of other silicates (cordierite, enstatite, diopside and illite) were present in NA, in addition to quartz, as visible in Figure 6.7.

The UND1 sample (Figure 6.8) contained the main minerals found in its constituents (RC, RA, BT, and NA). Some traces of ferrous (gladiusite) and serpentine (antigorite) minerals were also observed in this fraction.

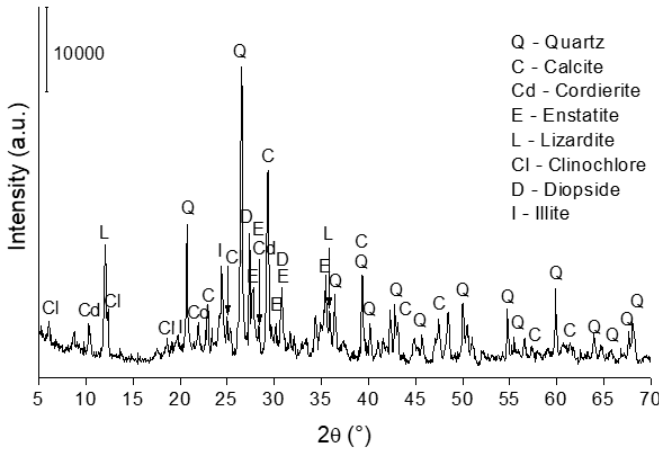


Figure 6.7 - XRD output pattern of NA

Crystalline phases detected from XRD analysis revealed the presence of aluminosilicates in all CDW constituents, in line with XRD outputs of other investigations [30], [389], [390], [391]. These results confirmed the potential of CDW fines to be precursors of alkali-activation processes. In fact, the AA method requires the existence of aluminosilicates for the development of chemical reactions [203]. Moreover, it is interesting to highlight the positive presence of mica-group minerals (muscovite, phengite) in almost all constituents, which suggested the further potential of these materials to undergo alkali-activation. According to Choquette et al. [392], minerals from mica-group are the most reactive among the different aluminosilicate phases.

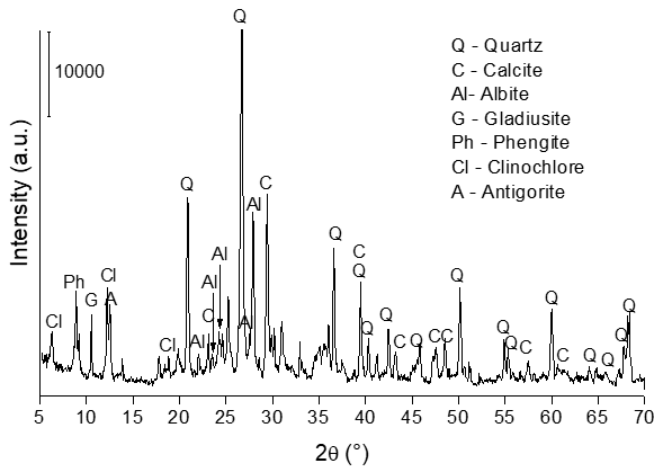


Figure 6.8 - XRD output pattern of UNDI

Table 6.2 summarizes the output of the semi-quantitative phase analysis based on the relative intensity of XRD peaks. Mineral phases, differentiated in aluminosilicates, mica-group minerals, carbonates, and quartz are expressed in percentage of the whole mixture. A significant content of aluminosilicates minerals was found in all fines, thus proving, once again, the feasibility of these products to be chemically activated with alkaline solutions. BT and UND1 fines were characterized by the highest content of aluminosilicates and mica-group phases, while a great amount of carbonate phases was detected in RC, due to the presence of moderately high peaks of calcite (CaCO_3). Looking at the results of UND2, some differences with the UND1 sample are appreciable. It confirmed that, in addition to particles of RC, RA, BT, and NA, other elements were present in UND1, which cannot be recognized and quantified in the size lower than 0.125 mm.

XRF results, reported in Table 6.3, were consistent with the outcomes of XRD indexing analysis. All samples contained a significant abundance of silica (SiO_2) and alumina (Al_2O_3), with the highest quantities in BT and UND1 constituents. The elemental characterization of UND1 was consistent with XRF results reported by Bianchini et al. [393], who compared the chemical and mineralogical properties of different CDW materials. BT powder contained more than 50% of SiO_2 and 10% of Fe_2O_3 . The relevant content of iron justifies the reddish appearance of this ceramic waste [387]. A relevant amount of CaO was detected in all CDW powders and especially in RC (24.8%). It is a consequence of the residual adhered cement and calcium-rich aggregates in concrete waste [382]. CO_2 was always present in significant quantities, apart from BT sample. The abundance of calcium carbonate (1) in natural aggregates and (2) as a result of cement carbonation can be regarded the main causes of CO_2 copiousness. The low content of CO_2 in BT fines is related to the fact that the calcium carbonate decomposes due to the high-temperature treatments of these ceramics [394], [395]. It is worth mentioning that calcium carbonate is typically employed as a melting agent in ceramic materials sintering [396]. Lastly, small percentages of MgO , SO_3 , and K_2O were also found in all constituents.

Table 6.2 - Mineral phases in the CDW fines

Mineral phases	RC	RA	BT	NA	UND1	UND2
Aluminosilicates (%)	23.3	29.7	63.6	30.1	56.8	36.7
Minerals from mica-group (%)	15.2	11.9	30.3	n.d. ¹	22.7	19.1
Carbonates (%)	26.0	13.9	6.1	17.2	11.8	15.8
Quartz (%)	9.1	9.9	22.2	8.5	14.7	12.4

Note: ⁽¹⁾ n.d. = non-detected

Table 6.3 - XRF results on the six CDW fines

Component	mass (%)					
	RC	RA	BT	NA	UND1	UND2
SiO ₂	32.90	36.39	56.40	44.30	42.60	40.70
Al ₂ O ₃	6.31	6.34	18.61	8.41	12.80	8.72
CaO	24.80	4.12	4.14	11.20	11.50	11.80
CO ₂	23.44	38.70	1.20	16.87	15.90	21.28
Fe ₂ O ₃	4.29	3.69	10.40	5.85	6.84	4.20
MgO	4.93	6.92	4.19	10.60	6.00	10.70
SO ₃	1.42	1.22	0.14	0.20	0.59	0.56
K ₂ O	1.08	1.10	3.05	1.43	2.19	1.16
TiO ₂	0.43	0.31	1.25	0.46	0.76	0.41
P ₂ O ₅	0.11	0.09	0.00	0.13	0.35	0.11
MnO	0.19	0.14	0.25	0.30	0.28	0.13
Cr ₂ O ₃	0.00	0.07	0.08	0.12	0.00	0.07
Na ₂ O	0.00	0.82	0.00	0.00	0.00	0.00
NiO	0.03	0.04	0.04	0.06	0.05	0.03
CuO	0.00	0.00	0.00	0.00	0.02	0.00
ZnO	0.00	0.01	0.03	0.00	0.03	0.00
Rb ₂ O	0.00	0.00	0.02	0.01	0.02	0.01
SrO	0.06	0.02	0.03	0.04	0.04	0.02
ZrO ₂	0.01	0.02	0.12	0.02	0.03	0.10
PbO	0.00	0.00	0.05	0.00	0.00	0.00
Total	100.00	100.00	100.00	100.00	100.00	100.00

Table 6.4 compares the elemental composition of CDW fines in terms of SiO₂, Al₂O₃, and CaO content and SiO₂/Al₂O₃ and SiO₂/(Al₂O₃+CaO) ratios with XRF results of precursors successfully submitted to the AA from literature. This comparison allows to understand if the chemical composition of CDW fines is consistent with typical precursors of the AA process. Moreover, some habitual ranges of silica and alumina content (which are a requirement for the AA process) can be identified. It is well known that the presence of Si and Al elements is fundamental for the formation of alkali-activated products [397], since hardening properties of this category of binders involves chemical reactions between aluminosilicate oxides and alkali-polysilicates to form Si-O-Al bonds [225], [297]. Xu and Van Deventer [224] studied 16 alkali-activated minerals characterized by different content of SiO₂ and Al₂O₃ and pointed out that it is not possible to predict qualitatively a specific content of alumina and silica or their combination for a suitable geopolymerization process.

Table 6.4 - Comparison between elemental composition from XRF results of CDW powders and literature, with indication of SiO₂/Al₂O₃ and SiO₂/(Al₂O₃+CaO) ratios

Author	Material	XRF (%)			SiO ₂ /Al ₂ O ₃	SiO ₂ /(Al ₂ O ₃ +CaO)
		SiO ₂	Al ₂ O ₃	CaO		
Data from elemental analysis of Table 6.3	RC	32.9	6.3	24.8	5.2	1.1
	RA	36.4	6.3	4.1	5.8	3.5
	BT	56.4	18.6	4.1	3.0	2.5
	NA	44.3	8.4	11.2	5.3	2.3
	UND1	42.6	12.8	11.5	3.3	1.8
	UND2	40.7	8.7	11.8	4.7	2.0
Allahverdi and Kani [293]	RC	41.2	7.8	20.6	5.3	1.5
	BT	53.4	10.5	24.9	5.1	1.5
Allahverdi and Kani [29]	RC	40	8.6	25.1	4.7	1.2
	BT	58.6	9.1	19.8	6.4	2.0
Gonçalves Rapazote et al. [398]	RC	41.9	1.7	34.2	24.6	1.2
	BT	66.4	21.6	3.1	3.1	2.7
Kioupis et al. [399]	BT	51.3	14.6	6.3	3.5	2.5
Komnitsas [298]	RC	5.8	1.5	65.4	3.9	0.1
	BT	64.2	12.4	8.8	5.2	3.0
Pathak et al. [294]	BT	65.3	13.5	3.3	4.8	3.9
Reig et al. [290]	BT	51.0	16.9	9.9	3.0	1.9
Reig et al. [291]	BT	49.9	16.6	9.7	3.0	1.9
Robayo-Salazar et al. [292]	BT	65.9	20.1	0.7	3.3	3.2
Robayo-Salazar et al. [328]	RC	56.2	10.7	15.4	5.3	2.2
	BT	65.9	20.1	0.7	3.3	3.2
Sun et al. [289]	BT	65.5	21.0	6.0	3.1	2.4
Vasquez et al. [400]	RC	56.2	10.7	15.4	5.3	2.2
Zedan et al. [300]	RC	30.6	1.8	37.5	17.0	0.8
	BT	63.2	16.8	5.2	3.8	2.9
Horpibulsuk et al. [401]	FA ¹	39.2	22.6	11.3	1.7	1.2
Horpibulsuk et al. [402]	FA ¹	47.5	13.1	30.2	3.6	1.1
	WTS ²	67.3	22.5	0.7	3.0	2.9
Komnitsas et al. [403]	LCFS ³	32.7	8.3	3.7	3.9	2.7
Sathonsaowaphak et al. [243]	LBA ⁴	39.3	21.3	16.5	1.8	1.0
Suksiripattanapong et al. [404]	WTS ²	67.3	22.5	0.7	3.0	2.9
Antoni et al. [405]	VM ⁵	56.8	23.3	2.1	2.4	2.2
Ferone et al. [406]	RCS ⁶	49.4	16	8.6	3.1	2.0
Palmero et al. [234]	SM ⁷	36.5	8.8	12.3	4.1	1.7
Slavik et al. [407]	FBCBA ⁸	38.2	20.5	17.9	1.9	1.0

Notes: ⁽¹⁾ Fly Ash, ⁽²⁾ Water Treatment Sludge, ⁽³⁾ Low Calcium Ferronickel Slag, ⁽⁴⁾ Lignite Bottom Ash, ⁽⁵⁾ Vulcanic Mud, ⁽⁶⁾ Reservoir Clay Sediment, ⁽⁷⁾ Stone Mud, ⁽⁸⁾ Fluidized Bed Combustion Bottom Ash

Table 6.4 includes XRF results of CDW powders (especially from BT and RC components), as well as elemental analysis of other waste powders submitted to AA, such as water treatment sludge (WTS), lignite bottom ash (LBA), reservoir clay sediment (RCS), etc. The quantity of SiO_2 , Al_2O_3 , and CaO in all CDW constituents here investigated were consistent with literature ($5.8\div 67.3\%$ for SiO_2 , $1.5\div 23.7\%$ for Al_2O_3 , and $0.7\div 70.8\%$ for CaO). These wide ranges testify that the AA process is sufficiently versatile to tolerate significant variations in chemical compositions of precursors.

Considering the RC fraction, the content of 24.8% of CaO is in line with most of results in Table 6.4. The high content of calcium is usually reflected in the formation of C-S-H products as a consequence of the AA [397], thus improving the mechanical strength. Among CDW constituents, BT is the most appropriate for alkali-activation purposes due to the abundance of both silica and alumina [30]. From Table 6.4 it is evident that the amounts of SiO_2 and Al_2O_3 in BT were in the typical ranges of $49.9\div 66.4\%$ and $9.1\div 21.6\%$ observed in ceramic wastes used for alkali-activated binder production. For this constituent, the $\text{SiO}_2/\text{Al}_2\text{O}_3$ ratio equal to 3.0 is slightly lower than literature data. Komnitsas et al. [30] and Robayo-Salazar et al. [292] observed a general improvement of strength with the increase of $\text{SiO}_2/\text{Al}_2\text{O}_3$ ratio. It is worth noting that BT was characterized by a lower quantity of CaO when compared with the majority of data in literature [293], [29], [298], [399], [290], [291], [289], [300]. Calcium has a positive effect on the development of strength of alkali-activated binders [224] since it favours the formation of Ca-Al-Si gel, which improves the mechanical properties of hardened products [225], [408]. Considering other constituents (RA, NA, UND1, and UND2) no direct correlations with data of Table 6.4 can be achieved. However, the content of silica, alumina, and calcium are comparable with wastes successfully submitted to the AA, as well as the values of $\text{SiO}_2/\text{Al}_2\text{O}_3$ and $\text{SiO}_2/(\text{Al}_2\text{O}_3+\text{CaO})$ ratios.

The chemical characterization of CDW fines and the comparative analysis with literature suggested a proper composition in term of aluminosilicate presence for the AA purpose. However, due to the well-crystallized mineral phases detected from XRD analysis, only a partial dissolution of Si and Al phases in the alkaline medium was expected [234]. The dissolution of aluminosilicates in the alkaline medium is related to the crystallinity of these phases [225]. Many authors reported that for highly crystallized minerals an incomplete dissolution of aluminosilicate species usually occurs [222], [310], [409].

6.1.3 Viscosity of fresh mixtures

The viscosity of fresh pastes provided information on the workability of CDW-AS blends during mixing phase. In case of $l/s = 0.4$, fresh pastes appeared as a wet mouldable powder, not flowable at all. For this reason, the viscosity of mixtures with l/s equal to 0.4 could not be estimated as per the Brookfield viscometer method. It is worth mentioning that with this low amount of liquid phase, fresh mixtures could not be poured into the mould, but were transferred and manually compacted. Figure 6.9.a illustrates an example of consistency of fresh mixture of RA with AS-100% and $l/s = 0.4$, in comparison with the corresponding mixtures with AS-50% and $l/s = 0.6$ (Figure 6.9.b).

Viscosity results of CDW powders mixed with AS-75% and AS-50% with $l/s = 0.5$ are shown in Figure 6.10 and Figure 6.11 respectively. In case of mixture with BT powders and AS-75%, estimated values of viscosities were out of the measurement domain of Brookfield viscometer, therefore results were not reported. Considering other constituents, it is worth noting that UND1 was the more viscous paste, followed by RC, RA, and UND2. The NA-AS-75% paste was the most fluid, with values of η always lower than 20000 cP. When the AS was more diluted (i.e. AS-50%) a marked decrease of viscosities was evidenced for all constituents. For example, the viscosity of UND1 mixtures reduced from 57600 cP in case of AS-75% to 18500 cP of pastes with AS-50% (at a revolution speed of 20 rpm). For the same speed (20 rpm), the viscosity of NA mixtures decreased from 11300 to 3040 cP when passing from 75% to 50% concentrated AS.



Figure 6.9 - Consistency of fresh mixtures of RA powders with (a) AS-100% and $l/s = 0.4$ and (b) AS-50% and $l/s = 0.6$

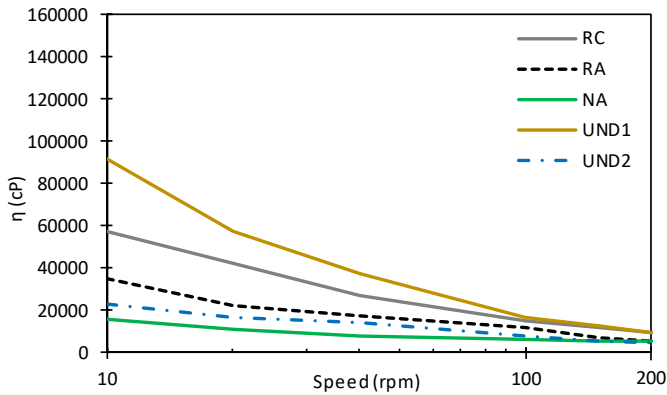


Figure 6.10 - Viscosity of fresh mixtures with a $l/s = 0.5$ and AS-75%

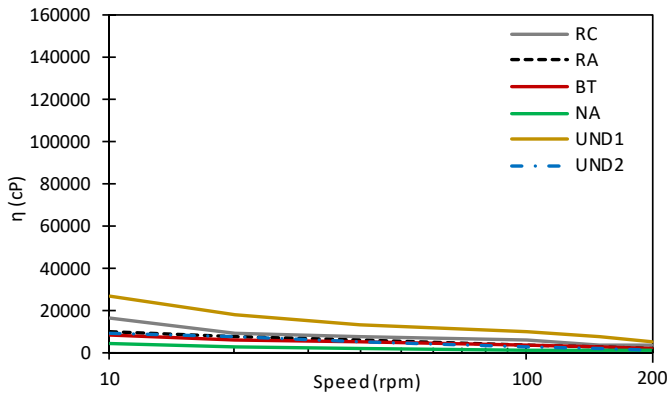


Figure 6.11 - Viscosity of fresh mixtures with a $l/s = 0.5$ and AS-50%

Figure 6.12, Figure 6.13, and Figure 6.14 summarize the evolution of η in function of the rotational speed for mixtures with $l/s = 0.6$ and AS-100%, AS-75%, and AS-50% respectively. Also in this case, it is clear the crucial role of the AS concentration on the viscosity of fresh pastes. The higher viscosity of sodium silicate (Na_2SiO_3) in comparison to water (Section 4.3) provided to the whole AS a certain viscosity, which tended to decrease with the dilution. The viscosity of the AS was directly reflected on the consistency of fresh pastes as indicated in results of Figure 6.12, Figure 6.13, and Figure 6.14. UND1, RC, and RA were found the most viscous constituents independently of the AS concentration. The high viscosity of RC may be attributed to the role of sodium silicate as setting time accelerator of cement hydration reactions [410], [411]. In case of UND1 the presence of particles with high specific area, such as silty-clayey grains [389] [412], can be considered the main cause of the high viscosity compared to other components. It is worth highlighting that at high rotational speeds, the differences of

viscosity significantly reduced. At a speed of 200 rpm, all pastes with AS-100% and l/s ratio equal to 0.6, exhibited a viscosity in the range 11400÷7300 cP.

Through the comparison of results of Figure 6.10 and Figure 6.13, it can be concluded that the addition of higher quantities of liquid phase in the mixtures determined an improvement of flowability of the fresh pastes. At 20 rpm of rotational speed, RC mixture with l/s = 0.6 was characterized by a viscosity of 19000 cP in comparison to $\eta = 42600$ cP observed for the same mixture with l/s = 0.5. For the same rotational speed, the mixture containing UND2 powders increased the viscosity from 9200 to 17133 cP when l/s ratio reduced from 0.6 to 0.5.

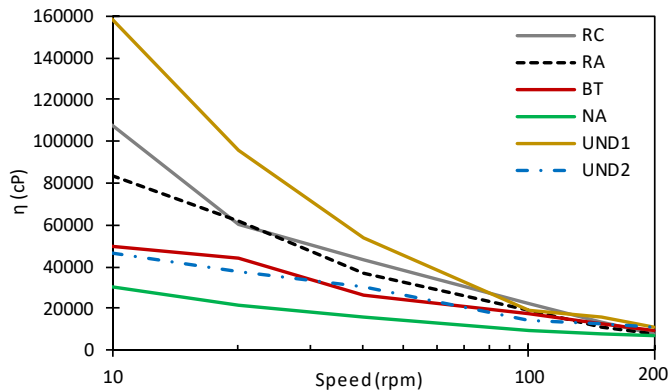


Figure 6.12 - Viscosity of fresh mixtures with a l/s = 0.6 and AS-100%

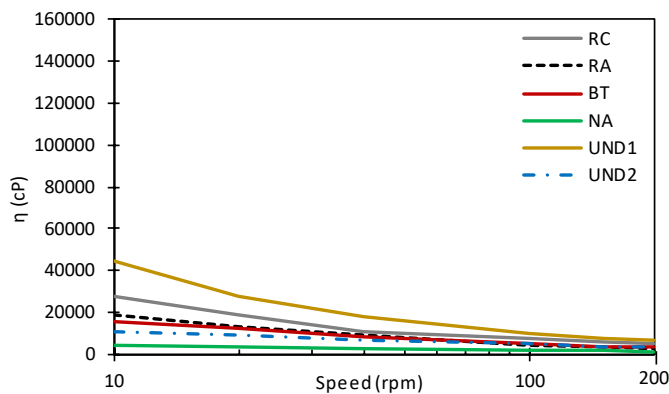


Figure 6.13 - Viscosity of fresh mixtures with a l/s = 0.6 and AS-75%

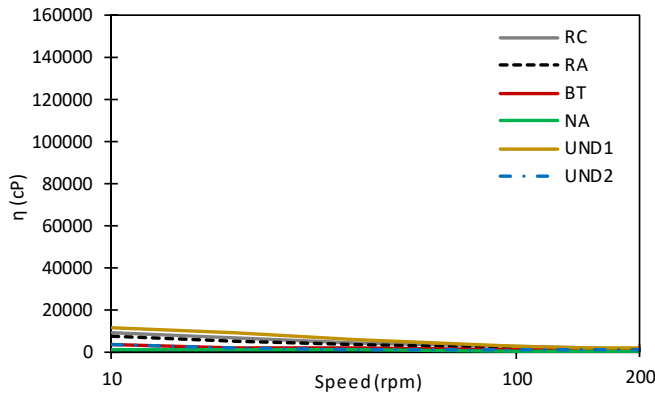


Figure 6.14 - Viscosity of fresh mixtures with a $l/s = 0.6$ and AS-50%

6.1.4 Strength of hardened specimens

Results of mechanical tests of 28-day cured specimens of alkali-activated CDW powders are reported in this section. As specified in Section 5.1.4, several parameters were derived from the stress-strain relationships. Mechanical performance of hardened and alkali-activated specimens were evaluated in terms of:

- maximum value of flexural and compressive strength ($\sigma_{f,max}$ and $\sigma_{c,max}$);
- tangent modulus of flexural and compressive stress-strain curves ($E_{T,f}$ and $E_{T,c}$);
- secant modulus of compression tests ($E_{S,c}$);
- toughness (T_f and T_c).

Flexural test results

The results of flexural strength tests are displayed in Figure 6.15. The best mechanical properties were exhibited by mixtures containing the totally concentrated solution (AS-100%). However, the AS concentrated at 75% (AS-75%) induced a good mechanical strength in RC, UND1, and UND2 samples, with $\sigma_{f,max}$ greater than 2.0 MPa. CDW fines activated with the less concentrated solution (AS-50%) never exceeded 1.0 MPa after 28 days of curing at room temperature. With the addition of AS-50%, BT and UND2 constituents were the most reactive. Powders of RC, RA, UND1 constituents, in the l/s ratio of 0.6, exhibited a greater flexural strength with AS-75% than AS-100%. The same behaviour was observed on UND2 specimens with $l/s = 0.5$, which achieved an average value of $\sigma_{f,max}$ close to 4.0 MPa. In all other cases, the highest flexural strengths were obtained with the undiluted AS (AS-100%). In this case, the mixture containing RC powders and l/s ratio of 0.5 displayed the average maximum value of 5.8 MPa of flexural strength.

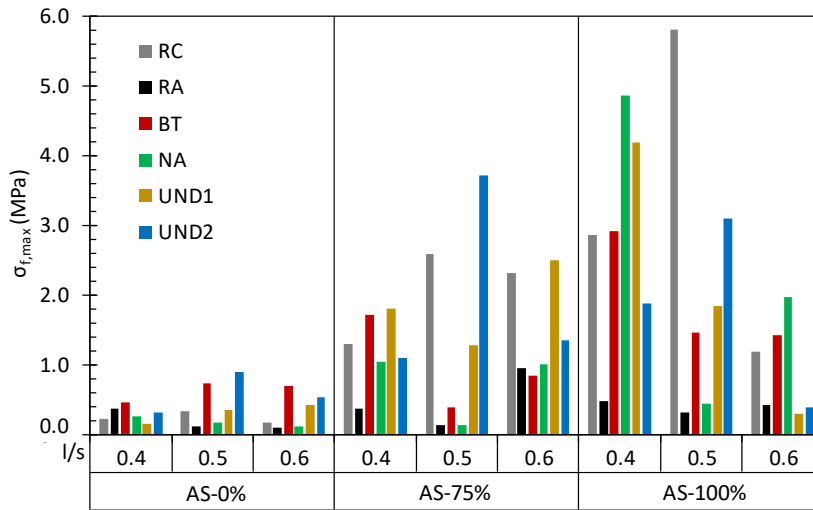


Figure 6.15 - Values of maximum flexural stresses ($\sigma_{f,max}$) of 28-cured specimens

Similarly, UND2 specimens with AS-100%, developed the greatest flexural properties with the $l/s = 0.5$. Differently, RA, BT, NA, UND1 specimens containing the AS-100% exhibited the highest value of $\sigma_{f,max}$ with the lowest quantity of AS ($l/s = 0.4$). Among these components, NA and UND1 were found the most alkali-reactive powders. These materials achieved flexural strengths of 4.9 and 4.2 MPa, respectively.

A systematic comparison with literature cannot be carried out, since no flexural strength results on alkali-activated CDW materials are available. Nevertheless, some flexural strength measurements obtained on others alkali-activated wastes or by-products can be considered for comparative purposes. Yamaguchi et al. [413], studied the alkali-activation of urban incinerator waste in mixtures characterized by a l/s ratio equal to 0.4 and cured at 80°C for 48 hours. The hardened specimens developed flexural strengths in the range 2.5÷15.0 MPa. In a parallel work, the same authors [414] obtained flexural results ranging from 4.0 to 5.5 MPa on specimens containing sewage sludge slag and FA activated with a chemical solution of sodium silicate and sodium hydroxide. Granizo et al. [415] performed flexural tests on metakaolin-based geopolymers, obtaining values of $\sigma_{f,max}$ between 6.3 and 13.9 MPa depending on the Na concentration in the chemical activator. A mixture of potassium hydroxide, sodium silicate and sodium hydroxide was used by Kamseu et al. [416] for the alkali-activation of metakaolin. After 28 days of curing at room temperature, specimens with Si/Al ratio equal to 1.9 and $l/s = 0.6$ achieved flexural strengths in the range 4.0÷6.2 MPa. Fernandez-Jimenez and Puertas [417] investigated a BFS-based geopolymer with a very similar AS to the AS-100%. The hardened specimens reached 5.6, 8.8, and 9.1 MPa of flexural strength

after 3, 7, and 28 days of curing, respectively. Zhao et al. [418] published the results of flexural strength of alkali-activated mortars containing a mixture of FA and BFS. After 28 days of curing, the mechanical properties tended to decrease from 8.5 to 6.1 MPa with the increase of FA content in the mortars.

It should be observed that CDW fines treated with the totally concentrated AS are likely characterized by flexural strength values in good agreement with the aforementioned literature, especially in case of RC with $l/s = 0.5$ and UND1 and NA with l/s ratio equal to 0.4. These constituents exhibited flexural strengths barely lower than those recorded for FA and BFS, which have been widely recognized to be excellent precursors for the AA process [419].

Tangent modulus ($E_{T,f}$) and toughness (T_f) derived from the stress-strain curves of flexural strength tests in function of AS concentration, l/s ratio and CDW constituent are reported in Figure 6.16 and Figure 6.17 respectively. For each combination, RA specimens showed the lowest values of $E_{T,f}$. Very low stiffness were also exhibited by hardened products with AS-50%. Significantly higher values were noticed when the AS concentration increased to 75% and 100%, as expected from strength results. In particular, for $l/s = 0.4$ and $l/s = 0.5$, the tangent modulus of alkali-activated mixtures with AS-100% was almost the double of that characterizing the specimens with AS-75%. Conversely, RC, RA, UND1, and UND2 mixtures showed higher $E_{T,f}$ with AS-75% compared to AS-100% (in the case of l/s equal to 0.6).

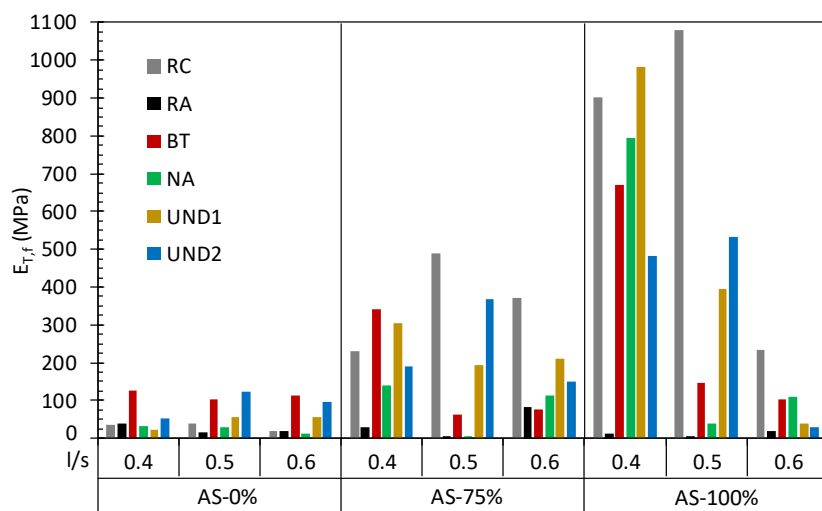


Figure 6.16 - Tangent modulus ($E_{T,f}$) results obtained from stress-strain curves of flexural test

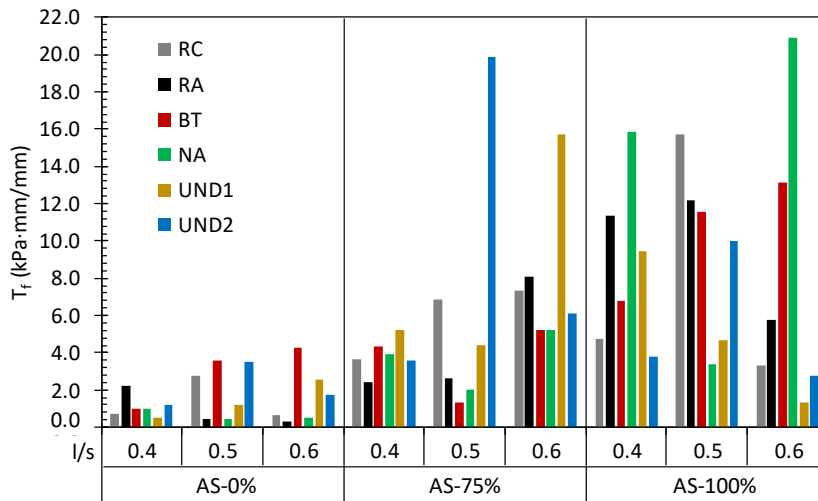


Figure 6.17 - Toughness (T_f) results derived from stress-strain curves of flexural test

The average values of T_f generally increased with the increment of AS concentration. In contrast to $\sigma_{f,\max}$ and $E_{T,f}$ trends, the toughness of the RA specimens was comparable to that of the other constituents. In fact, alkali-activated RA constituent displayed high strains at failure, which balanced the low stress in the toughness estimation. With the addition of AS-75%, the highest values of T_f were always put in evidence for specimens with l/s ratio equal to 0.6, with the exception of UND2. This last component was characterized by a mean T_f value equal to 19.9 $\text{kPa}\cdot\text{mm}/\text{mm}$ (for l/s = 0.5). In case of AA with AS-100%, no definite trends for T_f parameter were appreciated. In fact, UND1 had the highest failure energy with l/s = 0.4, RC, RA, and UND2 with l/s = 0.5, while BT and NA with l/s = 0.6.

Compression test results

Figure 6.18 illustrates the results of compression strength obtained on alkali-activated CDW fines. After a curing period of 28 days at room temperature, the compressive strength of mixtures containing the most diluted AS (AS-50%) was decisively low, independently of the component and the l/s ratio. This behaviour was also observed in flexural strength results. It is worth noting that $\sigma_{c,\max}$ values recorded on specimens with AS-50% were averagely the 11%, 20%, and 23% of the corresponding specimens with AS-100% and l/s ratios equal to 0.4, 0.5, and 0.6 respectively. Among the compressive strengths obtained on specimens containing AS-50%, only the UND2 component with l/s = 0.5 exceeded 2.0 MPa.

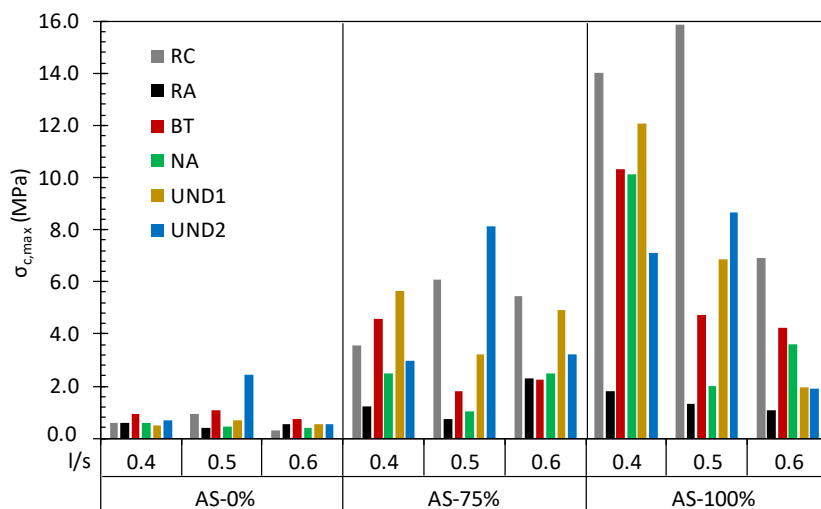


Figure 6.18 - Compressive strength results of alkali-activated CDW powders

The bar diagram of Figure 6.18 shows that $\sigma_{c,max}$ generally increased when passing from 75% to 100% concentrated AS. Only for RA, UND1, and UND2 with $l/s = 0.4$ an opposite trend can be appreciated. Considering all constituents, RA always exhibited the lowest compressive strengths, as already noticed in flexural strength tests. Among average results obtained on cured specimens with AS-75%, UND2 showed the best mechanical properties with l/s equal to 0.5 (average $\sigma_{c,max}$ of 8.1 MPa). Good results were also recorded on RC and UND1 powders independently of the l/s ratio. Differently, the negative effect on compressive strength caused by the increment of l/s ratio was clearly observed in mixture activated with AS-100%. All constituents halved the compressive strength when the l/s ratio increased from 0.4 to 0.6. However, it is important to highlight that RC and UND2 powders achieved their best performances with $l/s = 0.5$.

Table 6.5 lists several results from technical literature for comparison purposes. Most of data are related to BT and RC constituents, which are characterized by compressive strengths ranging in wide intervals. The best results of alkali-activated RC fines were consistent with values obtained by Vasquez et al. [400], who used a chemical activator similar to the AS-100%. RC powders activated with AS-100% and with the two l/s ratios of 0.4 and 0.5 exhibited higher values of $\sigma_{c,max}$ than those obtained by Komnitsas [298], Komnitsas et al. [30], and Zaharaki et al. [297] on RC specimens cured for 7 days and thermally treated.

Table 6.5 - Synthesis from literature of compressive strength results for alkali-activated CDW constituents.

Author	Material	l/s ratio	Temp. curing	Curing (days)	$\sigma_{c,max}$ (MPa)
Allahverdi and Kani [293]	BT	0.30	25°C	28	22.5÷40.0
	BT+RC	0.26	25°C	28	12.5÷18.5
Allahverdi and Kani [29]	BT	0.33	25°C	28	3.2÷16.1
	BT+RC	0.31	25°C	28	15.2÷48.0
Jha and Tuladhar [295]	UND	0.25	40°C	15	7.3
Komnitsas [298]	BT	0.30	80°C for 24 h	7	8.1÷25.0
	RC	0.30	80°C for 24 h	7	3.2÷10.0
Komnitsas et al. [30]	BT	0.38	90°C for 7 d	7	49.5
	RC	0.48	90°C for 7 d	7	13.0
Pathak et al. [294]	BT	0.50	60°C for 24 h	28	11.4
Robayo-Salazar et al. [292]	BT	0.25	25°C	28	3.0÷52.0
	BT	0.25	70°C for 24 h	28	6.0÷34.0
Robayo-Salazar et al. [328]	BT	0.23	25°C	28	9.0÷55.0
	RC	0.23	25°C	28	11.0÷25.0
Sun et al. [289]	BT	0.40	60°C for 28 d	28	52.2÷63.4
Vasquez et al. [400]	RC	0.22	25°C	28	12.5÷25.6
	RC	0.22	70°C for 24 h	28	22.5÷25.4
Zaharaki et al. [297]	BT	0.30	80°C for 24 h	7	38.8
	RC	0.30	80°C for 24 h	7	8.9

Hardened specimens containing BT powders showed generally compressive strengths lower than those achieved by other authors [30], [293], [297]. Komnitsas et al. [30] and Zaharaki et al. [297] applied a thermal curing at 90°C for 7 days and 80°C for 24 hours respectively, which markedly increased the final strengths. Results published by Sun et al. [289] demonstrated that the curing at 60°C extremely improved the alkali-activation efficiency, since BT specimens reached compressive strengths considerably higher (52.2÷63.4 MPa) than those recorded for alkali-activated BT with AS-100% and cured at room temperature (investigated here). Compressive strength results from Robayo-Salazar et al. [292], [328] vary in wide ranges depending on the $\text{SiO}_2/\text{Al}_2\text{O}_3$ and $\text{Na}_2\text{O}/\text{SiO}_2$ molar ratios. It is worth noting that the values of $\sigma_{c,max}$ obtained on both BT and RC constituents with AS-100% and $l/s = 0.4$ are close to the lower limit. The lower strengths of RC and BT specimens in comparison to results of Robayo-Salazar et al. [292], [328] can be justified by the significantly higher l/s ratio (0.4÷0.6 here investigated versus 0.23÷0.25 of Robayo-Salazar et al. [292], [328]). Allahverdi and Kani [293] studied the mechanical properties of alkali-activated BT powders at room temperature with an AS characterized by a significantly greater amount of Na_2O (silica

content of 34.3% in weight and $\text{SiO}_2/\text{Na}_2\text{O}$ of 0.86) than AS-100% (Section 4.3). According to the same authors [293] and to Duran Atis et al. [217], an increment of sodium concentration in the AS induces an improvement of the mechanical properties of final products, thus justifying the higher values measured by Allahverdi and Kani [293].

Fines derived directly from CDW sieving (UND1) and activated with AS-100% developed an average compressive strength higher than that observed by Jha and Tuladhar [295] on 15-day cured specimens with a preliminary 24-hour curing at 60°C .

Figure 6.19 and Figure 6.20 plot the values of tangent ($E_{T,c}$) and secant ($E_{S,c}$) moduli derived from the analysis of stress-strain relationships, as indicated in Section 5.1.4. It is evident a direct correspondence between the two parameters: $E_{S,c}$ is averagely the 70% of $E_{T,c}$. With the addition of AS-75%, the highest stiffness was achieved by alkali-activated RC and UND2 powders with an l/s ratio equal to 0.5. As observed in case of compressive strength, tangent and secant moduli systematically increased with an increment of the AS concentration. Only RA, UND1, and UND2 with $l/s = 0.6$ displayed an opposite trend. In case of AS-100%, it is worth noting the significant decrease of stiffness in RA, BT, NA, and UND1 specimens when the l/s ratio passed from 0.4 to 0.5. These trends highlighted the strong dependency of certain constituents on the variation of proportions between liquid and solid phases.

Toughness (T_c) values before failure are illustrated in Figure 6.21. Similar considerations to those carried out in the analysis of T_f results can be drawn. The energy before failure tended to increase with the increment of the AS concentration.

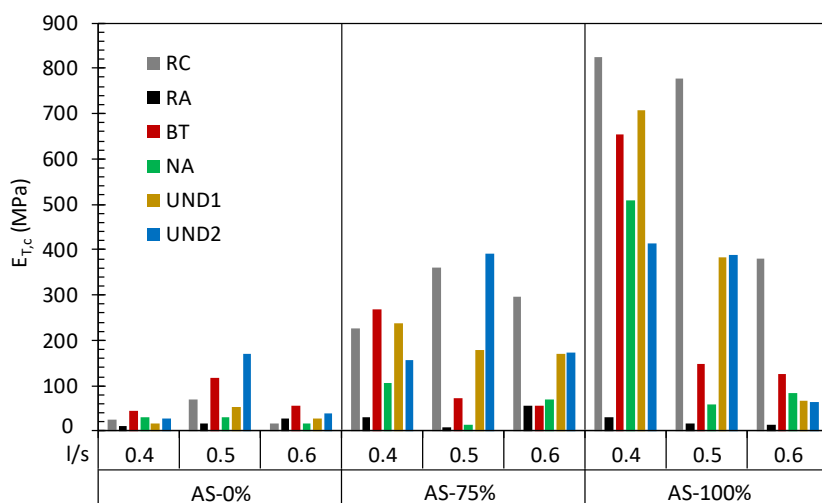


Figure 6.19 - Tangent modulus ($E_{T,c}$) results obtained from stress-strain curves of compressive test

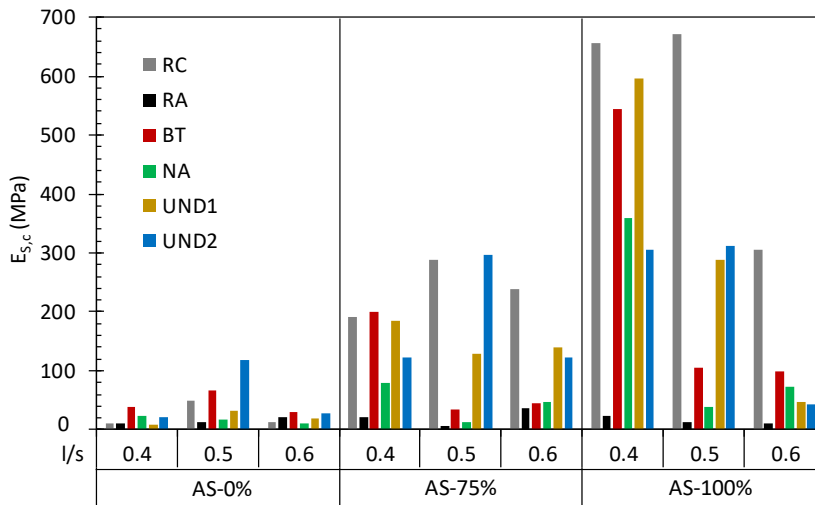


Figure 6.20 - Secant modulus ($E_{s,c}$) results obtained from stress-strain curves of compressive test

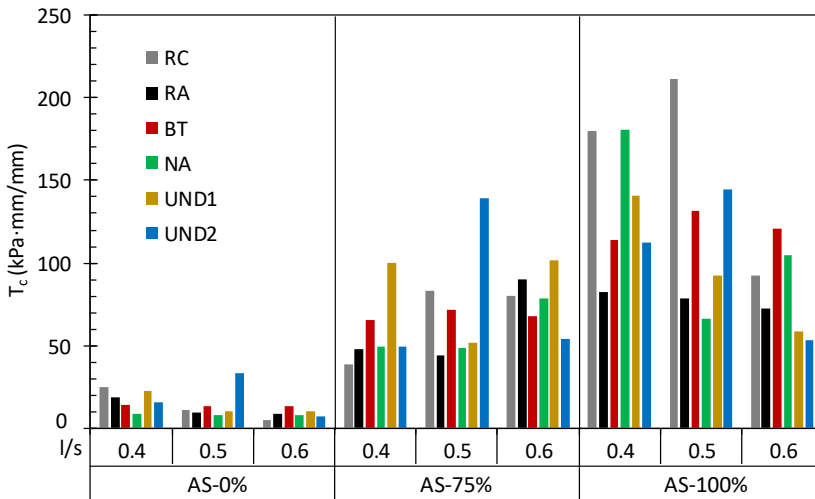


Figure 6.21 - Toughness (T_c) results derived from stress-strain curves of compressive test

With the AS-75%, the highest values of T_c were obtained on UND1 and UND2 fractions. It demonstrates that these two alkali-activated products dissipated more energy before failure than the others. Toughness of hardened mixtures activated with AS-100% reflected the trends already discussed on $\sigma_{c,max}$. The highest average value of $T_c = 211.6$ kPa·mm/mm was achieved by RC specimens with $l/s = 0.5$. As expected from T_f values, RA showed values of T_c comparable to those exhibited by the other

constituents, confirming that this alkali-activated material reached the failure with inadequate stresses, but at high strain levels.

Discussion

Flexural strength and compression strength results were in good agreement. The average magnitude of $\sigma_{f,max}$ was around the 50%, 36%, and 30% of the corresponding $\sigma_{c,max}$ in case of AS concentrated at 50%, 75% and 100% respectively. It implies that similar considerations for both parameters can be drawn. Marked differences in mechanical behaviour depending on the origin of alkali-activated powders were observed. These differences suggest that each constituent tended to react distinctively when an AS is added for triggering the AA process. It is reasonable to assume that BT and UND1 efficiently reacted with the totally concentrated activator (AS-100%), since they showed relevant mechanical strengths and comparable to results in literature. Both constituents were characterized by the highest amount of aluminosilicate and reactive mica-group phases (Table 6.2), whose presence is a requirement for the AA occurrence. These minerals induced the formation of aluminosilicate geopolymers with adequate flexural and compressive strengths. The assumption is confirmed by the fact that RA constituent, characterized by a significant lower quantity of aluminosilicates and minerals from mica-group achieved only 0.9 MPa and 2.3 MPa of average flexural and compressive strength respectively (with AS-75% and $l/s = 0.6$). Moreover, it is worth mentioning that after 28 days of curing at room temperature the majority of RA specimens were found partially humid, suggesting an extreme slow hardening kinetic. From the mechanical characterization of hardened products, it can be inferred that a content of aluminosilicates greater than 50% (from XRD analysis) with $SiO_2 > 40\%$ and $Al_2O_3 > 8\%$ (from XRF analysis) in raw powders of BT and UND1 component could lead to a satisfactory AA process. The relatively high content of CaO (Table 6.3) in UND1 and UND2 ensured a reduced microstructural porosity, forming Ca-Al-Si gel which likely led to an enhancement of final strengths [225].

Although the NA fines contained a lower proportion of aluminosilicates in comparison to BT and UND1, the mechanical properties of hardened products were comparable to the latter two constituents. Two reasons can explain these good mechanical results: (1) the highest densities of hardened specimens (Table 6.6) and (2) the lowest viscosity of fresh pastes (Section 6.1.3). Both factors contributed in producing a dense structure which expressed mechanical properties comparable with those of fines containing a greater amount of aluminosilicates. Considering the elemental composition of NA fractions (Table 6.3 and Table 6.4), it can be concluded that powders of natural origin are prone to geopolymerization process when the amount of silicon, aluminium and calcium oxides are greater than 40%, 8%, and 10% respectively. These values are in good agreement

with Palmero et al. [234], who positively submitted muds derived from cutting operations of aluminosilicate ornamental stones to the AA process (Table 6.4).

The highest mechanical strengths were shown by the RC powders, in which the combined presence of aluminosilicate and calcium-rich phases led to the formation of both aluminosilicate geopolymers and C-S-H species [408] [420], [421]. According to XRD and XRF analysis, RC constituent was characterized by the highest content of calcium carbonate (Table 6.2 and Table 6.3), which tends to dissolve under alkaline condition [345]. Solubilized calcium and residual unreacted silicates reacted with waste and silicon species of the AS, forming C-S-H species together to alkali-activated structures. This assumption is supported by the fact that the highest flexural and compressive strengths were achieved when more water was added (i.e. with $l/s = 0.5$). As previously mentioned (Section 6.1.3), the sodium silicate, plenty contained in the AS, acted also as setting accelerator of residual particle of cement ([410], [422]), thus promoting the formation of C-S-H products [423].

In contrast with literature, mechanical results revealed that BT exhibited a lower alkali-activation potential than RC. Two reasons can be associated to this unexpected behaviour. The first and the most important is related to the curing temperature: although BT is considered the most alkali-reactive constituent (of CDW) due to its chemical composition, the geopolymerization reactions of crystalline aluminosilicates (such as BT fines investigated here) is favoured under high-temperature curing conditions ($60\div 80^{\circ}\text{C}$) [30], [289], [290]. Vice versa, the strength development of RC is mainly caused by the hydration reactions of residual particles of cement, which normally occur at room temperature. The second reason of the lower strength exhibited by BT in comparison to literature can be attributed to the low $\text{SiO}_2/\text{Al}_2\text{O}_3$ ratio (Table 6.4). According to Komnitsas et al.[30], high $\text{SiO}_2/\text{Al}_2\text{O}_3$ ratios lead to higher compressive strength. Silva et al. [424] claimed that, at low $\text{SiO}_2/\text{Al}_2\text{O}_3$ ratios, an excess of Al_2O_3 content (as observed in BT samples investigated here) can cause a reduction of strengths.

Table 6.6 - Average densities of alkali-activated specimens before test

AS concentration	l/s ratio	Density (kg/m^3)					
		RC	RA	BT	NA	UND1	UND2
50	0.4	1691	1729	1761	1854	1764	1759
	0.5	1575	1737	1734	1902	1826	1544
	0.6	1488	1679	1609	1710	1605	1529
75	0.4	1927	1887	1865	1973	1764	1911
	0.5	1904	1951	1932	2085	1951	1737
	0.6	1767	1862	1958	1991	1833	1893
100	0.4	1835	1975	1536	1994	1974	1962
	0.5	1900	1939	1875	2016	1916	1908
	0.6	1908	1890	1973	2034	1934	1926

The l/s ratio and AS concentration influenced concurrently the mechanical properties of alkali-activated products. In Figure 6.22.a and Figure 6.22.b is displayed the evolution of $\sigma_{c,max}$ in function of the l/s ratio for specimens activated with AS-75% and AS-100% respectively. In case of 75% concentrated solution, RC and UND2 constituent reached the highest compressive strength, with the optimal l/s ratio equal to 0.5. Considering the mixture activated with the undiluted solution, there was often a drop of strength when passing from a l/s of 0.4 to 0.6. Both Reig et al. [290] and Komnitsas et al. [403] stated that an excess of water causes the formation of pores and cracks, which are detrimental for compressive strength development. Moreover, it is worth mentioning that a retardation of the hardening process was observed in case of l/s = 0.6 as a consequence of the excessive amount of liquid phase. In most cases, it was reflected in a reduction of the mechanical properties.

The concentration of the AS had a key role in the development of both flexural and compressive strengths, as reported by many authors [294], [307], [308], [309]. When the AS was diluted, a decrease of the sodium silicate and hydroxide content in the liquid phase took place, concurrently to a lowering of pH. It caused a reduction of the AA efficiency, which affected the development of mechanical strength. With high pH, the AS has usually a higher capability in dissolving aluminosilicate phases. As a consequence, a great amount of dissolved silica and alumina species was available for creating a strongly interconnected inorganic network during condensation stage [425]. It led to an enhancement of the mechanical properties of hardened materials, as recorded for almost all specimens.

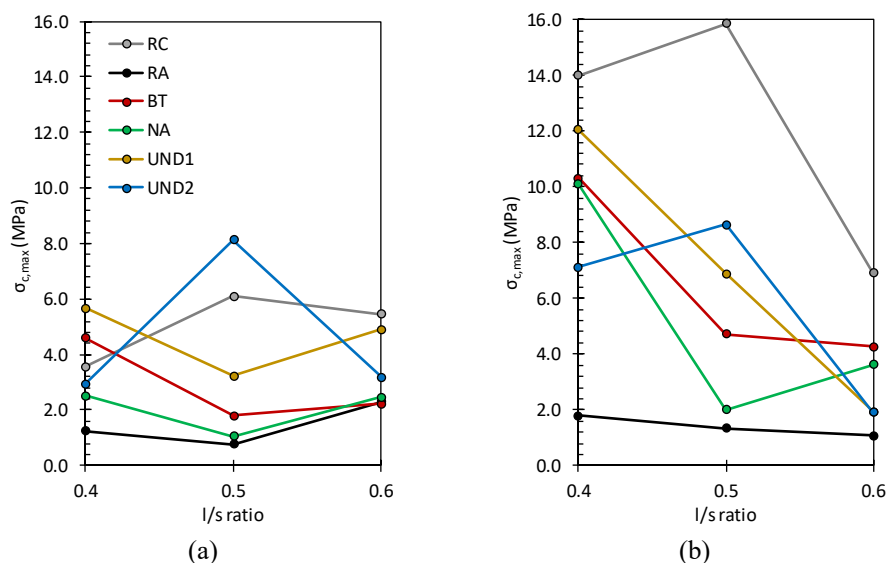


Figure 6.22 - Evolution of compressive strength as a function of l/s ratio for (a) AS-75% and (b) AS-100%

The role of pH was also discussed by Song et al. [426], who attributed to the higher pH the increment of precursors reactivity. This condition allowed to produce more resistant products characterized by a less porous microstructure.

Figure 6.23.a plots the comparison between flexural and compressive strengths of UND1 and UND2 specimens. The different behaviour of the two component is evident from the poor correlation between the two datasets. UND1 fines were obtained from sieving at 0.125 mm the starting CDW sample, thus they contained both particles of RC, RA, BT, NA and unidentifiable residual particles. Whereas UND2 sample was equally recomposed by RC, RA, BT, and NA fractions, exactly for comparison purposes (with UND1). UND1 fines tended to react differently from UND2 when submitted to alkali-activation, generally showing higher mechanical properties.

The graph of Figure 6.23.b correlates the average mechanical strength results of UND2 measured on hardened specimens ($\sigma_{\max}(\text{UND2}_{\text{meas}})$) with a prediction of strength values estimated with Eq. 30 ($\sigma_{\max}(\text{UND2}_{\text{pred}})$). In this equation, $\sigma_{\max}(C_{i,\text{meas}})$ is the strength of the i constituent, while the counter i varies from 1 to 4 and identifies the constituent (RC, RA, BT, NA).

$$\sigma_{\max}(\text{UND2}_{\text{pred}}) = \frac{\sum_{i=1}^4 \sigma_{\max}(C_{i,\text{meas}})}{4} \quad \text{Eq. 30}$$

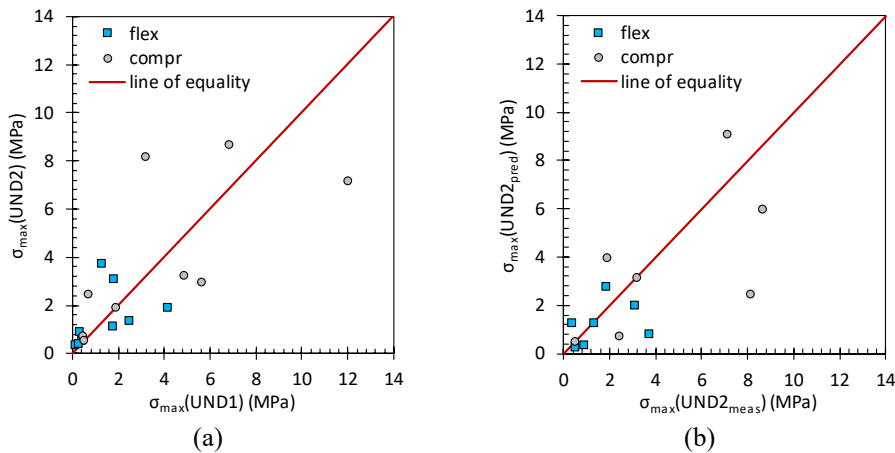


Figure 6.23 - Comparison between UND components: (a) UND1 versus UND2 strength results, (b) UND2 measured results versus UND2 predicted strength values

The significant deviation from the line of equality of both flexural and compressive strengths values suggests that the initial hypothesis was rejected, thus the expected mechanical properties cannot be estimated by the average results of strengths exhibited by the four constituting components. This consideration implies the existence of interactions between CDW components during the alkali-activation. It is reasonable to suppose that the strength development of UND1 fraction is governed also by phenomena of the second order.

In conclusion, CDW fines reacted when mixed with an AS (especially AS-100% and AS-75%) to form alkali-activated binders. Each component developed the best mechanical properties with a specific l/s ratio. RC with $l/s = 0.5$ and 0.4 , BT, NA, and UND1 with $l/s = 0.4$ exhibited flexural and compressive strengths comparable with literature results. The dilution of the AS caused a detrimental effect in the mechanical properties of hardened material.

The chemical-mineralogical composition of starting powders plays a key role in the formation of geopolymer products. The presence of Si and Al elements is a requirement for the development of alkali-activation reactions [397]. Khale and Chaudhary [397] suggested $3.3 \div 4.5$ as the range of SiO_2/Al_2O_3 to obtain strong alkali-activated products. According to the best mechanical results recorded on BT, UND1, and UND2 fractions, a content of $SiO_2 > 40\%$, $Al_2O_3 > 8\%$, and $4\% < CaO < 12\%$ produced alkali-activated binders with adequate strengths when cured at room temperature. It is worth pointing out that the chemical composition of BT constituent does not considerably differ from source to source (Table 6.4), thus these ranges can be considered as recommend values for a satisfactory alkali-activation. No specific references are available to set up the same comparison with UND1 and UND2 fractions. However, considering the average contents of SiO_2 , Al_2O_3 , and CaO from literature indicated in Table 6.4 (50.4% for SiO_2 , 14.6% for Al_2O_3 , and 14.0% for CaO), it is reasonable to assume that the chemical composition of undivided materials (UND1 and UND2) is a good reference for the alkali-activation of CDW fines coming from different plants. Although unselected CDW aggregates are composed of materials of different origin depending on the debris delivered to the recycling plants [20], Table 6.7 shows that the contents of silicon, aluminium, and calcium oxides fluctuate in limited ranges. The mean values are equal to $50.0 \pm 10.6\%$, $10.7 \pm 3.4\%$, and $14.2 \pm 5.1\%$ for SiO_2 , Al_2O_3 , and CaO respectively. These values are similar to the chemical characterization of RMA and RMCA suggested by Jiménez [20]: $40 \div 50\%$ of SiO_2 , $6 \div 8\%$ of Al_2O_3 , and $20 \div 28\%$ of CaO .

The abundance of SiO_2 , Al_2O_3 , and CaO found in UND1 and UND2 fractions (reported in the first two rows of Table 6.7), as well as the SiO_2/Al_2O_3 and $SiO_2/(Al_2O_3+CaO)$ ratios are consistent with literature data and can be referred as recommended values for

the adequate development of alkali-activation reactions at room temperature, independently of the provenience of waste.

In case of RC constituent, good mechanical strengths were measured with $\text{SiO}_2/\text{Al}_2\text{O}_3$ and $\text{SiO}_2/(\text{Al}_2\text{O}_3+\text{CaO})$ ratios equal to 5.2 and 1.1 respectively, in line with works of Allahverdi and Kani [29], [293].

Table 6.7 - Comparison between elemental composition from XRF results of undivided CDW powders and literature, with indication of $\text{SiO}_2/\text{Al}_2\text{O}_3$ and $\text{SiO}_2/(\text{Al}_2\text{O}_3+\text{CaO})$ ratios

Author	Size	XRF (%)			$\text{SiO}_2/\text{Al}_2\text{O}_3$	$\text{SiO}_2/(\text{Al}_2\text{O}_3+\text{CaO})$
		SiO_2	Al_2O_3	CaO		
UND1	d<0.063 mm	42.6	12.8	11.5	3.3	1.8
UND2		40.7	8.7	11.8	4.7	2.0
Bianchini et al. [393]	d<0.075 mm	36.6	8.6	22.0	4.3	1.2
		40.3	8.9	19.2	4.5	1.4
		41.4	10.4	18.7	4.0	1.4
		42.1	10.6	18.7	4.0	1.4
		48.5	10.6	14.5	4.6	1.9
		41.5	10.7	19.4	3.9	1.4
		44.5	11.1	16.7	4.0	1.6
Gao et al. [427]	n.d. ¹	60.5	18.9	1.1	3.2	3.0
		30.2	4.6	14.0	6.6	1.6
		48.3	6.5	15.1	7.4	2.2
		49.6	7.1	11.1	7.0	2.7
Angulo et al. [386]	d<0.150 mm	48.0	10.8	13.9	4.4	1.9
		48.3	12.9	11.1	3.7	2.0
		52.2	17.2	7.8	3.0	2.1
Saiz Martínez et al. [428]	d<4 mm	45.5	10.1	15.7	4.5	1.8
		63.5	6.6	11.6	9.6	3.5
Contreras et al. [181]	d<2 mm	75.5	9.8	6.1	7.7	4.7
Moreno-Pérez et al. [429]	d<4.75 mm	51.5	13.7	19.6	3.8	1.5
		59.6	14.3	12.3	4.2	2.2
		57.0	10.8	12.3	5.3	2.5
Cristelo et al. [28]	d<20 mm	64.3	9.9	17.0	6.5	2.4
Average	-	50.0	10.7	14.2	5.1	2.1
Dev.st	-	10.6	3.4	5.1	1.7	0.8

Note: (¹) n.d. = non-defined

6.1.5 Environmental assessment

The environmental compatibility of CDW materials was evaluated by means of leaching tests and pH measurements (Section 5.1.5). Results of environmental characterization of raw CDW powders are shown in Table 6.8, while those related to alkali-activated products are in Table 6.9. In addition to leaching test results, both tables contain the acceptance limits of (1) the Ministerial Decree of 5th February 1998 [65] for EoW criteria and (2) the Council Decision 2003/33/EC [139] for landfilling materials.

In most cases, raw powders of CDW constituents did not release any harmful substances. In fact, results of leaching test were below the threshold of the Italian requirement for the employment in road applications. However, it is worth noting that values of sulphates of RC and UND1 samples were outside the acceptance limits. Moreover, RC constituents released a quantity of total chromium double of the permitted value of the Ministerial Decree of 5th February 1998 [65].

Table 6.8 - Results of leaching test on raw CDW fines (bolded numbers indicate values outside the Italian acceptance limits)

Parameter	Unit of meas.	IT limits ¹	EU limits ²	RC	RA	BT	NA	UND1
Chlorides	(mg/l)	100	800	55	43	48	44	50
Fluorides	(mg/l)	1.5	10.0	0.6	0.1	0.7	0.2	0.1
Nitrates	(mg/l)	50	-	34	6	12	10	37
Sulphates	(mg/l)	250	1000	540	28	120	79	390
Arsenic	(µg/l)	50	500	0.6	2.4	3.5	1.3	4.1
Barium	(mg/l)	1.0	20	0.10	0.74	2.50	0.09	0.07
Beryllium	(µg/l)	10	-	0.000	0.000	0.000	0.000	0.000
Cadmium	(µg/l)	5.0	40	0.000	0.000	0.000	0.000	0.000
Cobalt	(µg/l)	250	-	0.28	0.13	0.11	0.18	0.31
Chromium ³	(µg/l)	50	500	110.0	0.9	42.0	1.3	4.1
Mercury	(µg/l)	1.0	10	0.000	0.000	0.000	0.000	0.000
Nickel	(µg/l)	10	400	0.00	4.00	0.00	3.70	2.10
Lead	(µg/l)	50	500	0.00	0.26	0.16	0.14	0.19
Copper	(mg/l)	0.05	2	0.008	0.002	0.004	0.002	0.009
Selenium	(µg/l)	10	100	1.0	0.0	1.1	0.0	1.3
Vanadium	(µg/l)	250	-	17.0	4.6	110.0	2.9	11.0
Zinc	(mg/l)	3.0	4.0	0.001	0.003	0.005	0.003	0.003
pH	(-)	5.5÷12	-	11.0	8.7	10.1	8.3	8.6

Notes: ⁽¹⁾ acceptance limits of the Ministerial Decree of 5th February 1998 [65] for EoW

⁽²⁾ acceptance limits of 2003/33/EC [139] for landfilling inert waste

⁽³⁾ total chromium

Several authors [183], [430], [431], [432], [433], [434] indicated that sulphates and chromium are the most critical elements recorded in leaching tests of CDW materials, especially for those containing high amount of RC. The release of sulphates is mainly due to the presence of gypsum residuals in unselected CDW and cement mortars in RC aggregates [81], [435], [436]. Gypsum is usually added to cement to regulate the hydration time and controlling the drying shrinkages [437], [438]. Residual particles of cement in RC caused also an increase of pH of the eluate, whose value reached 11.0. Values of total chromium recorded on RC were also consistent with the results of Galvín et al. [431] and Dosho [439]. The high leaching of chromium by cementitious materials is due to its presence in the raw materials used for clinker production [440]. A high release of barium was detected in the eluate of BT component, since barium carbonate (BaCO_3) is usually used in manufacturing process of ceramic materials [441]. The pH of BT sample was found around 10, while other constituents had a pH slightly higher than 8.

The results of leaching test on alkali-activated specimens with AS-100% and $l/s = 0.5$ are shown in Table 6.9. To better understand the effects of the AA on the environmental properties of CDW constituents, the values of leaching concentrations (in mg/l) of both raw powders before the AA and reacted samples after 28 days of curing are illustrated in the bar diagrams from Figure 6.24 to Figure 6.28. A general increase of the concentration of pollutants in the eluates as a consequence of AA is evidenced in all Figures. The leaching of sulphates (SO_4^{2-}) was rather high for alkali-activated RC (Figure 6.24) and UND1 (Figure 6.28) products. Its concentrations were outside the acceptance limits of the Ministerial Decree of 5th February 1998 [65]. Figure 6.25 reveals that the leaching of sulphates in RA constituent increased from 28 mg/l to 600 mg/l when these powders underwent to the AA process. Total chromium moderately increased its concentration in the eluate of the alkali-activated RA products. Similar trend can be observed also for other constituents. Among heavy metal, it is worth mentioning that alkali-activated RC fines tended to release excessive amounts of copper and vanadium, whose values exceeded the limits of the Italian permitted concentrations. The same observation is valid for reacted UND1 sample. In this constituent, also the concentration of nickel (58 $\mu\text{g/l}$) did not comply the limit of 10 $\mu\text{g/l}$ imposed by the Italian law. Similarly, quantities of nickel over the Italian acceptance limits were recorded in the eluates of alkali-activated RA and NA samples (Figure 6.25 and Figure 6.27 respectively).

Reacted BT products (Figure 6.26) released concentrations of lead and vanadium outside the acceptance limits. On the contrary, results of leaching tests revealed that the AA always reduced the concentration of barium. Alkali-earth metals (i.e. Mg, Ca, and Ba) are likely dissolved during the AA process [442], [443]. It is reasonable to suppose that Ba remained in the Al-Si network, thus resulting not available to be released.

Table 6.9 - Results of leaching test on alkali-activated CDW fines (bolded numbers indicate values outside the Italian acceptance limits)

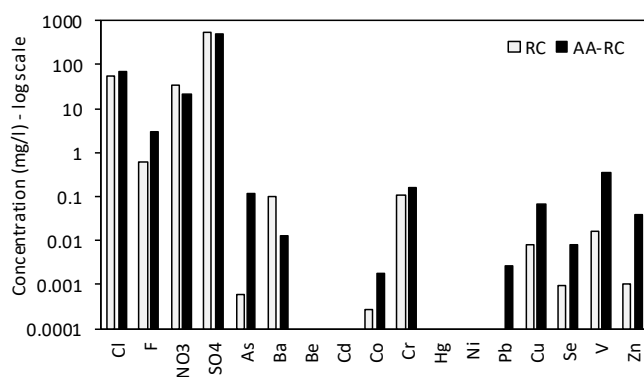
Parameter	Unit of meas.	IT limits ¹	EU limits ²	AA ³ RC	AA ³ RA	AA ³ BT	AA ³ NA	AA ³ UND1
Chlorides	(mg/l)	100	800	69	58	58	49	68
Fluorides	(mg/l)	1.5	10.0	3.1	0.5	0.9	0.0	0.9
Nitrates	(mg/l)	50	-	22	4	6	9	27
Sulphates	(mg/l)	250	1000	520	600	100	79	560
Arsenic	(µg/l)	50	500	120.0	66.0	210.0	69.0	180.0
Barium	(mg/l)	1.0	20	0.01	0.04	0.09	0.05	0.08
Beryllium	(µg/l)	10	-	0.000	0.250	0.000	0.110	0.140
Cadmium	(µg/l)	5.0	40	0.000	0.000	0.000	0.000	0.110
Cobalt	(µg/l)	250	-	1.80	6.50	1.00	2.10	7.90
Chromium ⁴	(µg/l)	50	500	160.0	21.0	25.0	15.0	13.0
Mercury	(µg/l)	1.0	10	0.000	0.000	0.000	0.000	0.240
Nickel	(µg/l)	10	400	0.00	76.00	0.00	19.00	58.00
Lead	(µg/l)	50	500	2.70	19.00	64.00	11.00	16.00
Copper	(mg/l)	0.05	2	0.067	0.047	0.026	0.064	0.230
Selenium	(µg/l)	10	100	8.1	3.3	2.9	0.0	3.9
Vanadium	(µg/l)	250	-	360.0	150.0	1200.0	140.0	580.0
Zinc	(mg/l)	3.0	4.0	0.040	0.094	0.067	0.120	0.058
pH	(-)	5.5÷12	-	11.8	12.2	11.5	12.1	12.0

Notes: ⁽¹⁾ acceptance limits of the Ministerial Decree of 5th February 1998 [65] for EoW

⁽²⁾ acceptance limits of 2003/33/EC [139] for landfilling inert waste

⁽³⁾ alkali-activated products with AS-100%, l/s=0.5, after 28 days of curing

⁽⁴⁾ total chromium

**Figure 6.24 - Concentration of pollutants in the eluates of raw and alkali-activated RC constituents**

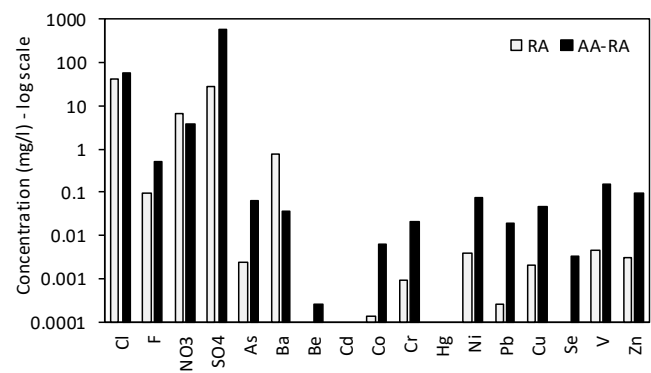


Figure 6.25 - Concentration of pollutants in the eluates of raw and alkali-activated RA constituents

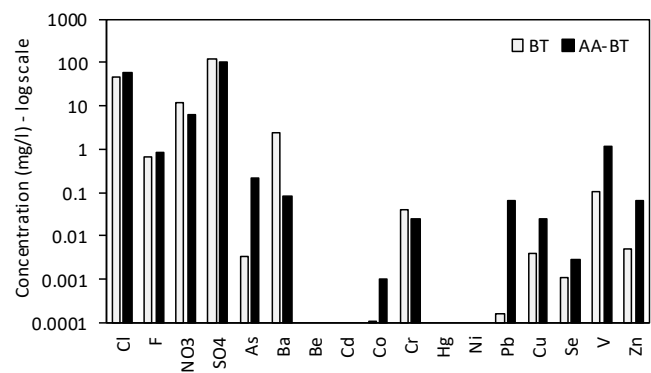


Figure 6.26 - Concentration of pollutants in the eluates of raw and alkali-activated BT constituents

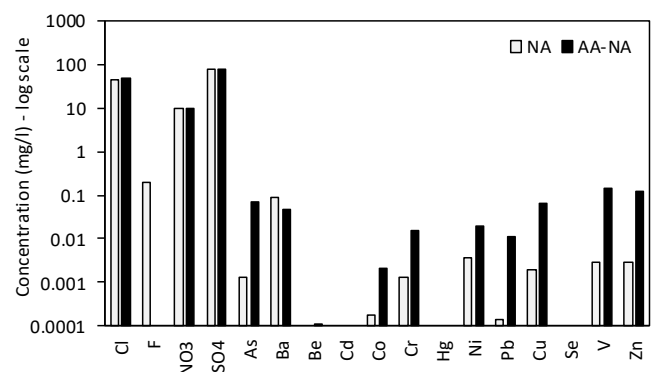


Figure 6.27 - Concentration of pollutants in the eluates of raw and alkali-activated NA constituents

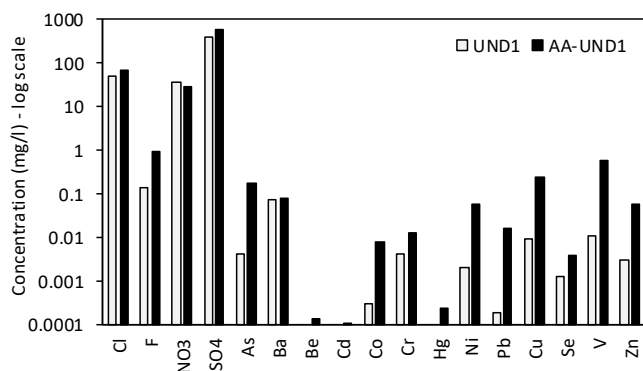


Figure 6.28 - Concentration of pollutants in the eluates of raw and alkali-activated UND1 constituents

With few exceptions (fluorides), anions (Cl^- , SO_4^{2-} and NO_3^-) generally maintained constant or slightly increased their concentrations as a consequence of the AA. The most reasonable hypothesis is that they reacted with NaOH to form sodium chloride, sodium nitrate and sodium sulphate, which tended to precipitate in the porosity of the structure and therefore were released in lower quantities. It is worth noting that all these species are highly soluble in water. For instance, Eq. 31 describes the chemical balance of the aqueous solution of sodium chloride (in which NaCl is completely dissociated).



Eq. 31

When the concentration of Na^+ is elevated, like in presence of AS-100%, the balance is shifted towards the non-ionized specie, which tend to precipitate in the porosity of material and are leached in lower concentrations.

Results presented here are partially inconsistent with few studies which recognized the ability of alkali-activated materials to immobilize certain hazardous metals [444], [445]. For example, the alkali-activation of FA studied by Palomo and Palacios [444] reduced the leaching of lead and not of chromium. Zhang et al. [446] stated that their FA-based geopolymers efficiently immobilized both Cu and Pb cations. Some heavy metals, in fact, tend to be incorporated in the geopolymeric network, thus minimizing their leaching [442], [447]. It is worth mentioning that the previously-cited studies [444], [447], [448] investigated the leaching of solid specimens, taking advantage of the highly compacted microstructure and the nanometric porosity of geopolymers to retain toxic substances. Moreover, literature investigations refer always to leaching behaviour of fully reacted products, obtained by more reactive precursors than those investigated here. In case of highly crystalline phases, such as CDW powders, the dissolution of aluminosilicates is usually incomplete, thus leading to partially reacted products (Section 6.1.2). For this

reason, it is reasonable to suppose that some metals were easily released because of their weak connection to the aluminosilicates network. However, no literature data are available on leaching behaviour of CDW alkali-activated materials for entering into a deep comparison.

Nevertheless, some hypotheses can be drawn for justifying the increment in concentration of released substances by alkali-activated CDW constituents. Unlike what happens with raw powders, alkali-activated materials were submitted to a double exposure of an aqueous medium. During the specimen preparation stage, in which raw powders were mixed with the AS, certain substances could have been partially released in the liquid medium. The second water exposure occurred during the 24 hours of leaching test, which caused the additional dissolution of anions and cations in the eluate. On the contrary, raw powders exhibited only the second exposure to water during the leaching test. An additional justification of the increment of leaching as a consequence of AA, can be found in the AA process itself. In fact, the exposure to an extremely basic solution produces a certain corrosion of the material, thus promoting the release of its constituents [392]. Consequently, all elements which did not take part in the chemical reactions and were not immobilized in the new geopolymeric matrix, being more reactive, tended to be released more easily. Furthermore, the addition of an AS with pH close to 14 caused a common increment of pH of all constituents, whose values ranged from 11.5 to 12.2. Some researches [352], [449], [450] demonstrated that leaching behaviour is strongly influenced by the pH, since it regulates the dissolution and adsorption process of certain substances. In particular, Van der Sloot and Dijkstra [451] reported that the concentration of cations and anions increases when the pH value moves towards the basicity. Luna Galiano et al. [452], who studied the leachability behaviour of municipal waste incineration fly ash-based geopolymers, stated that for acidic pH values, the concentration of released metals, such as Cd, Cr, Pb, and Zn, are generally lower than those observed for $\text{pH} > 7$.

Finally, it is worth evidencing the poor reproducibility of the leaching test of the EN 12457-2 [353] when compared to the in-field conditions of the material [431]. The real-scale application of any granular material, both in unbound and stabilized conditions, imposes its compaction in a dense structure characterized by a wide particle size distribution. On the contrary, the EN 12457-2 [353] envisages the grinding of the sample (dimension of particles lower than 4 mm) and the measure of leaching on loose material, resulting barely representative of the in-field conditions.

Although alkali-activated samples exhibited an excessive leaching of anions and heavy metals in relation to the threshold of the Ministerial Decree of 5th February 1998 [65], their concentrations completely fulfil the European Council Decision 2003/33/EC [139] for inert waste. As a consequence, CDW powders activated with the AS-100% can be

classified as inert, thus their environmental compatibility was considered satisfactory, even if the leaching of pollutants was generally greater than raw fines before the activation.

6.2 Stabilization of CDW aggregates with AA of fines

The mechanical properties of hardened specimens containing alkali-activated CDW powders demonstrated that finest particles of these materials are potentially reactive in alkaline environments. Promising results obtained in Exp. A allowed to widen the scale of investigation towards the evaluation of the effectiveness of AA as stabilization method for recycled granular mixture containing CDW aggregates. The results of Exp. B1 are collected and discussed in this section. Results of preliminary characterization of loose aggregates are firstly shown. These basic properties are preparatory to a complete understanding of the behaviour of compacted mixtures. Moreover, these measurements allow a direct comparison with similar materials investigated in other studies. In the second part, the mechanical properties of stabilized CDW materials are deeply examined referring to the results of RLT, UCS, and ITS tests. As last, FESEM images of hardened samples are provided and commented on.

6.2.1 Preliminary characterization of aggregates

Table 6.10 provides information on the composition of collected CDW material. The compositional analysis, carried out on a sample in the size range 10÷14 mm, revealed the presence of a high amount of NA particles, with a percentage of 40.8% of the total sample. This value is consistent with literature data, as well as, the percentage content of RC [160], [127]. The amount of RA (22.7%) was higher than other studies [160], [177], [453], in which the content of RA typically ranges from 2.0 to 9.2%.

Table 6.10 - Results of compositional analysis, particle density (γ_p), and water absorption (w_a) of CDW constituents (10÷14 mm)

Material	Composition (%)	γ_p (kg/m ³)	w_a (%)
RC	28.3	2628	6.3
RA	22.7	2591	1.4
BT	8.2	2637	15.1
NA	40.8	2733	1.1
Ref. NGM	-	2783	0.6

Ceramic residuals (BT) were present in less amount than the 29.5% and 26.6% showed by Cerni and Colagrande [160] and Jiménez et al. [22], respectively. Considering the classification of CDW aggregates reported in Table 5.3, CDW materials can be classified as RMA (recycled mixed aggregates), albeit the amount of RA was not smaller than 15%. In fact, the sum of RC, RA, and NA was significantly greater than 70%, and BT content was below the 30%.

In Table 6.10, the particle density (γ_p) and the water absorption (w_a) of the different constituent (RC, RA, BT, NA) are also reported. The same table contains values of γ_p and w_a measured on a reference natural granular material (NGM). RC and RA aggregates were characterized by lower particle densities than those of natural origin (i.e. NA and NGM), due to residual mortar and bitumen films attached [20]. The γ_p value of BT constituent was also lower than NA and NGM, due to the nature of ceramic materials contained in BT fraction. However, this value ($\gamma_p = 2637 \text{ kg/m}^3$) was in line with the particle density reported by Arulrajah et al. [15]. Natural aggregates derived from CDW sample (NA) exhibited a density comparable to that measured on the reference mixture (NGM). Since all specimens were compacted according to the reference grading curve of Table 4.1, an overall value of $\gamma_p = 2664 \text{ kg/m}^3$ was also measured on a sample with particle size in the range $0 \div 25 \text{ mm}$. This value was moderately higher than the typical range ($2010 \div 2290 \text{ kg/m}^3$) for CDW (classified as RMA) suggested by Jiménez [20].

Considering the results of water absorption, it is worth noting that BT aggregates displayed the highest values (15.1%) in agreement with ceramic materials investigated by Poon and Chan [454] and Jiménez et al. [455]. The water absorption of RC was equal to 6.3% and was higher than that of NA because of the porosity caused by the residual cement mortar coating the aggregates [20], [114]. RA particles in the range $10 \div 14 \text{ mm}$ exhibited a w_a value not dissimilar to the 1.0% recorded by Taha et al. [197]. As expected, NA and NGM were characterized by the lowest water absorption coefficients.

The results of fragmentation and F/T degradation resistance are summarized in Table 6.11. LA and F/T tests were performed on samples of (1) individual CDW constituents (RC, RA, BT, NA), (2) undivided CDW aggregates (CDW_{meas}), and (3) reference NGM. In all cases, the testing sample was composed by aggregates in the size fraction $10 \div 14 \text{ mm}$. Table 6.11 reports also the values of LA, $\text{LA}_{8\text{F/T}}$, ML coefficients estimated by the weighted average of the corresponding parameter exhibited by each constituents (CDW_{pred}). Each parameter ($p = \text{LA}$ or $\text{LA}_{8\text{F/T}}$ or ML) was defined according to Eq. 32, in which:

- $p(\text{CDW}_{\text{pred}})$ is the predicted parameter for the CDW sample;
- $\%_{\text{RC}}$, $\%_{\text{RA}}$, $\%_{\text{BT}}$, $\%_{\text{NA}}$ indicate the percentage content of RC, RA, BT, and NA respectively, included in Table 6.10;

- p_{RC} , p_{RA} , p_{BT} , p_{NA} are the values of the considered parameter (LA or $LA_{8F/T}$ or ML) recorded on RC, RA BT, and NA samples respectively.

$$p(CDW_{pred}) = \frac{\%_{RC} \cdot p_{RC} + \%_{RA} \cdot p_{RA} + \%_{BT} \cdot p_{BT} + \%_{NA} \cdot p_{NA}}{100} \quad \text{Eq. 32}$$

Results of Los Angeles test put in evidence that RC and BT were the two most susceptible CDW constituents in relation to the fragmentation degradation. The values of LA coefficient for RC and BT were consistent with those provided by Bazaz et al. [456] and Cavalline and Weggel [457], but slightly higher than the values observed by other authors [141], [15], [435], [458]. The high LA coefficient for RC was caused by the detachment and pulverization of mortar coating the aggregates. Figure 6.29 depicts the sample of RC before the test (a) and the two resulting fractions (b, retained at 1.6 mm sieve, c, passing at 1.6 mm sieve) at the end of degradation process. It is evident how the aggregates coming from LA were deprived from mortar and cement particles attached to them before the test [459].

The cause of the low fragmentation resistance exhibited by BT sample is related to the material itself. Bricks, tiles, and generic ceramic materials are poorly resistant to impacts. The high crushing of BT is attributable also to residual masonry mortar attached to grains [20]. RA particles were less sensitive to the degradation of LA, as confirmed by the low LA coefficient (21%). This value is lower than that measured for NA samples (25%) and equal to that obtained on the virgin NGM. The same consideration was confirmed by the experimental investigations carried out by Arulrajah et al. [199] and Vegas et al. [149]. It is reasonable to assume that the film of bitumen coating grains provided a residual cohesion to aggregates, preventing their complete breakdown. Moreover, it can be supposed that the viscoelastic nature of the asphaltic binder tended to soften the effect of impacts by steel spheres.

Table 6.11 - Results of LA and $LA_{8F/T}$ and ML after 8 F/T cycles

Material	LA (%)	$LA_{8F/T}$ (%)	ML (%)
RC	41	44	6.5
RA	21	21	1.0
BT	43	46	2.5
NA	25	25	0.7
CDW_{meas}	29	30	2.7
CDW_{pred}	30	31	2.6
NGM	21	21	0.4

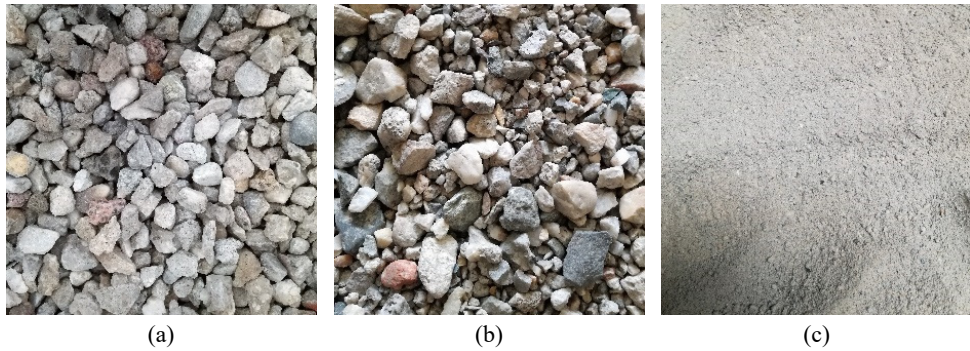


Figure 6.29 - Pictures of RC sample during Los Angeles test: (a) aggregates before test, (b) particles after test retained at 1.6 mm sieve, (c) particles grinded during test passing at 1.6 mm sieve

The LA coefficient of the mixed CDW fraction (CDW_{meas}) was equal to 29%, which is relatively lower than results obtained in other studies (31÷39%) [123], [149], [160], [177], [22]. It is logically associated to the higher content of RA materials in the sample and the lower content of BT. In particular, Vegas et al. [149] and Barbudo et al. [435] recognized that the BT constituent has the greatest influence on the resistance to fragmentation of the overall CDW granular material.

Values of $LA_{8F/T}$ evidenced that F/T degradation is detrimental for those components characterized by a low resistance to fragmentation. The worst performance was shown by the RC fraction, which increased LA coefficient from 41% to 44% after 8 cycles of F/T and exhibited a ML equal to 6.5 %. This latter value is significantly higher than the 2.9% and 2.4% determined by Woodside et al. [460] and Chidirouglu et al. [461] respectively. The F/T degradation of BT sample caused an increment of LA coefficient (from 43% to 46%) and a ML equal to 2.5%. The higher porosity and the greater water absorption (Table 6.10) can be considered the main reasons of the poor resistance of RC and BT elements when exposed to F/T degradation. When temperature goes below 4°C the volume of water embedded in pores increases causing internal stresses, which can lead to a potential breakdown of the grains [23]. No variations of LA coefficient after thermal degradation were detected on RA, NA and NGM samples. Accordingly, negligible values of ML were measured on these constituents. The undivided sample of CDW (CDW_{meas}) showed average values of $LA_{8F/T}$ and ML, in line with the results of Woodside et al. [460].

Finally, it is worth noting that values of LA, $LA_{8F/T}$, and ML for CDW_{meas} and CDW_{pred} were close to each other. It demonstrated that the degradation parameters (LA, $LA_{8F/T}$, ML) obtained on the unseparated sample (CDW_{meas}) were reasonably equal to the

weighted average of the values of the corresponding parameters obtained on the individual constituents (RC, RA, BT, NA).

6.2.2 Compaction properties of mixtures

Proctor compaction study

The results of Proctor compaction study are given in Figure 6.30. In detail, Figure 6.30.a illustrates the evolution of dry density (γ_d) as a function of the AS content (w_{AS}) in the CDW mixtures, while in Figure 6.30.b, γ_d is depicted as a function of the nominal water content (w_w). The AS was composed by a fixed percentage of water depending on its concentration (Section 4.3). Therefore, both w_w and w_{AS} have been considered in the results analysis. It is evident that the concentration of the AS added as liquid phase during compaction affected its optimum content ($w_{AS,opt}$). Compaction curves reported in Figure 6.30.a indicate that higher concentrations of AS required a greater amount of liquid phase to reach the optimum value. This behaviour can be explained considering the AS viscosity (Section 4.3), which increased passing from the reference liquid phase (i.e. water, AS-0%) to the totally concentrated AS (AS-100%). During compaction, a more viscous liquid phase tended to be less flowable than water, thus a larger quantity of fluid phase was required for satisfactorily lubricating grains.

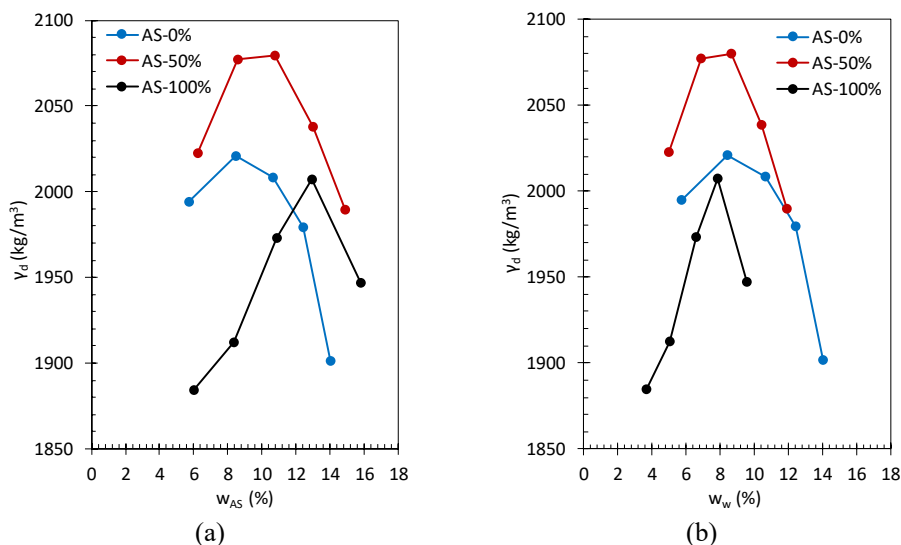


Figure 6.30 - Results of compaction study as per the Proctor method: dry density (γ_d) as a function of (a) AS content (w_{AS}) and (b) moisture content (w_w)

Conversely, when dry densities are represented in function of w_w (Figure 6.30.b), the optimum value ($w_{w,opt}$) converged around the 8.6%, independently of the AS concentration. For this reason, 8.6% was set as $w_{w,opt}$ for all mixtures of Exp. B1 independently of the AS concentration. Two variation of $\pm 2\%$ around the optimal value ($w_{w,opt}-2\%$ and $w_{w,opt}+2\%$) were also used for preparing additional specimens. This was useful for a comprehensive investigation of the effects of the variation of liquid phase on the mechanical behaviour of both un-stabilized (AS-0%) and alkali-activated CDW materials (AS-50% and AS-100%). The value of maximum dry density ($\gamma_{d,max}$) was in the range $2000 \div 2080 \text{ kg/m}^3$. The CDW mixture compacted with AS-100% exhibited the lower values of $\gamma_{d,max}$. It is attributable to the higher viscosity of AS with respect to water, which partially contrasted the compaction process and led to a less dense structure.

The results of Proctor study on the reference CDW mixture (i.e. CDW mixed with AS-0%) can be compared with numerous data available in literature. Considering values summarized in Table 6.12, it can be concluded that $w_{w,opt}$ obtained on CDW-AS-0% mixture was slightly lower than literature, probably due to the lower amount of ceramic particles [454]. The dry density ($\gamma_d = 2020 \text{ kg/m}^3$) was essentially consistent with the ranges reported by other authors [149], [25], [314]. Slight differences of Proctor parameters of Table 6.12 are mainly due to the different composition and gradation of the CDW materials.

The liquid phase is an aqueous solution containing H_2O and dissolved sodium silicate and hydroxide in fixed proportion depending on the AS concentration. For this reason, the amount of AS-50% and AS-100% added during compaction was greater than the value of w_w . According to Section 4.3, the AS-100% included 61% of H_2O , while AS-50% was composed by 80% of H_2O . Hence, for a fixed value of w_w , the amount of w_{AS} varied depending on its concentration. Table 6.13 lists both the theoretical water content (w_w) and the corresponding w_{AS} added during compaction.

Table 6.12 - Proctor compaction parameters of unselected CDW aggregates from literature

Author	$w_{w,opt}$ (%)	γ_d (kg/m^3)
Agrela et al. [191]	11.5÷12.5	1960÷1990
Bassani and Tefa [314]	9.5	1968÷2070
Cerni et al. [462]	12.0	1920
da Conceição Leite et al. [157]	13.5	1856
Del Rey et al. [25]	9.0÷12.5	1870÷2140
Jiménez et al. [177]	13.0	1830
Jiménez et al. [22]	12.7	1910
Pasetto [186]	9.0	2000
Vegas et al. [149]	5.0÷9.1	1884÷2067

Table 6.13 - Values of AS content (w_{AS}) corresponding to fixed water contents (w_w)

AS-conc. (%)	w_w (%)	w_{AS} (%)	γ_{wet}^1 (kg/m ³)	γ_d (kg/m ³)	e (-)	S (%)
0	6.6	6.6	2135	2003	0.33	53.3
	8.6	8.6	2194	2020	0.32	71.9
	10.6	10.6	2221	2009	0.33	86.5
50	6.6	8.3	2239	2068	0.29	64.6
	8.6	10.8	2302	2079	0.28	86.2
	10.6	13.3	2301	2032	0.31	96.1
100	6.6	10.8	2188	1974	0.35	56.9
	8.6	14.1	2262	1982	0.34	75.3
	10.6	17.4	2246	1914	0.39	81.4

Note: ⁽¹⁾ estimated by linear interpolation of values obtained during Proctor compaction

The degree of saturation S , estimated according to Eq. 33, is also provided in Table 6.13.

$$S = \frac{w_{AS} \cdot \gamma_p}{\gamma_{AS} \cdot e} \quad \text{Eq. 33}$$

In Eq. 33, the particle density is indicated as γ_p and is equal to 2664 kg/m³ (Section 6.2.1), γ_{AS} is the density of the AS depending on the concentration (Table 4.2), and e is the void index, estimated from the ratio between γ_p and γ_d .

Gyratory compaction and workability

As mentioned in Section 5.2.3, cylindrical specimens for mechanical characterization were compacted as per the gyratory compaction (GC) method. During the investigation, a loss of liquid phase as a consequence of compaction was noticed. Thus, the difference between the weight of loose CDW aggregates and AS (before compaction) and the weight of compacted specimen (after compaction) was estimated. Table 6.14 summarizes the average values of the AS loss (Δw_{AS}) measured on the nine mixtures depending on the AS concentration and w_w . These measurements revealed that Δw_{AS} was strongly related to the starting quantity of w_{AS} . With a water content equal to $w_{w,opt}-2\%$, Δw_{AS} assumed negligible values, while mixtures containing the optimal water content ($w_{w,opt}$) and the AS-100% demonstrated the tendency in losing moderate quantities of liquid phase during compaction ($\Delta w_{AS} = 0.8\%$). The same amount of Δw_{AS} was exhibited by mixtures compacted with water only (AS-0%) in a quantity of $w_{w,opt}+2\%$. The liquid phase expelled from mixtures with $w_{w,opt}+2\%$ and both AS-50% and AS-100% reached 1.2%. Results of Table 6.14 suggest that when the AS was greater than 13%, the excessive AS tended to bleed from the specimens during compaction.

Table 6.14 - AS loss (Δw_{AS}) during gyratory compaction

AS conc. (%)	Δw_{AS} (%)		
	$w_{w,opt}-2\%$	$w_{w,opt}$	$w_{w,opt}+2\%$
0	0.0	0.1	0.8
50	0.0	0.2	1.2
100	0.2	0.8	1.2

Figure 6.31 illustrates the compaction curves obtained from the analysis of the GC output data. Each curve was obtained through Eq. 34, where the compaction parameters ($C_{1,avg}$ and $k_{g,avg}$) are the average values of C_1 and k_g estimated on 12 specimens of the same mixture (i.e. specimens characterized by the same amount of w_w and AS concentration).

$$C_n = C_{1,avg} + k_{g,avg} \cdot \log(n) \quad \text{Eq. 34}$$

As detailed in Table 5.4, two cylindrical specimens of 100x200 mm and two cylindrical specimens of 100x100 mm, replicated for 3 different curing times, were compacted for each combination of AS concentration and w_w .

In case of CDW aggregates compacted with water only (AS-0%), the increase of w_w produced an upward shift of the compaction curve, with an increment of $C_{1,avg}$ and $C_{100,avg}$ values. The workability ($k_{g,avg}$) ranged from 6.5 of mixtures with $w_{w,opt}-2\%$ to 7.3 of mixtures containing the optimum value of water ($w_{w,opt}$). A different evolution of C_n characterized the mixtures with AS-50% and AS-100%.

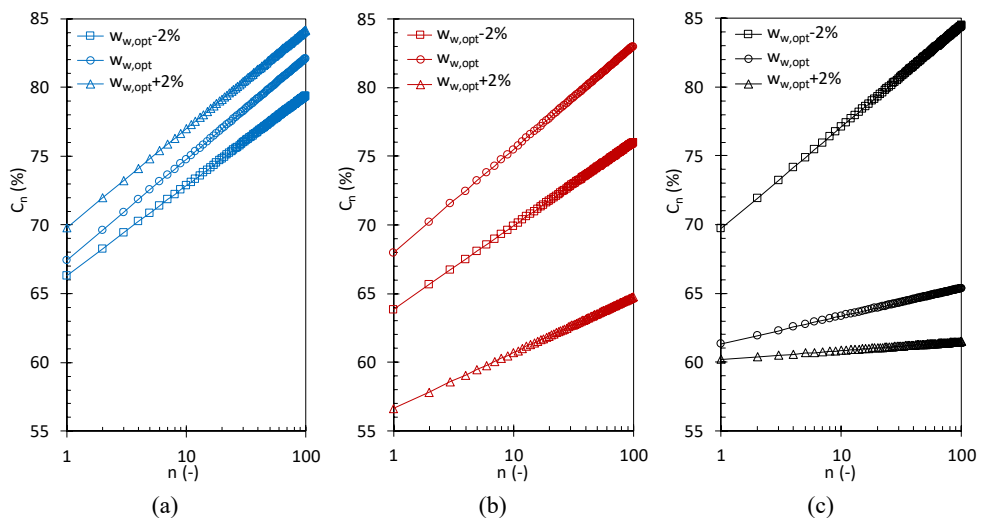


Figure 6.31 - Averages compaction curves for mixtures containing (a) AS-0%, (b) AS-50%, and (c) AS-100%

Compaction curves of Figure 6.31.b (related to CDW-AS-50% mixtures) displayed a marked variation of both $C_{1,avg}$ and $k_{g,avg}$ parameters. It is interesting to observe that the self-compaction and workability reduced to 56.6% and 4.1 respectively with $w_{w,opt}+2\%$. The excess of liquid phase affected also mixtures containing AS-100% (Figure 6.31.c). In this case, $C_{1,avg}$ passed from 69.7% for $w_{w,opt}-2\%$, to 61.3% for $w_{w,opt}$, and 60.2% for $w_{w,opt}+2\%$. For the same mixture, $k_{g,avg}$ decreased from 7.4 at $w_{w,opt}-2\%$, to 2.0 and 0.6 in case of $w_{w,opt}$ and $w_{w,opt}+2\%$ respectively. These very low values of workability were caused by both the excess of liquid phase in the mixtures and the high viscosity of AS-100%, which concurrently contrasted the compaction process. The viscous liquid phase influenced the packing action of the GSC and caused a drastic decrease of $k_{g,avg}$, especially for $w_{w,opt}$ and $w_{w,opt}+2\%$.

In addition to compaction parameters ($C_{1,avg}$, $k_{g,avg}$, $C_{100,avg}$), Table 6.15 contains also the values of corrected AS content ($w_{AS,real}$), the average values of final dry density (γ_d), as well as the estimated void content (v) and the degrees of saturation (S) of CDW mixtures prepared in Exp. B1. The void content was obtained from the following Eq. 34.

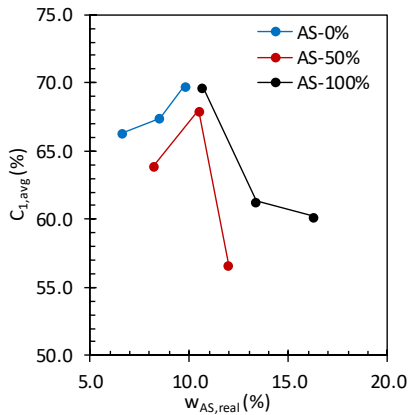
$$v = 100 - C_{100,avg} \quad \text{Eq. 35}$$

The $w_{AS,real}$ was estimated by the difference between the theoretical AS content (w_{AS}) and the amount of AS lost during compaction (Δw_{AS}). The higher γ_d values of CDW-AS-100% mixtures in comparison to those obtained in the Proctor study (Table 6.13) can be explained by the different compaction procedure. According to Cerni and Camilli [363], the impact compaction of Proctor method is less effective in the expulsion of water in comparison to GSC. Vice versa, the kneading action of GC favoured the expulsion of the excessive liquid phase and, consequently, the grains tended to get closer in a denser structure. Similarly, both non-cohesive and cohesive granular materials investigated by Mokwa et al. [463] reached slightly greater dry densities with GC method than with the modified Proctor compaction.

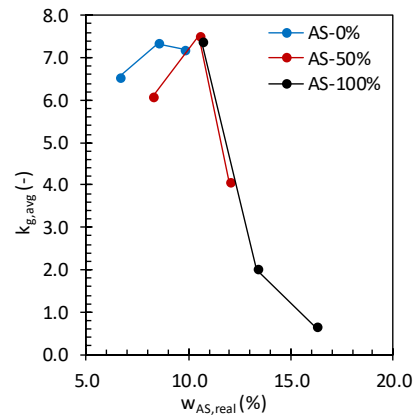
The evolution of $C_{1,avg}$ and $k_{g,avg}$, $C_{100,avg}$, and γ_d as a function of $w_{AS,real}$ is depicted in Figure 6.32. The highest values of compaction parameters were achieved for a w_{AS} content between 10 and 11%, independently of the AS concentration. The same observation is not valid in case of γ_d for mixtures with AS-0%, since they tended to reduce the dry density with the addition of water from 6.6 to 10.6%.

Table 6.15 - Synthesis of real AS contents ($w_{AS,real}$), compaction parameters ($C_{1,avg}$, $k_{g,avg}$, $C_{100,avg}$), final dry densities (γ_d), voids content (v) and degrees of saturation (S) of CDW mixtures prepared in Exp. B1

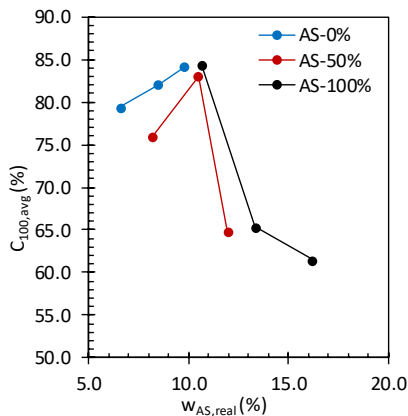
AS conc. (%)	w_w	$w_{AS,real}$ (%)	γ_d (kg/m ³)	$C_{1,avg}$ (%)	$k_{g,avg}$ (-)	$C_{100,avg}$ (%)	v (%)	S (%)
0	$w_{w,opt}-2\%$	6.6	2064	66.3	6.5	79.4	20.6	60.5
	$w_{w,opt}$	8.5	2056	67.4	7.3	82.1	17.9	76.6
	$w_{w,opt}+2\%$	9.8	2049	69.8	7.2	84.2	15.8	87.0
50	$w_{w,opt}-2\%$	8.2	2028	63.9	6.1	76.0	24.0	59.1
	$w_{w,opt}$	10.5	2056	68.0	7.5	83.0	17.0	80.2
	$w_{w,opt}+2\%$	12.0	2044	56.6	4.1	64.8	35.2	89.2
100	$w_{w,opt}-2\%$	10.7	2052	69.7	7.4	84.5	15.5	65.7
	$w_{w,opt}$	13.3	2023	61.3	2.0	65.3	34.7	77.3
	$w_{w,opt}+2\%$	16.2	1972	60.2	0.6	61.5	38.5	84.9



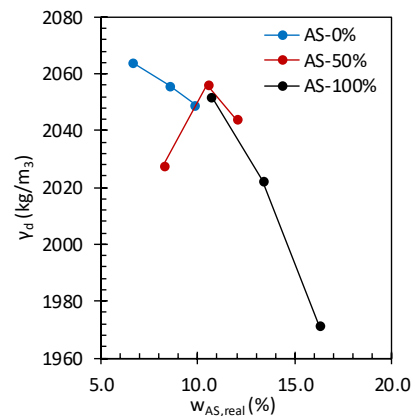
(a)



(b)



(c)



(d)

Figure 6.32 - Evolution of (a) $C_{1,avg}$, (b) $k_{g,avg}$, (c) $C_{100,avg}$, and (d) γ_d as a function of real AS content

6.2.3 Resilient behaviour

Resilient modulus results

All RM results are displayed in function of bulk stress (θ) in the log-log scale. With the aim of providing a better interpretation of this dependency, a regression line has been drawn for each set of data, including the coefficient of determination R^2 .

The positive effect of curing on both reference mixtures (i.e. CDW mixtures with AS-0%) and stabilized CDW aggregates with AA (i.e. mixtures containing AS-50% and AS-100%) is evident in Figure 6.33. In case of CDW-AS-0% mixtures with $w_{w,opt}$ -2%, a significant increment in stiffness was observed passing from 7 to 28 and 60 days of curing, especially for low stress conditions (Figure 6.33.a). The main cause is reasonably attributable to the self-cementing phenomenon induced by particles of cementitious materials with residual pozzolanic reactivity of RC constituent [146], [147], [26], [464]. The addition of water during compaction produced the rehydration of residual unreacted cement particles, which caused new weak bonds and improved the overall mechanical behaviour [148], [465]. The enhancement of stiffness with curing time for CDW mixtures containing AS-50% and AS-100% is attributed to both the self-cementing phenomenon and, in particular, the effects of alkaline activation.

The stiffness improvement from 28 to 60 days was significant: at the intermediate stress condition (i.e. 8th loading sequence, $\theta = 344.6$ kPa), RM increased from 238.5 to 306.1 MPa in case of mixtures containing AS-50% and from 481.8 to 624.1 MPa for CDW-AS-100% mixtures. The behaviour of CDW-AS-50% mixture with $w_{w,opt}$ -2% was unexpected since exhibited higher RM values after 7 days of curing than after 28 days (Figure 6.33.b). The same trend was observed in the region of low θ for CDW-AS-100% specimens containing $w_{w,opt}$ -2% (Figure 6.33.c). These results confirmed the key role of the AS concentration and content on the resilient behaviour of AA stabilized CDW aggregates.

The effect of AS concentration can be clearly appreciated in Figure 6.34, in which RM data recorded on CDW aggregates with $w_{w,opt}$ are reported. The addition of AS-100% induced a significant improvement of stiffness at each curing time. After 7 days (Figure 6.34.a), RM of mixtures containing AS-100% was equal to 267.1 MPa for the lowest stress state (1st loading sequence, $\theta = 82.8$ kPa) and 562.5 MPa for the most severe stress condition (15th loading sequence, $\theta = 689.5$ kPa). For the same two stress conditions, specimen with AS-0% exhibited RM values of 69.2 and 322.0 MPa respectively. The addition of AS-100% induced an excellent stabilization of CDW aggregates, evidenced by the highest RM values showed by CDW-AS-100% mixtures.

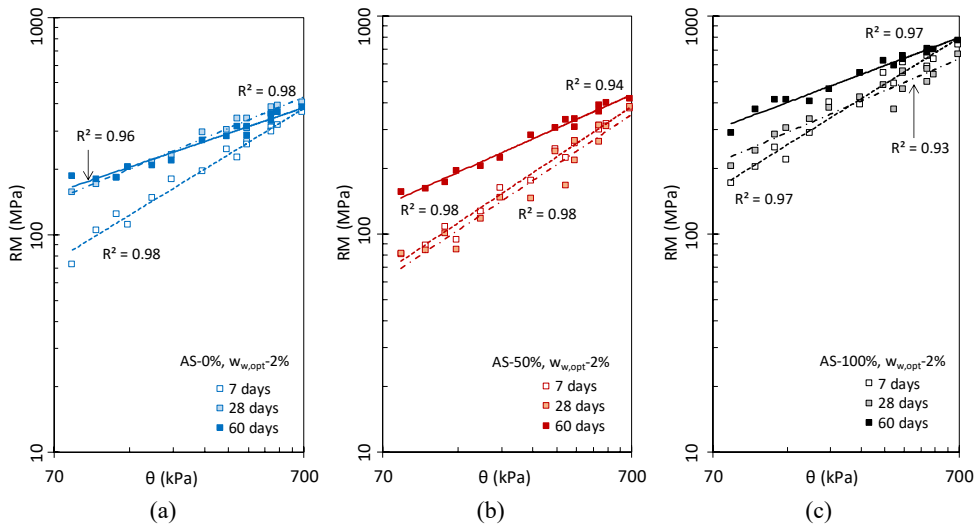


Figure 6.33 - RM of CDW-AS mixtures with $w_{w,opt}=2\%$ after 7, 28, and 60 days of curing, for different AS concentrations: (a) AS-0%, (b) AS-50%, and (c) AS-100%

Conversely, the resilient behaviour of CDW-AS-50% mixtures was similar to that of the reference mixtures (AS-0%). It confirmed that the 50% concentrated AS did not trigger the AA process due to the excessive dilution of the chemical activator, according to observations carried out in Exp. A (Section 6.1.4). After 7 (Figure 6.34.a) and 60 (Figure 6.34.c) days of curing, slightly lower RM values were recorded on mixtures with AS-50% in comparison to the reference un-stabilized mixtures (AS-0%). This behaviour was attributed to the higher amount of AS in the mixtures containing AS-50%, which led to a lower overall stiffness. Although both specimens had the same $w_{w,opt}$, to reach this water content, a different w_{AS} was added depending on the AS concentration (Section 6.2.2). The AS content ($w_{AS,real}$) was equal to 10.5% for AS-50% and 8.5% for AS-0% and that difference likely affected the resilient behaviour of the compacted CDW material. The same consideration is not valid for the AS-100%, since the negative effect of an even greater quantity of $w_{AS,real}$ (13.3%) was largely counterbalanced by the development of a binding phase which improved the mechanical properties.

The influence of water content on the resilient behaviour of granular materials is widely recognized in technical literature [368]. An increment of w_w usually induces a decrease of the resilient modulus [466], [467], [468], [469], [470], [471]. The effects produced by the increment of water content from $w_{w,opt}-2\%$ to $w_{w,opt}+2\%$ on both un-stabilized and alkali-activated CDW mixtures is reported in Figure 6.35 and Figure 6.36.

The comparative analysis of RM values after 28 days of curing (Figure 6.35) highlighted a more marked influence of w_w for the reference mixtures (AS-0%) than for the stabilized

ones. The greater the amount of water, the lower the stiffness of the mixture, consistently with literature [472]. At the intermediate loading condition (i.e. $\theta = 344.6$ kPa), RM decreased from 304.9 to 192.4 MPa when water content increased from $w_{w,opt}-2\%$ to $w_{w,opt}+2\%$.

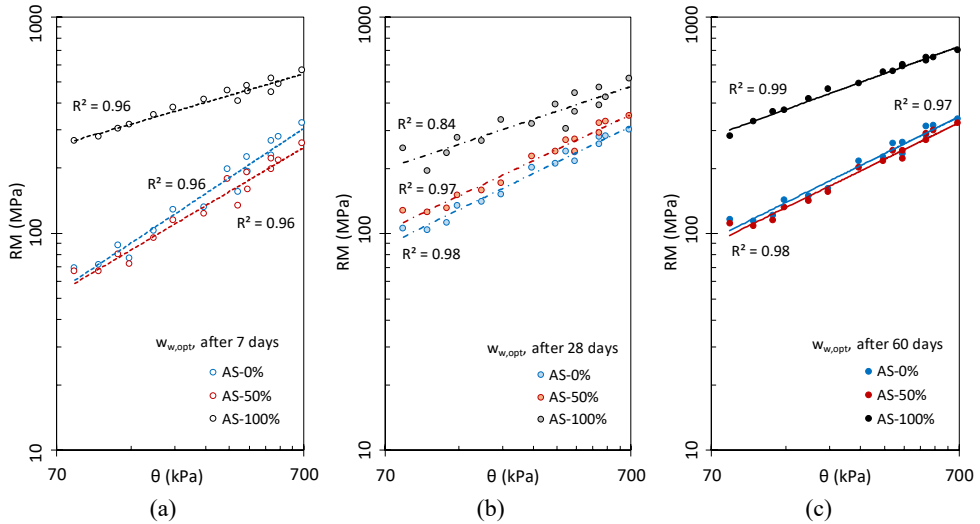


Figure 6.34 - RM of CDW-AS mixtures containing AS in three different concentration (0%, 50%, and 100%) and $w_{w,opt}$, after (a) 7, (b) 28, and (c) 60 days of curing

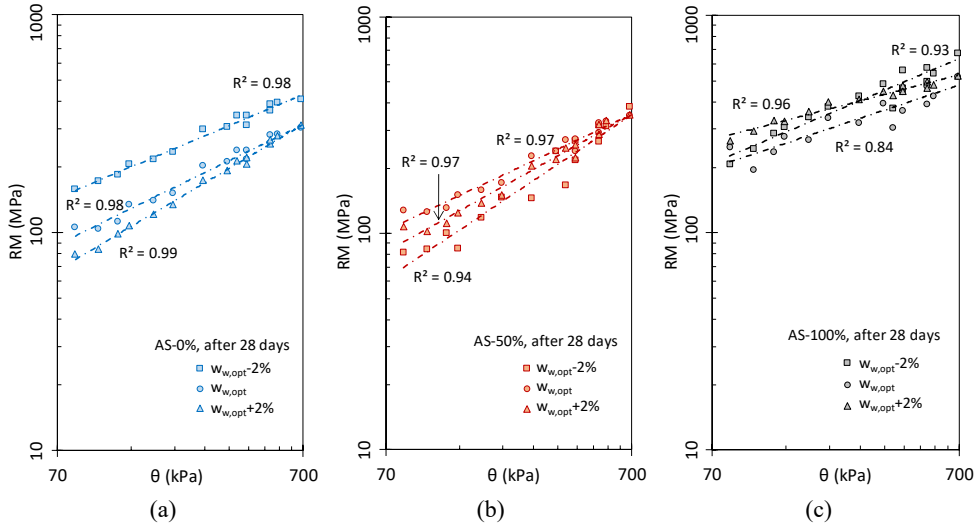


Figure 6.35 - RM of 28-day cured CDW-AS mixtures with three different water contents ($w_{w,opt}-2\%$, $w_{w,opt}$, $w_{w,opt}+2\%$) and (a) AS-0%, (b) AS-50%, (c) AS-100%

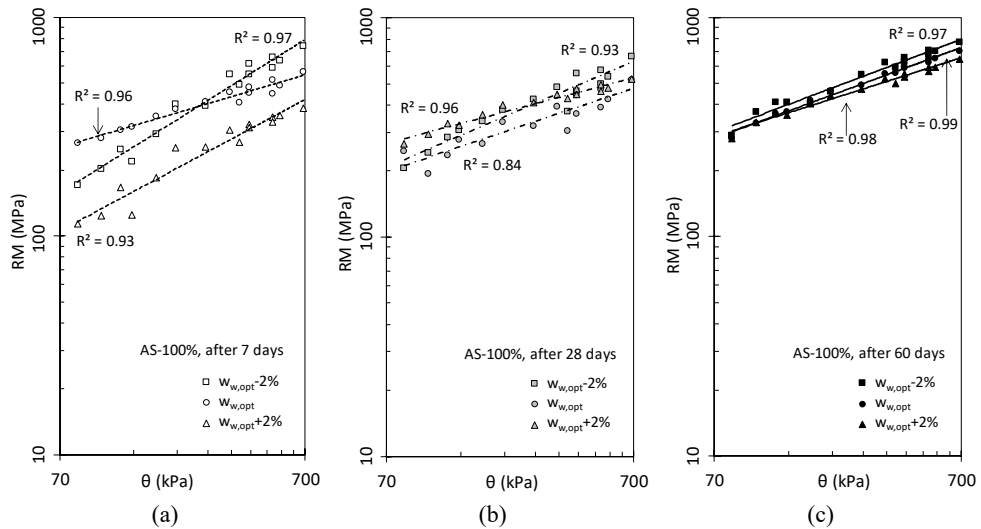


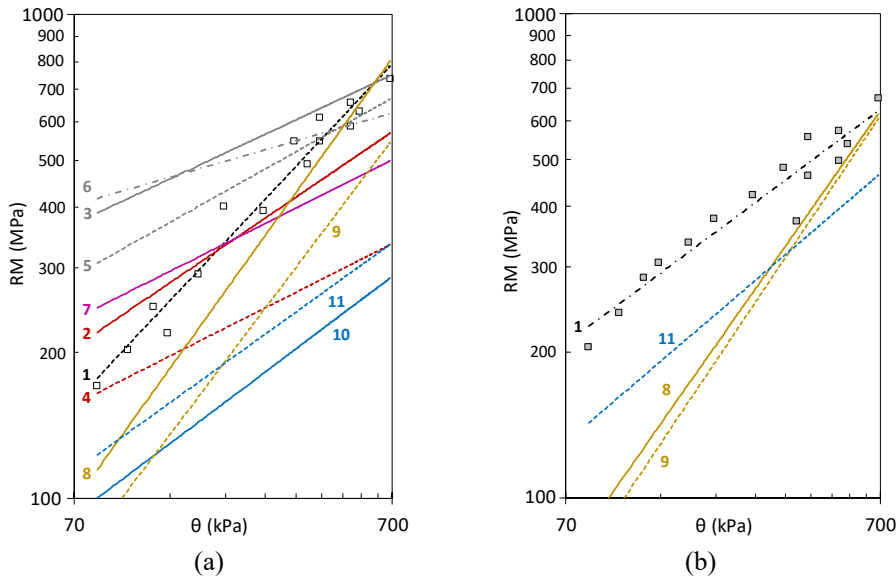
Figure 6.36 - RM of CDW-AS mixtures with AS-100% for three water contents ($w_{w,opt}-2\%$, $w_{w,opt}$, $w_{w,opt}+2\%$) after (a) 7, (b) 28, and (c) 60 days of curing

Mixtures containing AS-50% and AS-100% were less sensitive to moisture variations because of the effect of alkali-activation. In case of CDW-AS-50% mixtures cured for 28 days (Figure 6.35.b), RM with w_w was similar to the reference mixture (AS-0%): at low stress state, the negative effect of the increment of liquid phase (or AS content) was significant, while moving towards higher values of θ , RM tended to converge into a unique value. It suggests that the strong dependency of stiffness on the AS content reduced at high stress conditions. CDW granular materials with the addition of AS-100% (Figure 6.35.c) exhibited a different resilient behaviour depending on the liquid content. After 28 days of curing, mixture with $w_{w,opt}$ (i.e. $w_{AS,real} = 13.3\%$) had the lowest values of RM. In the region of low stress condition, mixtures containing $w_{w,opt}+2\%$ showed higher values of stiffness than those of mixtures with $w_{w,opt}-2\%$. The trend was completely reversed for high stress states ($\theta > 275.6$ kPa, 7th loading sequence). This behaviour suggests that the excess of the AS improved the binding effect and the overall stabilization of the mixture, at least for low stress states. On the other hand, the abundance of liquid phase during compaction generated a solid matrix with more voids which were detrimental for supporting high stresses, thus justifying the lower values of RM in the region of high θ . According to Table 6.15, mixtures with $w_{w,opt}+2\%$ were characterized by an average value of voids equal to 38.5%. Vice versa, mixtures compacted with $w_{w,opt}-2\%$ had an average value of void content of 15.5%. Similarly, the low stiffness of CDW-AS-100% mixtures with $w_{w,opt}$ can be attributed to the moderately high void content ($v = 34.7\%$).

Figure 6.36 displays the evolution of RM of specimens stabilized with AS-100% for different w_w (or w_{AS}). After 7 days, specimens compacted with $w_{w,opt}$ and $w_{w,opt}-2\%$ behaved similarly to the 28-day cured mixture with $w_{w,opt}+2\%$ and $w_{w,opt}-2\%$ previously described. The high void content of CDW mixtures with $w_{w,opt}+2\%$, at low stress states, was not detrimental and the larger amount of liquid phase led to an enhancement of stiffness. In fact, it is supposed that the abundance of the AS produced more geopolymer bonds in the structures. Conversely, at higher loading conditions, the denser structure (i.e. with lower void content) of specimens compacted with $w_{w,opt}-2\%$ was considerably stiffer (i.e. with high RM values) although characterized by a reduced binding matrix (due to the lower w_{AS}).

The most interesting consideration derived from Figure 6.36 is related to the attenuation of the RM differences (caused by w_w) as a consequence of curing time. Longer periods of curing led to a better development of the AA process, which was more extended in mixtures with higher w_{AS} . It can be considered a promising result for real scale applications, since, after an adequate curing time, local variations of the w_{AS} would not significantly affect the stiffness of the stabilized layer made of alkali-activated CDW materials.

Several results concerning the resilient behaviour of recycled aggregates stabilized with ordinary and alternative binders are available in literature. Figure 6.37 shows a comparative analysis between the RM of the stiffest CDW-AS mixture (investigated here) with data obtained on different materials from literature. After 7 days of curing (Figure 6.37.a), the RM of CDW mixtures stabilized with AS-100% and $w_{w,opt}-2\%$ was significantly higher than those indicated by Rout et al. [473] and Zhu [474] concerning natural cohesive soil stabilized with OPC and CKD respectively. At low stress conditions, granular materials including single CDW constituent (BT and RC) stabilized with 10% in mass of alkali-activated BFS [206] and 4% of alkali-activated FA [27] showed higher RM values than the CDW-AS-100% mixture. However, in the region of high θ , differences of stiffness between CDW aggregates stabilized with AS-100% and literature results can be considered negligible. From results of Figure 6.37, it can be concluded that the stabilization with AS-100% led to RM values comparable to those measured on recycled aggregates stabilized with high-performance geopolymeric binder based on BFS and FA. Moreover, this stabilization technique seemed to be more effective than the stabilization of the similar recycled materials with the addition of OPC and CKD investigated by Bassani et al. [26]. Analogous considerations can be drawn from the comparison between RM values after 28 days of curing, shown in Figure 6.37.b.



- Notes: (1) CDW-AS-100% with $w_{w,opt}=2\%$ ($w_{AS,real}=10.7\%$)
 (2) BT aggregates stabilized with 10% of alkali-activated BFS [206]
 (3) RC aggregates stabilized with 10% of alkali-activated BFS [206]
 (4) BT aggregates stabilized with 4% of alkali-activated FA [27]
 (5) RC aggregates stabilized with 4% of alkali-activated FA [27]
 (6) RC aggregates stabilized with 4% of OPC [24]
 (7) RA aggregates stabilized with 4% of OPC [195]
 (8) unselected CDW (0-25mm) stabilized with 2% of OPC [26]
 (9) unselected CDW (0-25mm) stabilized with 10% of CKD [26]
 (10) CH soil (ASTM D2487 [475]) with 6% of lime and 3% of OPC [473]
 (11) A-2-4 soil (AASHTO M [476]) stabilized with 15% of CKD [474]

Figure 6.37 - Comparative analysis between RM of CDW-AS-100% mixtures ($w_{w,opt}=2\%$) and literature results on stabilized recycled and natural granular materials after (a) 7 and (b) 28 days of curing

MEPDG modelling

According to Section 5.2.4, RM results were fitted through the generalized model of MEPDG (Eq. 22). Regression parameters k_1 , k_2 , and k_3 were calibrated with the least square method, and their values are summarized in Table 6.16. In order to evaluate the fitting procedure, Table 6.16 includes also the standard error ratio (S_e/S_y) and the adjusted determination coefficient (R^2_{adj}). S_e/S_y ratios were always below 0.25, attesting the excellent goodness-of-fit of the calibration coefficients [372]. The values of R^2_{adj} were close to the unity, confirming again the excellent quality of the fitting.

Table 6.16 - Results of MEPDG model fitting

AS concentration	Water content	Curing	k_1	k_2	k_3	S_e/S_y	R_{adj}^2
AS-0%	$w_{w,opt}-2\%$	7	1027	0.61	0.20	0.11	0.99
		28	1809	0.53	-0.28	0.05	1.00
		60	1822	0.46	-0.20	0.15	0.98
	$w_{w,opt}$	7	669	0.63	0.54	0.16	0.98
		28	1128	0.62	-0.27	0.07	0.99
		60	1196	0.65	-0.29	0.08	0.99
	$w_{w,opt}+2\%$	7	570	0.80	0.18	0.09	0.99
		28	877	0.71	-0.12	0.05	1.00
		60	690	0.83	-0.18	0.04	1.00
AS-50%	$w_{w,opt}-2\%$	7	892	0.69	0.21	0.11	0.99
		28	753	0.59	0.72	0.17	0.97
		60	1686	0.57	-0.24	0.06	1.00
	$w_{w,opt}$	7	649	0.54	0.53	0.16	0.97
		28	1289	0.62	-0.28	0.11	0.99
		60	1119	0.62	-0.19	0.10	0.99
	$w_{w,opt}+2\%$	7	557	0.76	0.45	0.13	0.98
		28	1038	0.74	-0.27	0.12	0.99
		60	802	0.81	-0.33	0.11	0.99
AS-100%	$w_{w,opt}-2\%$	7	2182	0.54	0.34	0.18	0.97
		28	2381	0.28	0.68	0.07	0.99
		60	3537	0.38	0.12	0.15	0.98
	$w_{w,opt}$	7	2787	0.23	0.35	0.14	0.98
		28	2124	0.21	0.69	0.24	0.94
		60	3330	0.37	0.09	0.10	0.99
	$w_{w,opt}+2\%$	7	1418	0.49	0.18	0.25	0.94
		28	2970	0.23	0.20	0.16	0.97
		60	3275	0.30	0.16	0.11	0.99

The k_1 parameter, which is proportional to the stiffness of material, generally increased with curing time. With the exception of CDW-AS-50% at $w_{w,opt}-2\%$ and CDW-AS-100% at $w_{w,opt}$ mixtures, k_1 became greater passing from 7 to 28 days of curing. Furthermore, the increment of curing period induced a stiffening of the materials, since k_1 was always higher after 60 days of curing than after 7 days.

Stabilized mixtures with AS-100% showed k_1 values approximately twice of those obtained on CDW aggregates stabilized with AS-50% and AS-0%. When the amount of w_w increased from 6.6% ($w_{w,opt}-2\%$) to 10.6% ($w_{w,opt}+2\%$), a systematic reduction of k_1 coefficients was observed, in line with results of Nazzal and Mohammad [477].

The regression coefficient k_2 specifies the sensitivity of the RM to the stress state expressed in terms of bulk stress (θ). Since k_2 was always positive, it is reasonable to suppose that an increase of θ produced a hardening effect on the material, independently of the AS content and concentration. This stress-hardening behaviour is typical of unbound and stabilized granular materials used in base and subbase layers of road pavements [478], [479]. Lower values of k_2 were shown by the stiffest mixtures (i.e. those containing the AS-100%), consistently with the fact that the higher the stiffness, the lower the stress-state dependency. In case of AS-0%, k_2 generally increased with the increment of water content from $w_{w,opt}-2\%$ to $w_{w,opt}+2\%$. These results suggest that the stress-state dependency of the un-stabilized material tended to increase with the amount of water in the mixtures. Conversely, in case of AS-50%, no defined evolution of k_2 parameter with investigated variables (AS concentration, w_w , and curing time) was identified. In fact, k_2 assumed values ranging from 0.57 to 0.69 with $w_{w,opt}-2\%$, and from 0.54 to 0.62 when the water content was optimal. Values slightly higher were observed in case of $w_{w,opt}+2\%$ (0.74÷0.81).

Similarly, k_3 parameter was characterized by no defined trends depending on the investigated variables. Positive values of the exponent of the octahedral shear stress (k_3) indicate a shear-hardening behaviour, while negative values point out a lowering of RM when the τ_{oct} increases, i.e. a shear-softening behaviour [480]. The fitting of RM results as per the MEPDG model (Eq. 22) led to k_3 values always positive for 7-day cured mixtures, independently of the AS concentration and w_w . Specimens cured for longer times (28 and 60 days) with AS-0% and AS-50% showed a shear-softening behaviour, since values of k_3 were negative in most cases. Conversely, a general shear-hardening behaviour was evident for CDW-AS-100% mixtures after each curing time. Specifically, k_3 assumed values between 0.18 and 0.35 after 7 days, slightly increased after 28 days, and tended to zero after 60 days of curing.

Table 6.17 lists values of MEPDG regression coefficients of Eq. 22 obtained for un-stabilized [481], [164], [482], [479] and stabilized granular materials [26], [483], [318]. Before comparing results, it is worth remembering that fitting parameters reported in Table 6.17 and related to un-stabilized materials was obtained immediately after compaction (with the exception of CDW aggregates investigated after 30 days of curing by Farias et al. [481]). Conversely, literature on k_1 , k_2 , k_3 values associated to stabilized granular material is referred to 28-day cured specimens. Substantial differences can be appreciated between un-stabilized and stabilized materials: if for un-stabilized materials k_1 is commonly below 1500, the stabilization induced an increment of RM, with k_1 values usually higher than 1000. k_2 and k_3 coefficients are more variable and no defined trend can be observed. In details, k_2 is positive and very close to zero for stabilized soils investigated by Solanki et al. [318]. Contrarily, k_3 is generally negative (in the range

between -3.44 and -0.09), with the exceptions of CDW aggregates tested by Farias et al. [481], and the A-2-4 and A-2-6 soils stabilized with 3% of OPC by MacDonald [483]. According to this literature, it can be concluded that mixtures with AS-0% and AS-50% were characterized by k_1 parameters similar to those of un-stabilized materials (877÷1809 for AS-0%, 753÷1289 for AS-50%), while CDW-AS-100% specimens showed k_1 parameters more similar to values of stabilized materials (in the range 2124÷2970). The same mixtures (CDW-AS-100%) were characterized by k_2 values ranging between 0.21 and 0.28 in accordance to literature. Conversely, k_3 positive values were rarely observed for stabilized materials. These comparisons support the hypothesis that the addition of the AS-100% to CDW aggregates successfully generated the alkali-activation of fines particles, that acted as a binder of coarser particles, stabilizing the overall mixture.

Table 6.17 - Fitting parameters (k_1 , k_2 , k_3) from literature

Author	Material	k_1	k_2	k_3
Farias et al. [481]	CDW aggregates after 30 days	1302	0.01	1.25
Dong and Huang [164]	RA aggregates (0÷19mm)	1450	0.98	-0.09
Hanifa et al. [482]	RC aggregates (0÷25 mm)	1008÷1263	0.82÷0.85	-0.22÷-0.20
Hossain [479]	A-1-b ¹ soil	954	0.46	-2.52
	A-2-4 ¹ soil	483÷1428	0.06÷0.65	-2.84÷-0.88
	CDW with 2%OPC (28 days)	1117	1.66	-2.88
Bassani et al. [26]	CDW with 10%CKD (28 days)	1014	1.84	-3.44
	A-2-6 ¹ soil with 3%OPC (28 days)	1465÷2953	0.47÷1.01	-0.11÷0.22
MacDonald [483]	A-2-4 ¹ soil with 3%OPC (28 days)	2394÷2913	0.39÷0.77	-0.09÷0.57
	A-4 ¹ soil with 9%lime (28 days)	8462	0.01	-1.93
Solanki et al. [318]	A-4 ¹ soil with 10%FA (28 days)	3705	0.02	-1.23
	A-4 ¹ soil with 10%CKD (28 days)	3725	-0.02	-0.71

Note: (1) according to AASHTO M 145 classification [476]

6.2.4 Strengths

Unconfined compression strength

Results of UCS tests are listed in Figure 6.38 in function of the AS concentration, the water content, and the curing time. UCS values were averaged between two measurements carried out on:

- one specimen used for RM determination and then submitted to UCS test;
- one specimen exclusively prepared for the UCS test.

Considering that RLT is a non-destructive test and negligible differences between two measurements were recorded, both values have been averaged into a unique result.

From Figure 6.38, it is evident the effect of the AS concentration on strength development. Specimens containing AS-100% showed highest UCS values, around 5 and 10 times greater than those of mixtures with AS-50% and AS-0% respectively. After 7 days of curing, UCS reached 0.51 MPa with $w_{w,opt}+2\%$, 1.72 MPa with $w_{w,opt}$, and 2.99 MPa with $w_{w,opt}-2\%$. The latter result was consistent with the range of UCS values required by the Italian technical specifications [313] for stabilized natural materials to be employed in bases and subbases after 7 days of curing (2.50÷4.50 MPa). For longer curing times, mechanical strengths tended to increase achieving the maximum value of 4.05 MPa after 60 days for mixtures containing $w_{w,opt}-2\%$.

Table 6.18 summarizes the values of UCS after 7- and 28-day stabilized recycled and natural materials from literature. CDW-AS-100% mixtures with $w_{w,opt}-2\%$ exhibited comparable values of UCS to those recorded on single CDW constituents (RC, RA, or BT) stabilized with CKD and OPC by Arulrajah et al. [199], Behiry [193], and Mohammadinia et al. [24]. The stabilization of CDW aggregates with AS-100% induced higher compressive strengths than those observed by Bassani et al. [26] on CDW aggregates stabilized with OPC after both 7 and 28 days of curing. Recycled aggregates stabilized with 10% of CDK of the same authors (Bassani et al. [26]) exhibited UCS values in line with the CDW-AS-100% mixtures investigated here. After 7 days of curing, the addition of AS-100% (in the corresponding quantity of $w_{w,opt}$ and $w_{w,opt}-2\%$) induced a binding matrix which led to higher compressive strengths than the stabilization of both CDW and natural aggregates with alkali-activated FA obtained by Cristelo et al. [28]. Vice versa, after 28 days, mixtures studied by Cristelo et al. [28] were characterized by higher compressive strengths.

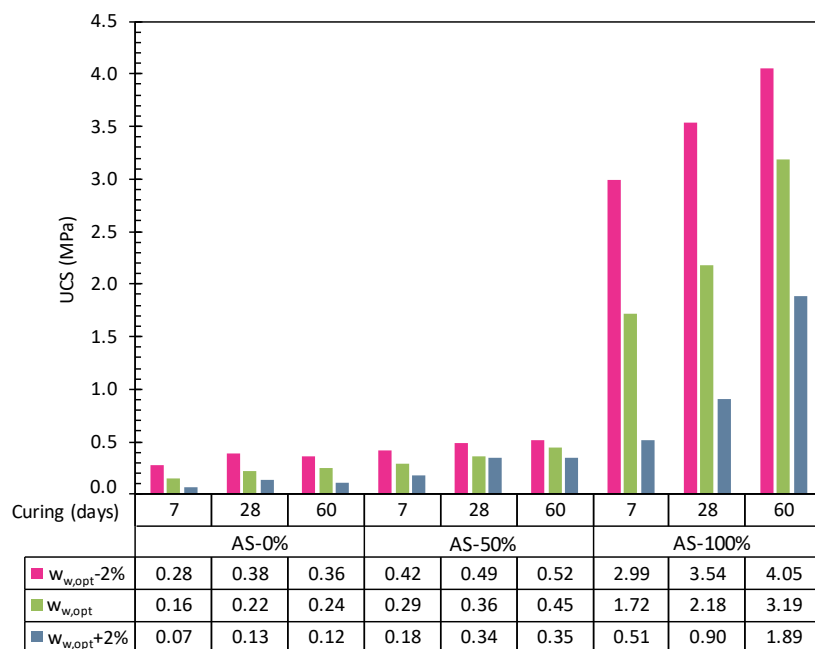


Figure 6.38 - UCS results of CDW-AS mixtures including three different AS concentrations after 7, 28, and 60 days of curing

Data from literature listed in Table 6.18 suggests that UCS recorded on CDW aggregates with AS-100% were within the ranges reported by Del Rey et al. [25] concerning the stabilization of recycled aggregates with OPC. Moreover, the comparison with NGM and soils stabilized with both ordinary [484], [485], [486] and alternative [487] binders revealed comparable results in terms of UCS.

It is worth noting that when CDW aggregates were mixed with a AS in the corresponding amount of $w_{w,opt}+2\%$, UCS values were moderately lower than results from literature. In this case, the compressive strength increased significantly only after 60 days of curing, achieving an average value of 1.89 MPa. The addition of the AS-50% did not determine significant strength developments. In fact, UCS values were approximately one fifth of those obtained with AS-100%. On the contrary, highly concentrated activators are beneficial for strength development [294], [415], [307], [308], [488], [489]. According to Komljenovic et al. [490], higher amounts of dissolved silicon in the aqueous solution induces an increment of reaction kinetic, which leads to higher strengths [237]. Moreover, the lowering of pH, as a consequence of the AS dilution, decreased the dissolution of aluminosilicates, reducing the amount of silica and alumina species for the AA process development.

Results of Figure 6.38 highlight the negative effect of an AS content increment in the material. The UCS systematically decreased when passing from $w_{w,opt}-2\%$ to $w_{w,opt}+2\%$, for each AS concentration. This trend was more empathized in AS-100% mixtures. For instance, after 28 days of curing, the UCS equal to 3.54 MPa recorded on mixtures with $w_{w,opt}-2\%$ decreased to 2.18 MPa with $w_{w,opt}$, and dropped to 0.90 MPa with $w_{w,opt}+2\%$. An excessive amount of liquid phase, which for $w_{w,opt}+2\%$ corresponded to a $w_{AS,real}$ of 16.2%, did not guarantee an adequate compaction of the material. In fact, the average value of void content of these mixtures, greater than 38% (Table 6.15), influenced the capability of loading support. The denser CDW-AS-100% mixture containing $w_{w,opt}-2\%$, characterized by a void content equal to 15.5%, was able to reach almost four times the UCS of the corresponding mixture with $w_{w,opt}+2\%$. Furthermore, few literature contributions indicated that alkali-activated materials are incompatible with water curing [491]. Hence, the additional water ($w_{w,opt}+2\%$) might have contributed to a reduction of the geopolymerization rate and, consequently, to an overall strength lowering.

Table 6.18 - UCS results from literature related to stabilized granular materials (recycled and natural) with ordinary and alternative binders

Author	Materials	UCS (MPa)	
		7-day cured	28-day cured
Arulrajah et al. [199]	RA with 30%CKD (0÷12 mm)	2.5	-
	RC with 30%CKD (0÷20 mm)	2.5	-
	RC with 30%FA (0÷20 mm)	0.5	-
	BT with 30%CKD (0÷20 mm)	2.0	-
Bassani et al. [26]	CDW with 2%OPC (0÷25 mm)	1.6	2.6
	CDW with 2%OPC (0÷8 mm)	1.4	1.8
	CDW with 10%CKD (0÷25 mm)	2.3	3.1
	CDW with 10%CKD (0÷8 mm)	2.0	3.1
Behiry [193]	RC with 5%OPC	2.6	3.5
Cristelo et al. [28]	CDW with 20%FA-AA	1.6	6.1
	NGM with 20%FA-AA	1.0	4.5
Del Rey et al. [25]	CDW with 3%OPC (0÷40 mm)	2.5÷3.5	3.1÷4.2
	CDW with 3%OPC (0÷8 mm)	2.6÷3.4	3.3÷4.4
Kien et al. [194]	BT with 5%OPC	-	0.8
	RC with 5%OPC	-	1.5
	NGM with 5%OPC (0÷5 mm)	-	1.0
Mohammadinia et al. [24]	BT with 2%OPC (0÷20 mm)	2.9	3.1
	RC with 2%OPC (0÷20 mm)	2.8	3.3
	RA with 2%OPC (0÷20 mm)	3.1	4.2
Biswal et al. [484]	GW ¹ soil with 3%OPC	2.5	2.9
	SW ¹ with 3%OPC	2.8	3.9
Lim and Zollinger [485]	NGM with 4%OPC	3.2÷4.3	3.8÷7.0
Piratheepan et al. [487]	Soil with BFS and lime	-	3.4
Davis et al. [486]	Weak soil + 4%OPC (0÷25 mm)	1.2÷3.0	-

Note: (1) according to ASTM D2487 classification [475]

The strength development is mainly attributed to the alkaline reactions between the liquid activator and the finer particles of CDW materials. However, considering the presence of highly-crystalline raw powders and the curing at room temperature, the solidification of sodium silicate may be regarded partially responsible for the increase of strength. Some studies indicated that the sodium silicate can be used to solidify clayey soils as per injection method [492], [493] and as a soil stabilizer [494], [495]. Allahverdi and Kani [29] stated that sodium silicate provides a strong interface between un-reacted particles and the gel matrix, thus contributing to the overall mechanical strength. Nevertheless, the presence of sodium silicate is considered pivotal since supplies soluble silica species (Si-O-), which promotes the formation of geopolymeric structures [219], [309]. Robayo-Salazar et al. [328] proved that the increase of mechanical strength of BT and RC materials is favoured by the addition of sodium silicate. However, the authors recorded a non-negligible mechanical strength development (up to 10 MPa) also in sodium silicate-free specimens, even when cured at room temperature. They attributed the strength development to the NaOH-activation of the waste particles.

Accordingly, the development of UCS in CDW-AS mixtures (investigated here) was correlated to the synergic effect of sodium silicate solidification and AA of the finest fraction. The latter hypothesis is supported by the increment of mechanical strength from 7 to 60 days of curing. Hence, the strength development during time suggested an evolution of both geopolymerization and hydration reactions triggered by the AS addition. In case of AS-100%, UCS increased by 35%, 86%, and 267% for mixtures containing $w_{w,opt}-2\%$, $w_{w,opt}$, and $w_{w,opt}+2\%$ respectively when passing from 7 to 60 days of curing. For CDW-AS-50% mixtures, the increment of UCS from 7 to 60 days was less marked than CDW-AS-100% (+25% for $w_{w,opt}-2\%$, +53% for $w_{w,opt}$, +98% for $w_{w,opt}+2\%$). The greatest intensification of strength of mixtures with $w_{w,opt}+2\%$ is related to the higher content of AS, which increased the amount of binding phase.

The self-cementing phenomena characterizing CDW materials and already observed on RM results (Section 6.2.3), were similarly noticeable in the UCS characterization. Mixtures containing only water (AS-0%) exhibited an enhancement of compressive strength from 7 to 60 days of curing (from 0.28 to 0.36 MPa for $w_{w,opt}-2\%$, from 0.16 to 0.24 MPa for $w_{w,opt}$, from 0.07 to 0.12 MPa for $w_{w,opt}+2\%$). Analogously Bassani et al. [26] attributed to self-cementing phenomena the huge improvement of UCS of un-stabilized CDW aggregates (0÷8 mm) from 0.2 MPa after 7 days of curing to 1.9 MPa after 365 days. Results of un-stabilized CDW aggregates (AS-0%) were in line with UCS values obtained by Arulrajah et al. [496] on specimens containing separately RC, BT, and RA. Conversely, RC materials investigated by Gabr and Cameron [161] and cured for 28 days without any binders exhibited higher UCS values (0.69÷0.88 MPa) than the CDW-AS-0% mixtures (UCS = 0.13÷0.38 MPa for $w_{w,opt}-2\%$).

Indirect tensile strength

Figure 6.39 summarizes the results of ITS test. A similar trend to that of UCS (Figure 6.38) is evident, hence all considerations carried out can be confirmed. In this case, the differences in mechanical proprieties due to the AS concentration were even more pronounced. Mixtures with AS-100% showed ITS values averagely 15 and 9 times greater than those recorded on mixtures with AS-0% and AS-50% respectively. CDW aggregates compacted with AS-100% reached excellent results. After 7 days of curing, the two most performing mixtures (AS-100% with $w_{w,opt}-2\%$ and $w_{w,opt}$) exceeded the minimum threshold of 0.25 MPa indicated by the Italian technical specifications for cement-stabilized granular materials to be used in subbase layers [313]. The CDW-AS-100% mixture with $w_{w,opt}$ demonstrated a comparable ITS to that recorded by Behiry [193] on RC aggregates stabilized with 3% of OPC (after 7 days of curing), while the same mixture, but with $w_{w,opt}-2\%$, exceeded of twice that literature data. After 28 days of curing, the ITS of AS-100% mixtures reached values of 0.71 and 0.39 MPa for $w_{w,opt}-2\%$ and $w_{w,opt}$ respectively. The totally concentrated AS acted as an activator of the alkaline reactions, generating new bonds in the materials. This binding phase coating coarser grains was able in supporting adequate tensile stress.

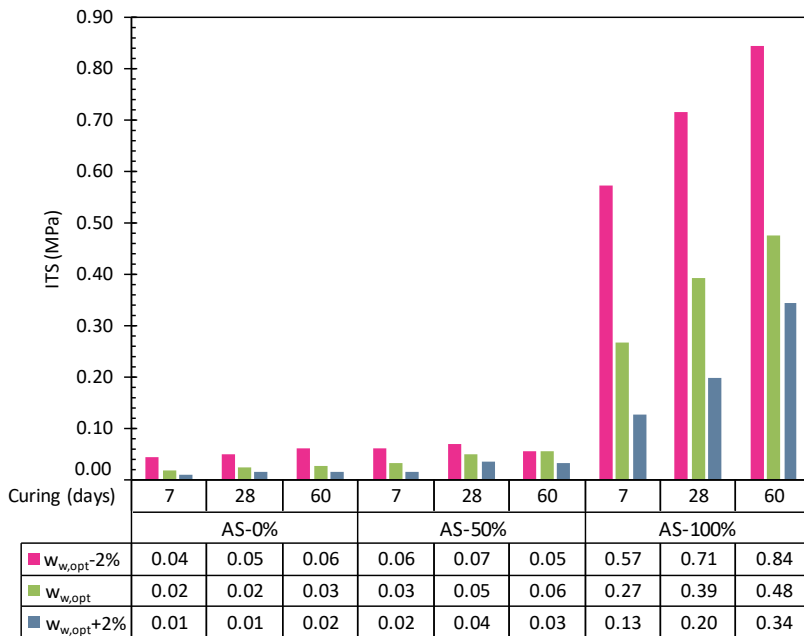


Figure 6.39 - ITS results of CDW-AS mixtures including three different AS concentrations after 7, 28, and 60 days of curing

The effectiveness of this stabilization technique is demonstrated by the fact that recorded strengths were comparable to literature data related to both recycled and natural aggregates stabilized with OPC. For instance, Kien et al. [194] measured the ITS on 28-day cured BT, RC, and a natural quarry material stabilized with 10% of OPC, obtaining values of 0.35 MPa, 0.77 MPa and 0.58 MPa respectively. Recycled granular materials including 50% of RC and 50% of BT investigated by Taherkhani and Amani [497] exhibited ITS values of 0.75 MPa and 1.33 MPa after 28 days of curing with the addition of 3% and 10% of OPC respectively.

The mixture with AS-100% and $w_{w,opt}+2\%$ did not comply the requirement of the Italian technical specification. In fact, the addition of an excessive quantitative of AS was detrimental for the ITS development. Results of Figure 6.39 give evidence of this drastic reduction of tensile strength with the increase of w_w (or w_{AS}). CDW aggregates compacted with AS-100% and cured for 7 days decreased the ITS from 0.57 to 0.13 MPa when passing from a real AS content of 10.7% (corresponding to $w_{w,opt}-2\%$) to 16.2% (corresponding to $w_{w,opt}+2\%$). A decrement of around 70% of ITS from the lowest amount of liquid phase ($w_{w,opt}-2\%$) to the greatest one ($w_{w,opt}+2\%$) was also recorded on mixtures with AS-50% and AS-0%.

Once again, the increase of curing time was beneficial for the strength development, both in mixtures with the AS and in those containing only water. Recycled aggregates treated with AS-100% and $w_{w,opt}$ ($w_{AS,real} = 13.3\%$) exhibited an improvement of 47% of ITS passing from 7 to 28 days of curing, and of 21% passing from 28 to 60 days of curing. As already discussed for UCS results, the enhancement of the mechanical properties over time was attributed to the development of hydration and alkali-activation reactions. Also the ITS of mixtures with AS-0% and $w_{w,opt}$ increased with curing time. Specifically, these mixtures exhibited an improvement of ITS of 31% and 11% when passing from 7 to 28 and from 28 to 60 days of curing. In this case, the self-cementing phenomenon was considered as the main cause of this moderate increment of strength.

6.2.5 FESEM and EDS analysis

Figure 6.40 depicts FESEM images of a fragment of a specimen containing only water (AS-0%) in the optimal amount ($w_{w,opt}$), while the morphology of a sample with the AS-50% is shown in Figure 6.41. It is evident a similarity in the two microstructures: CDW particles of different dimensions were recognizable at lower magnifications, while a poorly compacted structure with voids of different sizes was detectable at higher magnifications. Conversely, the microstructure of CDW-AS-100% mixtures with $w_{w,opt}$ (Figure 6.42) appeared denser and compact. In this case, some micro-cracks were visible in both magnifications, which typically occur in geopolymers [498], [499], [500] and are

caused by internal stresses of glassy geopolymer arisen during the hardening phase [501]. However, these micro-defects did not compromise the structural integrity of the materials, as confirmed by mechanical properties previously commented. Figure 6.43 compares two magnifications of specimens with AS-0% and AS-100% compacted at $w_{w,opt}$. A well faceted uncoated particle of material containing only water (AS-0%) gives no evidences of binding phases (Figure 6.43.a). Conversely, Figure 6.43.b shows a particle surrounded by a continuous rough coating, identifiable in the alkali-activated product induced by the addition of AS-100%.

To confirm this hypothesis from a chemical point of view, EDS analyses were carried out on different areas of CDW-AS-100% fragments. Table 6.19 summarizes the elemental composition (in terms of percentage Si, Na, Al, Ca) of four different samples.

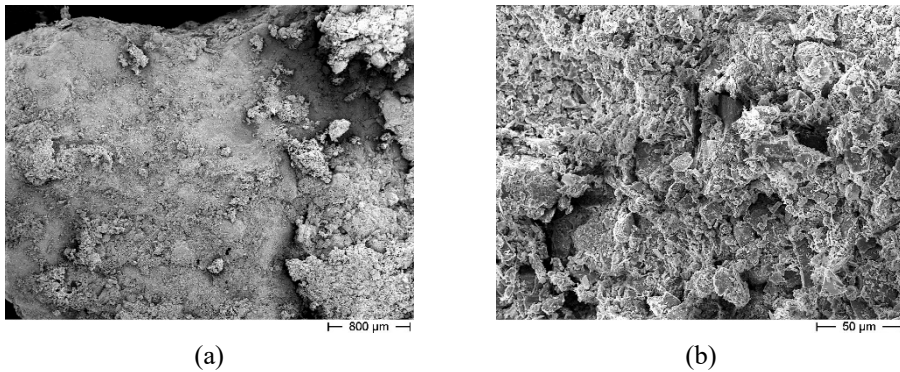


Figure 6.40 - FESEM images of CDW sample prepared with AS-0% and $w_{w,opt}$: (a) 30x and (b) 500x magnification

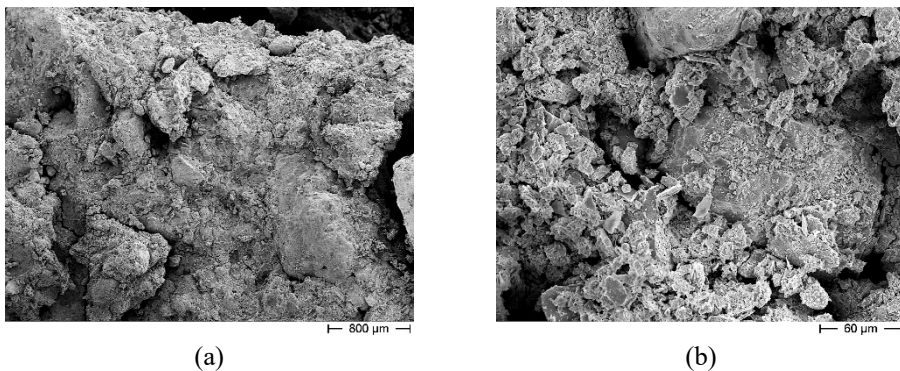


Figure 6.41 - FESEM images of CDW sample prepared with AS-50% and $w_{w,opt}$: (a) 30x and (b) 400x magnification

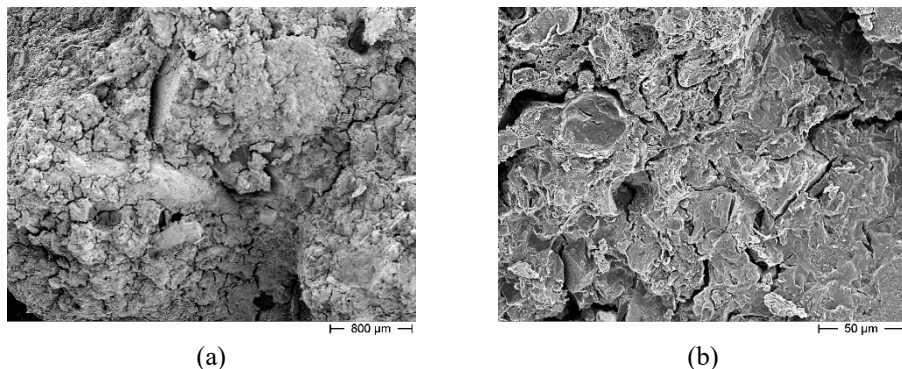


Figure 6.42 - FESEM images of CDW sample prepared with AS-100% and $w_{w,opt}$: (a) 30x and (b) 500x magnification

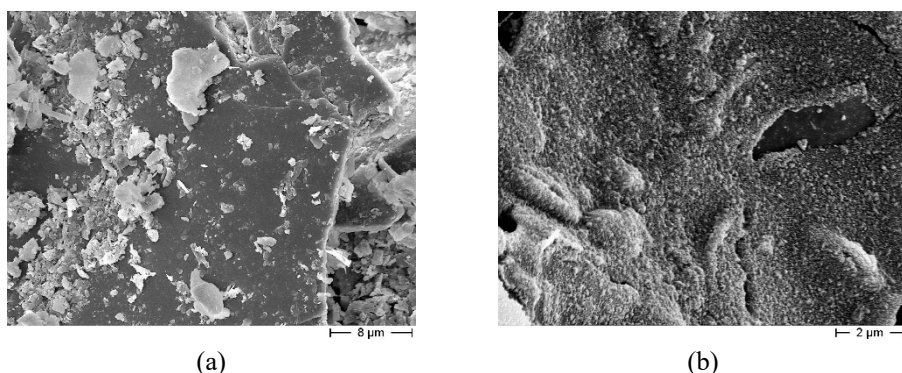


Figure 6.43 - FESEM images of CDW sample prepared with (a) AS-0% and (b) AS-100%, both compacted at $w_{w,opt}$

For each fragment, two different zones were analysed: (1) a clearly identifiable particle of aggregate and (2) the surrounding coating layer, in which the presence of alkali-activated binder was hypothesized. Results of EDS analysis suggest that in the binding zones there was an abundance of Na in comparison to the primary particle of aggregates. In these zones, the Na/Si molar ratio was in the range $0.8 \div 1.5$, which is consistent with the Na/Si molar ratio of the AS-100% equal to 1.3 (Section 4.3). Moreover, Al and Ca elements were systematically detected on different coating zones, suggesting a preferential dissolution of these ions from aggregate particle, as a consequence of the alkaline attack. Chemical results of Table 6.19 confirm that the continuous sodium silicate-based coating likely derived from the partial alkaline reaction between the AS-100% and finer particles of CDW aggregates.

Table 6.19 - Results of EDS analysis coupled with FESEM observations

Sample	Zone	Element ¹ (%)				Ratios		
		Si	Na	Al	Ca	Na/Si	Si/Al	Al/Na
1	aggregate	14.28	0.46	8.52	n.d. ²	0.03	1.68	18.52
	binder	8.34	7.28	2.04	1.40	0.87	4.09	0.28
2	aggregate	44.98	1.05	0.57	0.47	0.02	78.91	0.54
	binder	11.42	9.08	1.98	2.03	0.80	5.77	0.22
3	aggregate	13.20	0.71	9.02	n.d. ²	0.05	1.46	12.70
	binder	6.27	9.27	1.62	2.35	1.48	3.87	0.17
4	aggregate	17.19	2.89	15.28	n.d. ²	0.17	1.13	5.29
	binder	8.28	11.88	2.26	2.61	1.43	3.66	0.19

Notes: ⁽¹⁾ reported only elements of interest, others were also present (C, O, Mg, K, Fe)

⁽²⁾ n.d. = non-detected

FESEM images of Figure 6.44 and Figure 6.45 depict fragments of specimens containing AS-100% with $w_{w,opt}-2\%$ and $w_{w,opt}+2\%$ respectively. The excess of AS content led to a widespread porosity in the microstructure (Figure 6.45). Conversely, the morphology of the sample prepared with $w_{w,opt}-2\%$ appeared entirely compacted with no evidences of porosity.

The characteristics of the microstructures observed through FESEM were consistent with the mechanical properties measured on cured specimens: (1) only the AS-100% was able in producing a binding matrix around grains, (2) the excessive amount of liquid phase added during compaction negatively affected the strength and the stiffness of the overall mixture.

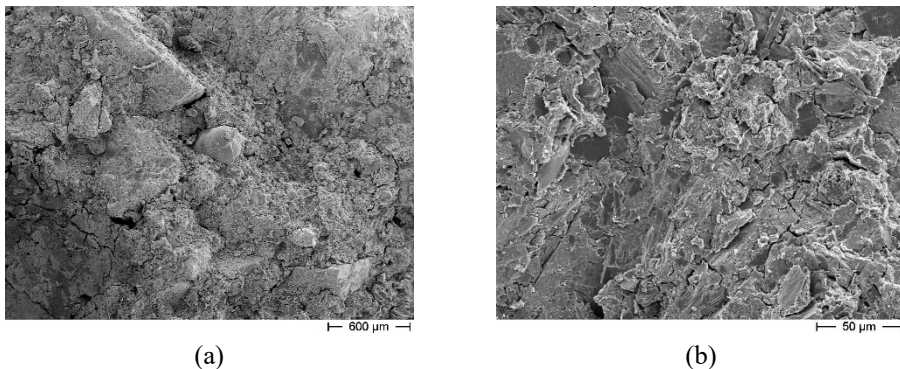


Figure 6.44 - FESEM images of CDW sample prepared with AS-100% and $w_{w,opt}-2\%$: (a) 40x and (b) 500x magnification

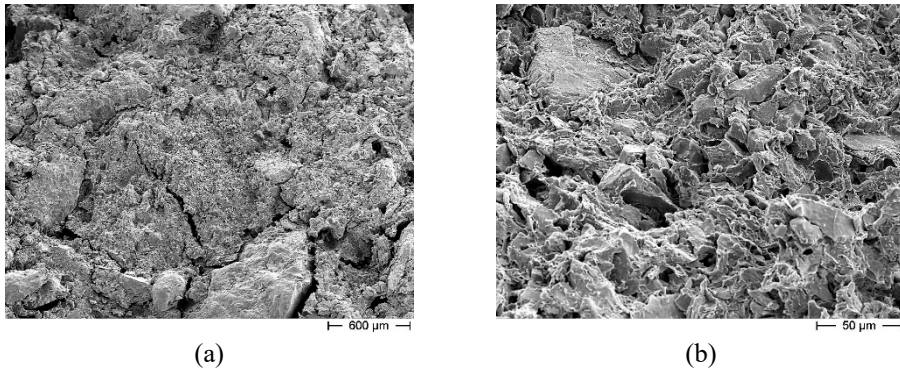


Figure 6.45 - FESEM images of CDW sample prepared with AS-100% and $w_{w,opt}+2\%$: (a) 40x and (b) 500x magnification

6.3 Durability of stabilized CDW-AS mixtures

This section evaluates the mechanical properties of CDW-AS-100% mixtures subjected to F/T degradation. With the aim of comparing the durability of these mixtures with an ordinary material typically employed in road bases and subbases (Section 3.2.3), a NGM stabilized with OPC was submitted to the same degradation process. Both CDW aggregates and NGM were optimized in terms of quantity of liquid content to be added during compaction. Results of compaction and workability properties are reported in this section, as well as the evolution of mechanical properties (in terms of RM, UCS, and ITS) depending on the F/T degradation severity level.

6.3.1 Compaction properties of mixtures

The compaction study of Exp. B2 involved the use of the GSC only. In line with Proctor test, the adopted approach envisaged the compaction of several specimens with different w_{AS} for identifying the optimal content corresponding to the greatest values of workability and dry density. The results of GC on CDW-AS-100% mixtures are summarized in Figure 6.46. It is evident that $w_{AS} = 11\%$ maximized both k_g and γ_d , consistently with results of Exp. B1 (Section 6.2.2). Hence, 11.0% was selected as optimum value of AS to be added during compaction for preparing cylindrical specimen of CDW aggregates.

In case of NGM-OPC mixtures, the optimal quantity of water ($w_{w,opt}$) was selected on the basis of results of Figure 6.47. With a water content of 6.5%, all compaction parameters were maximized, as well as the γ_d . It is worth mentioning that the specimen

with $w_w = 6.0\%$ visually resulted too dry, while a loss of water was observed during compaction of the specimen with $w_w = 7\%$. This suggested that the amount of water in this specimen was excessive and thus was expelled during compaction. For these reasons and for the results of Figure 6.47, the optimal amount of water for compacting NGM-OPC mixtures was set equal to 6.5%.

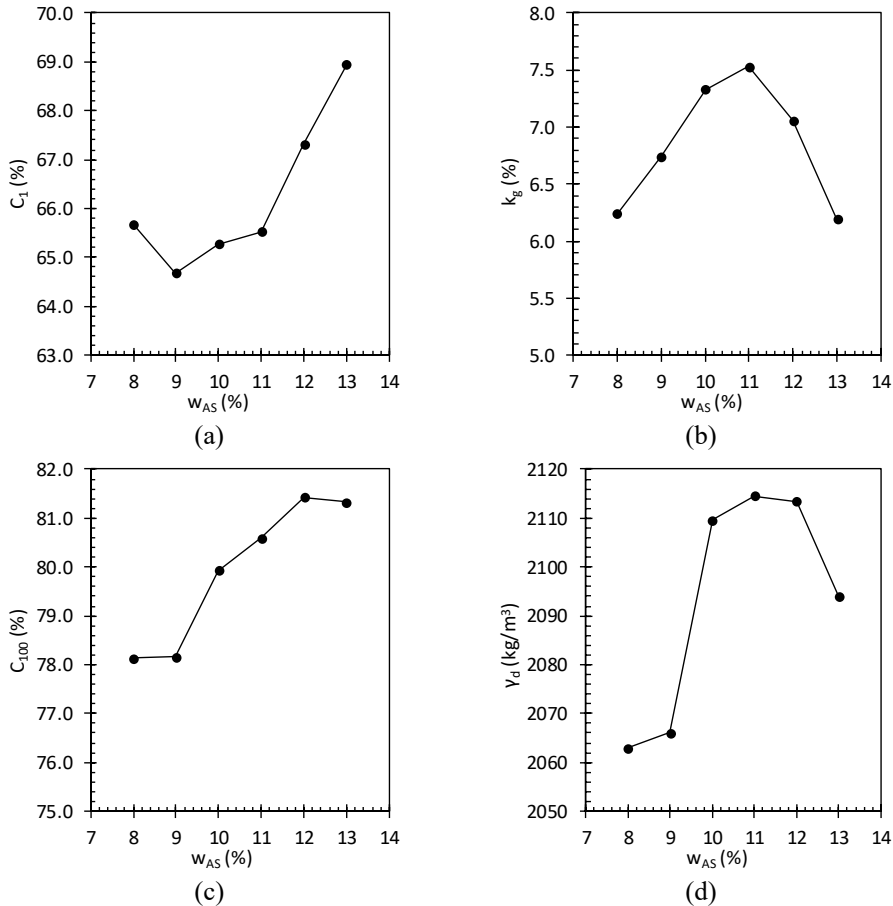


Figure 6.46 - Evolution of compaction parameters for CDW-AS-100% mixtures as a function of AS content (w_{AS})

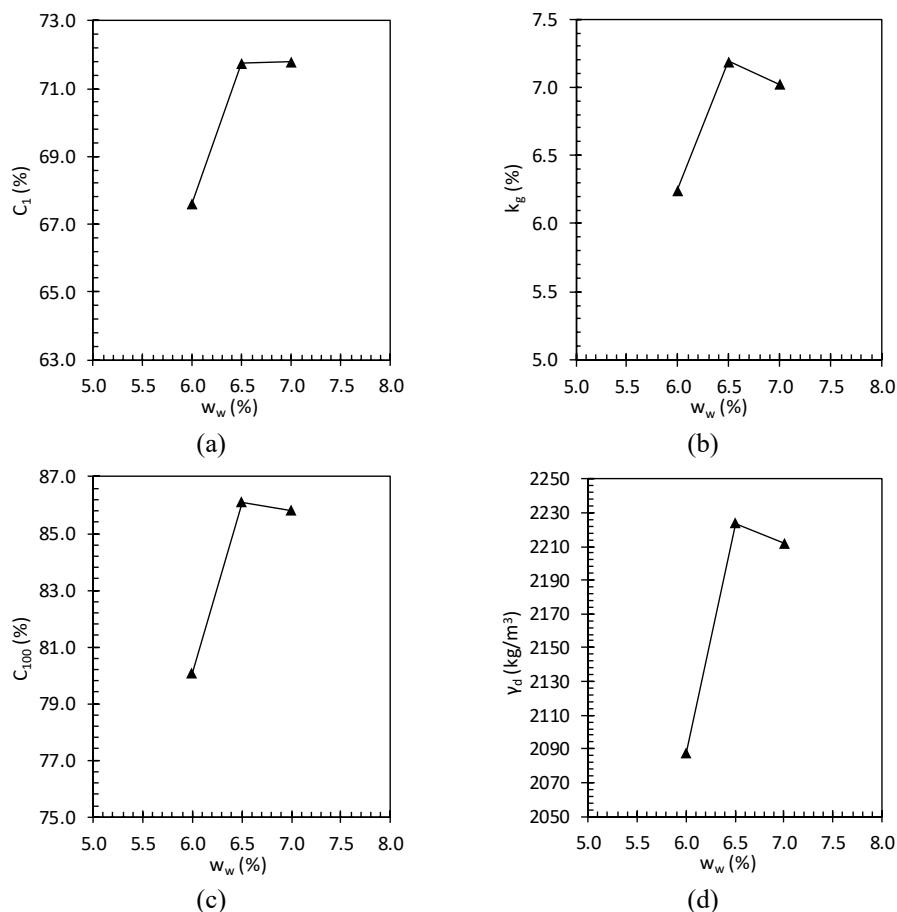


Figure 6.47 - Evolution of compaction parameters for NGM-OPC mixtures as a function of water content (w_w)

6.3.2 Effect of F/T degradation on mechanical properties

Resilient behaviour

The effect of F/T degradation on the RM of CDW-AS-100% mixtures for different curing periods is illustrated in Figure 6.48. The F/T treatment always affected the resilient behaviour of CDW aggregates. The reduction of RM due to F/T cycles was dependant on the curing time of specimens. After 7 days of curing, the geopolymerization reactions induced by the addition of AS-100% in the CDW mixtures were not yet fully developed, thus the F/T cycles provoked a significant abatement of RM values (Figure 6.48.a). At the intermediate stress condition (i.e. 8th loading sequence,

$\theta = 344.6$ kPa), the RM decreased from 628 MPa of the untreated specimen, to 290 MPa recorded on the specimen subjected to 4 F/T cycles. However, after 8 and 12 F/T cycles, an improvement of stiffness in comparison to the degradation condition of 4 F/T was evident.

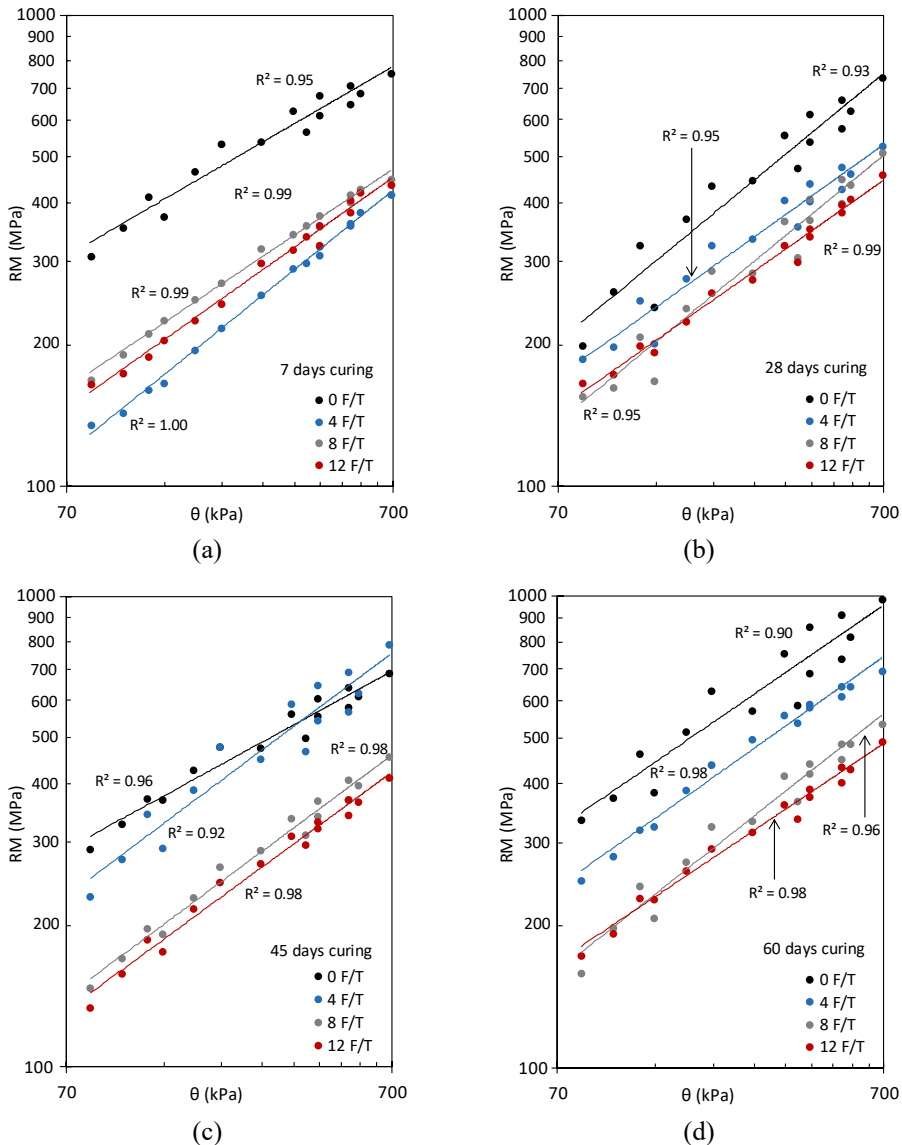


Figure 6.48 - Effect of F/T degradation on RM of CDW-AS-100% mixtures after (a) 7, (b) 28, (c) 45, and (d) 60 days of curing

Apparently, it can be assumed that during the degradation period alkaline reactions evolved leading to an increment of RM. In fact, each F/T cycle lasted for 2 days, thus specimens exposed to 4, 8, and 12 F/T cycles were tested at the 15th, 23rd, and 31st day after compaction respectively. Results evidenced that the additional time favoured an improvement of resilient response, although the curing conditions were characterized by thermal variations. The slight decrease of RM recorded on specimens after 12 F/T cycles in comparison to the corresponding specimens exposed to 8 F/T cycles testified that the stiffness of CDW-AS-100 materials was affected by the highest level of degradation severity. It is worth noting that the beneficial effect attributed to the additional curing occurring during F/T cycles was valid only for specimens cured for 7 days before the degradation treatment. RM values of all specimens initially cured for more than 7 days tended to decrease progressively with the increment of the F/T severity level. This trend is shown in Figure 6.49, which highlights the reduction (in percentage of the untreated specimen) of RM measured at the 8th loading sequence ($\theta = 344.6$ kPa) due to F/T degradation.

After 28 days of curing the effects of F/T degradation was less relevant than that detected after 7 days (Figure 6.48.b). Considering the 8th loading sequence ($\theta = 344.6$ kPa), the exposure to 4 F/T cycles led to a reduction of RM equal to 27% in relation to the reference specimen (0 F/T). For the same loading sequence, the degradation from 4 to 8 F/T reduced the RM from 405 to 366 MPa, while after 12 F/T cycles, the RM dropped to 325 MPa.

Results of RLT tests on 45-day cured specimens demonstrated negligible differences in RM values between the undisturbed specimen (0 F/T) and that submitted to 4 F/T cycles (Figure 6.48.c). Conversely, a significant reduction of RM was noticed for higher degradation levels. For instance, at the 15th loading sequence ($\theta = 689.5$ kPa), the RM of mixture exposed to 8 F/T exhibited a decrement of 34% in comparison to the untreated condition (0 F/T). At the same stress level ($\theta = 689.5$ kPa), the reduction of stiffness between 8 F/T and 12 F/T cycles was modest and estimated around 10%.

CDW mixtures cured for 60 days (Figure 6.48.d) showed a similar behaviour in terms of stiffness evolution with F/T degradation. In this case, the difference between RM results of undisturbed (0 F/T) and 4 F/T-degraded specimens varied from 8 to 30% depending on the stress level (θ). The stiffness reduction was even more relevant when the degradation severity increased from 4 to 8 cycles. Specifically, at the 1st loading sequence ($\theta = 82.8$ kPa), the RM dropped from 250 to 159 MPa passing from 4 to 8 F/T cycles. At the last loading sequence (i.e. 15th loading sequence, $\theta = 689.5$ kPa), RM value decreased from 698 to 539 MPa passing, once again, from 4 to 8 F/T cycles.

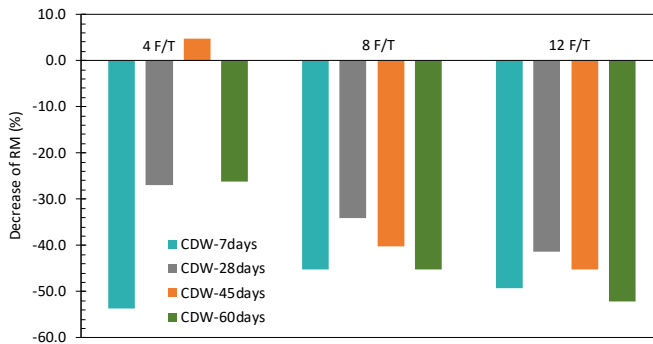


Figure 6.49 - Percentage of decrease in RM results (8th loading sequence, $\theta = 344.6$ kPa) due to F/T degradation

The trend of RM with curing time is plotted in Figure 6.50. It is worth noting that 60-day cured mixtures had the highest RM independently of the applied degradation level. The evolution of resilient behaviour of undisturbed mixtures (0 F/T cycles) for different curing times can be read in Figure 6.50.a. Just after 7 days of curing, the CDW-AS-100% mixture reached excellent RM values, which were slightly lower than those recorded on the 60-day cured specimen. However, after 28 days the RM tended to reduce, especially for low stress conditions. The most relevant differences in curing time were observed on specimens which underwent to 4 F/T cycles. Results of Figure 6.50.b highlight the poor resilient response of 7- and 28-day cured mixtures. Vice versa, after 45 and 60 days of curing, RM results were considerably higher than those shown by less cured specimens (7 and 28 days).

Data of Figure 6.50.c and Figure 6.50.d suggest that after 8 and 12 F/T cycles, the differences due to curing were reduced. It means that the RM of CDW-AS-100% mixture after 8 and 12 F/T cycles settled to approximately constant values independently of the initial curing.

The resilient behaviour of the NGM stabilized with 3% of OPC and exposed to F/T degradation is shown in Figure 6.51. After 7 days of curing the NGM-OPC mixture was not influenced by the F/T degradation. In fact, specimens submitted to 4 and 12 F/T cycles exhibited RM values relatively higher than those measured on the reference specimen (0 F/T). These results were in line with observations of Khoury and Brooks [502] on limestone aggregates stabilized with 10% of FA and cured for 3 days, who detected an improvement of stiffness after 12 F/T cycles. Considering the 8th loading sequence ($\theta = 344.6$ kPa), RM increased from 539 MPa of the undisturbed mixture (0 F/T), to 605 and 654 MPa recorded on specimens after 4 and 12 F/T cycles respectively (Figure 6.51.a). This behaviour is interpreted with similar considerations

previously carried out on 7-day cured CDW-AS-100% mixtures. Although the conditions of F/T degradation process were not ideal for the curing of material, the additional time contributed to the evolution of hydration reactions, which led to an improvement of the overall resilient behaviour. In other words, at short curing times, the supplementary time from the end of standard curing period and the testing moment partially contrasted the detrimental action of F/T cycles.

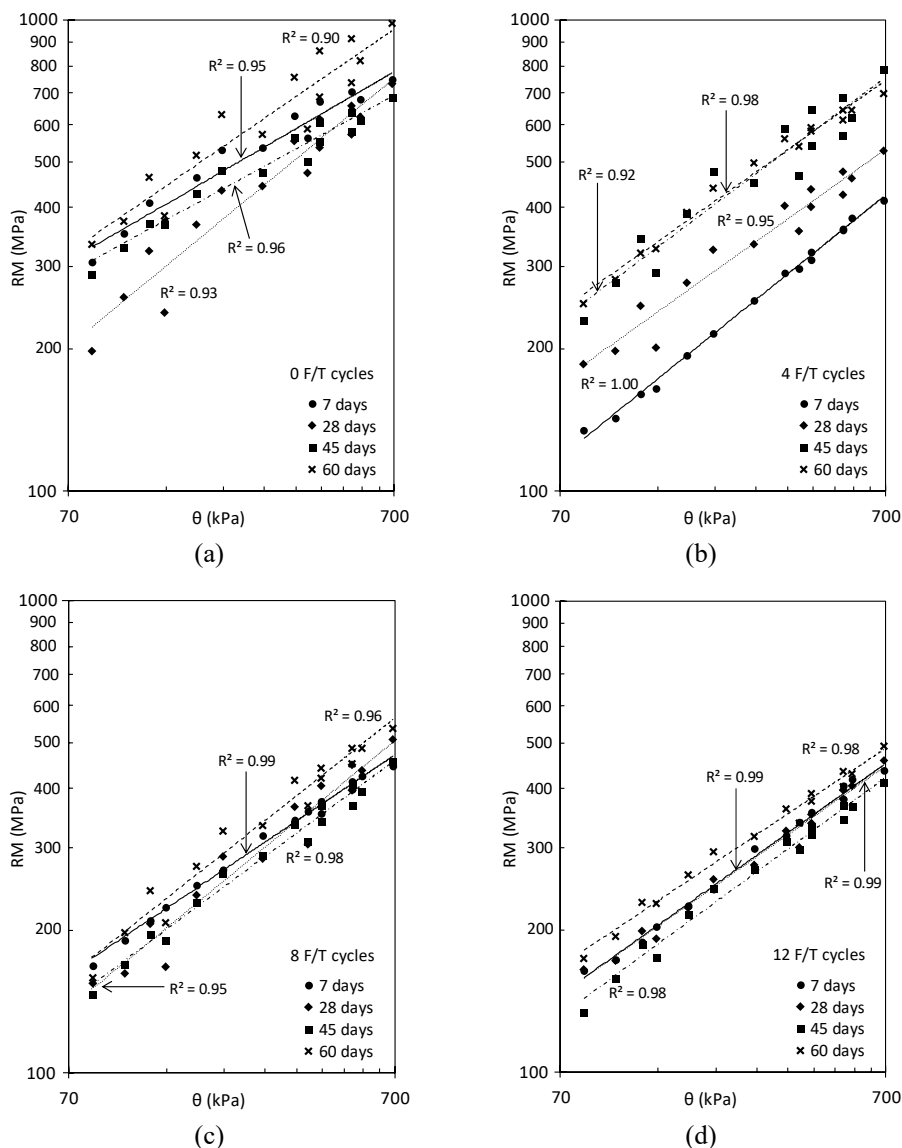


Figure 6.50 - Effect of curing on CDW-AS-100% mixture. Evolution of RM for (a) reference specimens (0 F/T) and those exposed to (b) 4, (c) 8, and (d) 12 F/T cycles

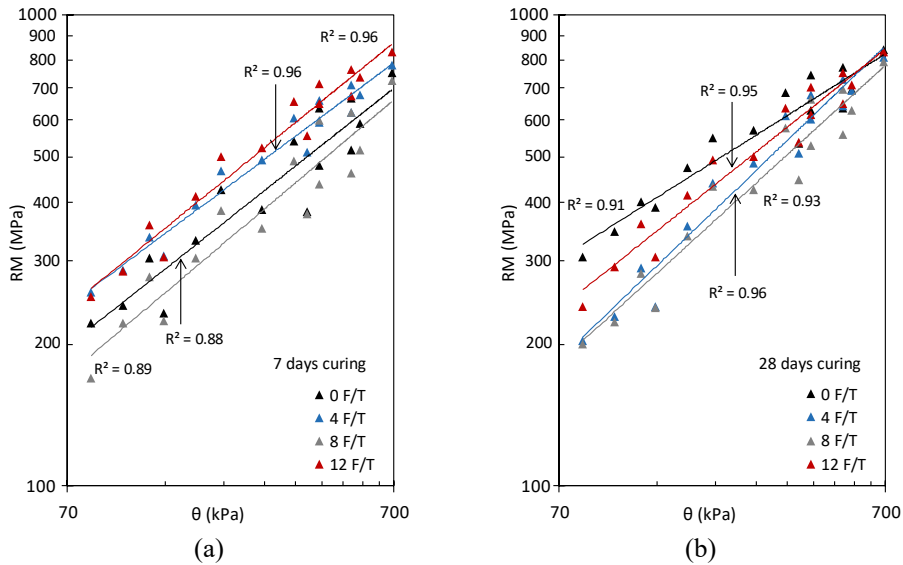


Figure 6.51 - Resilient behaviour of NGM-OPC mixtures after (a) 7 and 28 days of curing for different F/T degradation levels

The same trend was not evidenced on 28-day cured specimens, since most of hydration reactions were supposed to be completed [503]. In this case, the F/T degradation caused a reduction of RM, especially after 4 and 8 cycles. From Figure 6.51.b it is evident that differences in the resilient behaviour were more relevant for low stress conditions Vice versa, negligible differences were observed at high levels of θ .

Figure 6.52 compares the resilient response of CDW and NGM stabilized with AA process and OPC respectively. After 7 days of curing, recycled aggregates stabilized with AS-100% were more rigid than the NGM stabilized with OPC, demonstrating the excellent resilient response of the CDW-AS-100% mixture. At the 8th loading sequence ($\theta = 344.6$ kPa), the CDW-AS-100% mixture exhibited a RM equal to 628 MPa, while in case of NGM-OPC, the RM was equal to 539 MPa. On the other hand, Figure 6.52.a highlights that CDW granular material was definitely more susceptible to F/T degradation in comparison to the natural one. After 28 days of curing (Figure 6.52.b), cement-stabilized NGM mixtures exhibited slightly higher stiffness than CDW aggregates. At the highest stress state of the RLT test ($\theta = 689.5$ kPa), the differences between two materials were almost equal to 13%, while these disparities were greater for lower loading sequences. However, it is worth noting that the 60-day cured specimen made up of CDW aggregates and AS-100% displayed higher RM values than those measured on NGM-OPC mixtures (and cured 28 days). As well as recorded for 7-day

cured mixtures, recycled materials demonstrated a considerable weakness to F/T degradation also after 28 days of curing.

RM of non-degraded CDW-AS-100% mixtures was comparable to that measured on a reference NGM stabilized with OPC. However, stabilized CDW aggregates were notably sensitive to the degradation caused by F/T actions. No literature data on alkali-activated CDW aggregates were found to set up a direct comparison. Nevertheless, the same F/T degradation procedure was proposed by some authors for studying the durability of compacted granular materials and soils. For instance, Bassani and Tefa [314] analysed the resilient response of three different unbound CDW materials under F/T degradation. They found a relevant growth of RM values after 4 and 8 F/T, indicating in (1) the self-cementing phenomena and in (2) the production of fine particles due to the degradation process the main causes of these increments. F/T degradation of un-stabilized recycled aggregates was also studied by Bozyurt et al. [317]. They compared the resilient behaviour of compacted RC and RA aggregates demonstrating that the decrease of RM measured on RA specimens was moderate as the F/T degradation occurred. In case of RC specimens, the RM decreased after 5 F/T cycles, while the self-cementing attitude and the fine produced as a consequence of degradation led to a significant increase of RM after the exposure to more than 5 cycles. The same conclusion was pointed out by Soleimanbeigi et al. [175], who recognized an improvement in RM of compacted RC aggregates equal to 33% after 20 cycles of F/T in comparison to the reference mixture (0 F/T).

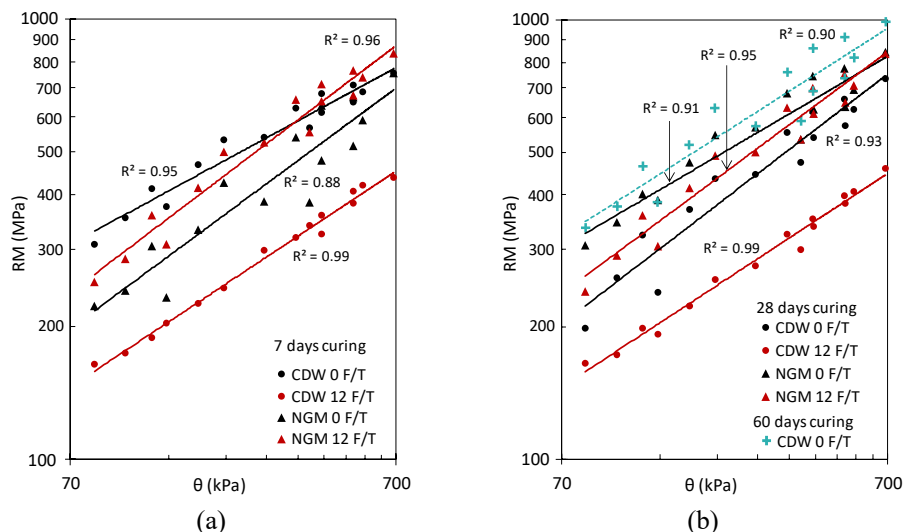


Figure 6.52 - Comparison between resilient behaviour of CDW-AS-100% and NGM-OPC mixtures after (a) 7 and (b) 28 days of curing

All these studies showed a good durability of un-stabilized recycled aggregates when subjected to F/T degradation and are partially in contrast with the resilient response of CDW-AS-100% mixtures presented here. Results of alkali-activated granular materials revealed that CDW-AS-100% were more susceptible to F/T degradation than un-stabilized ones. Generally speaking, the stabilization induces a great increment of stiffness, thus small alterations of the bound and rigid structure tend to be more evident in the overall resilient response. It is reasonable to suppose that un-stabilized specimens, although compacted, tend to deform more easily as a consequence of ice lens formation, while in a stabilized and bound matrix, the expansion of water freezing, is partially contrasted from the rigidity of the structure itself. For this reason, F/T degradation is usually more detrimental to the overall response of the stabilized material. This assumption is supported by literature data, which demonstrated that the durability in terms of resilient behaviour of stabilized granular materials is negatively affected by F/T degradation. Rosa et al. [504] attributed to the repetition of retardation and acceleration of cementitious reactions the main cause of reduction of RM of both coarse- and fine-grained geomaterials stabilized with FA. Camargo et al. [200] explained that the slight decrease in RM of FA-stabilized recycled aggregates (derived from RA and road surface gravel) is caused by the breakdown of binder bonds during freezing. Lee et al. [505] studied the effect of 0, 1, 2, 3 F/T cycles on resilient behaviour of cohesive soils classified as CL according to ASTM D2487 [475]. They observed that just one cycle caused a 30÷50% reduction of the RM, while additional cycles did not affect relevantly the resilient behaviour. Khalife et al. [506] found that some CH soils drastically reduced their resilient response after one F/T cycle independently if stabilized with 6% of lime, 10% of CKD or 10% of FA. Khoury and Zaman [316] evaluated the durability of limestone aggregates stabilized with different cementitious binders. 28-day cured NGM mixtures containing 15% of CKD exhibited a reduction of 49% of RM due to the exposure of 8 cycles of F/T from -25°C to 21°C. For the same material stabilized with 10% of FA and subjected to the same degradation severity, an average decrement of 42% in the RM was observed. The authors attributed the drop of resilient response of compacted and cured specimens to the formation of ice which led to a distortion of the material structure. Similarly, Zaman et al. [315] applied some F/T cycles on compacted CKD-stabilized NGM in partially saturated conditions and quantified the deleterious effects of freezing in terms of variation of the RM in comparison to regularly cured specimens. For a bulk stress of 414 kPa (9th loading sequence), the RM of 7-day cured specimens reduced by 25%, 96%, and 48% after 4, 8 and 12 F/T cycles. They measured that, after 12 F/T cycles, the stiffness of material was greater than that recorded after 8 F/T cycles, consistently with results of CDW-AS-100% materials after 7 days of curing and NGM-OPC mixtures after 28 days of curing.

In conclusion, the comparison of the resilient behaviour of stabilized CDW aggregates with AS-100% and un-stabilized CDW materials examined by Bassani and Tefa [314] is proposed in Figure 6.53. This shows the worst results exhibited by CDW-AS-100% mixtures (after 7 and 28 days of curing) and best values of RM recorded by Bassani and Tefa [314] on un-stabilized CDW aggregates subjected to F/T degradation. It is worth mentioning that un-stabilized mixtures had the same particle size distribution considered in the present investigation (Figure 4.1), but different composition: mixture A (Figure 6.53.a) was composed by 32% of RC, 9% of RA, 14% of BT, and 45% of NA, while mixture B (Figure 6.53.b) contained 71% of RC, 3% of RA, 4% of BT, and 22% of NA. Although the significant drop of RM due to F/T cycles exhibited by alkali-activated CDW aggregates, their stiffness was always greater than the best values obtained on un-stabilized CDW specimens (compacted with a water content of 7.5%) and degraded with F/T cycles.

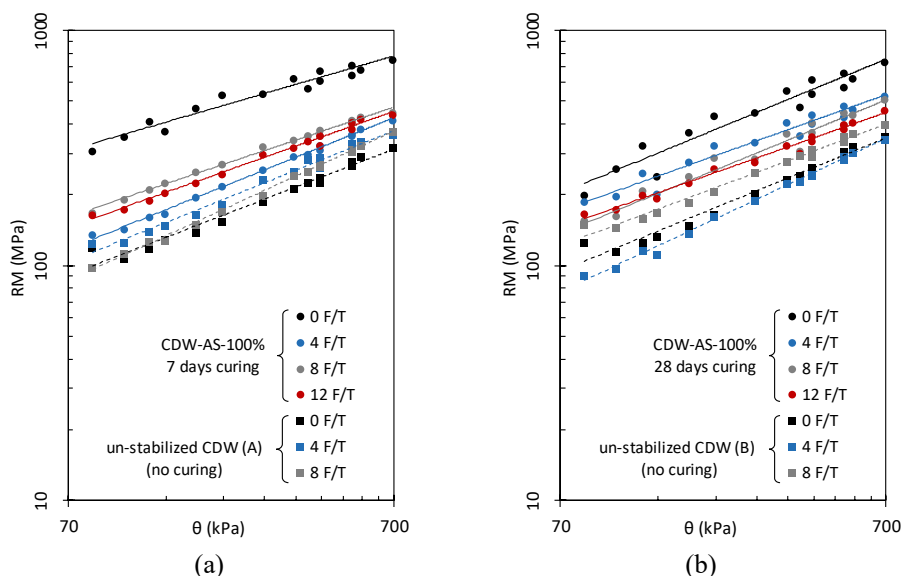


Figure 6.53 - Comparison between resilient behaviour of CDW-AS-100% and un-stabilized CDW materials subjected to F/T degradation without curing, investigated by Bassani and Tefa [314]

MEPDG modelling

Table 6.20 summarizes the results of the fitting procedure of MEPDG model. As well as performed in Exp. B1, the regression parameters of Eq. 22 (k_1 , k_2 , and k_3) were obtained as per the least square method, while the goodness of fitting was evaluated through the standard error ratio (S_e/S_y) and the adjusted determination coefficient (R^2_{adj}). Low values of S_e/S_y ratios and R^2_{adj} very close to the unity suggested the excellent capability of MEPDG model in interpreting the RLT test results.

After 7 days of curing, the trend of k_1 parameter was not defined for both CDW and NGM mixtures, reflecting the fluctuation of the RM results with the F/T degradation previously discussed. In case of CDW-AS-100% materials, the k_1 parameter after 4 F/T was less than the half of the corresponding one obtained on the undisturbed specimen. From 4 to 8 F/T cycles, k_1 increased from 1470 to 1998, then reduced to 1809 after the treatment with 12 F/T cycles. Also in case of 7-day cured NGM stabilized with OPC, the values of k_1 coefficient were consistent with the evolution of RM previously described. From data of Table 6.20, it can be observed that F/T degradation did not substantially influence the RM. For longer curing times, k_1 generally decreased when the CDW material was degraded through F/T cycles, advising a reduction of material stiffness. It is worth noting that variations of k_1 between CDW-AS-100% mixtures degraded 8 and 12 F/T cycles were limited, demonstrating that the stiffness tended towards an asymptotic value after a certain number of F/T cycles. Moreover, it is interesting to observe that specimens exposed to 8 and 12 F/T, exhibited a progressive increase of k_1 from 28 to 60 days of curing.

The stress-hardening behaviour of all mixtures was demonstrated by the positive values of k_2 coefficient. Considering the 7-day cured CDW-AS-100% mixtures, the parameter k_2 was higher in specimens which underwent to F/T degradation, meaning that the material tended to be more dependent upon the bulk stress as a consequence of F/T actions. Specimens of the same mixture cured for 28 days showed k_2 values limited in the range $0.41 \div 0.46$, while for those cured 45 and 60 days, k_2 generally increased after the degradation treatment. Apart from CDW-AS-100% mixture cured for 28 days, undisturbed materials (0 F/T) were characterized by lower k_2 coefficients ($0.26 \div 0.30$) than those obtained on specimens exposed to F/T degradation. This is consistent with the fact that stiffer materials tend to denote a resilient behaviour less dependent upon the stress condition. Moreover, it is worth observing that CDW-AS-100% mixtures submitted to 8 and 12 F/T cycles demonstrated a systematic reduction of k_2 values with the progression of curing time. In case of k_3 parameter, no defined evolution was detected. Positive values of k_3 indicate a relevant shear-hardening behaviour of material, while k_3 values close to zero suggest that the material is poorly sensitive to the octahedral shear stress [480]. Cement-stabilized NGM mixtures were characterized by values of k_3 moderately greater than those obtained on recycled materials, suggesting that their RM results were more influenced by the τ_{oct} . Furthermore, a decrement of k_3 from 7- to 28-day cured mixtures after 0, 4, and 8 F/T cycles is noticeable. The k_3 coefficient of CDW-AS-100% mixtures cured for 7 days decreased from positive to negative values, showing an inversion in the shear-dependency behaviour.

Table 6.20 - Results of MEPDG model fitting

Material	Curing	F/T cycles	k ₁	k ₂	k ₃	S _e /S _y	R _{adj} ²
CDW-AS-100%	7 days	0	3586	0.30	0.30	0.19	0.96
		4	1470	0.55	0.01	0.06	1.00
		8	1998	0.48	-0.12	0.06	1.00
		12	1809	0.54	-0.19	0.07	1.00
	28 days	0	2450	0.43	0.47	0.26	0.93
		4	1946	0.41	0.36	0.23	0.95
		8	1601	0.46	0.45	0.19	0.96
		12	1687	0.42	0.28	0.10	0.99
	45 days	0	3293	0.27	0.34	0.16	0.98
		4	2726	0.30	0.69	0.17	0.97
		8	1715	0.41	0.31	0.11	0.99
		12	1596	0.44	0.19	0.14	0.98
	60 days	0	3547	0.27	0.80	0.17	0.97
		4	3002	0.44	0.07	0.15	0.98
		8	2006	0.45	0.25	0.18	0.97
		12	1978	0.38	0.27	0.09	0.99
NGM-OPC	7 days	0	2217	0.30	0.94	0.20	0.96
		4	2851	0.39	0.42	0.18	0.97
		8	2021	0.27	1.06	0.15	0.98
		12	2963	0.44	0.36	0.21	0.95
	28 days	0	3431	0.26	0.61	0.23	0.95
		4	2462	0.52	0.38	0.21	0.96
		8	2224	0.39	0.81	0.22	0.95
		12	2897	0.40	0.47	0.19	0.96

Unconfined compression strength

The influence of F/T actions on mechanical strengths was investigated through UCS and ITS tests. Each UCS result given in Figure 6.54 is the average of two measurements, as explained in Section 5.3.2. In most cases, the evolution of strength was consistent with the resilient behaviour previously discussed. Firstly, it is interesting to observe the equivalent UCS values between non-degraded (0 F/T) alkali-activated CDW aggregates and cement-stabilized NGM.

After 7 days of curing, recycled aggregates stabilized with AS-100% reached the inferior limit of 2.50 MPa suggested by the Italian technical specifications for stabilized natural materials to be used in bases and subbases layers [313], while the NGM-OPC mixture exhibited a slightly lower value (2.33 MPa). Specimens of both materials (CDW and NGM) cured for 28 days faintly exceeded 4.00 MPa.

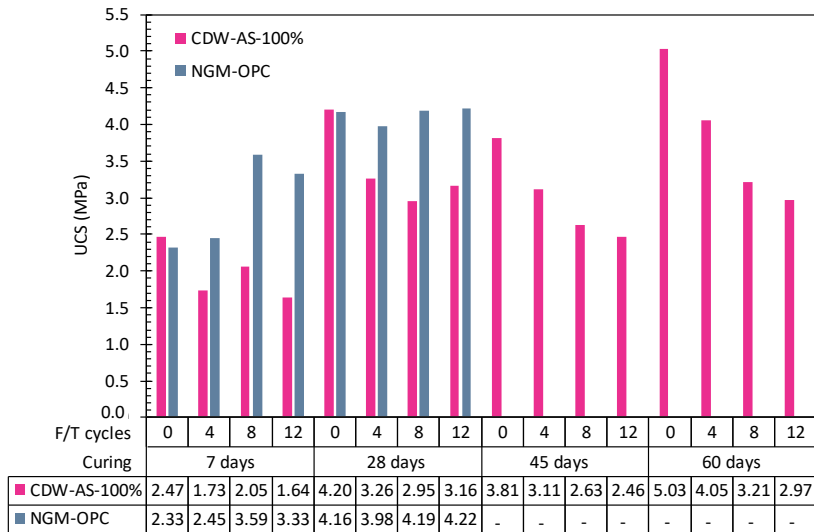


Figure 6.54 - UCS results of CDW-AS-100% and NGM-OPC mixtures exposed to F/T degradation

After 60 days of curing, CDW-AS-100% materials were characterized by UCS values of 5.03 MPa, demonstrating the continuous evolution of AA reactions during time at room temperature. Data displayed in Figure 6.54 indicate that CDW materials were more sensitive to frost action than NGM. Independently of the curing time, the UCS of CDW-AS-100% mixtures decreased as a consequence of F/T cycles. Specimens cured for 7 days exhibited a reduction of UCS from 2.47 to 1.73 MPa after 4 F/T cycles, while after 8 cycles the strength slightly increased to 2.05 MPa. A degradation of 4, 8, and 12 F/T on 28-day cured CDW material stabilized with AS-100% led to an UCS reduction of 23, 30, and 25% in relation to the strength exhibited by the mixture not subjected to F/T. For longer curing times, a systematic reduction of compressive strength with the increment of degradation severity level was evidenced. It is worth noting that 60-day cured specimens exhibited a greater reduction of UCS than those cured for 45 days.

NGM-OPC mixtures cured for 7 days showed a significant improvement of UCS after 8 and 12 F/T cycles. For instance, specimens undergone to 8 F/T exhibited an UCS equal to 3.59 MPa, which is 54% greater than the value achieved by non-degraded specimens (0 F/T). The increase of strength at early stages can be attributed to the evolution of hydration reactions of cement binder. A similar behaviour was observed in cement-stabilized NGM investigated by Theivakularatnam and Gnanendran [507]. They measured an increase of UCS from 1.70 to 2.40 MPa between un-degraded specimens and those subjected to 8 F/T cycles. Miller and Zaman [508] ascribed to the loss of water observed during F/T cycles, the slight increment of UCS exhibited by soil specimens

stabilized with CKD and subjected to 12 F/T cycles. Conversely, a detrimental effect of F/T degradation on stabilized subgrade soils with FA-CKD or lime was pointed out by Solanki et al. [509] and Hotineanu et al. [510] respectively. The UCS results recorded on CDW-AS-100% mixtures were in contrast with data reported by Camargo et al. [200]. These authors noticed that after 5 F/T cycles, aggregates derived from the recycling of road surface gravel (RSG) and stabilized with FA exhibited a slight improvement of compressive strength. Conversely, negligible changes were detected for RA aggregates stabilized with FA. Considering the results of non-degraded specimens obtained by Camargo et al. [200] reported in Table 6.21, it is interesting to observe that CDW-AS-100% specimens not subjected to F/T cycles exhibited better results for each curing time. It demonstrates, once again, the effectiveness of alkali-activation of fine particles as stabilization method for CDW materials in relation to more traditional stabilization techniques.

Table 6.21 - UCS results in MPa obtained by Camargo et al. [200] on specimens not exposed to F/T cycles

Material	Curing (days)		
	7	28	56
RSG with 10% FA	0.8	1.0	1.1
RA with 10% FA	1.4	1.8	2.5

Indirect tensile strength

The average results of ITS obtained from two identical specimens are provided in Figure 6.55. The evolution of ITS values depending on curing times and F/T degradation was analogous to that observed for UCS results (Figure 6.54). The ITS results were averagely the 13 and 16% of the UCS for CDW and NGM respectively. Considering undisturbed specimens (0 F/T), ITS progressively increased with curing time for both recycled and natural materials. CDW-AS-100% mixtures fulfilled the requirement of minimum 0.25 MPa (of ITS) after 7 days of curing of the Italian technical standard for cement-stabilized materials [313]. After 28 days of curing, the ITS of these mixtures achieved 0.62 MPa, while, at 60 days of curing, the ITS (0.82 MPa) was more than the double of that recorded on 7-day cured specimens (0.40 MPa). The F/T degradation affected the behaviour of CDW mixtures stabilized with AS-100%, in line with results of UCS. According to data of Figure 6.55, it is evident that 4 F/T cycles were enough to moderately reduce the strength. The worst results were shown by mixtures cured for 7 and 45 days, for which the ITS halved after 4 F/T in comparison to the values exhibited by the reference specimens (0 F/T).

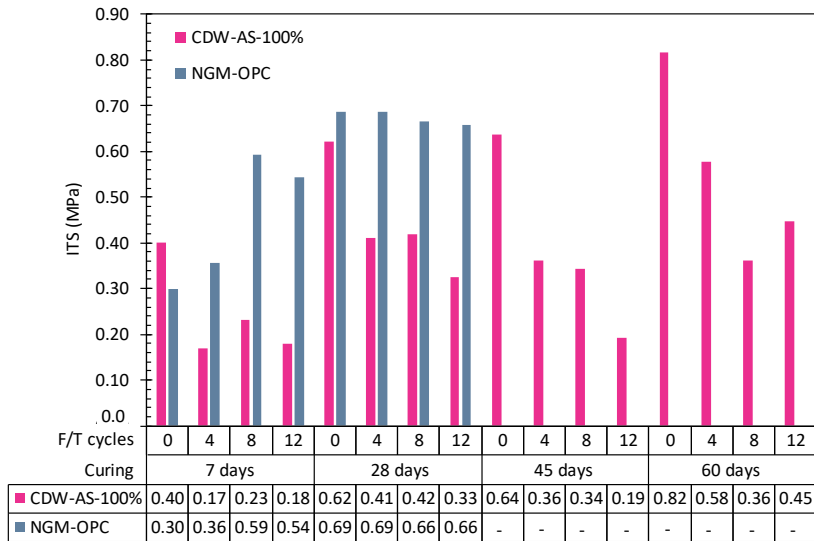


Figure 6.55 - ITS results of CDW-AS-100% and NGM-OPC mixtures exposed to F/T degradation

Conversely, NGM stabilized with OPC seemed insensitive to F/T degradation. After 7 days of curing, the ITS increased progressively from 0 to 8 F/T cycles, supporting the idea that, at early stages, the positive effects of additional curing were prevalent than the detrimental influence of the degradation. Since each F/T cycle lasted for 2 days, specimens tested after a certain number cycles were cured for more time than the undisturbed material (0 F/T). After 12 cycles, the trend was reversed with an ITS value lower than that obtained on specimens degraded for 8 cycles. An identical behaviour was evident in case of UCS of the same mixtures (Figure 6.54). The influence of F/T degradation on 28-day cured NGM-OPC mixtures can be considered negligible. The comparative analysis between CDW aggregates and NGM revealed that undisturbed mixtures (0 F/T) were able in supporting an equal amount of indirect tensile stress.

Discussion

All mechanical tests indicated that un-degraded CDW aggregates stabilized as per the AA method performed similarly to a cement-stabilized NGM. Undisturbed specimens (0 F/T) showed comparable and, sometimes better, results in terms of strength and stiffness when compared to literature data on similar materials stabilized with traditional binders [200]. However, CDW-AS-100% mixtures were found more sensitive to freezing actions than NGM stabilized with OPC. This is partially in contrast with most of literature which attributes to geopolymer materials a good F/T resistance [30], [285], [287]. It is worth mentioning that typical geopolymer products derive from amorphous

and semi-crystalline phases of raw powders, such as calcined clays, FA, BFS [511], [512], [513]. These precursors are highly reactive [222], [514] in comparison to the crystalline and mineral phases detected in fine particles of CDW (Section 6.1.2). In this condition, the dissolution of aluminosilicate is less efficient and the final products exhibit a lower geopolymerization rate [515]. The curing temperature is also a crucial factor in the formation of the bonds for alkali-activated material [30], [516]. Many authors stated that low temperatures of curing are not adequate for developing a structurally sound geopolymer [421], [397]. According to Temuujin et al. [515], products with partially dissolved aluminosilicates are more sensitive to F/T degradation. Hence, the weak F/T resistance exhibited by CDW-AS-100% mixtures can be attributed to the low reactivity rate of the alkali-activated binder which allowed the penetration of water and the detrimental effect of frost actions.

It is worth pointing out that literature references, which state the good F/T resistance of alkali-activated products, deal with the durability assessment of the binder only. For this reason, a comparison with granular materials stabilized with AS-100% (investigated here) cannot be easily carried out.

Although it is reasonable to assume that the binding phase was not a completely reacted geopolymer and its properties were affected by freezing phenomena, compacted material in its complete particle size distribution appeared as a network of CDW grains weakly bound by a geopolymeric matrix. Alkali-activated fine particles acted as a binder for coarser CDW aggregates, which became harder with the evolution of the AA reactions (Figure 6.56.a). The excellent mechanical properties induced by the alkali-activated binder were demonstrated both in Exp. B1 and Exp. B2. The first one showed that the addition of AS-100% considerably increased the values of RM, UCS and ITS in comparison to mixtures compacted with only water (AS-0%). In Exp. B2, these mechanical properties were found comparable to those exhibited by a cement-stabilized NGM, confirming the good performance of the proposed stabilization technique. Against this background, it is reasonable to suppose that this poor durability under F/T degradation exhibited by CDW-AS-100% can be imputable to the low soundness of recycled aggregates. The volumetric expansion due to the freezing of water present in the AS entrapped in voids between grains induced internal stresses. In a hardened and non-deformable structure, the progressive repetition of this phenomenon tended to break the weaker particles of CDW (Figure 6.56.b), such as RC and BT (Table 6.11), leading to the abatement of the mechanical properties of the overall mixtures. Actually, RC and BT materials had the highest values of water absorption (Table 6.10), which contributed to the damage of these weak grains in presence of water and freezing conditions. Unfortunately, no literature data on stabilized CDW aggregates with ordinary or alternative binders subjected to F/T are available for supporting these assumptions.

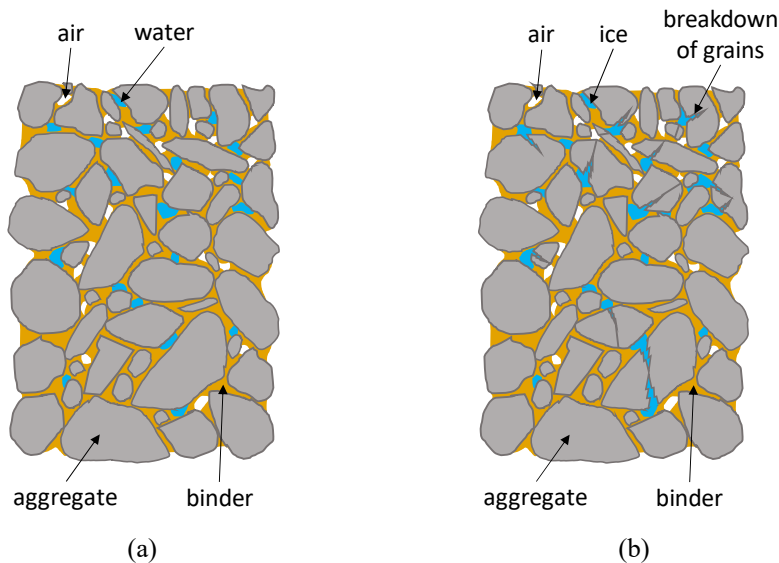


Figure 6.56 - Schematic representation of (a) CDW aggregates bound with the alkali-activated binder and (b) breakdown of coarser particles due to the ice formation

A similar behaviour was not shown by the NGM stabilized with OPC. In this case, two considerations should be taken into account. The main cause is related to the natural origin of aggregates, which ensured a greater resistance to internal stresses induced by freezing actions. It is justified by data of Table 6.10 and Table 6.11, which indicate that NGM had a lower water absorption and a greater F/T resistance when compared to CDW aggregates. Secondly, it is reasonable to suppose that freezing conditions between CDW-AS-100% and NGM-OPC mixtures were dissimilar. In the first case, water was used for mixing the material and dissolving sodium silicate and hydroxide present in the AS. In alkali-activation processes, water is consumed only during the dissolution of aluminosilicate species [223], [517]. Conversely, gelation and polycondensation are water-releasing phases in the AA process [518], [519]. Therefore, it may be assumed that water was not part of the AA reaction, thus remaining constant and free during curing.

Conversely, the hydration of cement added in NGM required a certain amount of water [520], thus part of H_2O was consumed by the chemical reaction of cement. Hence, free water was reduced and, consequently, the negative effect caused by its expansion during freezing was mitigated. Considering that the stoichiometric water for the complete hydration of cement is equal to the ratio 0.42 [520] (i.e. each 100 g of dry binder, 42 g of water are required for its hydration), almost the 20% of water added during compaction was required for the hydration reactions; thus it was consumed during curing. The estimates included in Table 6.23 indicate that a quantity equal to 1.3% was

consumed by cement-hydration reactions. As a consequence, the free water involved in F/T cycles was reduced to an amount of 5.2%. It means that, during F/T treatment, NGM-OPC mixtures had almost 30% less of water than CDW materials. The reduced amount of w_w in comparison to recycled aggregates contributes to explain the better response of NGM-OPC mixtures when F/T degradation occurred.

Table 6.22 - Estimates of water involved in F/T cycles for both CDW and NGM aggregates

Material	Compaction w_w	w_w required for chemical reactions	w_w involved in F/T cycles
	(%)	(%)	(%)
CDW-AS-100%	6.7	0.0	6.7
NGM-OPC	6.5	1.3	5.2

6.4 Environmental compatibility of CDW-AS mixtures

Table 6.23 synthetizes the results of leaching test carried on both recycled aggregates stabilized with AA of fines (CDW-AS-100%) and virgin natural aggregates stabilized with 3% of cement (NGM-OPC). In addition, the leaching behaviour of raw CDW aggregates before the activation treatment was also evaluated for comparison purposes.

Looking at the column of CDW aggregates without any treatment (raw CDW), it is possible to ascertain their perfect fulfilment of acceptance limits imposed by the Italian law [65] for aggregates to be used in road applications. Comparing these data with those recorded on raw powders of UND1 sample (Section 6.1.5), a lower release of pollutants from the CDW aggregates samples is evident. It is due to the different particle size distribution of two samples:

- UND1 was a powder with dimension of particles lower than 0.125 mm;
- CDW aggregates have been ground to obtain particles with dimensions lower than 4 mm according to EN 12457-2 [353].

Accordingly, Peters [521] and Townsend et al. [522] found that the leaching efficiency is greater for smaller particles than for samples with coarser aggregates.

As previously observed at the scale of fine particles (Section 6.1.5), the AA produced a negative effect in the pollutants leaching behaviour of CDW aggregates. The concentrations of certain metals, such as beryllium, cadmium, cobalt, nickel, and selenium, tended to slightly increase in comparison to the untreated sample. Arsenic and vanadium were present in higher concentration in the eluate of the CDW-AS-100% mixtures than in that of raw CDW. These two heavy metals, together with nickel, exceeded the threshold of the Ministerial Decree of 5th February 1998 [65]. The same

three cations (As, Ni, V) exhibited a significant increment of concentration in leaching test carried out on alkali-activated UND1 powders (Table 6.9).

In case of activation of CDW mixtures, the concentration of lead grew from 0.3 µg/l in the raw material to 130.0 µg/l in the sample containing CDW stabilized through the AA. The common increase of the leaching of metals from alkali-activated products can be ascribed to the same causes reported in Section 6.1.5. It could be supposed that (1) a double exposure to a liquid medium, (2) the increment of pH, and (3) the alkali-activation process itself, produced an enhancement of the reactivity of certain elements that tended to be released more easily in contact with the leaching agent.

Results of Table 6.23 suggest that all anions (Cl^- , F^- , NO_3^- , SO_4^{2-}) were released in lower concentrations by alkali-activated CDW mixtures compared to the starting untreated aggregates. This is attributable to the reaction with NaOH, which resulted in the formation of sodium chloride, sodium fluoride, sodium nitrate, and sodium sulphate. It was hypothesized that these non-ionized species have precipitated in the structure porosities, thus resulting less available to be leached (Section 6.1.5).

Of particular interest is definitely the reduction in sulphates concentrations, whose leaching has been reported critical for CDW materials by many authors [431], [432], [523], [524], [525]. In fact, it decreased from 180 mg/l in the raw material to 110 mg/l in the activated products. The reduction of chromium can be considered another good result, since its leaching has been always considered a discriminating factor for using CDW materials in civil applications [432], [526], [527].

Comparing the results with the European acceptance limits, it can be concluded that CDW granular materials stabilized with the addition of AS-100% can be considered inert waste, thus confirming the total environmental compatibility of the proposed stabilization technique.

As expected, the leaching of pollutants from NGM-OPC mixtures were generally minimal since they included natural-origin aggregates and soil. The concentration of cations and anions were commonly lower in case of cement-stabilized NGM than CDW-AS-100% mixtures. However, it is worth noting the high concentration of cobalt and chromium in the eluate caused by the addition of cement as a stabilizer [81]. Lastly, from data of Table 6.23 can be deduced that cement contributed to the increment of pH up to a value of 12.0. This value was even higher than the 11.4 recorded on the eluate of the CDW-AS-100% mixture.

Table 6.23 - Results of leaching test on raw CDW, alkali-activated CDW, and cement-stabilized natural aggregates (bolded values are outside the Italian acceptance limits)

Parameter	Unit of meas.	IT limits ¹	EU limits ²	Raw CDW	CDW-AS ³	NGM-OPC
Chlorides	(mg/l)	100	800	6.0	5.4	1.3
Fluorides	(mg/l)	1.5	10.0	0.3	0.3	0.1
Nitrates	(mg/l)	50	-	7.3	3.4	0.0
Sulphates	(mg/l)	250	1000	180	110	18
Arsenic	(µg/l)	50	500	1.6	76.0	0.4
Barium	(mg/l)	1.0	20	0.02	0.00	0.02
Beryllium	(µg/l)	10	-	0.000	0.020	0.000
Cadmium	(µg/l)	5.0	40	0.010	0.690	0.010
Cobalt	(µg/l)	250	-	0.3	2.7	3.4
Chromium ⁵	(µg/l)	50	500	25	13	40
Mercury	(µg/l)	1.0	10	0.07	0.08	0.09
Nickel	(µg/l)	10	400	2.0	17.0	5.8
Lead	(µg/l)	50	500	0.3	130.0	0.5
Copper	(mg/l)	0.05	2	0.012	0.046	0.007
Selenium	(µg/l)	10	100	0.7	2.0	0.0
Vanadium	(µg/l)	250	-	22.0	310.0	2.4
Zinc	(mg/l)	3.0	4.0	0.026	0.036	0.003
pH	(-)	5.5÷12	-	10.9	11.4	12.0

Notes: ⁽¹⁾ limits of the Ministerial Decree of 5th February 1998 [65] for EoW

⁽²⁾ limits of the 2003/33/EC [139] for landfilling inert waste

⁽³⁾ CDW aggregates stabilized with AA method after 28 days of curing

⁽⁴⁾ natural granular material stabilized with 3% of ordinary Portland cement

⁽⁵⁾ total chromium

7. CONCLUSIONS

Despite many laboratory and full-scale investigations demonstrating that unselected construction and demolition waste (CDW) aggregates can be effectively used in road pavements, their effective employment is still limited to low trafficked roads. As a result, several attempts have been made to improve their mechanical and durability properties through stabilization. With the aim of reducing the use of ordinary Portland cement (OPC), considered environmentally unfriendly, different by-products have been employed as alternative binders for CDW aggregates stabilization. Some authors tried to stabilize granular materials by the addition of alkali-activated precursors, such as fly-ash (FA), blast furnace slag (BFS), and cement kiln dust (CKD). Recently, powders (or fines) derived from CDW were also found to be sufficiently reactive in alkaline conditions.

The investigation presented here takes advantage of the alkaline activation (AA) of finer particles ($d < 0.125$ mm) regularly present in unselected CDW aggregates for stabilization purposes. Unlike what happens with the addition of alkali-activated by-products, the formation of internal bonds responsible for the stabilization of CDW aggregates appears to be induced by the chemical reactions between aluminosilicates (present in finer granular fractions) and a liquid activating solution. As a result, with this new technology, finer particles of CDW recycled aggregates can act as self-stabilizer.

7.1 Key findings

The laboratory investigation employed a multiscale approach with the objective of verifying, at a smaller scale, the alkali-reactivity of the finest particles only and, at a larger scale, the feasibility of the alkali-activation of fines as a stabilization method for CDW mixtures in their complete particle size distribution. At this scale of investigation, freeze and thaw (F/T) degradation tests were also performed to assess the durability of these mixtures.

7.1.1 Alkali-activation of CDW fines

In the small-scale investigation (Exp. A), the reactivity of individual constituents (recycled concrete, RC; reclaimed asphalt, RA, bricks and tiles, BT; and natural aggregates, NA) and a mix of unselected CDW fines (UND1, and UND2) was evaluated. The preliminary chemical and mineralogical characterization carried out by means of x-ray diffraction (XRD) and x-ray fluorescence (XRF) analyses on single fractions of different origin identified the presence of aluminosilicate and mica-group minerals potentially reactive in alkaline conditions. The highest amounts of SiO_2 and Al_2O_3 were detected in the BT, NA, and UND1 samples. The abundance of silicon, aluminium, and calcium oxides in RC, BT, UND1, and UND2 fractions was found consistent with literature data related to successful experiences of AA of waste materials.

The fresh mixtures (powders and alkaline solution) exhibited markedly variable viscosity depending on the l/s ratio, alkaline solution (AS) concentration, and constituents (i.e. origin of the powders). As a result, the casting procedures were decided on mixture consistency: fluid pastes (with l/s = 0.6, and AS concentration of 75% and 50%) were simply poured into moulds, while undiluted solutions (AS-100%) and low l/s ratios (equal to 0.4 and 0.5) produced very viscous pastes, which were compacted into the moulds.

The effectiveness of alkali-activation reactions were assessed in terms of development of mechanical strengths after 28 days of curing at room temperature. Flexural and compressive strength tests yielded consistent results. The key findings can be stated as follows:

- the AS concentration played a key role in the development of mechanical strength which is consistent with several results from geopolymer-oriented literature;
- the AS-50% did not trigger the AA of aluminosilicates included in CDW powders, since hardened specimens exhibited lower strengths in comparison to the two more concentrated AS;
- RC and UND1 showed the highest values of flexural and compressive strength with AS-100%;
- 28-day cured specimens made up of UND1 powders and AS-100% in the l/s ratio equal to 0.4 achieved 4.2 and 12.0 MPa of flexural and compressive strength respectively;
- RC fines required more liquid phase (l/s = 0.5) to develop average flexural and compressive strengths of 5.8 and 15.8 MPa respectively.

The relevant mechanical properties exhibited by UND1 were attributed mainly to the formation of aluminosilicate geopolymer structures due to the abundance of aluminosilicate-rich phases in the raw powders. From the perspective of using

alkali-activation as a stabilization method for CDW mixtures, the good mechanical behaviour of UND1 would guarantee some economic benefits, since fines typically present in the unselected material can be activated without the addition of other precursors. Although the unselected fraction of CDW material is expected to be characterized by a marked compositional heterogeneity, the comparative analysis with literature data showed that the content of SiO_2 , Al_2O_3 , and CaO elements does not vary in wide ranges. The chemical-mineralogical composition of UND1 constituent can be recommended for a satisfactory AA, and thus for an adequate development of mechanical properties. From a practical point of view, it can be concluded that the undivided fraction of CDW material can be considered as an alternative precursor in the alkali-activation process independently of the provenience of waste, due to the adequate combination of Si, Al, and Ca minerals always present in these materials.

The excellent mechanical strengths of RC were ascribed to the good balance between calcium-rich and aluminosilicate phases, which led to the formation of both alkali-activated products and C-S-H species as a consequence of the AS addition.

Leaching tests proved that the AA process increased the potential release of pollutants. Some alkali-reacted samples exceeded the Italian limits of the Ministerial Decree of 5th February 1998 [65]. However, considering the less conservative limitations of European Council Decision 2003/33/EC [139], all alkali-activated products met the requirements of pollutants concentration limits and can be regarded as inert waste.

The small-scale investigation demonstrated that CDW fines, when mixed with a highly concentrated AS, developed interesting mechanical strength values. In contrast to most literature studies, in which thermal curing ($60\div 80^\circ\text{C}$) was the norm, the alkali-activation occurred at room temperature inducing relatively high mechanical strengths. This latter aspect is of fundamental importance in road constructions, where this technology could be applied. The promising results for the reactivity of fine particles of CDW acted as a spur for new experiments at a larger scale concerning the effective stabilization of CDW aggregates with this technique.

7.1.2 Stabilization of CDW aggregates

The objective of Exp. B1 was an assessment of the alkali-activation of fine particles of CDW as a new stabilization method for whole mixtures containing both fine and coarse grains. Fines normally present in CDW mixtures correspond to the UND1 fraction of Exp. A, thus no distinctions between constituents were investigated in Exp. B1 and Exp. B2.

The preliminary characterization of loose aggregates revealed, as expected, that CDW aggregates are more susceptible to fragmentation and F/T degradation than natural ones. However, when compacted in cylindrical specimens with an aqueous solution of sodium hydroxide and silicate instead of water, their mechanical properties improved significantly. The mechanical characterization results for 7-, 28-, and 60-day cured specimens reflected the main findings outlined in the small-scale investigation (Exp. A). Also in this case, the AS concentration had a key role in the development of mechanical strength values of cured specimens. No noticeable improvements in resilient modulus (RM), unconfined compression strength (UCS), and indirect tensile strength (ITS) were observed for mixtures containing AS-50% (i.e. the AS diluted by 50%) in comparison to the reference specimens (i.e. specimens compacted with water only, AS-0%). An excessive dilution of the AS drastically reduced its capability of triggering the alkali-activation of aluminosilicates of fine CDW particles. Conversely, the addition of the AS-100% induced a binding matrix that led to a marked improvement in mechanical behaviour for all curing times.

The following general key findings arose from Exp. B1:

- despite the AS being characterized by significantly different viscosities depending on the concentration, the best compaction results were obtained with a $w_{AS} = 10\div 11\%$ of aggregate mass independently of the AS concentration;
- variations in the content of AS (w_{AS} or w_w) had a significant effect on the mechanical behaviour of cured specimens for each concentration;
- excessive quantities of AS during the compaction phase caused a high void content in specimens, which inevitably had a negative effect on strength and stiffness properties. Only in the case of AS-100%, the long-term resilient behaviour (i.e. after 60 days of curing) appear to be uncompromised by the excessive quantity of the AS;
- modelling of RLT test results revealed a shear hardening behaviour of mixtures prepared with AS-100% for all the investigated curing times
- independently of the AS concentration, the best RM, UCS, and ITS results were obtained with 60-day cured specimens containing $w_{w,opt} \sim 2\%$;
- the addition of AS-100% effectively stabilized CDW materials, which showed stiffness and strength results comparable to those of similar materials stabilized with more valuable binders documented in literature;
- self-cementing phenomena were observed in specimens containing water only (AS-0%).

FESEM observations coupled with EDS analysis confirmed the occurrence of a binding phase which surrounds the aggregate particles, which can be attributed to the products of alkali-activation reactions.

These promising results offer a new perspective in the stabilization technique for recycled aggregates in road construction. The addition of AS-100% in lieu of water during compaction induced the alkali-activation of fine particles, with an overall enhancement of the mechanical properties of CDW mixtures. After 7 days of curing, UCS and ITS results satisfied the minimum requirements of Italian regulation for cement-stabilized natural granular materials (NGM) for subbase layers of road pavements [313]. The development of mechanical properties over time can reasonably be attributed to the formation of geopolymer products which created bonds between coarser grains stabilizing the whole mixtures.

7.1.3 Durability of AA-CDW mixtures

The second investigation (Exp. B2) assessed the durability of CDW-AS-100% mixtures when subjected to F/T degradation. The degradation was applied to compacted and cured cylindrical specimens, and the evolution of mechanical properties (i.e. RM, UCS, and ITS) between undisturbed specimens (not subjected to F/T degradation, 0 F/T) and those subjected to a different number of F/T cycles (4, 8, and 12 cycles) was considered to evaluate its detrimental effect. The analogous treatment was applied to a NGM stabilized with 3% of OPC for comparison purposes.

The optimal amount of AS content was determined as per the gyratory compaction method, obtaining a value equal to 11%, in line with observations from Exp. B1.

CDW-AS-100% not exposed to F/T degradation (0 F/T) exhibited a slight improvement in mechanical properties when passing from 7 to 60 days of curing. Consistently with the key findings from Exp. B1, this improvement is attributable to the evolution of alkali-activation reactions between fines, which create a binding matrix between coarser grains able to stabilize the material. Despite curing at room temperature, CDW-AS-100% mixtures achieved excellent UCS and ITS values after only 7 days of curing, meeting the limits of the Italian specification [313]. These results provided further evidences of the effectiveness of the proposed stabilization method, in line with the considerations made in Exp. B1. However, it emerged that CDW-AS-100% mixtures were markedly sensitive to temperature variations induced by F/T cycles. The most significant outcomes of F/T characterization are as follows:

- after 7 days of curing, a sort of balancing between the negative effect of F/T cycles and the positive influence of additional curing time of CDW-AS-100% specimens exposed to degradation was observed; in fact, after 4 F/T cycles there was a decline in mechanical properties, albeit they experienced a slight recovery after 8 and 12 F/T cycles;

- the same phenomenon is evident with NGM-OPC mixtures cured for 7 days and exposed to F/T degradation;
- the exposure to F/T degradation significantly reduced the stiffness and strength of CDW materials cured for more than 7 days;
- the analysis of regression parameters of MEPDG modelling revealed that variations in the k_1 model parameter between CDW-AS-100% mixtures subjected to 8 and 12 F/T cycles are limited, suggesting that stiffness tended to an asymptotic value after a certain number of F/T cycles;
- differently from CDW material, the mechanical properties of 28-day cured cement-stabilized NGM were not affected by frost degradation.

The greater sensitivity of CDW mixtures in comparison to NGM is mainly attributable to the weaker nature of recycled aggregates. The mechanical characterization of non-degraded CDW-AS-100% mixtures, carried out in both Exp. B1 and Exp. B2, demonstrated the excellent behaviour of the hybrid binder produced from the AA of CDW fines. For this reason, it is reasonable to suppose that the reduction in the stiffness and strength properties of CDW-AS-100% mixtures after F/T degradation was mainly caused by the breakdown of recycled aggregates. This supposition was also supported by preliminary observations on fragmentation and F/T resistance in Exp. B1. The greater toughness of natural-origin aggregates ensured a greater resistance of the NGM-OPC mixtures to F/T degradation.

Despite the fact that CDW-AS-100% mixtures were found to be markedly sensitive to F/T degradation, a comparison with the best RM results obtained by Bassani and Tefa [314] with similar but un-stabilized materials, evidenced that stabilized materials maintained a higher RM even after 12 F/T cycles.

Lastly, a leaching test showed that the AA of CDW fines was beneficial to a reduction in the concentration of chlorides, fluorides, nitrates, and sulphates. In contrast, the level of arsenic, nickel, lead and vanadium had increased in the eluate of alkali-activated product. Nevertheless, CDW-AS-100% mixtures met the requirements of European Council Decision 2003/33/EC [139] and can be classified as inert waste materials.

7.2 Final considerations and future perspectives

The experimental investigation documented in this thesis demonstrates that the alkali-activation of CDW fines is an alternative method for the stabilization of CDW granular materials. The majority of CDW constituent materials were found to be reactive in alkaline conditions even without any specific thermal treatment. At both small- and

large-scale, the excessive dilution of the AS was detrimental to mechanical strength development.

The use of mixtures of recycled aggregates with the AS-100% can effectively be considered an innovative option for new road constructions and rehabilitative works. In that it avoids the use of natural resources (i.e. natural aggregates) and environmentally unfriendly materials (i.e. OPC). Moreover, it is worth noting that the cost of CDW material is currently lower than that of natural aggregates, thus entailing conspicuous savings in the construction of base and subbase layers of pavement structures.

The stabilization method to be adopted for full-scale applications is not dissimilar to the one commonly used for lime- or cement-stabilized granular materials. Tank trucks can distribute the binding agent (in this case the AS) on the layer and construction machines, like the Pulvimixer, can mix CDW aggregates (Figure 7.1). After compaction by rollers, the improved layer made up of CDW and AS initiates the hardening process without any specific thermal treatment. The combination of the chemical activator and recycled aggregates can occur also at the mixing plant, with subsequent transport, laying and compaction operations.

Notwithstanding the promising results documented here, certain aspects require further investigation in the future. With respect to CDW powders, the effect of curing and mixing temperature on the kinetics of alkali-reactions and on the development of mechanical strength is of interest, especially considering the main findings in geopolymer-oriented literature. The optimization of the AS in terms of a reduction of those components having the greatest environmental and economic impact (i.e. sodium silicate and hydroxide) can be considered another element for future investigation.

The second-order effects observed on UND1 and UND2 samples and attributed to the interaction between CDW constituents can be further investigated, as well as the controversial leaching behaviour exhibited by alkali-activated products. In this direction, the employment of advanced technologies, such as solid state nuclear magnetic resonance [528], synchrotron infrared microscopy, and x-ray fluorescence microscopy would help in achieving a greater understanding of the geopolymer structure and chemistry and the whole AA phenomenon [529], [530].

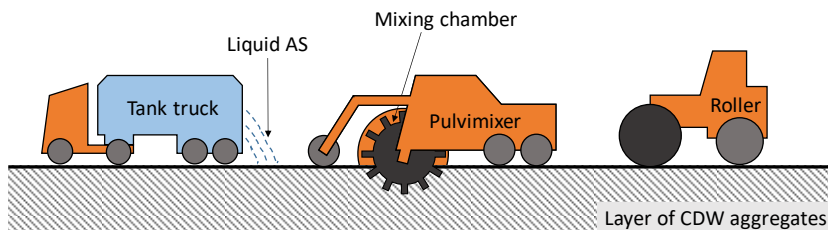


Figure 7.1 - Stabilization of CDW aggregates with Pulvimixer

At the scale of granular mixtures, durability is the most critical aspect. Although CDW-AS-100% mixtures exhibited strength and stiffness values comparable to those of ordinary stabilized materials in base and subbase pavement layers, increased levels of durability in the face of F/T degradation are necessary. In the future, specific experiments to determine if the reduction in mechanical properties was caused by the breakdown of CDW aggregates or by the excessive degradation of alkali-activated binder will be conducted. To address this gap, twin small- and large-scale investigations could be performed to study, on the one hand, the F/T resistance of alkali-activated CDW powders and, on the other, the mechanical behaviour of CDW aggregates stabilized with ordinary binders and subject to the analogous F/T degradation documented here.

Lastly, the innovative stabilization method proposed in the framework of this thesis could be effectively adopted in road pavement constructions only after further investigations of the real-scale mechanical and durability properties. In addition, a specific study of the life cycle assessment of the AA process will confirm the environmental and economic sustainability of the stabilization method.

8. REFERENCES

1. European Builders Confederation. (2018). *ECB's annual report 2017/2018* (Annual Report). Brussels, Belgium: European Builders Confederation.
2. Shen, L.-Y., Hao, J. L., Tam, V. W.-Y., & Yao, H. (2007). A checklist for assessing sustainability performance of construction projects. *Journal of civil engineering and management*, (4), 9.
3. Sjostrom, C., & Bakens, W. (1999). CIB Agenda 21 for sustainable construction: why, how and what. *Building Research & Information*, 27(6), 347–353. doi:10.1080/096132199369174
4. Di Maria, F., Bianconi, F., Micale, C., Baglioni, S., & Marionni, M. (2016). Quality assessment for recycling aggregates from construction and demolition waste: An image-based approach for particle size estimation. *Waste Management*, 48, 344–352. doi:10.1016/j.wasman.2015.12.005
5. World Commission on Environment and Development. (1987). *Our Common Future* (No. A/42/427). New York, NY, US: United Nations.
6. Bourdeau, L. (1999). Sustainable development and the future of construction: a comparison of visions from various countries. *Building Research & Information*, 27(6), 354–366. doi:10.1080/096132199369183
7. Kibert, C. J. (1994). Establishing principles and a model for sustainable construction. In *Proceedings of the first international conference on sustainable construction* (pp. 6–9). Tampa, FA, US.
8. Huovila, P., & Koskela, L. (1998). Contribution of the principles of lean construction to meet the challenges of sustainable development. In *6th Annual Conference of the International Group for Lean Construction*. São Paulo, Brazil.
9. Berardi, U. (2012). Sustainability Assessment in the Construction Sector: Rating Systems and Rated Buildings: Sustainability Assessment in the Construction Sector. *Sustainable Development*, 20(6), 411–424. doi:10.1002/sd.532
10. Sev, A. (2009). How can the construction industry contribute to sustainable development? A conceptual framework. *Sustainable Development*, 17(3), 161–173. doi:10.1002/sd.373
11. Vanegas, J. A., DuBose, J. R., & Pearce, A. R. (1995). Sustainable technologies for the building construction industry. In *Symposium on Design for the Global Environment*. Atlanta, GA, US.
12. Kylili, A., & Fokaides, P. A. (2017). Policy trends for the sustainability assessment of construction materials: A review. *Sustainable Cities and Society*, 35, 280–288. doi:10.1016/j.scs.2017.08.013
13. Marzouk, M., & Azab, S. (2014). Environmental and economic impact assessment of construction and demolition waste disposal using system dynamics. *Resources, Conservation and Recycling*, 82, 41–49. doi:10.1016/j.resconrec.2013.10.015
14. Yeheyis, M., Hewage, K., Alam, M. S., Eskicioglu, C., & Sadiq, R. (2013). An overview of construction and demolition waste management in Canada: a lifecycle analysis approach to sustainability. *Clean Technologies and Environmental Policy*, 15(1), 81–91. doi:10.1007/s10098-012-0481-6
15. Arulrajah, A., Piratheepan, J., Disfani, M. M., & Bo, M. W. (2013). Geotechnical and Geoenvironmental Properties of Recycled Construction and Demolition Materials in Pavement Subbase Applications. *Journal of Materials in Civil Engineering*, 25(8), 1077–1088. doi:10.1061/(ASCE)MT.1943-5533.0000652

16. European Commission. Communication from the Commission to the European Parliament, the Council, the European economic and social Committee and the Committee of the regions. Closing the loop - An EU action plan for the circular economy. Official Journal of the European Union COM/2015/0614 (2015).
17. Adams, K. T., Osmani, M., Thorpe, T., & Thornback, J. (2017). Circular economy in construction: current awareness, challenges and enablers. *Proceedings of the Institution of Civil Engineers - Waste and Resource Management*, 170(1), 15–24. doi:10.1680/jwarm.16.00011
18. Schut, E., Crielaard, M., & Mesman, M. (2015). *Circular economy in the Dutch construction sector. A perspective for the market and government* (Final Report No. 2016– 0024) (p. 58). Bilthoven, The Netherlands: National Institute for Public Health and the Environment.
19. de Brito, J., & Saikia, N. (2013). *Recycled Aggregate in Concrete*. London: Springer London.
20. Jiménez, J. R. (2013). Recycled aggregates (RAs) for roads. In *Handbook of Recycled Concrete and Demolition Waste* (pp. 351–377). Elsevier. doi:10.1533/9780857096906.3.351
21. European Parliament. Directive 2008/98/EC of the European parliament and of the council of 19 November 2008 on waste and repealing certain directives (waste framework directive). 312(11-2b). Official Journal of the European Union 2008/98/EC (2008).
22. Jiménez, J. R., Ayuso, J., Agrela, F., López, M., & Galvín, A. P. (2012). Utilisation of unbound recycled aggregates from selected CDW in unpaved rural roads. *Resources, Conservation and Recycling*, 58, 88–97. doi:10.1016/j.resconrec.2011.10.012
23. Cardoso, R., Silva, R. V., Brito, J. de, & Dhir, R. (2016). Use of recycled aggregates from construction and demolition waste in geotechnical applications: A literature review. *Waste Management*, 49, 131–145. doi:10.1016/j.wasman.2015.12.021
24. Mohammadinia, A., Arulrajah, A., Sanjayan, J., Disfani, M. M., Bo, M. W., & Darmawan, S. (2014). Laboratory Evaluation of the Use of Cement-Treated Construction and Demolition Materials in Pavement Base and Subbase Applications. *Journal of Materials in Civil Engineering*, 27(6), 04014186. doi:10.1061/(ASCE)MT.1943-5533.0001148
25. Del Rey, I., Ayuso, J., Barbudo, A., Galvín, A. P., Agrela, F., & de Brito, J. (2016). Feasibility study of cement-treated 0–8 mm recycled aggregates from construction and demolition waste as road base layer. *Road Materials and Pavement Design*, 17(3), 678–692. doi:10.1080/14680629.2015.1108221
26. Bassani, M., Riviera, P. P., & Tefa, L. (2016). Short-Term and Long-Term Effects of Cement Kiln Dust Stabilization of Construction and Demolition Waste. *Journal of Materials in Civil Engineering*, 29(5), 04016286. doi:10.1061/(ASCE)MT.1943-5533.0001797
27. Mohammadinia, A., Arulrajah, A., Sanjayan, J., Disfani, M. M., Win Bo, M., & Darmawan, S. (2016). Stabilization of Demolition Materials for Pavement Base/Subbase Applications Using Fly Ash and Slag Geopolymers: Laboratory Investigation. *Journal of Materials in Civil Engineering*, 28(7), 04016033. doi:10.1061/(ASCE)MT.1943-5533.0001526
28. Cristelo, N., Fernández-Jiménez, A., Vieira, C., Miranda, T., & Palomo, Á. (2018). Stabilisation of construction and demolition waste with a high fines content using alkali activated fly ash. *Construction and Building Materials*, 170, 26–39. doi:10.1016/j.conbuildmat.2018.03.057
29. Allahverdi, A., & Kani, E. N. (2013). Use of construction and demolition waste (CDW) for alkali-activated or geopolymer cements. In *Handbook of recycled concrete and demolition waste* (pp. 439–475). Elsevier.
30. Komnitsas, K., Zaharaki, D., Vlachou, A., Bartzas, G., & Galetakis, M. (2015). Effect of synthesis parameters on the quality of construction and demolition wastes (CDW) geopolymers. *Advanced Powder Technology*, 26(2), 368–376. doi:10.1016/j.appt.2014.11.012
31. Symonds Group, Argus, COWI Consulting Engineers and Planners, & PRC Bouwcentrum. (1999). *Construction and demolition waste management practices and their economic impacts* (Final Report No. B4- 3040/97/000659/MAR/E3). Brussels, Belgium: European Commission.
32. United States Environmental Protection Agency. (2009). *Estimating 2003 Building-Related Construction and Demolition (C&D) Materials Amounts*. Washington, D.C.: U.S.

- Environmental Protection Agency, Materials Conservation and Recycling Branch, Resource Conservation and Sustainability Division, EPA Office of Resource Conservation and Recovery.
33. Canavese, P., Mondini, N., Zambito, P., Bianco, A., Simonelli, A., & Pavan, S. (2018). *Gli aggregati riciclati nelle opere edili pubbliche e private: le opportunità ambientali ed economiche* (Technical Report) (p. 48). Turin, Italy: Associazione nazionale produttori aggregati riciclati.
 34. Huang, W.-L., Lin, D.-H., Chang, N.-B., & Lin, K.-S. (2002). Recycling of construction and demolition waste via a mechanical sorting process. *Resources, Conservation and Recycling*, 37(1), 23–37.
 35. del Río Merino, M., Izquierdo Gracia, P., & Weis Azevedo, I. S. (2010). Sustainable construction: construction and demolition waste reconsidered. *Waste management & research*, 28(2), 118–129.
 36. Eurostat. (2017). Waste statistics - Statistics Explained. Retrieved 4 December 2017, from http://ec.europa.eu/eurostat/statistics-explained/index.php/Waste_statistics
 37. United States Environmental Protection Agency. (2016). *Advancing Sustainable Materials Management: 2014 Tables and Figures*. Washington, D.C.: U.S. Environmental Protection Agency, Materials Conservation and Recycling Branch, Resource Conservation and Sustainability Division, EPA Office of Resource Conservation and Recovery.
 38. ISPRA. (2016). *Rapporto Rifiuti Speciali* (Report 2016 No. 246). Rome, Italy: Istituto Superiore per la protezione e la ricerca ambientale.
 39. Williams, P. T. (2005). *Waste treatment and disposal* (2nd ed.). Chichester, West Sussex, England ; Hoboken, NJ, USA: Wiley.
 40. European Parliament. Decision 1386/2013/EU of the European Parliament and of the Council of 20 November 2013 on a General Union Environment Action Programme to 2020 ‘Living well, within the limits of our planet’. Official Journal of the European Union 1386/2013/EU (2013).
 41. European Commission Directorate-General for the Environment. (2012). *Handbook on the implementation of EU environmental legislation* (Vol. KH-06-16-004-EN-N). Brussels, Belgium: Hulla & Co Human Dynamics.
 42. Cameron, J., & Abouchar, J. (1991). The precautionary principle: a fundamental principle of law and policy for the protection of the global environment. *BC Int'l & Comp. L. Rev.*, 14, 1.
 43. Gharfalkar, M., Court, R., Campbell, C., Ali, Z., & Hillier, G. (2015). Analysis of waste hierarchy in the European waste directive 2008/98/EC. *Waste Management*, 39, 305–313. doi:10.1016/j.wasman.2015.02.007
 44. Parlamento della Repubblica Italiana. Decreto Legislativo 3 aprile 2006, n.152. Norme in materia ambientale. Supplemento Ordinario n. 96 Gazzetta Ufficiale n. 88 del 14 aprile 2006 (2006).
 45. Parlamento della Repubblica Italiana. Decreto Legislativo 3 dicembre 2010, n.205. Disposizioni di attuazione della direttiva 2008/98/CE del Parlamento europeo e del Consiglio del 19 novembre 2008 relativa ai rifiuti e che abroga alcune direttive. Supplemento ordinario n. 269/L Gazzetta Ufficiale n. 288 del 10 dicembre 2010 (2010).
 46. Ministero dell’Ambiente e della Tutela del Territorio e del Mare. Decreto 7 ottobre 2013. Adozione e approvazione del Programma nazionale prevenzione rifiuti. Serie generale n. 245 Gazzetta Ufficiale del 18 ottobre 2013 (2013).
 47. Parlamento della Repubblica Italiana. Legge 27 dicembre 2013, n.147. Disposizioni per la formazione del bilancio annuale e pluriennale dello Stato (Legge di stabilità 2014). Supplemento ordinario n. 87 Gazzetta Ufficiale del 27-12-2013 n. 302 (2013).
 48. Parlamento della Repubblica Italiana. Legge 28 dicembre 2015, n.221. Disposizioni in materia ambientale per promuovere misure di green economy e per il contenimento dell’uso eccessivo di risorse naturali. Serie Generale n.13 Gazzetta Ufficiale del 18-01-2016 (2015).

49. El-Fadel, M., Findikakis, A. N., & Leckie, J. O. (1997). Environmental Impacts of Solid Waste Landfilling. *Journal of Environmental Management*, 50(1), 1–25. doi:10.1006/jema.1995.0131
50. John, V. M., Angulo, S. C., Miranda, L. F., Agopyan, V., & Vasconcellos, F. (2004). Strategies for innovation in construction demolition waste management in Brazil. In *CIB World Building Congress*.
51. Garbarino, E., & Blengini, G. A. (2013). The economics of construction and demolition waste (C&DW) management facilities. In F. Pacheco-Torgal, V. W. Y. Tam, J. A. Labrincha, Y. Ding, & J. de Brito (Eds.), *Handbook of Recycled Concrete and Demolition Waste* (pp. 108–138). Woodhead Publishing. doi:10.1533/9780857096906.1.108
52. Duran, X., Lenihan, H., & O'Regan, B. (2006). A model for assessing the economic viability of construction and demolition waste recycling—the case of Ireland. *Resources, Conservation and Recycling*, 46(3), 302–320. doi:10.1016/j.resconrec.2005.08.003
53. Zhao, W., Leefstink, R. B., & Rotter, V. S. (2010). Evaluation of the economic feasibility for the recycling of construction and demolition waste in China—The case of Chongqing. *Resources, Conservation and Recycling*, 54(6), 377–389. doi:10.1016/j.resconrec.2009.09.003
54. Bio Intelligence Service, ARCADIS, & Institute European Environmental Policy. (2011). *European Commission, SERVICE CONTRACT ON MANAGEMENT OF CONSTRUCTION AND DEMOLITION WASTE* (Final Report Task 2). Paris, France.
55. Zhu, Q., Geng, Y., & Sarkis, J. (2013). Motivating green public procurement in China: An individual level perspective. *Journal of Environmental Management*, 126, 85–95. doi:10.1016/j.jenvman.2013.04.009
56. Testa, F., Annunziata, E., Iraldo, F., & Frey, M. (2016). Drawbacks and opportunities of green public procurement: an effective tool for sustainable production. *Journal of Cleaner Production*, 112, 1893–1900. doi:10.1016/j.jclepro.2014.09.092
57. Palmujoki, A., Parikka-Alhola, K., & Ekroos, A. (2010). Green Public Procurement: Analysis on the Use of Environmental Criteria in Contracts: GREEN PUBLIC PROCUREMENT. *Review of European Community & International Environmental Law*, 19(2), 250–262. doi:10.1111/j.1467-9388.2010.00681.x
58. Rainville, A. (2017). Standards in green public procurement – A framework to enhance innovation. *Journal of Cleaner Production*, 167, 1029–1037. doi:10.1016/j.jclepro.2016.10.088
59. Ministero dell'Ambiente e della Tutela del Territorio. Decreto Ministeriale 8 maggio 2003. Norme affinché gli uffici pubblici e le società a prevalente capitale pubblico coprano il fabbisogno annuale di manufatti e beni con una quota di prodotti ottenuti da materiale riciclato nella misura non inferiore al 30% del fabbisogno medesimo. , Supplemento ordinario n. 180 Gazzetta Ufficiale del 5 agosto 2003 (2003).
60. Deloitte Touche Tohmatsu Limited. (2015). *Screening template for Construction and Demolition Waste management in Italy* (No. V2).
61. European Commission, Joint Research Centre, & Institute for Prospective Technological Studies. (2009). *End of waste criteria. Final report*. Luxembourg: Publications Office of the European Union.
62. European Commission, Joint Research Centre, & Institute for Prospective Technological Studies. (2010). *Study on the selection of waste streams for end-of-waste assessment: final report*. Luxembourg: Publications Office of the European Union.
63. Böhmer, S., Moser, G., Neubauer, C., Peltoniemi, M., Schachermayer, E., Tesar, M., ... Winter, B. (2008). *Aggregates case study. Final report* (Final Report No. 150787- 2007 FISC-AT) (p. 282). Wien, Austria: Umweltbundesamt.
64. Hjelmar, O., van der Sloot, H. A., Comans, R. N. J., & Wahlström, M. (2013). EoW Criteria for Waste-Derived Aggregates. *Waste and Biomass Valorization*, 4(4), 809–819. doi:10.1007/s12649-013-9261-8
65. Ministero dell'Ambiente. Decreto 5 febbraio 1998. Individuazione dei rifiuti non pericolosi sottoposti alle procedure semplificate di recupero ai sensi degli articoli 31 e 33 del decreto

- legislativo 5 febbraio 1997, n. 22. Supplemento ordinario n. 88 Gazzetta Ufficiale del 16 aprile 1998 (1998).
66. European Committee for Standardization. Aggregates for unbound and hydraulically bound materials for use in civil engineering work and road construction. EN 13242:2008 (2008).
 67. European Committee for Standardization. Aggregates for bituminous mixtures and surface treatments for roads, airfields and other trafficked areas. EN 13043:2004 (2004).
 68. European Committee for Standardization. Aggregates for railway ballast. EN 13450:2003 (2003).
 69. European Committee for Standardization. Aggregates for concrete. EN 12620:2008 (2008).
 70. UNI Ente Nazionale Italiano di Unificazione. Campionamento manuale, preparazione del campione ed analisi degli eluati. UNI 10802:2013 (2013).
 71. European Committee for Standardization. Aggregates for mortar. EN 13139:2003 (2003).
 72. European Committee for Standardization. Armourstone - Part 1: Specification. EN 13383-1:2003 (2003).
 73. Kourmpanis, B., Papadopoulos, A., Moustakas, K., Stylianou, M., Haralambous, K. J., & Loizidou, M. (2008). Preliminary study for the management of construction and demolition waste. *Waste Management & Research*, 26(3), 267–275. doi:10.1177/0734242X07083344
 74. Coelho, A., & de Brito, J. (2011). Economic analysis of conventional versus selective demolition—A case study. *Resources, Conservation and Recycling*, 55(3), 382–392. doi:10.1016/j.resconrec.2010.11.003
 75. Kien, T. T., Thanh, L. T., & Lu, P. V. (2013). Recycling construction demolition waste in the world and in Vietnam. In *The International Conference on Sustainable Built Environment for Now and the Future. Hanoi* (Vol. 26, p. 27).
 76. Rodríguez-Robles, D. (2016). *Ceramic and mixed construction and demolition wastes (CDW): a technically viable and environmentally friendly source of coarse aggregates for the concrete manufacture*. Ghent University.
 77. Evertsson, M. (2000). *Cone Crusher Performance*. Chalmers University of Technology Machine and Vehicle Design, Göteborg, Sweden.
 78. Bressi, G., Volpe, G., & Pavesi, E. (2011). *The production of recycled aggregates from inert waste*. Milan, Italy: Tecnitalia Consultants.
 79. Cecala, A., O'Brien, A., Schall, J., Colinet, J., Fox, W., Franta, R., ... Schultz, M. (2012). *Dust control handbook for industrial minerals mining and processing*. U.S. Department of Health and Human Services, Public Health Service, Centers for Disease Control and Prevention, National Institute for Occupational Safety and Health. doi:10.26616/NIOSHPUB2012112
 80. Tam, V. W. Y., & Tam, C. M. (2006). A review on the viable technology for construction waste recycling. *Resources, Conservation and Recycling*, 47(3), 209–221. doi:10.1016/j.resconrec.2005.12.002
 81. Vegas, I., Broos, K., Nielsen, P., Lambertz, O., & Lisbona, A. (2015). Upgrading the quality of mixed recycled aggregates from construction and demolition waste by using near-infrared sorting technology. *Construction and Building Materials*, 75, 121–128. doi:10.1016/j.conbuildmat.2014.09.109
 82. Chong, W. K., & Hermreck, C. (2010). Understanding transportation energy and technical metabolism of construction waste recycling. *Resources, Conservation and Recycling*, 54(9), 579–590. doi:10.1016/j.resconrec.2009.10.015
 83. Nunes, K. R. A., Mahler, C. F., Valle, R., & Neves, C. (2007). Evaluation of investments in recycling centres for construction and demolition wastes in Brazilian municipalities. *Waste Management*, 27(11), 1531–1540. doi:10.1016/j.wasman.2006.09.007
 84. Coelho, A., & de Brito, J. (2013). Economic viability analysis of a construction and demolition waste recycling plant in Portugal – part I: location, materials, technology and economic analysis. *Journal of Cleaner Production*, 39, 338–352. doi:10.1016/j.jclepro.2012.08.024
 85. Blengini, G. A., & Garbarino, E. (2010). Resources and waste management in Turin (Italy): the role of recycled aggregates in the sustainable supply mix. *Journal of Cleaner Production*, 18(10), 1021–1030. doi:10.1016/j.jclepro.2010.01.027

86. Coelho, A., & Brito, J. de. (2013). Environmental analysis of a construction and demolition waste recycling plant in Portugal – Part I: Energy consumption and CO2 emissions. *Waste Management*, 33(5), 1258–1267. doi:10.1016/j.wasman.2013.01.025
87. Vegas, I. (2015). *Innovative Strategies for High-Grade Material Recovery from Construction and Demolition Waste* (Final Report Summary No. 265212). Spain: Fundacion Tecnalia Research and Innovation.
88. Paranhos, R. S., Cazacliu, B. G., Sampaio, C. H., Petter, C. O., Neto, R. O., & Huchet, F. (2016). A sorting method to value recycled concrete. *Journal of Cleaner Production*, 112, 2249–2258. doi:10.1016/j.jclepro.2015.10.021
89. Bovea, M. D., & Powell, J. C. (2016). Developments in life cycle assessment applied to evaluate the environmental performance of construction and demolition wastes. *Waste Management*, 50, 151–172. doi:10.1016/j.wasman.2016.01.036
90. Mercante, I. T., Bovea, M. D., Ibáñez-Forés, V., & Arena, A. P. (2012). Life cycle assessment of construction and demolition waste management systems: a Spanish case study. *The International Journal of Life Cycle Assessment*, 17(2), 232–241. doi:10.1007/s11367-011-0350-2
91. Estanqueiro, B., Dinis Silvestre, J., de Brito, J., & Duarte Pinheiro, M. (2018). Environmental life cycle assessment of coarse natural and recycled aggregates for concrete. *European Journal of Environmental and Civil Engineering*, 22(4), 429–449. doi:10.1080/19648189.2016.1197161
92. Cabeza, L. F., Rincón, L., Vilariño, V., Pérez, G., & Castell, A. (2014). Life cycle assessment (LCA) and life cycle energy analysis (LCEA) of buildings and the building sector: A review. *Renewable and Sustainable Energy Reviews*, 29, 394–416. doi:10.1016/j.rser.2013.08.037
93. International organization for standardization. Environmental management - Life cycle assessment - Requirements and guidelines. ISO 14044 (2006).
94. Tillman, A.-M. (2000). Significance of decision-making for LCA methodology. *Environmental Impact Assessment Review*, 20(1), 113–123. doi:10.1016/S0195-9255(99)00035-9
95. Ugwu, O. O., & Haupt, T. C. (2007). Key performance indicators and assessment methods for infrastructure sustainability—a South African construction industry perspective. *Building and Environment*, 42(2), 665–680. doi:10.1016/j.buildenv.2005.10.018
96. Hossain, M. U., Poon, C. S., Lo, I. M. C., & Cheng, J. C. P. (2016). Comparative environmental evaluation of aggregate production from recycled waste materials and virgin sources by LCA. *Resources, Conservation and Recycling*, 109, 67–77. doi:10.1016/j.resconrec.2016.02.009
97. Simion, I. M., Fortuna, M. E., Bonoli, A., & Gavrilescu, M. (2013). Comparing environmental impacts of natural inert and recycled construction and demolition waste processing using LCA. *Journal of Environmental Engineering and Landscape Management*, 21(4), 273–287. doi:10.3846/16486897.2013.852558
98. Ghanbari, M., Abbasi, M. A., & Ravanshadian, M. (2017). Environmental life cycle assessment and cost analysis of aggregate production industries compared with hybrid scenario. *Applied Ecology and Environmental Research*, 15(3), 1577–1593. doi:10.15666/aeer/1503_15771593
99. Blengini, G. A. (2009). Life cycle of buildings, demolition and recycling potential: A case study in Turin, Italy. *Building and Environment*, 44(2), 319–330. doi:10.1016/j.buildenv.2008.03.007
100. Balaguera, A., Carvajal, G. I., Albertí, J., & Fullana-i-Palmer, P. (2018). Life cycle assessment of road construction alternative materials: A literature review. *Resources, Conservation and Recycling*, 132, 37–48. doi:10.1016/j.resconrec.2018.01.003
101. Chowdhury, R., Apul, D., & Fry, T. (2010). A life cycle based environmental impacts assessment of construction materials used in road construction. *Resources, Conservation and Recycling*, 54(4), 250–255. doi:10.1016/j.resconrec.2009.08.007

102. Rosado, L. P., Vitale, P., Penteado, C. S. G., & Arena, U. (2017). Life cycle assessment of natural and mixed recycled aggregate production in Brazil. *Journal of Cleaner Production*, 151, 634–642. doi:10.1016/j.jclepro.2017.03.068
103. Penteado, C. S. G., & Rosado, L. P. (2016). Comparison of scenarios for the integrated management of construction and demolition waste by life cycle assessment: A case study in Brazil. *Waste Management & Research*, 34(10), 1026–1035. doi:10.1177/0734242X16657605
104. Butera, S., Christensen, T. H., & Astrup, T. F. (2015). Life cycle assessment of construction and demolition waste management. *Waste Management*, 44, 196–205. doi:10.1016/j.wasman.2015.07.011
105. Mroueh, U.-M., Eskola, P., & Laine-Ylijoki, J. (2001). Life-cycle impacts of the use of industrial by-products in road and earth construction. *Waste Management*, 7.
106. Marinković, S., Radonjanin, V., Malešev, M., & Ignjatović, I. (2010). Comparative environmental assessment of natural and recycled aggregate concrete. *Waste Management*, 30(11), 2255–2264. doi:10.1016/j.wasman.2010.04.012
107. Parajuli, S. P., Naizghi, M. S., Warshay, B., & Arafat, H. A. (2011). A comparative life cycle assessment (LCA) of using virgin crushed aggregate (VCA) and recycled waste concrete aggregate (RCA) in road construction. *International Conference on Water, Energy and Environment*, 312–316.
108. Gschösser, F., Wallbaum, H., & Boesch, M. E. (2012). Life-cycle assessment of the production of Swiss road materials. *Journal of Materials in Civil Engineering*, 24(2), 168–176. doi:10.1061/(ASCE)MT.1943-5533.0000375
109. Yazdanbakhsh, A., Bank, L. C., Baez, T., & Wernick, I. (2018). Comparative LCA of concrete with natural and recycled coarse aggregate in the New York City area. *The International Journal of Life Cycle Assessment*, 23(6), 1163–1173. doi:10.1007/s11367-017-1360-5
110. Ding, T., Xiao, J., & Tam, V. W. Y. (2016). A closed-loop life cycle assessment of recycled aggregate concrete utilization in China. *Waste Management*, 56, 367–375. doi:10.1016/j.wasman.2016.05.031
111. Knoeri, C., Sanyé-Mengual, E., & Althaus, H.-J. (2013). Comparative LCA of recycled and conventional concrete for structural applications. *The International Journal of Life Cycle Assessment*, 18(5), 909–918. doi:10.1007/s11367-012-0544-2
112. Colangelo, F., Forcina, A., Farina, I., & Petrillo, A. (2018). Life Cycle Assessment (LCA) of Different Kinds of Concrete Containing Waste for Sustainable Construction. *Buildings*, 8(5), 70. doi:10.3390/buildings8050070
113. Yuan, H., & Shen, L. (2011). Trend of the research on construction and demolition waste management. *Waste Management*, 31(4), 670–679. doi:10.1016/j.wasman.2010.10.030
114. Sherwood, P. T. (2001). *Alternative materials in road construction: a guide to the use of waste, recycled materials and by-products* (Second edition.). London: Thomas Telford.
115. Rao, A., Jha, K. N., & Misra, S. (2007). Use of aggregates from recycled construction and demolition waste in concrete. *Resources, Conservation and Recycling*, 50(1), 71–81. doi:10.1016/j.resconrec.2006.05.010
116. Silva, R. V., de Brito, J., & Dhir, R. K. (2014). Properties and composition of recycled aggregates from construction and demolition waste suitable for concrete production. *Construction and Building Materials*, 65, 201–217. doi:10.1016/j.conbuildmat.2014.04.117
117. Vieira, C. S., & Pereira, P. M. (2015). Use of recycled construction and demolition materials in geotechnical applications: A review. *Resources, Conservation and Recycling*, 103, 192–204. doi:10.1016/j.resconrec.2015.07.023
118. Limbachiya, M. C., Leelawat, T., & Dhir, R. K. (2000). Use of recycled concrete aggregate in high-strength concrete. *Materials and structures*, 33(9), 574–580.
119. Etxeberria, M., Mari, A. R., & Vázquez, E. (2007). Recycled aggregate concrete as structural material. *Materials and Structures*, 40(5), 529–541. doi:10.1617/s11527-006-9161-5
120. Huda, S. B., & Shahria Alam, M. (2015). Mechanical and Freeze-Thaw Durability Properties of Recycled Aggregate Concrete Made with Recycled Coarse Aggregate. *Journal of Materials in Civil Engineering*, 27(10), 04015003. doi:10.1061/(ASCE)MT.1943-5533.0001237

121. Evangelista, L., & de Brito, J. (2007). Mechanical behaviour of concrete made with fine recycled concrete aggregates. *Cement and Concrete Composites*, 29(5), 397–401. doi:10.1016/j.cemconcomp.2006.12.004
122. Sagoe-Crentsil, K. K., Brown, T., & Taylor, A. H. (2001). Performance of concrete made with commercially produced coarse recycled concrete aggregate. *Cement and concrete research*, 31(5), 707–712.
123. Rodríguez-Robles, D., García-González, J., Juan-Valdés, A., Morán-del Pozo, J., & Guerra-Romero, M. (2014). Quality Assessment of Mixed and Ceramic Recycled Aggregates from Construction and Demolition Wastes in the Concrete Manufacture According to the Spanish Standard. *Materials*, 7(8), 5843–5857. doi:10.3390/ma7085843
124. Poon, C. S., Kou, S. C., & Lam, L. (2002). Use of recycled aggregates in molded concrete bricks and blocks. *Construction and Building Materials*, 16(5), 281–289. doi:10.1016/S0950-0618(02)00019-3
125. Kwan, W. H., Ramli, M., Kam, K. J., & Sulieman, M. Z. (2011). Influence of the amount of recycled coarse aggregate in concrete design and durability properties. *Construction and Building Materials*. doi:10.1016/j.conbuildmat.2011.06.059
126. López Gayarre, F., López-Colina, C., Serrano, M. A., & López-Martínez, A. (2013). Manufacture of concrete kerbs and floor blocks with recycled aggregate from C&DW. *Construction and Building Materials*, 40, 1193–1199. doi:10.1016/j.conbuildmat.2011.11.040
127. Mas, B., Cladera, A., Olmo, T. del, & Pitarch, F. (2012). Influence of the amount of mixed recycled aggregates on the properties of concrete for non-structural use. *Construction and Building Materials*, 27(1), 612–622. doi:10.1016/j.conbuildmat.2011.06.073
128. Mas, B., Cladera, A., Bestard, J., Muntaner, D., López, C. E., Piña, S., & Prades, J. (2012). Concrete with mixed recycled aggregates: Influence of the type of cement. *Construction and Building Materials*, 34, 430–441. doi:10.1016/j.conbuildmat.2012.02.092
129. de Brito, J., Pereira, A. S., & Correia, J. R. (2005). Mechanical behaviour of non-structural concrete made with recycled ceramic aggregates. *Cement and Concrete Composites*, 27(4), 429–433. doi:10.1016/j.cemconcomp.2004.07.005
130. Paine, K. A., & Dhir, R. K. (2010). Recycled aggregates in concrete: a performance-related approach. *Magazine of Concrete Research*, 62(7), 519–530. doi:10.1680/mac.2010.62.7.519
131. Bravo, M., de Brito, J., Pontes, J., & Evangelista, L. (2015). Durability performance of concrete with recycled aggregates from construction and demolition waste plants. *Construction and Building Materials*, 77, 357–369. doi:10.1016/j.conbuildmat.2014.12.103
132. Santos, E. C. G., & Vilar, O. M. (n.d.). Use of recycled construction and demolition wastes (RCDW) as backfill of reinforced soil structures. In *4th European Conference on Geosynthetics e EUROGEO* (Vol. 4, p. 8). Edinburgh, United Kingdom.
133. Santos, E. C. G., Palmeira, E. M., & Bathurst, R. J. (2013). Behaviour of a geogrid reinforced wall built with recycled construction and demolition waste backfill on a collapsible foundation. *Geotextiles and Geomembranes*, 39, 9–19. doi:10.1016/j.geotexmem.2013.07.002
134. Aqil, U., Tatsuoka, F., Uchimura, T., Lohani, T. N., Tomita, Y., & Matsushima, K. (2005). Strength and deformation characteristics of recycled concrete aggregate as a backfill material. *Soils and Foundations*, 45(5), 53–72. doi:10.3208/sandf.45.5_53
135. Arulrajah, A., Rahman, M. A., Piratheepan, J., Bo, M. W., & Imteaz, M. A. (2013). Interface Shear Strength Testing of Geogrid-Reinforced Construction and Demolition Materials. *Advances in Civil Engineering Materials*, 2(1), 20120055. doi:10.1520/ACEM20120055
136. Arulrajah, A., Rahman, M. A., Piratheepan, J., Bo, M. W., & Imteaz, M. A. (2014). Evaluation of Interface Shear Strength Properties of Geogrid-Reinforced Construction and Demolition Materials Using a Modified Large-Scale Direct Shear Testing Apparatus. *Journal of Materials in Civil Engineering*, 26(5), 974–982. doi:10.1061/(ASCE)MT.1943-5533.0000897
137. Vieira, C. S., & Pereira, P. M. (2016). Interface shear properties of geosynthetics and construction and demolition waste from large-scale direct shear tests. *Geosynthetics International*, 23(1), 62–70. doi:10.1680/jgein.15.00030

138. Vieira, C. S., Pereira, P. M., & Lopes, M. de L. (2016). Recycled Construction and Demolition Wastes as filling material for geosynthetic reinforced structures. Interface properties. *Journal of Cleaner Production*, 124, 299–311. doi:10.1016/j.jclepro.2016.02.115
139. European Parliament. Council Decision of 19 December 2002 establishing criteria and procedures for the acceptance of waste at landfills pursuant to Article 16 of and Annex II to Directive 1999/31/EC. Official Journal of the European Communities 2003/33/EC (2003).
140. Sivakumar, V., McKinley, J. D., & Ferguson, D. (2004). Reuse of construction waste: performance under repeated loading. *Proceedings of the Institution of Civil Engineers - Geotechnical Engineering*, 157(2), 91–96. doi:10.1680/geng.2004.157.2.91
141. Rahman, M. A., Imteaz, M., Arulrajah, A., & Disfani, M. M. (2014). Suitability of recycled construction and demolition aggregates as alternative pipe backfilling materials. *Journal of Cleaner Production*, 66, 75–84. doi:10.1016/j.jclepro.2013.11.005
142. Nawagamuwa, U. P., Madarasinghe, D., Goonatillake, M., Karunaratna, H., & Gunaratne, M. (2012). Sustainable reuse of Brownfield properties in Sri Lanka as a gabion fill material. In *ICSBE-2012: International Conference on Sustainable Built Environment* (p. 8). Kandy, Sri Lanka.
143. Papagiannakis, A. T., & Masad, E. A. (2008). *Pavement Design and Materials* (1 edition.). Hoboken, N.J: Wiley.
144. Hill, A. R., Dawson, A. R., & Mundy, M. (2001). Utilisation of aggregate materials in road construction and bulk fill. *Resources, Conservation and Recycling*, 32(3–4), 305–320. doi:10.1016/S0921-3449(01)00067-2
145. Cristelo, N., Vieira, C. S., & de Lurdes Lopes, M. (2016). Geotechnical and Geoenvironmental Assessment of Recycled Construction and Demolition Waste for Road Embankments. *Procedia Engineering*, 143, 51–58. doi:10.1016/j.proeng.2016.06.007
146. Sangiorgi, C., Lantieri, C., & Dondi, G. (2015). Construction and demolition waste recycling: an application for road construction. *International Journal of Pavement Engineering*, 16(6), 530–537. doi:10.1080/10298436.2014.943134
147. Arm, M. (2001). Self-cementing properties of crushed demolished concrete in unbound layers: results from triaxial tests and field tests. *Waste Management*, 21(3), 235–239. doi:10.1016/S0956-053X(00)00095-7
148. Poon, C.-S., Qiao, X. C., & Chan, D. (2006). The cause and influence of self-cementing properties of fine recycled concrete aggregates on the properties of unbound sub-base. *Waste Management*, 26(10), 1166–1172. doi:10.1016/j.wasman.2005.12.013
149. Vegas, I., Ibañez, J. A., Lisbona, A., Sáez de Cortazar, A., & Frías, M. (2011). Pre-normative research on the use of mixed recycled aggregates in unbound road sections. *Construction and Building Materials*, 25(5), 2674–2682. doi:10.1016/j.conbuildmat.2010.12.018
150. O'Mahony, M. M., & Milligan, G. (1991). Use of recycled materials in subbase layers. *Transportation Research Record*, (1310).
151. British Standards Institution. Specification of Highway Works (1986).
152. Collins, R. J., & Ciesielski, S. K. (1994). *Recycling and use of waste materials and by-products in highway construction*. Washington, DC: Transportation Research Board.
153. Goulías, D., Aydilek, A., & Zhang, Y. (2016). *Recycled Material Availability in Maryland – A Synthesis Study* (Final Report No. SP509B4F). Baltimore, MD, US: Maryland State Highway Administration.
154. Bennert, T., Papp Jr, W., Maher, A., & Gucunski, N. (2000). Utilization of construction and demolition debris under traffic-type loading in base and subbase applications. *Transportation research record: journal of the transportation research board*, (1714), 33–39.
155. Nataatmadja, A., & Tan, Y. L. (2001). Resilient Response of Recycled Concrete Road Aggregates. *Journal of Transportation Engineering*, 127(5), 450–453. doi:10.1061/(ASCE)0733-947X(2001)127:5(450)
156. Molenaar, A., & van Niekerk, A. (2002). Effects of gradation, composition, and degree of compaction on the mechanical characteristics of recycled unbound materials. *Transportation Research Record: Journal of the Transportation Research Board*, (1787), 73–82.

157. Leite, F. da C., Motta, R. dos S., Vasconcelos, K. L., & Bernucci, L. (2011). Laboratory evaluation of recycled construction and demolition waste for pavements. *Construction and Building Materials*, 25(6), 2972–2979. doi:10.1016/j.conbuildmat.2010.11.105
158. Arulrajah, A., Piratheepan, J., Disfani, M. M., & Bo, M. W. (2013). Resilient Moduli Response of Recycled Construction and Demolition Materials in Pavement Subbase Applications. *Journal of Materials in Civil Engineering*, 25(12), 1920–1928. doi:10.1061/(ASCE)MT.1943-5533.0000766
159. Bozyurt, O., Tinjum, J. M., Son, Y.-H., Edil, T. B., & Benson, C. H. (2012). Resilient Modulus of Recycled Asphalt Pavement and Recycled Concrete Aggregate (pp. 3901–3910). American Society of Civil Engineers. doi:10.1061/9780784412121.400
160. Cerni, G., & Colagrande, S. (2012). Resilient Modulus of Recycled Aggregates Obtained by Means of Dynamic Tests in a Triaxial Apparatus. *Procedia - Social and Behavioral Sciences*, 53, 475–484. doi:10.1016/j.sbspro.2012.09.898
161. Gabr, A. R., & Cameron, D. A. (2011). Properties of recycled concrete aggregate for unbound pavement construction. *Journal of Materials in Civil Engineering*, 24(6), 754–764.
162. Cerni, G., Cardone, F., & Bocci, M. (2012). Permanent deformation behaviour of unbound recycled mixtures. *Construction and Building Materials*, 37, 573–580. doi:10.1016/j.conbuildmat.2012.07.062
163. Arulrajah, A., Piratheepan, J., & Disfani, M. M. (2014). Reclaimed Asphalt Pavement and Recycled Concrete Aggregate Blends in Pavement Subbases: Laboratory and Field Evaluation. *Journal of Materials in Civil Engineering*, 26(2), 349–357. doi:10.1061/(ASCE)MT.1943-5533.0000850
164. Dong, Q., & Huang, B. (2013). Laboratory evaluation on resilient modulus and rate dependencies of RAP used as unbound base material. *Journal of Materials in Civil Engineering*, 26(2), 379–383.
165. Ayan, V., Khavandi, A., Omer, J. R., & Limbachiya, M. C. (2016). Toughness performance of recycled aggregates for use in road pavement. *International Journal of Transportation Engineering*, 3(3), 171–180.
166. Rustom, R. N., Taha, S., Badarnah, A., & Barahma, H. (2015). Properties of recycled aggregate in concrete and road pavement applications. *IUG Journal of Natural Studies*, 15(2).
167. Park, T. (2003). Application of construction and building debris as base and subbase materials in rigid pavement. *Journal of Transportation Engineering*, 129(5), 558–563.
168. Wartman, J., Grubb, D. G., & Nasim, A. S. M. (2004). Select Engineering Characteristics of Crushed Glass. *Journal of Materials in Civil Engineering*, 16(6), 526–539. doi:10.1061/(ASCE)0899-1561(2004)16:6(526)
169. Grubb, D. G., Davis, A. F., Sands, S. C., Carnivale, M., Wartman, J., & Gallagher, P. M. (2006). Field Evaluation of Crushed Glass–Dredged Material Blends. *Journal of Geotechnical and Geoenvironmental Engineering*, 132(5), 577–590. doi:10.1061/(ASCE)1090-0241(2006)132:5(577)
170. Disfani, M. M., Arulrajah, A., Bo, M. W., & Hankour, R. (2011). Recycled crushed glass in road work applications. *Waste Management*, 31(11), 2341–2351. doi:10.1016/j.wasman.2011.07.003
171. Herrador, R., Pérez, P., Garach, L., & Ordóñez, J. (2012). Use of Recycled Construction and Demolition Waste Aggregate for Road Course Surfacing. *Journal of Transportation Engineering*, 138(2), 182–190. doi:10.1061/(ASCE)TE.1943-5436.0000320
172. Kuo, S.-S., Mahgoub, H., & Nazef, A. (2002). Investigation of recycled concrete made with limestone aggregate for a base course in flexible pavement. *Transportation Research Record: Journal of the Transportation Research Board*, (1787), 99–108.
173. Neves, J., Freire, A. C., Roque, A. J., Martins, I. M., Antunes, M. L., & Faria, G. (2013). Utilization of recycled materials in unbound granular layers validated by experimental test sections. In *9th International Conference on the Bearing Capacity of Roads, Railways and Airfields* (p. 8). Trondheim, Norway.

174. Saride, S., Puppala, A. J., & Williammee, R. (2010). Assessing recycled/secondary materials as pavement bases. *Proceedings of the Institution of Civil Engineers - Ground Improvement*, 163(1), 3–12. doi:10.1680/grim.2010.163.1.3
175. Soleimanbeigi, A., Shedivy, R. F., Tinjum, J. M., & Edil, T. B. (2015). Climatic effect on resilient modulus of recycled unbound aggregates. *Road Materials and Pavement Design*, 16(4), 836–853. doi:10.1080/14680629.2015.1060250
176. Tavira, J., Jiménez, J. R., Ayuso, J., Sierra, M. J., & Ledesma, E. F. (2018). Functional and structural parameters of a paved road section constructed with mixed recycled aggregates from non-selected construction and demolition waste with excavation soil. *Construction and Building Materials*, 164, 57–69. doi:10.1016/j.conbuildmat.2017.12.195
177. Jiménez, J. R., Ayuso, J., Galvín, A. P., López, M., & Agrela, F. (2012). Use of mixed recycled aggregates with a low embodied energy from non-selected CDW in unpaved rural roads. *Construction and Building Materials*, 34, 34–43. doi:10.1016/j.conbuildmat.2012.02.042
178. Del Rey, I., Ayuso, J., Galvín, A., Jiménez, J., & Barbudo, A. (2016). Feasibility of Using Unbound Mixed Recycled Aggregates from CDW over Expansive Clay Subgrade in Unpaved Rural Roads. *Materials*, 9(11), 931. doi:10.3390/ma9110931
179. Vegas, I., Ibañez, J. A., San José, J. T., & Urzelai, A. (2008). Construction demolition wastes, Waelz slag and MSWI bottom ash: A comparative technical analysis as material for road construction. *Waste Management*, 28(3), 565–574. doi:10.1016/j.wasman.2007.01.016
180. Angulo, S. C., & Mueller, A. (2009). Determination of construction and demolition recycled aggregates composition, in considering their heterogeneity. *Materials and Structures*, 42(6), 739–748. doi:10.1617/s11527-008-9417-3
181. Contreras, M., Teixeira, S. R., Lucas, M. C., Lima, L. C. N., Cardoso, D. S. L., da Silva, G. A. C., ... dos Santos, A. (2016). Recycling of construction and demolition waste for producing new construction material (Brazil case-study). *Construction and Building Materials*, 123, 594–600. doi:10.1016/j.conbuildmat.2016.07.044
182. Pasandín, A. R., & Pérez, I. (2013). Laboratory evaluation of hot-mix asphalt containing construction and demolition waste. *Construction and Building Materials*, 43, 497–505. doi:10.1016/j.conbuildmat.2013.02.052
183. Butera, S., Christensen, T. H., & Astrup, T. F. (2014). Composition and leaching of construction and demolition waste: Inorganic elements and organic compounds. *Journal of Hazardous Materials*, 276, 302–311. doi:10.1016/j.jhazmat.2014.05.033
184. Tränkler, J. O. V., Walker, I., & Dohmann, M. (1996). Environmental impact of demolition waste - An overview on 10 years of research and experience. *Waste Management*, 16(1–3), 21–26. doi:10.1016/S0956-053X(96)00061-X
185. Xuan, D. X., Houben, L. J. M., Molenaar, A. A. A., & Shui, Z. H. (2012). Mechanical properties of cement-treated aggregate material – A review. *Materials & Design*, 33, 496–502. doi:10.1016/j.matdes.2011.04.055
186. Pasetto, M. (2000). The re-utilisation of discarded building materials in cement-stabilised layers of road and airfield pavements. In G. R. Woolley, J. J. J. M. Goumans, & P. J. Wainwright (Eds.), *Waste Management Series* (Vol. 1, pp. 548–566). Elsevier. doi:10.1016/S0713-2743(00)80066-5
187. Gobianandh, V., & Jayakody, S. (n.d.). Evaluate the strength of cement treated recycled construction and demolition aggregates as a pavement material. In *The 7th International Conference on Sustainable Built Environment* (p. 6). Kandy, Sri Lanka.
188. Reis, J. H. C., Soares Silva, S., Ildefonso, J. S., & Yshiba, J. K. (2014). Evaluation of Soil, Cement and Construction and Demolition Waste (CDW) Mixtures for Use in Road Pavement Base and Sub-Base Applications. *Key Engineering Materials*, 634, 247–255. doi:10.4028/www.scientific.net/KEM.634.247
189. Xuan, D., Houben, L. J. M., Molenaar, A. A. A., & Shui, Z. (2010). Cement treated recycled demolition waste as a road base material. *Journal of Wuhan University of Technology-Mater. Sci. Ed.*, 25(4), 696–699. doi:10.1007/s11595-010-0073-4

190. Disfani, M. M., Arulrajah, A., Haghighi, H., Mohammadinia, A., & Horpibulsuk, S. (2014). Flexural beam fatigue strength evaluation of crushed brick as a supplementary material in cement stabilized recycled concrete aggregates. *Construction and Building Materials*, 68, 667–676. doi:10.1016/j.conbuildmat.2014.07.007
191. Agrela, F., Barbudo, A., Ramírez, A., Ayuso, J., Carvajal, M. D., & Jiménez, J. R. (2012). Construction of road sections using mixed recycled aggregates treated with cement in Malaga, Spain. *Resources, Conservation and Recycling*, 58, 98–106. doi:10.1016/j.resconrec.2011.11.003
192. Pérez, P., Agrela, F., Herrador, R., & Ordoñez, J. (2013). Application of cement-treated recycled materials in the construction of a section of road in Malaga, Spain. *Construction and Building Materials*, 44, 593–599. doi:10.1016/j.conbuildmat.2013.02.034
193. Behiry, A. E. A. E.-M. (2013). Utilization of cement treated recycled concrete aggregates as base or subbase layer in Egypt. *Ain Shams Engineering Journal*, 4(4), 661–673. doi:10.1016/j.asej.2013.02.005
194. Kien, T. T., Thanh, L. T., & Lu, P. V. (2013). Utilisation of construction demolition waste as stabilised materials for road base applications. In *The International Conference on Sustainable Built Environment for Now and the Future. Hanoi* (Vol. 26, p. 27).
195. Puppala, A. J., Hoyos, L. R., & Potturi, A. K. (2011). Resilient moduli response of moderately cement-treated reclaimed asphalt pavement aggregates. *Journal of Materials in Civil Engineering*, 23(7), 990–998.
196. Xuan, D. X., Molenaar, A. A. A., & Houben, L. J. M. (2015). Evaluation of cement treatment of reclaimed construction and demolition waste as road bases. *Journal of Cleaner Production*, 100, 77–83. doi:10.1016/j.jclepro.2015.03.033
197. Taha, R., Al-Harthy, A., Al-Shamsi, K., & Al-Zubeidi, M. (2002). Cement Stabilization of Reclaimed Asphalt Pavement Aggregate for Road Bases and Subbases. *Journal of Materials in Civil Engineering*, 14(3), 239–245. doi:10.1061/(ASCE)0899-1561(2002)14:3(239)
198. Taha, R. (2003). Evaluation of Cement Kiln Dust-Stabilized Reclaimed Asphalt Pavement Aggregate Systems in Road Bases. *Transportation Research Record: Journal of the Transportation Research Board*, 1819, 11–17. doi:10.3141/1819b-02
199. Arulrajah, A., Mohammadinia, A., D'Amico, A., & Horpibulsuk, S. (2017). Cement kiln dust and fly ash blends as an alternative binder for the stabilization of demolition aggregates. *Construction and Building Materials*, 145, 218–225. doi:10.1016/j.conbuildmat.2017.04.007
200. Camargo, F. F., Edil, T. B., & Benson, C. H. (2013). Strength and stiffness of recycled materials stabilised with fly ash: a laboratory study. *Road Materials and Pavement Design*, 14(3), 504–517. doi:10.1080/14680629.2013.779299
201. Hoy, M., Horpibulsuk, S., & Arulrajah, A. (2016). Strength development of Recycled Asphalt Pavement – Fly ash geopolymer as a road construction material. *Construction and Building Materials*, 117, 209–219. doi:10.1016/j.conbuildmat.2016.04.136
202. Shi, C., Roy, D., & Krivenko, P. (2006). *Alkali-Activated Cements and Concretes*. CRC Press.
203. Provis, J. L. (2014). Geopolymers and other alkali activated materials: why, how, and what? *Materials and Structures*, 47(1–2), 11–25. doi:10.1617/s11527-013-0211-5
204. Hoy, M., Horpibulsuk, S., Rachan, R., Chinkulkijniwat, A., & Arulrajah, A. (2016). Recycled asphalt pavement – fly ash geopolymers as a sustainable pavement base material: Strength and toxic leaching investigations. *Science of The Total Environment*, 573, 19–26. doi:10.1016/j.scitotenv.2016.08.078
205. Mohammadinia, A., Arulrajah, A., Sanjayan, J., Disfani, M. M., Bo, M. W., & Darmawan, S. (2016). Strength Development and Microfabric Structure of Construction and Demolition Aggregates Stabilized with Fly Ash–Based Geopolymers. *Journal of Materials in Civil Engineering*, 28(11), 04016141. doi:10.1061/(ASCE)MT.1943-5533.0001652
206. Arulrajah, A., Mohammadinia, A., Phummiphan, I., Horpibulsuk, S., & Samingthong, W. (2016). Stabilization of Recycled Demolition Aggregates by Geopolymers comprising Calcium Carbide Residue, Fly Ash and Slag precursors. *Construction and Building Materials*, 114, 864–873. doi:10.1016/j.conbuildmat.2016.03.150

207. Vitale, E., Russo, G., Dell'Agli, G., Ferone, C., & Bartolomeo, C. (2017). Mechanical Behaviour of Soil Improved by Alkali Activated Binders. *Environments*, 4(4), 80. doi:10.3390/environments4040080
208. Li, C., Sun, H., & Li, L. (2010). A review: The comparison between alkali-activated slag (Si+Ca) and metakaolin (Si+Al) cements. *Cement and Concrete Research*, 40(9), 1341–1349. doi:10.1016/j.cemconres.2010.03.020
209. Purdon, A. O. (1940). The action of alkalis on blast-furnace slag. *Journal of the Society of Chemical Industry*, 59(9), 191–202.
210. Glukhovskiy, V. D. (1959). Soil silicates. *Gosstroyizdat, Kiev*, 154.
211. Glukhovskiy, V. D., Rostovskaja, G. S., & Rumyna, G. V. (1980). High strength slag-alkaline cements. In *Proceedings of the 7th international congress on the chemistry of cement, Paris* (pp. 164–168).
212. Davidovits, J. (2002). 30 years of successes and failures in geopolymers applications. Market trends and potential breakthroughs. In *Keynote Conference on Geopolymer Conference*.
213. Leonelli, C., & Romagnoli, M. (2011). *Geopolimeri. Polimeri Inorganici Chimicamente Attivati*.
214. Wastiels, J., Wu, X., Faignet, S., & Patfoort, G. (1994). Mineral polymer based on fly ash. *The Journal of resource management and technology*, 22, 135–141.
215. Duxson, P., & Provis, J. L. (2008). Designing Precursors for Geopolymer Cements. *Journal of the American Ceramic Society*, 91(12), 3864–3869. doi:10.1111/j.1551-2916.2008.02787.x
216. Bondar, D., Lynsdale, C. J., Milestone, N. B., Hassani, N., & Ramezaniannpour, A. A. (2011). Effect of type, form, and dosage of activators on strength of alkali-activated natural pozzolans. *Cement and Concrete Composites*, 33(2), 251–260. doi:10.1016/j.cemconcomp.2010.10.021
217. Duran Atiş, C., Bilim, C., Çelik, Ö., & Karahan, O. (2009). Influence of activator on the strength and drying shrinkage of alkali-activated slag mortar. *Construction and Building Materials*, 23(1), 548–555. doi:10.1016/j.conbuildmat.2007.10.011
218. Provis, J. L. (2009). Activating solution chemistry for geopolymers. In *Geopolymers* (pp. 50–71). Elsevier.
219. Pacheco-Torgal, F., Castro-Gomes, J., & Jalali, S. (2008). Alkali-activated binders: A review. Part 1. Historical background, terminology, reaction mechanisms and hydration products. *Construction and Building Materials*, 22(7), 1305–1314. doi:10.1016/j.conbuildmat.2007.10.015
220. Juenger, M. C. G., Winnefeld, F., Provis, J. L., & Ideker, J. H. (2011). Advances in alternative cementitious binders. *Cement and Concrete Research*, 41(12), 1232–1243. doi:10.1016/j.cemconres.2010.11.012
221. Liew, Y.-M., Heah, C.-Y., Mohd Mustafa, A. B., & Kamarudin, H. (2016). Structure and properties of clay-based geopolymer cements: A review. *Progress in Materials Science*, 83, 595–629. doi:10.1016/j.pmatsci.2016.08.002
222. Tchadjie, L. N., & Ekolü, S. O. (2018). Enhancing the reactivity of aluminosilicate materials toward geopolymer synthesis. *Journal of Materials Science*, 53(7), 4709–4733. doi:10.1007/s10853-017-1907-7
223. Duxson, P., Fernández-Jiménez, A., Provis, J. L., Lukey, G. C., Palomo, A., & van Deventer, J. S. J. (2007). Geopolymer technology: the current state of the art. *Journal of Materials Science*, 42(9), 2917–2933. doi:10.1007/s10853-006-0637-z
224. Xu, H., & Van Deventer, J. S. J. (2000). The geopolymerisation of aluminosilicate minerals. *International Journal of Mineral Processing*, 59(3), 247–266. doi:10.1016/S0301-7516(99)00074-5
225. Komnitsas, K., & Zaharaki, D. (2007). Geopolymerisation: A review and prospects for the minerals industry. *Minerals Engineering*, 20(14), 1261–1277. doi:10.1016/j.mineng.2007.07.011
226. Wang, H., Li, H., & Yan, F. (2005). Synthesis and mechanical properties of metakaolinite-based geopolymer. *Colloids and Surfaces A: Physicochemical and Engineering Aspects*, 268(1–3), 1–6. doi:10.1016/j.colsurfa.2005.01.016

227. Pacheco-Torgal, F., Castro-Gomes, J., & Jalali, S. (2008). Alkali-activated binders: A review. Part 2. About materials and binders manufacture. *Construction and Building Materials*, 22(7), 1315–1322. doi:10.1016/j.conbuildmat.2007.03.019
228. Cuisinier, O., Deneele, D., & Masrouri, F. (2009). Shear strength behaviour of compacted clayey soils percolated with an alkaline solution. *Engineering Geology*, 108(3–4), 177–188. doi:10.1016/j.enggeo.2009.07.012
229. Slaty, F., Khoury, H., Wastiels, J., & Rahier, H. (2013). Characterization of alkali activated kaolinitic clay. *Applied Clay Science*, 75–76, 120–125. doi:10.1016/j.clay.2013.02.005
230. Alonso, S., & Palomo, A. (2001). Alkaline activation of metakaolin and calcium hydroxide mixtures: influence of temperature, activator concentration and solids ratio. *Materials Letters*, 47(1–2), 55–62. doi:10.1016/S0167-577X(00)00212-3
231. Duxson, P., Mallicoat, S. W., Lukey, G. C., Kriven, W. M., & van Deventer, J. S. J. (2007). The effect of alkali and Si/Al ratio on the development of mechanical properties of metakaolin-based geopolymers. *Colloids and Surfaces A: Physicochemical and Engineering Aspects*, 292(1), 8–20. doi:10.1016/j.colsurfa.2006.05.044
232. Molino, B., De Vincenzo, A., Ferone, C., Messina, F., Colangelo, F., & Cioffi, R. (2014). Recycling of Clay Sediments for Geopolymer Binder Production. A New Perspective for Reservoir Management in the Framework of Italian Legislation: The Occhito Reservoir Case Study. *Materials*, 7(8), 5603–5616. doi:10.3390/ma7085603
233. Messina, F., Ferone, C., Molino, A., Roviello, G., Colangelo, F., Molino, B., & Cioffi, R. (2017). Synergistic recycling of calcined clayey sediments and water potabilization sludge as geopolymer precursors: Upscaling from binders to precast paving cement-free bricks. *Construction and Building Materials*, 133, 14–26. doi:10.1016/j.conbuildmat.2016.12.039
234. Palmero, P., Formia, A., Tulliani, J.-M., & Antonaci, P. (2017). Valorisation of aluminosilicate stone muds: From wastes to source materials for innovative alkali-activated materials. *Cement and Concrete Composites*, 83, 251–262. doi:10.1016/j.cemconcomp.2017.07.011
235. Zhang, Y. J., Zhao, Y. L., Li, H. H., & Xu, D. L. (2008). Structure characterization of hydration products generated by alkaline activation of granulated blast furnace slag. *Journal of Materials Science*, 43(22), 7141–7147. doi:10.1007/s10853-008-3028-9
236. Ben Haha, M., Le Saout, G., Winnefeld, F., & Lothenbach, B. (2011). Influence of activator type on hydration kinetics, hydrate assemblage and microstructural development of alkali activated blast-furnace slags. *Cement and Concrete Research*, 41(3), 301–310. doi:10.1016/j.cemconres.2010.11.016
237. Palomo, A., Grutzeck, M. W., & Blanco, M. T. (1999). Alkali-activated fly ashes: a cement for the future. *Cement and concrete research*, 29(8), 1323–1329.
238. Hardjito, D., Cheak, C. C., & Ing, C. H. L. (2008). Strength and setting times of low calcium fly ash-based geopolymer mortar. *Modern applied science*, 2(4), 3.
239. Kumar, S., Kumar, R., & Mehrotra, S. P. (2010). Influence of granulated blast furnace slag on the reaction, structure and properties of fly ash based geopolymer. *Journal of Materials Science*, 45(3), 607–615. doi:10.1007/s10853-009-3934-5
240. Marjanović, N., Komljenović, M., Bašćarević, Z., Nikolić, V., & Petrović, R. (2015). Physical–mechanical and microstructural properties of alkali-activated fly ash–blast furnace slag blends. *Ceramics International*, 41(1), 1421–1435. doi:10.1016/j.ceramint.2014.09.075
241. Buchwald, A., & Schulz, M. (2005). Alkali-activated binders by use of industrial by-products. *Cement and Concrete Research*, 35(5), 968–973. doi:10.1016/j.cemconres.2004.06.019
242. Brew, D. R. M., & MacKenzie, K. J. D. (2007). Geopolymer synthesis using silica fume and sodium aluminate. *Journal of Materials Science*, 42(11), 3990–3993. doi:10.1007/s10853-006-0376-1
243. Sathonsaowaphak, A., Chindaprasit, P., & Pimraksa, K. (2009). Workability and strength of lignite bottom ash geopolymer mortar. *Journal of Hazardous Materials*, 168(1), 44–50. doi:10.1016/j.jhazmat.2009.01.120
244. American Concrete Institute. ACI-ITG-10R: Practitioner’s Guide for Alternative Cements. , Pub. L. No. ITG-10R-18 (2018).

245. Huntzinger, D. N., & Eatmon, T. D. (2009). A life-cycle assessment of Portland cement manufacturing: comparing the traditional process with alternative technologies. *Journal of Cleaner Production*, 17(7), 668–675. doi:10.1016/j.jclepro.2008.04.007
246. Hendriks, C. A., Worrell, E., De Jager, D., Blok, K., & Riemer, P. (1998). Emission reduction of greenhouse gases from the cement industry. In *Proceedings of the 4th International Conference on greenhouse gas control technologies* (pp. 939–944). Interlaken, Austria.
247. Newman, J., & Choo, B. S. (2003). *Advanced Concrete Technology Constituent materials*. Burlington, MA, US: Elsevier.
248. Bizzozero, J., Gosselin, C., & Scrivener, K. L. (2014). Expansion mechanisms in calcium aluminate and sulfoaluminate systems with calcium sulfate. *Cement and Concrete Research*, 56, 190–202. doi:10.1016/j.cemconres.2013.11.011
249. Damtoft, J. S., Lukasik, J., Herfort, D., Sorrentino, D., & Gartner, E. M. (2008). Sustainable development and climate change initiatives. *Cement and Concrete Research*, 38(2), 115–127. doi:10.1016/j.cemconres.2007.09.008
250. Scrivener, K. L., Cabiron, J.-L., & Letourneux, R. (1999). High-performance concretes from calcium aluminate cements. *Cement and Concrete Research*, 29(8), 1215–1223. doi:10.1016/S0008-8846(99)00103-9
251. Sharp, J. H., Lawrence, C. D., & Yang, R. (1999). Calcium sulfoaluminate cements - low-energy cements, special cements or what? *Advances in Cement Research*, 11(1), 3–13. doi:10.1680/adcr.1999.11.1.3
252. Li, Y., & Chen, B. (2013). Factors that affect the properties of magnesium phosphate cement. *Construction and Building Materials*, 47, 977–983. doi:10.1016/j.conbuildmat.2013.05.103
253. Tonelli, M., Martini, F., Calucci, L., Fratini, E., Geppi, M., Ridi, F., ... Baglioni, P. (2016). Structural characterization of magnesium silicate hydrate: towards the design of eco-sustainable cements. *Dalton Transactions*, 45(8), 3294–3304. doi:10.1039/C5DT03545G
254. Yang, N., Shi, C., Yang, J., & Chang, Y. (2014). Research Progresses in Magnesium Phosphate Cement-Based Materials. *Journal of Materials in Civil Engineering*, 26(10), 04014071. doi:10.1061/(ASCE)MT.1943-5533.0000971
255. Grounds, T., Nowell, D., & Wilburn, F. (2003). Resistance of supersulfated cement to strong sulfate solutions. *Journal of Thermal Analysis and Calorimetry*, 72(1), 181–190. doi:10.1023/A:1023928021602
256. Matschei, T., Bellmann, F., & Stark, J. (2005). Hydration behaviour of sulphate-activated slag cements. *Advances in Cement Research*, 17(4), 167–178. doi:10.1680/adcr.2005.17.4.167
257. Niu, Q. L., Li, C. Z., & Zhao, S. Q. (2011). Properties of a low-carbon cement with 90% of industrial refuse. In *Key Engineering Materials* (Vol. 477, pp. 91–94). Trans Tech Publ. doi:https://doi.org/10.4028/www.scientific.net/KEM.477.91
258. Yang, K.-H., Jung, Y.-B., Cho, M.-S., & Tae, S.-H. (2015). Effect of supplementary cementitious materials on reduction of CO₂ emissions from concrete. *Journal of Cleaner Production*, 103, 774–783. doi:10.1016/j.jclepro.2014.03.018
259. Imbabi, M. S., Carrigan, C., & McKenna, S. (2012). Trends and developments in green cement and concrete technology. *International Journal of Sustainable Built Environment*, 1(2), 194–216. doi:10.1016/j.ijsbe.2013.05.001
260. Li, Y., Hao, L., & Chen, X. (2016). Analysis of MSWI Bottom Ash Reused as Alternative Material for Cement Production. *Procedia Environmental Sciences*, 31, 549–553. doi:10.1016/j.proenv.2016.02.084
261. Saikia, N., Kato, S., & Kojima, T. (2007). Production of cement clinkers from municipal solid waste incineration (MSWI) fly ash. *Waste Management*, 27(9), 1178–1189. doi:10.1016/j.wasman.2006.06.004
262. Gartner, E., & Hirao, H. (2015). A review of alternative approaches to the reduction of CO₂ emissions associated with the manufacture of the binder phase in concrete. *Cement and Concrete Research*, 78, 126–142. doi:10.1016/j.cemconres.2015.04.012
263. Puertas, F., García-Díaz, I., Barba, A., Gazulla, M. F., Palacios, M., Gómez, M. P., & Martínez-Ramírez, S. (2008). Ceramic wastes as alternative raw materials for Portland cement clinker

- production. *Cement and Concrete Composites*, 30(9), 798–805. doi:10.1016/j.cemconcomp.2008.06.003
264. Flower, D. J. M., & Sanjayan, J. G. (2007). Green house gas emissions due to concrete manufacture. *The International Journal of Life Cycle Assessment*, 12(5), 282–288. doi:10.1065/lca2007.05.327
265. Zhou, Q., Milestone, N. B., & Hayes, M. (2006). An alternative to Portland Cement for waste encapsulation - The calcium sulfoaluminate cement system. *Journal of Hazardous Materials*, 136(1), 120–129. doi:10.1016/j.jhazmat.2005.11.038
266. Scrivener, K. L., John, V. M., & Gartner, E. M. (2018). Eco-efficient cements: Potential economically viable solutions for a low-CO₂ cement-based materials industry. *Cement and Concrete Research*, 114, 2–26. doi:10.1016/j.cemconres.2018.03.015
267. Angulski da Luz, C., & Hooton, R. D. (2015). Influence of curing temperature on the process of hydration of supersulfated cements at early age. *Cement and Concrete Research*, 77, 69–75. doi:10.1016/j.cemconres.2015.07.002
268. Burris, L. E., Alapati, P., Moser, R. D., Ley, M. T., Berke, N., & Kurtis, K. E. (2015). Alternative cementitious materials: challenges and opportunities. In *International Workshop on Durability and Sustainability of Concrete Structures*. Bologna, Italy.
269. Komnitsas, K. A. (2011). Potential of geopolymer technology towards green buildings and sustainable cities. *Procedia Engineering*, 21, 1023–1032. doi:10.1016/j.proeng.2011.11.2108
270. Davidovits, J. (2005). Geopolymer chemistry and sustainable development. The poly (sialate) terminology: a very useful and simple model for the promotion and understanding of green-chemistry. In *Proceedings of the world congress Geopolymer* (pp. 9–15). Saint Quentin, France.
271. van Deventer, J. S. J., Provis, J. L., Duxson, P., & Brice, D. G. (2010). Chemical Research and Climate Change as Drivers in the Commercial Adoption of Alkali Activated Materials. *Waste and Biomass Valorization*, 1(1), 145–155. doi:10.1007/s12649-010-9015-9
272. McLellan, B. C., Williams, R. P., Lay, J., van Riessen, A., & Corder, G. D. (2011). Costs and carbon emissions for geopolymer pastes in comparison to ordinary portland cement. *Journal of Cleaner Production*, 19(9–10), 1080–1090. doi:10.1016/j.jclepro.2011.02.010
273. Teh, S. H., Wiedmann, T., Castel, A., & de Burgh, J. (2017). Hybrid life cycle assessment of greenhouse gas emissions from cement, concrete and geopolymer concrete in Australia. *Journal of Cleaner Production*, 152, 312–320. doi:10.1016/j.jclepro.2017.03.122
274. Salas, D. A., Ramirez, A. D., Ulloa, N., Baykara, H., & Boero, A. J. (2018). Life cycle assessment of geopolymer concrete. *Construction and Building Materials*, 190, 170–177. doi:10.1016/j.conbuildmat.2018.09.123
275. Passuello, A., Rodríguez, E. D., Hirt, E., Longhi, M., Bernal, S. A., Provis, J. L., & Kirchheim, A. P. (2017). Evaluation of the potential improvement in the environmental footprint of geopolymers using waste-derived activators. *Journal of Cleaner Production*, 166, 680–689. doi:10.1016/j.jclepro.2017.08.007
276. Rodríguez, E. D., Bernal, S. A., Provis, J. L., Paya, J., Monzo, J. M., & Borrachero, M. V. (2013). Effect of nanosilica-based activators on the performance of an alkali-activated fly ash binder. *Cement and Concrete Composites*, 35(1), 1–11. doi:10.1016/j.cemconcomp.2012.08.025
277. Habert, G., d'Espinose de Lacaillerie, J. B., & Roussel, N. (2011). An environmental evaluation of geopolymer based concrete production: reviewing current research trends. *Journal of Cleaner Production*, 19(11), 1229–1238. doi:10.1016/j.jclepro.2011.03.012
278. Turner, L. K., & Collins, F. G. (2013). Carbon dioxide equivalent (CO₂-e) emissions: A comparison between geopolymer and OPC cement concrete. *Construction and Building Materials*, 43, 125–130. doi:10.1016/j.conbuildmat.2013.01.023
279. Provis, J. L., & Bernal, S. A. (2014). Geopolymers and Related Alkali-Activated Materials. *Annual Review of Materials Research*, 44(1), 299–327. doi:10.1146/annurev-matsci-070813-113515

280. Wang, S.-D., Pu, X.-C., Scrivener, K. L., & Pratt, P. L. (1995). Alkali-activated slag cement and concrete: a review of properties and problems. *Advances in Cement Research*, 7(27), 93–102. doi:10.1680/adcr.1995.7.27.93
281. Rashad, A. M. (2013). Alkali-activated metakaolin: A short guide for civil Engineer - An overview. *Construction and Building Materials*, 41, 751–765. doi:10.1016/j.conbuildmat.2012.12.030
282. Singh, B., Ishwarya, G., Gupta, M., & Bhattacharyya, S. K. (2015). Geopolymer concrete: A review of some recent developments. *Construction and Building Materials*, 85, 78–90. doi:10.1016/j.conbuildmat.2015.03.036
283. Fernández-Jiménez, A., Palomo, J. G., & Puertas, F. (1999). Alkali-activated slag mortars: mechanical strength behaviour. *Cement and Concrete Research*, 29(8), 1313–1321.
284. Pelisser, F., Guerrino, E. L., Menger, M., Michel, M. D., & Labrincha, J. A. (2013). Micromechanical characterization of metakaolin-based geopolymers. *Construction and Building Materials*, 49, 547–553. doi:10.1016/j.conbuildmat.2013.08.081
285. Davidovits, J. (1994). Properties of geopolymer cements. In *First international conference on alkaline cements and concretes* (Vol. 1, pp. 131–149).
286. Jang, J. G., Lee, N. K., & Lee, H. K. (2014). Fresh and hardened properties of alkali-activated fly ash/slag pastes with superplasticizers. *Construction and Building Materials*, 50, 169–176. doi:10.1016/j.conbuildmat.2013.09.048
287. Pacheco-Torgal, F., Abdollahnejad, Z., Camões, A. F., Jamshidi, M., & Ding, Y. (2012). Durability of alkali-activated binders: A clear advantage over Portland cement or an unproven issue? *Construction and Building Materials*, 30, 400–405. doi:10.1016/j.conbuildmat.2011.12.017
288. Provis, J. L. (2018). Alkali-activated materials. *Cement and Concrete Research*, 114, 40–48. doi:10.1016/j.cemconres.2017.02.009
289. Sun, Z., Cui, H., An, H., Tao, D., Xu, Y., Zhai, J., & Li, Q. (2013). Synthesis and thermal behavior of geopolymer-type material from waste ceramic. *Construction and Building Materials*, 49, 281–287. doi:10.1016/j.conbuildmat.2013.08.063
290. Reig, L., Tashima, M. M., Soriano, L., Borrachero, M. V., Monzó, J., & Payá, J. (2013). Alkaline Activation of Ceramic Waste Materials. *Waste and Biomass Valorization*, 4(4), 729–736. doi:10.1007/s12649-013-9197-z
291. Reig, L., Tashima, M. M., Borrachero, M. V., Monzó, J., Cheeseman, C. R., & Payá, J. (2013). Properties and microstructure of alkali-activated red clay brick waste. *Construction and Building Materials*, 43, 98–106. doi:10.1016/j.conbuildmat.2013.01.031
292. Robayo-Salazar, R. A., Mulford, A., Munera, J., & Mejía de Gutiérrez, R. (2016). Alternative cements based on alkali-activated red clay brick waste. *Construction and Building Materials*, 128, 163–169. doi:10.1016/j.conbuildmat.2016.10.023
293. Allahverdi, A., & Kani, E. N. (2009). Construction wastes as raw materials for geopolymer binders. *Int J Civil Eng*, 7(3), 154–160.
294. Pathak, A., Kumar, S., & Jha, V. K. (2014). Development of Building Material from Geopolymerization of Construction and Demolition Waste (CDW). *Transactions of the Indian Ceramic Society*, 73(2), 133–137. doi:10.1080/0371750X.2014.922429
295. Jha, V. K., & Tuladhar, A. (2013). An attempt of geopolymer synthesis from construction waste. *Journal of Nepal Chemical Society*, 28, 29–33.
296. Payá, J., Borrachero, M. V., Monzó, J., Soriano, L., & Tashima, M. M. (2012). A new geopolymeric binder from hydrated-carbonated cement. *Materials Letters*, 74, 223–225. doi:10.1016/j.matlet.2012.01.132
297. Zaharaki, D., Galetakis, M., & Komnitsas, K. (2016). Valorization of construction and demolition (C&D) and industrial wastes through alkali activation. *Construction and Building Materials*, 121, 686–693. doi:10.1016/j.conbuildmat.2016.06.051
298. Komnitsas, K. (2016). Co-valorization of marine sediments and construction and demolition wastes through alkali activation. *Journal of Environmental Chemical Engineering*. doi:10.1016/j.jece.2016.11.003

299. Ahmari, S., Ren, X., Toufigh, V., & Zhang, L. (2012). Production of geopolymeric binder from blended waste concrete powder and fly ash. *Construction and Building Materials*, 35, 718–729. doi:10.1016/j.conbuildmat.2012.04.044
300. Zedan, S. R., Mohamed, M. R., Ahmed, D. A., & Mohammed, A. H. (2015). Effect of demolition/construction wastes on the properties of alkali activated slag cement. *HBRC Journal*. doi:10.1016/j.hbrj.2015.12.001
301. Silva, R. V., de Brito, J., & Dhir, R. K. (2017). Availability and processing of recycled aggregates within the construction and demolition supply chain: A review. *Journal of Cleaner Production*, 143, 598–614. doi:10.1016/j.jclepro.2016.12.070
302. Santagata, F. A. (2016). *Strade - Teoria e tecnica delle costruzioni stradali* (Vols 1-2, Vol. 1). Torino: Pearson.
303. Kézdi, A. (1979). *Stabilized Earth Roads*. New York, NY, US: Elsevier Scientific Publishing Company.
304. Yoder, E. J., & Witczak, M. W. (1975). *Principles of Pavement Design*. John Wiley & Sons.
305. Provis, J. (2013). *Alkali activated materials: state-of-the-art report, RILEM TC 224-AAM*. New York: Springer.
306. Pathak, A., & Jha, V. K. (2013). Synthesis of Geopolymer from Inorganic Construction Waste. *Journal of Nepal Chemical Society*, 30, 45–51.
307. Parthiban, K., & Saravana Raja Mohan, K. (2014). Effect of Sodium Hydroxide Concentration and Alkaline Ratio on the Compressive Strength of Slag Based Geopolymer Concrete. *International Journal of ChemTech Research*, 6, 974–4290.
308. Malkawi, A. B., Nuruddin, M. F., Fauzi, A., Almattarneh, H., & Mohammed, B. S. (2016). Effects of Alkaline Solution on Properties of the HCFA Geopolymer Mortars. *Procedia Engineering*, 148, 710–717. doi:10.1016/j.proeng.2016.06.581
309. Duxson, P., Provis, J. L., Lukey, G. C., Mallicoat, S. W., Kriven, W. M., & van Deventer, J. S. J. (2005). Understanding the relationship between geopolymer composition, microstructure and mechanical properties. *Colloids and Surfaces A: Physicochemical and Engineering Aspects*, 269(1–3), 47–58. doi:10.1016/j.colsurfa.2005.06.060
310. Diaz, E. I., Allouche, E. N., & Eklund, S. (2010). Factors affecting the suitability of fly ash as source material for geopolymers. *Fuel*, 89(5), 992–996. doi:10.1016/j.fuel.2009.09.012
311. Weng, L., Sagoe-Crentsil, K., Brown, T., & Song, S. (2005). Effects of aluminates on the formation of geopolymers. *Materials Science and Engineering: B*, 117(2), 163–168. doi:10.1016/j.mseb.2004.11.008
312. Kumar, S., Kristály, F., & Mucsi, G. (2015). Geopolymerisation behaviour of size fractioned fly ash. *Advanced Powder Technology*, 26(1), 24–30. doi:10.1016/j.appt.2014.09.001
313. Centro Interuniversitario Sperimentale di Ricerca Stradale. Norme Tecniche Prestazionali per Capitolati Speciali d'Appalto (2001).
314. Bassani, M., & Tefa, L. (2018). Compaction and freeze-thaw degradation assessment of recycled aggregates from unseparated construction and demolition waste. *Construction and Building Materials*, 160, 180–195. doi:10.1016/j.conbuildmat.2017.11.052
315. Zaman, M., Zhu, J.-H., & Laguros, J. (1999). Durability effects on resilient moduli of stabilized aggregate base. *Transportation Research Record: Journal of the Transportation Research Board*, (1687), 29–38.
316. Khoury, N. N., & Zaman, M. M. (2007). Environmental Effects on Durability of Aggregates Stabilized with Cementitious Materials. *Journal of Materials in Civil Engineering*, 19(1), 41–48. doi:10.1061/(ASCE)0899-1561(2007)19:1(41)
317. Bozyurt, O., Keene, A. K., Tinjum, J. M., Edil, T. B., & Fratta, D. (2013). Freeze-Thaw Effects on Stiffness of Unbound Recycled Road Base. In H. Zubeck & Z. Yang (Eds.), *Mechanical Properties of Frozen Soil* (pp. 1–19). 100 Barr Harbor Drive, PO Box C700, West Conshohocken, PA 19428-2959: ASTM International. doi:10.1520/STP156820130014
318. Solanki, P., Zaman, M., & Dean, J. (2010). Resilient Modulus of Clay Subgrades Stabilized with Lime, Class C Fly Ash, and Cement Kiln Dust for Pavement Design. *Transportation*

- Research Record: Journal of the Transportation Research Board*, 2186, 101–110. doi:10.3141/2186-11
319. Pandey, A., & Rabbani, A. (2017). Soil stabilisation using cement. *International Journal of Civil Engineering and Technology (IJCET)*, 8(6), 316–322.
 320. Fernández-Jiménez, A., & Puertas, F. (1997). Alkali-activated slag cements: Kinetic studies. *Cement and Concrete Research*, 27(3), 359–368. doi:10.1016/S0008-8846(97)00040-9
 321. Mo, B., Zhu, H., Cui, X., He, Y., & Gong, S. (2014). Effect of curing temperature on geopolymerization of metakaolin-based geopolymers. *Applied Clay Science*, 99, 144–148. doi:10.1016/j.clay.2014.06.024
 322. Sindhunata, van Deventer, J. S. J., Lukey, G. C., & Xu, H. (2006). Effect of Curing Temperature and Silicate Concentration on Fly-Ash-Based Geopolymerization. *Industrial & Engineering Chemistry Research*, 45(10), 3559–3568. doi:10.1021/ie051251p
 323. European Committee for Standardization. Tests for general properties of aggregates - Part 1: Methods for sampling. EN 932-1:1996 (1996).
 324. European Committee for Standardization. Geotechnical investigation and testing - Laboratory testing of soil - Part 1: Determination of water content. EN ISO 17892-1:2014 (2014).
 325. European Committee for Standardization. Tests for geometrical properties of aggregates - Part 1: Determination of particle size distribution - Sieving method. EN 933-1:2012 (2012).
 326. Temuujin, J., Williams, R. P., & van Riessen, A. (2009). Effect of mechanical activation of fly ash on the properties of geopolymer cured at ambient temperature. *Journal of Materials Processing Technology*, 209(12–13), 5276–5280. doi:10.1016/j.jmatprotec.2009.03.016
 327. Assi, L. N., Eddie Deaver, E., & Ziehl, P. (2018). Effect of source and particle size distribution on the mechanical and microstructural properties of fly Ash-Based geopolymer concrete. *Construction and Building Materials*, 167, 372–380. doi:10.1016/j.conbuildmat.2018.01.193
 328. Robayo-Salazar, R. A., Rivera, J. F., & Mejía de Gutiérrez, R. (2017). Alkali-activated building materials made with recycled construction and demolition wastes. *Construction and Building Materials*, 149, 130–138. doi:10.1016/j.conbuildmat.2017.05.122
 329. Petrillo, A., Cioffi, R., Ferone, C., Colangelo, F., & Borrelli, C. (2016). Eco-sustainable Geopolymer Concrete Blocks Production Process. *Agriculture and Agricultural Science Procedia*, 8, 408–418. doi:10.1016/j.aaspro.2016.02.037
 330. Liew, Y. M., Kamarudin, H., Mustafa Al Bakri, A. M., Bnhussain, M., Luqman, M., Khairul Nizar, I., ... Heah, C. Y. (2012). Optimization of solids-to-liquid and alkali activator ratios of calcined kaolin geopolymeric powder. *Construction and Building Materials*, 37, 440–451. doi:10.1016/j.conbuildmat.2012.07.075
 331. International organization for standardization. Viscosity of water. ISO/TR 3666 (1998).
 332. Yang, X., Zhu, W., & Yang, Q. (2008). The Viscosity Properties of Sodium Silicate Solutions. *Journal of Solution Chemistry*, 37(1), 73–83. doi:10.1007/s10953-007-9214-6
 333. Little, D. N., & Nair, S. (2009). *Recommended practice for stabilization of subgrade soils and base materials*. National Cooperative Highway Research Program, Transportation Research Board of the National Academies.
 334. Ridolfi, S., & Garbin, F. (2010). *Geologia e geotecnica stradale - I materiali e la loro caratterizzazione*. Palermo, Italy: Dario Flaccovio Editore.
 335. European Committee for Standardization. Cement - Part 1: Composition, specifications and conformity criteria for common cements. , EN 197-1:2011 (2011).
 336. Wanogho, S., Gettinby, G., & Caddy, B. (1987). Particle size distribution analysis of soils using laser diffraction. *Forensic Science International*, 33(2), 117–128. doi:10.1016/0379-0738(87)90147-2
 337. Blott, S. J., Croft, D. J., Pye, K., Saye, S. E., & Wilson, H. E. (2004). Particle size analysis by laser diffraction. *Geological Society, London, Special Publications*, 232(1), 63–73. doi:10.1144/GSL.SP.2004.232.01.08
 338. European Committee for Standardization. Tests for mechanical and physical properties of aggregates - Part 7: Determination of the particle density of filler - Pycnometer method. EN 1097-7:2008 (2008).

339. Nikolaides, A. (2014). *Highway Engineering: Pavements, Materials and Control of Quality*. CRC Press.
340. European Committee for Standardization. Tests for mechanical and physical properties of aggregates - Part 4: Determination of the voids of dry compacted filler. EN 1097-4:2008 (2008).
341. Ryland, A. L. (1958). X-ray diffraction. *Journal of chemical education*, 35(2), 4.
342. Skoog, D. A., Holler, F. J., & Crouch, S. R. (2017). *Principles of Instrumental Analysis*. Cengage Learning.
343. Callister, W. D. (2007). *Materials science and engineering: an introduction* (7th ed.). New York: John Wiley & Sons.
344. Leng, Y. (2013). *Materials Characterization: Introduction to Microscopic and Spectroscopic Methods*. Weinheim, Germany: Wiley-VCH Verlag GmbH & Co. KGaA. doi:10.1002/9783527670772
345. Zhou, X., Liu, D., Bu, H., Deng, L., Liu, H., Yuan, P., ... Song, H. (2018). XRD-based quantitative analysis of clay minerals using reference intensity ratios, mineral intensity factors, Rietveld, and full pattern summation methods: A critical review. *Solid Earth Sciences*, 3(1), 16–29. doi:10.1016/j.sesci.2017.12.002
346. Shackley, M. S. (2011). An Introduction to X-Ray Fluorescence (XRF) Analysis in Archaeology. In M. S. Shackley (Ed.), *X-Ray Fluorescence Spectrometry (XRF) in Geoarchaeology* (pp. 7–44). New York, NY: Springer New York. doi:10.1007/978-1-4419-6886-9_2
347. Jenkins, R. (1999). *X-ray fluorescence spectrometry* (2nd ed.). New York: Wiley.
348. Brookfield Engineering Laboratories. (2005). *More solutions to sticky problems*. Middleboro, MA, USA.
349. Mamlouk, M. S., & Zaniewski, J. P. (2011). *Materials for civil and construction engineers*. Prentice Hall Upper Saddle River, NJ.
350. European Committee for Standardization. Methods of testing cement - Part 1: Determination of strength. , EN 196-1:2016 (2016).
351. Rokade, S., Agarwal, P. K., & Shrivastava, R. (2012). Drainage and flexible pavement performance. *International Journal of Engineering Science and Technology*, 4, 4.
352. Hill, A. R. (2004). *Leaching of alternative pavement materials* (Ph.D.). University of Nottingham.
353. European Committee for Standardization. Characterisation of waste - Leaching - Compliance test for leaching of granular waste materials and sludges - Part 2: One stage batch test at a liquid to solid ratio of 10 l/kg for materials with particle size below 4 mm (without or with size reduction). EN 12457-2:2004 (2004).
354. Poon, C., Yu, A. T., & Ng, L. (2001). On-site sorting of construction and demolition waste in Hong Kong. *Resources, Conservation and Recycling*, 32(2), 157–172. doi:10.1016/S0921-3449(01)00052-0
355. European Committee for Standardization. Tests for mechanical and physical properties of aggregates - Part 6: Determination of particle density and water absorption. EN 1097-6:2013 (2013).
356. European Committee for Standardization. Tests for mechanical and physical properties of aggregates - Part 2: Methods for the determination of resistance to fragmentation. EN 1097-2:2010 (2010).
357. European Committee for Standardization. Tests for thermal and weathering properties of aggregates - Part 1: Determination of resistance to freezing and thawing. EN 1367-1:2007 (2007).
358. Mallick, R. B., & El-Korchi, T. (2013). *Pavement Engineering: Principles and Practice* (2nd ed.). CRC Press.
359. Yaghoubi, E., Disfani, M. M., Arulrajah, A., & Kodikara, J. (2018). Impact of compaction method on mechanical characteristics of unbound granular recycled materials. *Road Materials and Pavement Design*, 19(4), 912–934. doi:10.1080/14680629.2017.1283354

360. European Committee for Standardization. Unbound and hydraulically bound mixtures - Part 2: Test methods for laboratory reference density and water content - Proctor compaction. EN 13286-2:2010 (2010).
361. Lambert, N., Denny, K., Sukumaran, B., & Mehta, Y. (2009). Evaluation of the Compaction Characteristics of Unbound Material Using the Superpave Gyratory Compactor. In *Asphalt Material Characterization, Accelerated Testing, and Highway Management* (pp. 65–71).
362. Kim, W., Labuz, J. F., & Dai, S. (2007). Resilient Modulus of Base Course Containing Recycled Asphalt Pavement. *Transportation Research Record: Journal of the Transportation Research Board*, 2005(1), 27–35. doi:10.3141/2005-04
363. Cerni, G., & Camilli, S. (2011). Comparative Analysis of Gyratory and Proctor Compaction Processes of Unbound Granular Materials. *Road Materials and Pavement Design*, 12(2), 397–421. doi:10.3166/rmpd.12.397-421
364. Riviera, P. P., Bellopede, R., Marini, P., & Bassani, M. (2014). Performance-based re-use of tunnel muck as granular material for subgrade and sub-base formation in road construction. *Tunnelling and Underground Space Technology*, 40, 160–173. doi:10.1016/j.tust.2013.10.002
365. Du, Y., Liu, P., Tian, J., Zhang, J., & Zheng, Y. (2018). Preliminary Investigation of the Feasibility of Using a Superpave Gyratory Compactor to Design Cement-Treated Aggregate Mixture. *Applied Sciences*, 8(6), 946. doi:10.3390/app8060946
366. American Association of State and Highway Transportation Officials. Standard method of test for preparing and determining the density of asphalt mixture specimens by means of the superpave gyratory compactor. AASHTO T 312-15 (2015).
367. Seed, H. B., Chan, C. K., & Lee, C. E. (1962). Resilience characteristics of subgrade soils and their relation to fatigue failures in asphalt pavements. In *International Conference on the Structural Design of Asphalt Pavements. Supplement* University of Michigan, Ann Arbor.
368. Lekarp, F., Isacsson, U., & Dawson, A. (2000). State of the Art. I: Resilient Response of Unbound Aggregates. *Journal of Transportation Engineering*, 126(1), 66–75. doi:10.1061/(ASCE)0733-947X(2000)126:1(66)
369. American Association of State and Highway Transportation Officials. Standard method of test for determining the resilient modulus of soils and aggregate materials. AASHTO T 307-99 (2013).
370. American Association of State Highway and Transportation Officials. (2015). *Mechanistic-empirical pavement design guide: a manual of practice*.
371. Pellinen, T., & Witczak, M. (2002). Use of stiffness of hot-mix asphalt as a simple performance test. *Transportation Research Record: Journal of the Transportation Research Board*, (1789), 80–90.
372. Witczak, M. W., Kaloush, K., Pellinen, T., El-Basyouny, M., & Von Quintus, H. (Eds.). (2002). *Simple performance test for Superpave mix design*. Washington, D.C: National Academy Press.
373. Hudson, W. R., & Kennedy, T. W. (1968). *An indirect tensile test for stabilized materials* (Research report No. 98–1). Austin, Texas, U.S.: Center for Highway Research, University of Texas at Austin.
374. Anagnos, J. N., & Kennedy, T. W. (1972). *Practical method of conducting the indirect tensile test*. Center for Highway Research University of Texas at Austin.
375. European Committee for Standardization. Unbound and hydraulically bound mixtures - Part 42: Test method for the determination of the indirect tensile strength of hydraulically bound mixtures. EN 13286-42:2003 (2003).
376. Watt, I. M. (1997). *The Principles and Practice of Electron Microscopy*. Cambridge University Press.
377. Alyamani, A., & Lemine, O. M. (2012). FE-SEM characterization of some nanomaterial. In *Scanning Electron Microscopy*. Rijeka, Croatia: InTech.
378. Goldstein, J., Newbury, D. E., Joy, D. C., Lyman, C. E., Echlin, P., Lifshin, E., ... Michael, J. R. (2003). *Scanning Electron Microscopy and X-Ray Microanalysis* (Third.). Springer US.

379. Brodusch, N., Demers, H., & Gauvin, R. (2018). *Field Emission Scanning Electron Microscopy. New Perspectives for Materials Characterization*. Singapore: Springer Singapore. doi:10.1007/978-981-10-4433-5
380. Solanki, P., & Zaman, M. (2012). Microstructural and Mineralogical Characterization of Clay Stabilized Using Calcium-Based Stabilizers. *Scanning Electron Microscopy*. doi:10.5772/34176
381. Dhir, R. K., Limbachiya, M. C., & Leelawat, T. (1999). Suitability of recycled concrete aggregate for use in BS 5328 designated mixes (Vol. 134).
382. Limbachiya, M. C., Marrocchino, E., & Koulouris, A. (2007). Chemical–mineralogical characterisation of coarse recycled concrete aggregate. *Waste Management*, 27(2), 201–208. doi:10.1016/j.wasman.2006.01.005
383. Alexandridou, C., Angelopoulos, G. N., & Coutelieris, F. A. (2014). Physical, Chemical and Mineralogical Characterization of Construction and Demolition Waste Produced in Greece. *International Journal of Civil, Environmental, Structural, Construction and Architectural Engineering*, 8(9), 6.
384. Abbaspour, A., Tanyu, B. F., & Cetin, B. (2016). Impact of aging on leaching characteristics of recycled concrete aggregate. *Environmental Science and Pollution Research*, 23(20), 20835–20852. doi:10.1007/s11356-016-7217-9
385. Bhanumathidas, N., & Kalidas, N. (2004). Dual role of gypsum: set retarder and strength accelerator. *Indian Concr J*, 78(3), 1–4.
386. Angulo, S. C., Ulsen, C., John, V. M., Kahn, H., & Cincotto, M. A. (2009). Chemical–mineralogical characterization of C&D waste recycled aggregates from São Paulo, Brazil. *Waste Management*, 29(2), 721–730. doi:10.1016/j.wasman.2008.07.009
387. Pacheco-Torgal, F., & Jalali, S. (2010). Reusing ceramic wastes in concrete. *Construction and Building Materials*, 24(5), 832–838. doi:10.1016/j.conbuildmat.2009.10.023
388. Lavat, A. E., Trezza, M. A., & Poggi, M. (2009). Characterization of ceramic roof tile wastes as pozzolanic admixture. *Waste Management*, 29(5), 1666–1674. doi:10.1016/j.wasman.2008.10.019
389. Rodrigues, F., Carvalho, M. T., Evangelista, L., & de Brito, J. (2013). Physical–chemical and mineralogical characterization of fine aggregates from construction and demolition waste recycling plants. *Journal of Cleaner Production*, 52, 438–445. doi:10.1016/j.jclepro.2013.02.023
390. Medina, C., Zhu, W., Howind, T., Frías, M., & Sánchez de Rojas, M. I. (2015). Effect of the constituents (asphalt, clay materials, floating particles and fines) of construction and demolition waste on the properties of recycled concretes. *Construction and Building Materials*, 79, 22–33. doi:10.1016/j.conbuildmat.2014.12.070
391. Mejía, E., Tobón, J. I., Osorno, L., & Osorio, W. (2015). Mineralogical characterization of urban construction and demolition waste: potential use as a nutrient source for degraded soils. In *WIT Transactions on Ecology and The Environment* (Vol. 194, pp. 399–413). Medellin, Colombia: WIT Press. doi:10.2495/SC150351
392. Choquette, M., Berube, M.-A., & Locat, J. (1991). Behavior of common rock-forming minerals in a strongly basic NaOH solution. *The Canadian Mineralogist*, 29(1), 163–173.
393. Bianchini, G., Marrocchino, E., Tassinari, R., & Vaccaro, C. (2005). Recycling of construction and demolition waste materials: a chemical–mineralogical appraisal. *Waste Management*, 25(2), 149–159. doi:10.1016/j.wasman.2004.09.005
394. Hyatt, E. P., Cutler, I. B., & Wadsworth, M. E. (1958). Calcium Carbonate Decomposition in Carbon Dioxide Atmosphere. *Journal of the American Ceramic Society*, 41(2), 70–74. doi:10.1111/j.1151-2916.1958.tb13521.x
395. Hills, A. W. D. (1968). The mechanism of the thermal decomposition of calcium carbonate. *Chemical Engineering Science*, 23(4), 297–320. doi:10.1016/0009-2509(68)87002-2
396. Cultrone, G., Rodriguez-Navarro, C., Sebastian, E., Cazalla, O., & De La Torre, M. J. (2001). Carbonate and silicate phase reactions during ceramic firing. *European Journal of Mineralogy*, 13(3), 621–634. doi:10.1127/0935-1221/2001/0013-0621

397. Khale, D., & Chaudhary, R. (2007). Mechanism of geopolymerization and factors influencing its development: a review. *Journal of Materials Science*, 42(3), 729–746. doi:10.1007/s10853-006-0401-4
398. Gonçalves Rapazote, J., Laginhas, C., & Teixeira-Pinto, A. (2010). Development of Building Materials through Alkaline Activation of Construction and Demolition Waste (CDW) - Resistance to Acid Attack. *Advances in Science and Technology*, 69, 156–163. doi:10.4028/www.scientific.net/AST.69.156
399. Kioupis, D., AggelikiSkaropoulou, Tsivilis, S., & GlikeriaKakali. (2018). Alkali leaching control of construction and demolition waste based geopolymers. *MATEC Web of Conferences*, 149, 01064. doi:10.1051/mateconf/201814901064
400. Vásquez, A., Cárdenas, V., Robayo, R. A., & de Gutiérrez, R. M. (2016). Geopolymer based on concrete demolition waste. *Advanced Powder Technology*, 27(4), 1173–1179. doi:10.1016/j.appt.2016.03.029
401. Horpibulsuk, S., Munsrakes, V., Udomchai, A., Chinkulkijniwat, A., & Arulrajah, A. (2014). Strength of sustainable non-bearing masonry units manufactured from calcium carbide residue and fly ash. *Construction and Building Materials*, 71, 210–215. doi:10.1016/j.conbuildmat.2014.08.033
402. Horpibulsuk, S., Suksiripattanapong, C., Samingthong, W., Rachan, R., & Arulrajah, A. (2016). Durability against Wetting–Drying Cycles of Water Treatment Sludge–Fly Ash Geopolymer and Water Treatment Sludge–Cement and Silty Clay–Cement Systems. *Journal of Materials in Civil Engineering*, 28(1), 04015078. doi:10.1061/(ASCE)MT.1943-5533.0001351
403. Komnitsas, K., Zaharaki, D., & Perdikatsis, V. (2007). Geopolymerisation of low calcium ferronickel slags. *Journal of Materials Science*, 42(9), 3073–3082. doi:10.1007/s10853-006-0529-2
404. Suksiripattanapong, C., Horpibulsuk, S., Chanprasert, P., Sukmak, P., & Arulrajah, A. (2015). Compressive strength development in fly ash geopolymer masonry units manufactured from water treatment sludge. *Construction and Building Materials*, 82, 20–30. doi:10.1016/j.conbuildmat.2015.02.040
405. Antoni, Wiyono, D., Vianthi, A., Putra, P., Kartadinata, G., & Hardjito, D. (2014). Effect of Particle Size on Properties of Sidoarjo Mud-Based Geopolymer. *Materials Science Forum*, 803, 44–48. doi:10.4028/www.scientific.net/MSF.803.44
406. Ferone, C., Colangelo, F., Cioffi, R., Montagnaro, F., & Santoro, L. (2013). Use of reservoir clay sediments as raw materials for geopolymer binders. *Advances in Applied Ceramics*, 112(4), 184–189. doi:10.1179/1743676112Y.0000000064
407. Slavik, R., Bednarik, V., Vondruska, M., & Nemec, A. (2008). Preparation of geopolymer from fluidized bed combustion bottom ash. *Journal of Materials Processing Technology*, 200(1–3), 265–270. doi:10.1016/j.jmatprotec.2007.09.008
408. Xu, H., & Van Deventer, J. S. J. (2002). Geopolymerisation of multiple minerals. *Minerals Engineering*, 15(12), 1131–1139. doi:10.1016/S0892-6875(02)00255-8
409. Cristelo, N., Tavares, P., Lucas, E., Miranda, T., & Oliveira, D. (2016). Quantitative and qualitative assessment of the amorphous phase of a Class F fly ash dissolved during alkali activation reactions – Effect of mechanical activation, solution concentration and temperature. *Composites Part B: Engineering*, 103, 1–14. doi:10.1016/j.compositesb.2016.08.001
410. Aïtcin, P.-C., & Flatt, R. J. (2016). *Science and technology of concrete admixtures*. Cambridge, UK: Woodhead Publishing.
411. Lv, X., Shi, Y., Dong, Y., Gao, Z., & Li, B. (2017). The Performance and Mechanism Analysis of Cement Pastes Added to Aluminum Sulfate-Based Low-Alkali Setting Accelerator. *Advances in Materials Science and Engineering*, 2017, 1–10. doi:10.1155/2017/8906708
412. Llatas, C. (2013). Methods for estimating construction and demolition (C&D) waste. In F. Pacheco-Torgal, V. W. Y. Tam, J. A. Labrincha, Y. Ding, & J. de Brito (Eds.), *Handbook of Recycled Concrete and Demolition Waste* (pp. 25–52). Woodhead Publishing. doi:10.1533/9780857096906.1.25

413. Yamaguchi, N., Nagaishi, M., Kisu, K., Nakamura, Y., & Ikeda, K. (2013). Preparation of monolithic geopolymer materials from urban waste incineration slags. *Journal of the Ceramic Society of Japan*, 121(1417), 847–854. doi:10.2109/jcersj2.121.847
414. Yamaguchi, N., & Ikeda, K. (2010). Preparation of geopolymeric materials from sewage sludge slag with special emphasis to the matrix compositions. *Journal of the Ceramic Society of Japan*, 118(1374), 107–112. doi:10.2109/jcersj2.118.107
415. Granizo, M. L., Blanco-Varela, M. T., & Martínez-Ramírez, S. (2007). Alkali activation of metakaolins: parameters affecting mechanical, structural and microstructural properties. *Journal of Materials Science*, 42(9), 2934–2943. doi:10.1007/s10853-006-0565-y
416. Kamseu, E., Bignozzi, M. C., Melo, U. C., Leonelli, C., & Sglavo, V. M. (2013). Design of inorganic polymer cements: Effects of matrix strengthening on microstructure. *Construction and Building Materials*, 38, 1135–1145. doi:10.1016/j.conbuildmat.2012.09.033
417. Fernandez-Jimenez, A., & Puertas, F. (2003). Effect of activator mix on the hydration and strength behaviour of alkali-activated slag cements. *Advances in Cement Research*, (3), 8.
418. Zhao, F.-Q., Ni, W., Wang, H.-J., & Liu, H.-J. (2007). Activated fly ash/slag blended cement. *Resources, Conservation and Recycling*, 52(2), 303–313. doi:10.1016/j.resconrec.2007.04.002
419. Pacheco-Torgal, F., Tam, V. W. Y., Labrincha, J. A., Ding, Y., & de Brito, J. (2013). *Handbook of recycled concrete and demolition waste*. Woodhead Publishing Limited. doi:10.1533/9780857096906
420. Yip, C. K., Lukey, G. C., Provis, J. L., & van Deventer, J. S. J. (2008). Effect of calcium silicate sources on geopolymerisation. *Cement and Concrete Research*, 38(4), 554–564. doi:10.1016/j.cemconres.2007.11.001
421. Temuujin, J., van Riessen, A., & Williams, R. (2009). Influence of calcium compounds on the mechanical properties of fly ash geopolymer pastes. *Journal of Hazardous Materials*, 167(1–3), 82–88. doi:10.1016/j.jhazmat.2008.12.121
422. Coppola, L., Buoso, A., Coffetti, D., Kara, P., Lorenzi, S., & D'Alessandro, F. (2017). The Effect of Sodium Silicate on the Behaviour of Shotcretes for Tunnel Lining. *Journal of Scientific Research and Reports*, 14(2), 1–8. doi:10.9734/JSRR/2017/33641
423. Giannaros, P., Kanellopoulos, A., & Al-Tabbaa, A. (2016). Sealing of cracks in cement using microencapsulated sodium silicate. *Smart Materials and Structures*, 25(8), 084005. doi:10.1088/0964-1726/25/8/084005
424. Silva, P. D., Sagoe-Crenstil, K., & Sirivivatnanon, V. (2007). Kinetics of geopolymerization: Role of Al₂O₃ and SiO₂. *Cement and Concrete Research*, 37(4), 512–518. doi:10.1016/j.cemconres.2007.01.003
425. Davidovits, J. (2011). *Geopolymer Chemistry and Applications* (Third edition.). Saint-Quentin: Geopolymer Institute.
426. Song, S., Sohn, D., Jennings, H. M., & Mason, T. O. (2000). Hydration of alkali-activated ground granulated blast furnace slag. *Journal of Materials Science*, 35(1), 249–257.
427. Gao, X., Gu, Y., Xie, T., Zhen, G., Huang, S., & Zhao, Y. (2015). Characterization and environmental risk assessment of heavy metals in construction and demolition wastes from five sources (chemical, metallurgical and light industries, and residential and recycled aggregates). *Environmental Science and Pollution Research*, 22(12), 9332–9344. doi:10.1007/s11356-014-4058-2
428. Saiz Martínez, P., González Cortina, M., Fernández Martínez, F., & Rodríguez Sánchez, A. (2016). Comparative study of three types of fine recycled aggregates from construction and demolition waste (CDW), and their use in masonry mortar fabrication. *Journal of Cleaner Production*, 118, 162–169. doi:10.1016/j.jclepro.2016.01.059
429. Moreno-Pérez, E., Hernández-Ávila, J., Rangel-Martínez, Y., Cerecedo-Sáenz, E., Arenas-Flores, A., Reyes-Valderrama, M., & Salinas-Rodríguez, E. (2018). Chemical and Mineralogical Characterization of Recycled Aggregates from Construction and Demolition Waste from Mexico City. *Minerals*, 8(6), 237. doi:10.3390/min8060237
430. Engelsen, C. J., van der Sloot, H. A., Wibetoe, G., Justnes, H., Lund, W., & Stoltenberg-Hansson, E. (2010). Leaching characterisation and geochemical modelling of minor and trace

- elements released from recycled concrete aggregates. *Cement and Concrete Research*, 40(12), 1639–1649. doi:10.1016/j.cemconres.2010.08.001
431. Galvín, A. P., Ayuso, J., García, I., Jiménez, J. R., & Gutiérrez, F. (2014). The effect of compaction on the leaching and pollutant emission time of recycled aggregates from construction and demolition waste. *Journal of Cleaner Production*, 83, 294–304. doi:10.1016/j.jclepro.2014.07.074
 432. Del Rey, I., Ayuso, J., Galvín, A. P., Jiménez, J. R., López, M., & García-Garrido, M. L. (2015). Analysis of chromium and sulphate origins in construction recycled materials based on leaching test results. *Waste Management*, 46, 278–286. doi:10.1016/j.wasman.2015.07.051
 433. Maia, M. B., De Brito, J., Martins, I. M., & Silvestre, J. D. (2018). Toxicity of Recycled Concrete Aggregates: Review on Leaching Tests. *The Open Construction and Building Technology Journal*, 12(1), 187–196. doi:10.2174/1874836801812010187
 434. Wahlström, M., Laine-Ylijoki, J., Määttänen, A., Luotojärvi, T., & Kivekäs, L. (2000). Environmental quality assurance system for use of crushed mineral demolition wastes in road constructions. *Waste Management*, 20(2), 225–232.
 435. Barbudo, A., Agrela, F., Ayuso, J., Jiménez, J. R., & Poon, C. S. (2012). Statistical analysis of recycled aggregates derived from different sources for sub-base applications. *Construction and Building Materials*, 28(1), 129–138. doi:10.1016/j.conbuildmat.2011.07.035
 436. Weber, W. J., Jang, Y.-C., Townsend, T. G., & Laux, S. (2002). Leachate from Land Disposed Residential Construction Waste. *Journal of Environmental Engineering*, 128(3), 237–245. doi:10.1061/(ASCE)0733-9372(2002)128:3(237)
 437. Lerch, W. (1946). *The influence of gypsum on the hydration and properties of Portland cement pastes* (Vol. 46). Portland Cement Association.
 438. Bentur, A. (1976). Effect of gypsum on the hydration and strength of C3S pastes. *Journal of the American Ceramic Society*, 59(5–6), 210–213. doi:10.1111/j.1151-2916.1976.tb10935.x
 439. Dosho, Y. (2007). Development of a Sustainable Concrete Waste Recycling System. *Journal of Advanced Concrete Technology*, 5(1), 27–42. doi:10.3151/jact.5.27
 440. Sinyoung, S., Songsirittthigul, P., Asavapisit, S., & Kajitvichyanukul, P. (2011). Chromium behavior during cement-production processes: A clinkerization, hydration, and leaching study. *Journal of Hazardous Materials*, 191(1–3), 296–305. doi:10.1016/j.jhazmat.2011.04.077
 441. Andrés, A., Díaz, M. C., Coz, A., Abellán, M. J., & Viguri, J. R. (2009). Physico-chemical characterisation of bricks all through the manufacture process in relation to efflorescence salts. *Journal of the European Ceramic Society*, 29(10), 1869–1877. doi:10.1016/j.jeurceramsoc.2008.11.015
 442. Van Jaarsveld, J. G. S., Van Deventer, J. S. J., & Lorenzen, L. (1997). The potential use of geopolymeric materials to immobilise toxic metals: Part I. Theory and applications. *Minerals Engineering*, 10(7), 659–669. doi:10.1016/S0892-6875(97)00046-0
 443. Zhang, Z., Wang, H., & Provis, J. L. (2012). Quantitative study of the reactivity of fly ash in geopolymerization by FTIR. *Journal of Sustainable Cement-Based Materials*, 1(4), 154–166. doi:10.1080/21650373.2012.752620
 444. Palomo, A., & Palacios, M. (2003). Alkali-activated cementitious materials: Alternative matrices for the immobilisation of hazardous wastes Part II. Stabilisation of chromium and lead. *Cement and Concrete Research*, 7.
 445. Bankowski, P., Zou, L., & Hodges, R. (2004). Reduction of metal leaching in brown coal fly ash using geopolymers. *Journal of Hazardous Materials*, 114(1–3), 59–67. doi:10.1016/j.jhazmat.2004.06.034
 446. Zhang, Y., Sun, W., She, W., & Sun, G. (2009). Synthesis and heavy metal immobilization behaviors of fly ash based gepolymer. *Journal of Wuhan University of Technology-Mater. Sci. Ed.*, 24(5), 819–825. doi:10.1007/s11595-009-5819-5
 447. Ahmari, S., & Zhang, L. (2013). Durability and leaching behavior of mine tailings-based geopolymer bricks. *Construction and Building Materials*, 44, 743–750. doi:10.1016/j.conbuildmat.2013.03.075

448. Guo, X. L., & Shi, H. S. (2011). Leaching Behaviour of Heavy Metals from the Class C Fly Ash-Based Geopolymers. *Advanced Materials Research*, 194–196, 798–801. doi:10.4028/www.scientific.net/AMR.194-196.798
449. Van der Sloot, H. A. (1996). Developments in evaluating environmental impact from utilization of bulk inert wastes using laboratory leaching tests and field verification. *Waste Management*, 16(1), 65–81. doi:10.1016/S0956-053X(96)00028-1
450. Galvín, A. P., Ayuso, J., Jiménez, J. R., & Agrela, F. (2012). Comparison of batch leaching tests and influence of pH on the release of metals from construction and demolition wastes. *Waste Management*, 32(1), 88–95. doi:10.1016/j.wasman.2011.09.010
451. Van der Sloot, H. A., & Dijkstra, J. J. (2004). *Development of horizontally standardized leaching tests for construction materials: a material based or release based approach?* (ECN-C-04-060 report No. 2003.06.089). Petten, the Netherlands: Dutch Ministry of Housing, Spatial Planning and the Environment (VROM), Soil, Water and Rural Environment Directorate.
452. Luna Galiano, Y., Fernández Pereira, C., & Vale, J. (2011). Stabilization/solidification of a municipal solid waste incineration residue using fly ash-based geopolymers. *Journal of Hazardous Materials*, 185(1), 373–381. doi:10.1016/j.jhazmat.2010.08.127
453. Agrela, F., Sánchez de Juan, M., Ayuso, J., Gerales, V. L., & Jiménez, J. R. (2011). Limiting properties in the characterisation of mixed recycled aggregates for use in the manufacture of concrete. *Construction and Building Materials*, 25(10), 3950–3955. doi:10.1016/j.conbuildmat.2011.04.027
454. Poon, C. S., & Chan, D. (2006). Feasible use of recycled concrete aggregates and crushed clay brick as unbound road sub-base. *Construction and Building Materials*, 20(8), 578–585. doi:10.1016/j.conbuildmat.2005.01.045
455. Jiménez, J. R., Ayuso, J., López, M., Fernández, J. M., & de Brito, J. (2013). Use of fine recycled aggregates from ceramic waste in masonry mortar manufacturing. *Construction and Building Materials*, 40, 679–690. doi:10.1016/j.conbuildmat.2012.11.036
456. Bazaz, J. B., Khayati, M., & Akrami, N. (2006). Performance of concrete produced with crushed bricks as the coarse and fine aggregate. In *The Geological Society of London* (Vol. 10). Citeseer.
457. Cavalline, T. L., & Weggel, D. C. (2013). Recycled brick masonry aggregate concrete: Use of brick masonry from construction and demolition waste as recycled aggregate in concrete. *Structural Survey*, 31(3), 160–180. doi:10.1108/SS-09-2012-0029
458. Rahman, M. A., Arulrajah, A., Piratheepan, J., Bo, M. W., & Imteaz, M. A. (2014). Resilient Modulus and Permanent Deformation Responses of Geogrid-Reinforced Construction and Demolition Materials. *Journal of Materials in Civil Engineering*, 26(3), 512–519. doi:10.1061/(ASCE)MT.1943-5533.0000824
459. de Juan, M. S., & Gutiérrez, P. A. (2009). Study on the influence of attached mortar content on the properties of recycled concrete aggregate. *Construction and Building Materials*, 23(2), 872–877. doi:10.1016/j.conbuildmat.2008.04.012
460. Woodside, A. R., Woodward, W., Farmer, D., & Collins, R. J. (1996). The assessment of the suitability of waste materials for use in highway construction. In *Roads: finance, provision and operation. Proceedings of seminar G held at the PTRC European transport forum*. London, UK: PTRC Education and Research Services Limited.
461. Chidioglou, I., Goodwin, A. K., Laycock, E., & O’Flaherty, F. (2008). Physical properties of demolition waste material. *Proceedings of the Institution of Civil Engineers - Construction Materials*, 161(3), 97–103. doi:10.1680/coma.2008.161.3.97
462. Cerni, G., Corradini, A., Pasquini, E., & Cardone, F. (2015). Resilient behaviour of unbound granular materials through repeated load triaxial test: influence of the conditioning stress. *Road Materials and Pavement Design*, 16(1), 70–88. doi:10.1080/14680629.2014.964294
463. Mokwa, R., Cuelho, E., & Browne, M. (2008). Laboratory Testing of Soil Using Superpave Gyrotory Compactor. *Transportation Research Board*.

464. Lancieri, F., Marradi, A., & Mannucci, S. (2006). C&D waste for road construction: long time performance of roads constructed using recycled aggregate for unbound pavement layers. In *WIT Transactions on Ecology and the Environment*, (Vol. 92, pp. 559–569). Southampton, UK: WIT Press. doi:10.2495/WM060571
465. Blankenagel, B., & Guthrie, W. (2006). Laboratory Characterization of Recycled Concrete for Use as Pavement Base Material. *Transportation Research Record: Journal of the Transportation Research Board*, 1952, 21–27. doi:10.3141/1952-03
466. Rada, G., & Witczak, M. W. (1981). Comprehensive evaluation of laboratory resilient moduli results for granular material. *Transportation Research Record*, (810).
467. Zaman, M., Chen, D., & Laguros, J. (1994). Resilient Moduli of Granular Materials. *Journal of Transportation Engineering*, 120(6), 967–988. doi:10.1061/(ASCE)0733-947X(1994)120:6(967)
468. Khoury, N., Brooks, R., Khoury, C., & Yada, D. (2012). Modeling Resilient Modulus Hysteretic Behavior with Moisture Variation. *International Journal of Geomechanics*, 12(5), 519–527. doi:10.1061/(ASCE)GM.1943-5622.0000140
469. Cary, C., & Zapata, C. (2010). Enhanced Model for Resilient Response of Soils Resulting from Seasonal Changes as Implemented in *Mechanistic-Empirical Pavement Design Guide*. *Transportation Research Record: Journal of the Transportation Research Board*, 2170, 36–44. doi:10.3141/2170-05
470. Li, J., & Qubain, B. (2003). Resilient Modulus Variations with Water Content. In G. Durham, W. DeGroff, & W. Marr (Eds.), *Resilient Modulus Testing for Pavement Components* (pp. 59–59–11). 100 Barr Harbor Drive, PO Box C700, West Conshohocken, PA 19428-2959: ASTM International. doi:10.1520/STP12522S
471. Puppala, A. J. (2008). *Estimating stiffness of subgrade and unbound materials for pavement design*. Washington, D.C: Transportation Research Board.
472. Tamrakar, P., & Nazarian, S. (2016). *Impact of Gradation and Moisture Content on Stiffness Parameters of Base Materials* (Final Report No. CAIT-UTC-054). El Paso, TX, US: Center for Advanced Infrastructure and Transportation.
473. Rout, R. K., Ruttanapornmakul, P., Valluru, S., & Puppala, A. J. (2012). Resilient moduli behavior of lime-cement treated subgrade soils. In *GeoCongress 2012: State of the Art and Practice in Geotechnical Engineering* (pp. 1428–1437).
474. Zhu, J. (1998). *Characterization of cement-kiln-dust stabilized base/subbase aggregate* (PhD thesis). University of Oklahoma, Norman, OK, U.S.
475. American Society for Testing Materials. Standard Practice for Classification of Soils for Engineering Purposes (Unified Soil Classification System). ASTM D2487-11 (2011).
476. American Association of State and Highway Transportation Officials. Specification for Classification of Soils and Soil-Aggregate Mixtures for Highway Construction Purposes. AASHTO M 145-91 (2012).
477. Nazzal, M. D., & Mohammad, L. N. (2010). Estimation of resilient modulus of subgrade soils for design of pavement structures. *Journal of Materials in Civil Engineering*, 22(7), 726–734.
478. Titi, H. H., Elias, M. B., & Helwany, S. (2006). *Determination of Typical Resilient Modulus Values for Selected Soils in Wisconsin* (Wisconsin Highway Research Program Project No. ID 0092-03-11). Milwaukee, WI: Wisconsin Department of Transportation Division of Transportation Infrastructure Development Research Coordination Section.
479. Hossain, M. (2009). Estimation of Subgrade Resilient Modulus for Virginia Soil. *Transportation Research Record: Journal of the Transportation Research Board*, 2101, 98–109. doi:10.3141/2101-12
480. Yau, A., & Von Quintus, H. L. (2002). *Study of LTPP Laboratory Resilient Modulus Test Data and Response Characteristics* (No. FHWA-RD-02-051). Georgetown Pike McLean, VA: Federal Highway Administration Office of Infrastructure Research and Development.
481. Farias, M., Gomez, A., & Quiñones Sinisterra, F. (2013). Use of recycled aggregates from construction and demolition wastes for the construction of flexible pavements. In *Third*

- International Conference on Geotechnique, Construction Materials and Environment*. Nagoya, Japan.
482. Hanifa, K., Abu-Farsakh, M. Y., & Gavin, G. (2015). *Design Values of Resilient Modulus for Stabilized and Non-Stabilized Base* (Final Report No. FHWA/LA.14/521). Baton Rouge, LA: Louisiana Department of Transportation and Development.
 483. MacDonald, W. M. (2008). *Resilient Modulus and Strength Index Properties of Stabilized Base for Tennessee Highways*. University of Tennessee, Knoxville.
 484. Biswal, D. R., Sahoo, U. C., & Dash, S. R. (2018). Strength and Stiffness Studies of Cement Stabilized Granular Lateritic Soil. In W. Frikha, S. Varaksin, & A. Viana da Fonseca (Eds.), *Soil Testing, Soil Stability and Ground Improvement* (pp. 320–336). Cham: Springer International Publishing. doi:10.1007/978-3-319-61902-6_25
 485. Lim, S., & Zollinger, D. (2003). Estimation of the compressive strength and modulus of elasticity of cement-treated aggregate base materials. *Transportation Research Record: Journal of the Transportation Research Board*, (1837), 30–38.
 486. Davis, K. A., Warr, L. S., Burns, S. E., & Hoppe, E. J. (2007). Physical and Chemical Behavior of Four Cement-Treated Aggregates. *Journal of Materials in Civil Engineering*, 19(10), 891–897. doi:10.1061/(ASCE)0899-1561(2007)19:10(891)
 487. Piratheepan, J., Gnanendran, C. T., & Lo, S.-C. (2009). Characterization of cementitiously stabilized granular materials for pavement design using unconfined compression and IDT testings with internal displacement measurements. *Journal of Materials in Civil Engineering*, 22(5), 495–505.
 488. Hou, Y., Wang, D., Zhou, W., Lu, H., & Wang, L. (2009). Effect of activator and curing mode on fly ash-based geopolymers. *Journal of Wuhan University of Technology-Mater. Sci. Ed.*, 24(5), 711–715. doi:10.1007/s11595-009-5711-3
 489. Patankar, S. V., Ghugal, Y. M., & Jamkar, S. S. (2014). Effect of Concentration of Sodium Hydroxide and Degree of Heat Curing on Fly Ash-Based Geopolymer Mortar. *Indian Journal of Materials Science*, 2014, 1–6. doi:10.1155/2014/938789
 490. Komljenović, M., Bašćarević, Z., & Bradić, V. (2010). Mechanical and microstructural properties of alkali-activated fly ash geopolymers. *Journal of Hazardous Materials*, 181(1–3), 35–42. doi:10.1016/j.jhazmat.2010.04.064
 491. Naghizadeh, A., & Ekelu, S. O. (2017). Pozzolanic materials and waste products for formulation of geopolymer cements in developing countries: a review. *Concrete Beton*, 151, 22–31.
 492. Moayedi, H., Huat, B., Moayedi, F., Asadi, A., & Parsaie, A. (2011). Effect of Sodium Silicate on Unconfined Compressive Strength of Soft Clay. *Electronic Journal of Geotechnical Engineering*, 16, 289–295.
 493. Madurwar, K. V., Dahale, P. P., & Burile, A. N. (2013). Comparative Study of Black Cotton Soil Stabilization with RBI Grade 81 and Sodium Silicate. *International Journal of Innovative Research in Science, Engineering and Technology*, 2(2).
 494. Hurley, C. H., & Thornburn, T. H. (1971). *Sodium silicate stabilization of soils: A review of the literature*. Soil Mechanics Laboratory, Department of Civil Engineering, Engineering Experiment Station, University of Illinois.
 495. Broderick, G. P., & Daniel, D. E. (1990). Stabilizing Compacted Clay against Chemical Attack. *Journal of Geotechnical Engineering*, 116(10), 1549–1567. doi:10.1061/(ASCE)0733-9410(1990)116:10(1549)
 496. Arulrajah, A., Disfani, M. M., Horpibulsuk, S., Suksiripattanapong, C., & Prongmanee, N. (2014). Physical properties and shear strength responses of recycled construction and demolition materials in unbound pavement base/subbase applications. *Construction and Building Materials*, 58, 245–257. doi:10.1016/j.conbuildmat.2014.02.025
 497. Taherkhani, H., & Amani, B. (2014). An investigation on the using of cement stabilized recycled concrete and brick in pavement layers. *Indian Journal of Scientific Research*, 1(2), 297–306.

498. Catauro, M., Papale, F., Lamanna, G., & Bollino, F. (2015). Geopolymer/PEG Hybrid Materials Synthesis and Investigation of the Polymer Influence on Microstructure and Mechanical Behavior. *Materials Research*, 18(4), 698–705. doi:10.1590/1516-1439.342814
499. Timakul, P., Rattanaprasit, W., & Aungkavattana, P. (2016). Improving compressive strength of fly ash-based geopolymer composites by basalt fibers addition. *Ceramics International*, 42(5), 6288–6295. doi:10.1016/j.ceramint.2016.01.014
500. Matakah, F., Soroushian, P., Balchandra, A., & Peyvandi, A. (2017). Characterization of Alkali-Activated Nonwood Biomass Ash-Based Geopolymer Concrete. *Journal of Materials in Civil Engineering*, 29(4), 04016270.
501. Ferone, C., Roviello, G., Colangelo, F., Cioffi, R., & Tarallo, O. (2013). Novel hybrid organic-geopolymer materials. *Applied Clay Science*, 73, 42–50. doi:10.1016/j.clay.2012.11.001
502. Khoury, N. N., & Brooks, R. (2010). Performance of a Stabilized Aggregate Base Subject to Different Durability Procedures. *Journal of Materials in Civil Engineering*, 22(5), 506–514. doi:10.1061/(ASCE)MT.1943-5533.0000055
503. Kohlhaas, B., & Labahn, O. (Eds.). (1982). *Cement Engineers Handbook* (4 edition.). Wiesbaden: Intl Public Service.
504. Rosa, M. G., Cetin, B., Edil, T. B., & Benson, C. H. (2017). Freeze–Thaw Performance of Fly Ash–Stabilized Materials and Recycled Pavement Materials. *Journal of Materials in Civil Engineering*, 29(6), 04017015. doi:10.1061/(ASCE)MT.1943-5533.0001844
505. Lee, W., Bohra, N. C., Altschaeffl, A. G., & White, T. D. (1995). Resilient modulus of cohesive soils and the effect of freeze-thaw. *Canadian Geotechnical Journal*, 32(4), 559–568.
506. Khalife, R., Solanki, P., & Zaman, M. M. (2012). Evaluation of Durability of Stabilized Clay Specimens Using Different Laboratory Procedures. *Journal of Testing and Evaluation*, 40(3), 104194. doi:10.1520/JTE104194
507. Theivakularatnam, M., & Gnanendran, C. T. (2015). Durability of Lightly Stabilised Granular Material Subjected to Freeze-Thaw and Wet-Dry Cycles. In *IFCEE 2015* (pp. 1410–1419). doi:10.1061/9780784479087.127
508. Miller, G., & Zaman, M. (2000). Field and laboratory evaluation of cement kiln dust as a soil stabilizer. *Transportation Research Record: Journal of the Transportation Research Board*, (1714), 25–32.
509. Solanki, P., Zaman, M., & Khalife, R. (2013). Effect of Freeze-Thaw Cycles on Performance of Stabilized Subgrade. In *Sound Geotechnical Research to Practice* (pp. 566–580). San Diego, California, United States: American Society of Civil Engineers. doi:10.1061/9780784412770.038
510. Hotineanu, A., Bouasker, M., Aldaood, A., & Al-Mukhtar, M. (2015). Effect of freeze–thaw cycling on the mechanical properties of lime-stabilized expansive clays. *Cold Regions Science and Technology*, 119, 151–157. doi:10.1016/j.coldregions.2015.08.008
511. Marín-López, C., Reyes Araiza, J. L., Manzano-Ramírez, A., Rubio Avalos, J. C., Perez-Bueno, J. J., Muñoz-Villareal, M. S., ... Vorobiev, Y. (2009). Synthesis and characterization of a concrete based on metakaolin geopolymer. *Inorganic Materials*, 45(12), 1429–1432. doi:10.1134/S0020168509120231
512. Rattanasak, U., & Chindaprasirt, P. (2009). Influence of NaOH solution on the synthesis of fly ash geopolymer. *Minerals Engineering*, 22(12), 1073–1078. doi:10.1016/j.mineng.2009.03.022
513. Somna, K., Jaturapitakkul, C., Kajitvichyanukul, P., & Chindaprasirt, P. (2011). NaOH-activated ground fly ash geopolymer cured at ambient temperature. *Fuel*, 90(6), 2118–2124. doi:10.1016/j.fuel.2011.01.018
514. Feng, D., Provis, J. L., & Deventer, J. S. J. (2012). Thermal Activation of Albite for the Synthesis of One-Part Mix Geopolymers. *Journal of the American Ceramic Society*, 95(2), 565–572. doi:10.1111/j.1551-2916.2011.04925.x
515. Temuujin, J., Minjigmaa, A., Davaabal, B., Bayarzul, U., Ankhtuya, A., Jadambaa, T., & MacKenzie, K. J. D. (2014). Utilization of radioactive high-calcium Mongolian flyash for the

- preparation of alkali-activated geopolymers for safe use as construction materials. *Ceramics International*, 40(10), 16475–16483. doi:10.1016/j.ceramint.2014.07.157
516. Lampris, C., Lupo, R., & Cheeseman, C. R. (2009). Geopolymerisation of silt generated from construction and demolition waste washing plants. *Waste Management*, 29(1), 368–373. doi:10.1016/j.wasman.2008.04.007
 517. Landi, E., Medri, V., Papa, E., Dedecek, J., Klein, P., Benito, P., & Vaccari, A. (2013). Alkali-bonded ceramics with hierarchical tailored porosity. *Applied Clay Science*, 73, 56–64. doi:10.1016/j.clay.2012.09.027
 518. Temuujin, J., Rickard, W., Lee, M., & van Riessen, A. (2011). Preparation and thermal properties of fire resistant metakaolin-based geopolymer-type coatings. *Journal of Non-Crystalline Solids*, 357(5), 1399–1404. doi:10.1016/j.jnoncrysol.2010.09.063
 519. Zuhua, Z., Xiao, Y., Huajun, Z., & Yue, C. (2009). Role of water in the synthesis of calcined kaolin-based geopolymer. *Applied Clay Science*, 43(2), 218–223. doi:10.1016/j.clay.2008.09.003
 520. Taylor, H. F. W. (1997). *Cement Chemistry* (Second edition.). London, UK: Thomas Telford.
 521. Peters, R. W. (1999). Chelant extraction of heavy metals from contaminated soils. *Journal of Hazardous Materials*, 66(1–2), 151–210. doi:10.1016/S0304-3894(99)00010-2
 522. Townsend, T. G., Jang, Y.-C., & Tolaymat, T. (2003). *Leaching Tests for Evaluating Risk in Solid Waste Management Decision Making* (Final Report No. 03–01) (p. 149). Gainesville, Florida, US: The Florida Center for Solid and Hazardous Waste Management.
 523. Barbudo, A., Galvín, A. P., Agrela, F., Ayuso, J., & Jiménez, J. R. (2012). Correlation analysis between sulphate content and leaching of sulphates in recycled aggregates from construction and demolition wastes. *Waste Management*, 32(6), 1229–1235. doi:10.1016/j.wasman.2012.02.005
 524. Devia, Y. P., & Suryo, E. A. (2017). Leachate of Demolition Waste. *MATEC Web of Conferences*, 138, 08002. doi:10.1051/mateconf/201713808002
 525. Saca, N., Dimache, A., Radu, L. R., & Iancu, I. (2017). Leaching behavior of some demolition wastes. *Journal of Material Cycles and Waste Management*, 19(2), 623–630. doi:10.1007/s10163-015-0459-7
 526. López-Uceda, A., Galvín, A. P., Ayuso, J., Jiménez, J. R., Vanwalleghem, T., & Peña, A. (2018). Risk assessment by percolation leaching tests of extensive green roofs with fine fraction of mixed recycled aggregates from construction and demolition waste. *Environmental Science and Pollution Research*. doi:10.1007/s11356-018-1703-1
 527. Milagre-Martins, I. M., Roque, A. J., Freire, A. C., Neves, J., & Antunes, M. L. (2015). Release of dangerous substances from construction and demolition recycled materials used in road pavements-Laboratory and field leaching tests. In *III Progress of Recycling in the Built Environment* (pp. 109–115). RILEM Publications SARL.
 528. Tsai, Y.-L., Hanna, J. V., Lee, Y.-L., Smith, M. E., & Chan, J. C. C. (2010). Solid-state NMR study of geopolymer prepared by sol–gel chemistry. *Journal of Solid State Chemistry*, 183(12), 3017–3022. doi:10.1016/j.jssc.2010.10.008
 529. Provis, J. L., Hajimohammadi, A., White, C. E., Bernal, S. A., Myers, R. J., Winarski, R. P., ... van Deventer, J. S. J. (2013). Nanostructural characterization of geopolymers by advanced beamline techniques. *Cement and Concrete Composites*, 36, 56–64. doi:10.1016/j.cemconcomp.2012.07.003
 530. Ananthapadmanaban, D. (2018). Summary of Some Selected Characterization Methods of Geopolymers. *Geopolymer Science and Applications*. doi:10.5772/intechopen.82208

ANNEXES

A. Small scale investigation (Exp. A)

A.1. Brookfield viscosity

Table A.1 - Viscosities (in cP) of fresh pastes with $l/s=0.5$

AS conc. (%)	Sample	Revolution speed (rpm)					
		10	20	40	100	150	200
75	RC	57540	42600	27000	15550	12000	9300
	RA	35567	22067	17367	11800	7433	5500
	BT	-	-	-	-	-	-
	NA	16060	11300	8367	6633	5627	5280
	UND1	91800	57600	37800	17100	13067	9500
	UND2	23200	17133	14633	7850	5600	4550
50	RC	16200	9700	7550	5773	4120	3450
	RA	10320	7900	6393	3933	2701	1813
	BT	8800	6400	5250	3350	2605	1773
	NA	4416	3040	2170	1717	1446	1343
	UND1	27000	18500	13600	9760	7455	5550
	UND2	9600	7550	5533	3221	2254	1707

Table A.2 - Viscosities (in cP) of fresh pastes with $l/s=0.6$

AS conc. (%)	Sample	Revolution speed (rpm)					
		10	20	40	100	150	200
100	RC	108000	60500	43700	22700	13950	8000
	RA	84000	61867	37200	19200	11100	7550
	BT	50000	44000	26700	17900	12910	9550
	NA	30800	21400	16300	9912	7800	7300
	UND1	159000	96000	54150	19200	16000	11400
	UND2	47000	37500	30750	14700	13000	11000
75	RC	28000	19000	11000	7600	6250	5450
	RA	18900	13067	9000	4687	3578	2827
	BT	15800	12367	8100	5133	3880	3193
	NA	4384	3280	2460	1773	1576	1455
	UND1	44333	27600	17700	9956	7830	6800
	UND2	10400	9200	6880	5216	3867	3756
50	RC	9280	6600	4900	2650	1920	1580
	RA	7900	5390	3960	1913	1453	1123
	BT	4079	2464	2050	1570	1384	1347
	NA	1600	1200	980	489	465	454
	UND1	11650	9080	6300	3250	2209	1900
	UND2	3536	2340	1520	1232	1019	956

A.2. Flexural strength tests

A.2.1 Recycled concrete (RC)

Table A.3 - Average results of flexural strength test of alkali-activated RC fines

l/s ratio	AS conc. (%)	Stat.	$\sigma_{f,max}$ (MPa)	$\varepsilon_f(\sigma_{f,max})$ (%)	$E_{T,f}$ (MPa)	T_f (kPa·mm/mm)	γ_g (kg/m ³)	n. obs.
0.4	50	avg.	0.23	0.640	36.4	0.73	1691	3
		st.dev.	0.01	0.140	6.5	0.18	8	
		CV (%)	3.9	21.8	17.8	24.0	0.5	
	75	avg.	1.30	0.568	229.4	3.66	1927	3
		st.dev.	0.16	0.037	43.2	0.20	44	
		CV (%)	12.6	6.5	18.8	5.6	2.3	
	100	avg.	2.86	0.328	903.1	4.76	1835	3
		st.dev.	0.32	0.027	173.4	0.31	51	
		CV (%)	11.2	8.2	19.2	6.6	2.8	
0.5	50	avg.	0.34	1.086	38.8	2.80	1575	3
		st.dev.	0.06	0.352	3.1	1.75	27	
		CV (%)	17.8	32.4	8.0	62.5	1.7	
	75	avg.	2.58	0.527	490.4	6.86	1904	5
		st.dev.	0.32	0.042	42.6	1.24	17	
		CV (%)	12.3	8.0	8.7	18.1	0.9	
	100	avg.	5.81	0.541	1079.0	15.74	1900	4
		st.dev.	0.59	0.007	114.1	1.51	5	
		CV (%)	10.2	1.4	10.6	9.6	0.3	
0.6	50	avg.	0.16	0.860	19.1	0.66	1488	5
		st.dev.	0.01	0.191	5.5	0.12	49	
		CV (%)	6.4	22.2	29.0	17.5	3.3	
	75	avg.	2.31	0.634	370.8	7.31	1767	3
		st.dev.	0.26	0.076	78.8	0.75	11	
		CV (%)	11.0	11.9	21.2	10.3	0.6	
	100	avg.	1.19	0.564	234.6	3.34	1908	5
		st.dev.	0.16	0.177	97.6	1.01	19	
		CV (%)	13.3	31.4	41.6	30.2	1.0	

A.2.2 Reclaimed asphalt (RA)

Table A.4 - Average results of flexural strength test of alkali-activated RA fines

l/s ratio	AS conc. (%)	Stat.	$\sigma_{f,max}$ (MPa)	$\varepsilon_f(\sigma_{f,max})$ (%)	$E_{T,f}$ (MPa)	T_f (kPa·mm/mm)	γ_g (kg/m ³)	n. obs.
0.4	50	avg.	0.37	1.089	37.5	2.20	1729	3
		st.dev.	0.09	0.030	7.7	0.59	25	
		CV (%)	24.1	2.8	20.5	26.7	1.4	
	75	avg.	0.37	1.256	29.8	2.44	1887	3
		st.dev.	0.10	0.273	2.0	1.18	70	
		CV (%)	27.9	21.8	6.6	48.2	3.7	
	100	avg.	0.47	4.412	11.9	11.35	1975	5
		st.dev.	0.05	0.460	1.0	1.88	26	
		CV (%)	10.3	10.4	8.6	16.5	1.3	
0.5	50	avg.	0.12	0.774	17.1	0.47	1737	4
		st.dev.	0.01	0.292	5.8	0.19	13	
		CV (%)	9.8	37.8	33.6	39.3	0.8	
	75	avg.	0.14	3.634	4.0	2.64	1951	3
		st.dev.	0.01	1.037	1.0	0.79	6	
		CV (%)	6.4	28.5	24.3	30.0	0.3	
	100	avg.	0.32	7.052	5.1	12.14	1939	5
		st.dev.	0.04	1.314	1.0	2.74	29	
		CV (%)	13.8	18.6	20.0	22.5	1.5	
0.6	50	avg.	0.10	0.579	20.3	0.32	1679	3
		st.dev.	0.03	0.155	8.6	0.08	44	
		CV (%)	28.6	26.7	42.4	24.3	2.6	
	75	avg.	0.95	1.452	83.8	8.05	1862	4
		st.dev.	0.11	0.231	15.4	2.11	36	
		CV (%)	11.4	15.9	18.3	26.2	1.9	
	100	avg.	0.43	2.464	19.5	5.74	1890	3
		st.dev.	0.03	0.240	1.1	1.02	43	
		CV (%)	6.0	9.8	5.4	17.8	2.3	

A.2.3 *Bricks and tiles (BT)***Table A.5 - Average results of flexural strength test of alkali-activated BT fines**

l/s ratio	AS conc. (%)	Stat.	$\sigma_{f,max}$ (MPa)	$\varepsilon_f(\sigma_{f,max})$ (%)	$E_{T,f}$ (MPa)	T_f (kPa·mm/mm)	γ_g (kg/m ³)	n. obs.
0.4	50	avg.	0.46	0.480	124.7	1.02	1761	3
		st.dev.	0.10	0.288	98.0	0.39	26	
		CV (%)	22.9	59.9	78.6	38.7	1.5	
	75	avg.	1.72	0.504	342.4	4.31	1865	3
		st.dev.	0.08	0.054	46.8	0.49	25	
		CV (%)	4.5	10.8	13.7	11.3	1.3	
	100	avg.	2.92	0.442	671.5	6.76	1536	5
		st.dev.	0.64	0.083	30.9	2.61	26	
		CV (%)	21.9	18.8	4.6	38.6	1.7	
0.5	50	avg.	0.73	0.915	104.3	3.55	1734	4
		st.dev.	0.15	0.390	38.8	1.39	10	
		CV (%)	21.2	42.6	37.2	39.0	0.6	
	75	avg.	0.39	0.654	62.8	1.32	1932	5
		st.dev.	0.03	0.085	9.0	0.18	13	
		CV (%)	6.8	13.0	14.4	13.7	0.7	
	100	avg.	1.45	1.063	147.1	11.57	1875	3
		st.dev.	0.31	0.072	37.3	4.17	25	
		CV (%)	21.3	6.8	25.4	36.1	1.3	
0.6	50	avg.	0.70	0.946	112.1	4.27	1609	3
		st.dev.	0.11	0.121	20.1	1.08	16	
		CV (%)	15.3	12.8	17.9	25.2	1.0	
	75	avg.	0.84	1.171	76.3	5.24	1958	4
		st.dev.	0.16	0.218	9.2	1.69	78	
		CV (%)	18.9	18.6	12.0	32.2	4.0	
	100	avg.	1.42	1.847	102.5	13.12	1973	5
		st.dev.	0.13	0.820	62.6	4.67	33	
		CV (%)	9.0	44.4	61.1	35.6	1.7	

A.2.4 Natural aggregates (NA)

Table A.6 - Average results of flexural strength test of alkali-activated RC fines

l/s ratio	AS conc. (%)	Stat.	$\sigma_{f,max}$ (MPa)	$\varepsilon_f(\sigma_{f,max})$ (%)	$E_{T,f}$ (MPa)	T_f (kPa·mm/mm)	γ_g (kg/m ³)	n. obs.
0.4	50	avg.	0.26	0.785	32.6	1.01	1854	3
		st.dev.	0.06	0.072	8.7	0.21	39	
		CV (%)	21.5	9.1	26.7	20.5	2.1	
	75	avg.	1.04	0.752	140.9	3.95	1973	4
		st.dev.	0.02	0.073	13.1	0.41	44	
		CV (%)	1.9	9.7	9.3	10.3	2.2	
	100	avg.	4.86	0.661	795.6	15.86	1994	5
		st.dev.	0.89	0.158	287.1	2.29	38	
		CV (%)	18.2	23.8	36.1	14.4	1.9	
0.5	50	avg.	0.16	0.593	29.6	0.48	1902	3
		st.dev.	0.02	0.184	11.9	0.16	8	
		CV (%)	10.0	31.1	40.3	32.9	0.4	
	75	avg.	0.13	2.806	5.3	2.04	2085	4
		st.dev.	0.02	0.661	0.5	0.82	25	
		CV (%)	17.8	23.6	8.8	40.0	1.2	
	100	avg.	0.45	1.339	40.6	3.37	2016	5
		st.dev.	0.03	0.173	7.6	0.17	14	
		CV (%)	7.7	12.9	18.8	5.1	0.7	
0.6	50	avg.	0.11	0.896	13.1	0.51	1710	5
		st.dev.	0.00	0.137	2.2	0.07	22	
		CV (%)	2.3	15.3	16.9	13.9	1.3	
	75	avg.	1.00	0.982	112.4	5.25	1991	4
		st.dev.	0.17	0.243	31.2	1.82	22	
		CV (%)	17.1	24.7	27.8	34.7	1.1	
	100	avg.	1.97	1.985	110.2	20.94	2034	3
		st.dev.	0.32	0.273	15.1	4.00	138	
		CV (%)	16.4	13.8	13.7	19.1	6.8	

A.2.5 Undivided fraction 1 (UND1)

Table A.7 - Average results of flexural strength test of alkali-activated UND1 fines

l/s ratio	AS conc. (%)	Stat.	$\sigma_{f,max}$ (MPa)	$\varepsilon_f(\sigma_{f,max})$ (%)	$E_{T,f}$ (MPa)	T_f (kPa·mm/mm)	γ_g (kg/m ³)	n. obs.
0.4	50	avg.	0.15	0.666	22.4	0.50	1764	3
		st.dev.	0.01	0.047	0.4	0.06	63	
		CV (%)	5.6	7.1	1.8	12.0	3.6	
	75	avg.	1.80	0.583	304.1	5.25	1764	3
		st.dev.	0.44	0.037	57.0	1.62	19	
		CV (%)	24.5	6.3	18.7	30.8	1.1	
	100	avg.	4.19	0.443	981.3	9.46	1974	5
		st.dev.	0.33	0.108	163.9	3.01	26	
		CV (%)	7.8	24.4	16.7	31.8	1.3	
0.5	50	avg.	0.34	0.710	54.6	1.23	1826	4
		st.dev.	0.03	0.290	21.6	0.54	13	
		CV (%)	8.4	40.8	39.5	44.0	0.7	
	75	avg.	1.28	0.670	194.0	4.38	1951	5
		st.dev.	0.23	0.076	29.2	1.12	4	
		CV (%)	18.2	11.3	15.1	25.5	0.2	
	100	avg.	1.83	0.492	394.0	4.66	1916	5
		st.dev.	0.31	0.124	75.2	1.58	17	
		CV (%)	17.1	25.1	19.1	33.9	0.9	
0.6	50	avg.	0.43	1.025	56.9	2.55	1605	3
		st.dev.	0.09	0.039	10.1	0.50	23	
		CV (%)	20.4	3.8	17.7	19.4	1.4	
	75	avg.	2.49	1.240	212.0	15.70	1833	5
		st.dev.	0.45	0.266	50.9	4.12	10	
		CV (%)	18.1	21.4	24.0	26.2	0.6	
	100	avg.	0.30	0.828	39.1	1.31	1934	5
		st.dev.	0.05	0.101	8.9	0.20	23	
		CV (%)	15.3	12.3	22.7	15.6	1.2	

A.2.6 Undivided fraction 2 (UND2)

Table A.8 - Average results of flexural strength test of alkali-activated UND2 fines

l/s ratio	AS conc. (%)	Stat.	$\sigma_{f,max}$ (MPa)	$\varepsilon_f(\sigma_{f,max})$ (%)	$E_{T,f}$ (MPa)	T_f (kPa·mm/mm)	γ_g (kg/m ³)	n. obs.
0.4	50	avg.	0.32	0.764	51.6	1.23	1759	3
		st.dev.	0.03	0.030	18.6	0.03	8	
		CV (%)	9.3	3.9	36.1	2.6	0.5	
	75	avg.	1.10	0.766	188.5	3.56	1911	4
		st.dev.	0.07	0.060	13.5	0.39	28	
		CV (%)	6.0	7.8	7.1	10.9	1.5	
	100	avg.	1.88	0.395	482.4	3.76	1962	4
		st.dev.	0.14	0.045	36.2	0.69	17	
		CV (%)	7.4	11.5	7.5	18.3	0.9	
0.5	50	avg.	0.89	0.806	122.8	3.55	1544	4
		st.dev.	0.10	0.233	53.2	0.84	22	
		CV (%)	11.6	28.9	43.3	23.7	1.4	
	75	avg.	3.71	1.039	369.5	19.85	1737	5
		st.dev.	0.54	0.251	59.9	7.39	14	
		CV (%)	14.4	24.2	16.2	37.2	0.8	
	100	avg.	3.10	0.604	532.4	10.00	1908	5
		st.dev.	0.16	0.116	87.6	2.92	40	
		CV (%)	5.1	19.1	16.5	29.2	2.1	
0.6	50	avg.	0.53	0.650	96.0	1.74	1529	4
		st.dev.	0.08	0.249	38.3	0.56	24	
		CV (%)	15.6	38.3	39.9	32.2	1.6	
	75	avg.	1.35	0.901	151.0	6.11	1893	4
		st.dev.	0.03	0.034	6.8	0.28	23	
		CV (%)	2.3	3.8	4.5	4.6	1.2	
	100	avg.	0.38	1.382	29.0	2.75	1926	5
		st.dev.	0.06	0.142	4.2	0.46	16	
		CV (%)	14.7	10.3	14.3	16.6	0.8	

A.3. Compressive strength tests

A.3.1 Recycled concrete (RC)

Table A.9 - Average results of compression strength test of alkali-activated RC fines

l/s ratio	AS conc. (%)	Stat.	$\sigma_{c,max}$ (MPa)	$\varepsilon_c(\sigma_{c,max})$ (%)	$E_{T,c}$ (MPa)	$E_{S,c}$ (MPa)	T_c (kPa·mm/mm)	n. obs.
0.4	50	avg.	0.61	5.596	24.5	11.1	24.9	4
		st.dev.	0.04	0.972	5.3	1.6	7.3	
		CV (%)	7.1	17.4	21.5	14.6	29.5	
	75	avg.	3.57	1.878	227.6	192.2	38.7	4
		st.dev.	0.21	0.175	39.0	28.3	1.8	
		CV (%)	6.0	9.3	17.2	14.7	4.5	
	100	avg.	14.00	2.150	823.7	656.5	179.9	10
		st.dev.	2.24	0.280	140.9	114.5	53.9	
		CV (%)	16.0	13.0	17.1	17.4	29.9	
0.5	50	avg.	0.91	1.938	68.5	49.2	10.8	9
		st.dev.	0.18	0.309	18.0	17.9	0.9	
		CV (%)	19.3	16.0	26.3	36.4	8.4	
	75	avg.	6.10	2.155	361.4	287.5	83.1	10
		st.dev.	0.41	0.307	49.6	38.3	20.5	
		CV (%)	6.7	14.2	13.7	13.3	24.7	
	100	avg.	15.85	2.378	778.1	671.9	211.6	10
		st.dev.	1.15	0.257	62.4	72.2	36.6	
		CV (%)	7.3	10.8	8.0	10.7	17.3	
0.6	50	avg.	0.32	2.541	17.2	12.9	4.9	9
		st.dev.	0.03	0.394	4.1	2.8	1.0	
		CV (%)	10.8	15.5	23.9	21.9	19.7	
	75	avg.	5.46	2.317	295.7	239.7	79.9	8
		st.dev.	0.24	0.303	53.7	37.5	15.9	
		CV (%)	4.4	13.1	18.2	15.6	19.9	
	100	avg.	6.92	2.290	379.8	305.9	92.4	10
		st.dev.	0.26	0.277	52.6	37.6	10.9	
		CV (%)	3.7	12.1	13.9	12.3	11.8	

A.3.2 Reclaimed asphalt (RA)

Table A.10 - Average results of compression strength test of alkali-activated RA fines

l/s ratio	AS conc. (%)	Stat.	$\sigma_{c,max}$ (MPa)	$\varepsilon_c(\sigma_{c,max})$ (%)	$E_{T,c}$ (MPa)	$E_{S,c}$ (MPa)	T_c (kPa·mm/mm)	n. obs.
0.4	50	avg.	0.60	5.935	10.6	10.2	18.3	4
		st.dev.	0.21	0.339	4.3	4.1	5.4	
		CV (%)	34.9	5.7	40.4	40.2	29.6	
	75	avg.	1.24	6.092	30.0	20.6	47.6	4
		st.dev.	0.08	0.694	5.1	2.5	6.2	
		CV (%)	6.0	11.4	17.0	12.2	13.1	
	100	avg.	1.79	7.633	31.0	23.4	82.2	10
		st.dev.	0.14	0.421	2.3	1.8	8.4	
		CV (%)	7.7	5.5	7.3	7.7	10.2	
0.5	50	avg.	0.42	3.477	18.0	12.2	9.1	8
		st.dev.	0.03	0.512	5.8	2.2	1.4	
		CV (%)	7.9	14.7	32.1	17.6	15.4	
	75	avg.	0.76	10.394	8.5	7.3	44.1	10
		st.dev.	0.04	0.491	0.9	0.5	3.0	
		CV (%)	5.2	4.7	10.2	6.8	6.8	
	100	avg.	1.32	10.285	15.9	13.0	78.5	10
		st.dev.	0.12	0.823	2.5	1.8	8.3	
		CV (%)	9.0	8.0	15.7	14.1	10.6	
0.6	50	avg.	0.55	2.632	27.7	21.4	8.7	5
		st.dev.	0.05	0.455	3.9	3.0	2.5	
		CV (%)	8.3	17.3	14.0	13.9	28.7	
	75	avg.	2.31	6.265	55.3	37.6	90.1	9
		st.dev.	0.23	0.780	13.0	7.5	11.0	
		CV (%)	10.1	12.4	23.6	20.1	12.2	
	100	avg.	1.08	11.380	12.8	9.8	72.3	10
		st.dev.	0.12	1.633	4.0	2.5	7.4	
		CV (%)	11.1	14.3	31.5	25.1	10.3	

A.3.3 Bricks and tiles (BT)

Table A.11 - Average results of compression strength test of alkali-activated BT fines

l/s ratio	AS conc. (%)	Stat.	$\sigma_{c,max}$ (MPa)	$\varepsilon_c(\sigma_{c,max})$ (%)	$E_{T,c}$ (MPa)	$E_{S,c}$ (MPa)	T_c (kPa·mm/mm)	n. obs.
0.4	50	avg.	0.94	2.513	44.9	37.9	13.7	4
		st.dev.	0.01	0.304	3.8	5.1	2.0	
		CV (%)	1.3	12.1	8.4	13.4	14.6	
	75	avg.	4.59	2.322	268.0	199.4	65.6	4
		st.dev.	0.25	0.285	49.5	20.7	9.7	
		CV (%)	5.5	12.3	18.5	10.4	14.8	
	100	avg.	10.31	1.916	654.3	544.0	113.9	10
		st.dev.	1.48	0.235	93.0	91.9	26.9	
		CV (%)	14.3	12.3	14.2	16.9	23.6	
0.5	50	avg.	1.06	1.861	118.5	67.1	13.0	5
		st.dev.	0.22	0.860	48.0	30.3	6.3	
		CV (%)	20.8	46.2	40.5	45.1	48.2	
	75	avg.	1.80	5.553	72.2	34.0	71.5	10
		st.dev.	0.08	1.000	15.0	9.7	15.9	
		CV (%)	4.7	18.0	20.7	28.6	22.2	
	100	avg.	4.70	4.584	147.2	104.5	131.4	8
		st.dev.	0.59	0.527	35.6	22.0	13.0	
		CV (%)	12.6	11.5	24.1	21.0	9.9	
0.6	50	avg.	0.73	2.626	55.9	29.9	13.4	4
		st.dev.	0.19	0.707	14.6	11.5	5.3	
		CV (%)	25.4	26.9	26.1	38.3	39.8	
	75	avg.	2.22	5.201	56.5	45.0	68.0	10
		st.dev.	0.28	1.131	16.9	12.9	16.2	
		CV (%)	12.8	21.7	29.9	28.7	23.9	
	100	avg.	4.26	4.661	124.8	98.9	120.8	10
		st.dev.	0.40	1.594	22.5	26.0	53.3	
		CV (%)	9.4	34.2	18.1	26.3	44.1	

A.3.4 Natural aggregates (NA)

Table A.12 - Average results of compression strength test of alkali-activated NA fines

l/s ratio	AS conc. (%)	Stat.	$\sigma_{c,max}$ (MPa)	$\varepsilon_c(\sigma_{c,max})$ (%)	$E_{T,c}$ (MPa)	$E_{S,c}$ (MPa)	T_c (kPa·mm/mm)	n. obs.
0.4	50	avg.	0.58	2.478	29.6	24.2	8.5	7
		st.dev.	0.03	0.451	6.2	4.3	1.8	
		CV (%)	5.5	18.2	20.9	18.0	21.5	
	75	avg.	2.51	3.236	106.4	80.5	49.0	4
		st.dev.	0.10	0.713	29.3	18.7	10.7	
		CV (%)	4.0	22.0	27.6	23.2	21.9	
	100	avg.	10.11	2.879	508.6	359.5	180.7	9
		st.dev.	1.20	0.426	99.8	79.4	29.8	
		CV (%)	11.8	14.8	19.6	22.1	16.5	
0.5	50	avg.	0.43	2.747	29.5	16.5	7.9	7
		st.dev.	0.08	0.589	11.6	5.6	1.3	
		CV (%)	18.6	21.4	39.3	33.8	17.1	
	75	avg.	1.05	8.359	14.1	12.6	48.5	8
		st.dev.	0.04	0.475	1.0	0.9	3.6	
		CV (%)	3.5	5.7	6.9	6.8	7.5	
	100	avg.	2.01	5.246	57.4	38.8	66.5	10
		st.dev.	0.17	0.580	10.6	6.3	9.6	
		CV (%)	8.6	11.1	18.4	16.3	14.5	
0.6	50	avg.	0.38	3.422	17.6	11.7	8.0	10
		st.dev.	0.07	0.909	7.5	3.5	2.2	
		CV (%)	19.0	26.6	42.4	29.6	27.0	
	75	avg.	2.48	5.171	69.5	48.2	78.9	6
		st.dev.	0.09	0.410	11.0	4.3	7.7	
		CV (%)	3.7	7.9	15.8	9.0	9.8	
	100	avg.	3.61	5.067	84.4	73.1	104.7	7
		st.dev.	0.65	1.325	17.7	12.4	38.7	
		CV (%)	18.1	26.1	20.9	17.0	37.0	

A.3.5 Undivided fraction 1 (UND1)

Table A.13 - Average results of compression strength test of alkali-activated UND1 fines

l/s ratio	AS conc. (%)	Stat	$\sigma_{c,max}$ (MPa)	$\varepsilon_c(\sigma_{c,max})$ (%)	$E_{T,c}$ (MPa)	$E_{S,c}$ (MPa)	T_c (kPa·mm/mm)	n. obs.
0.4	50	avg.	0.47	6.400	17.6	7.6	22.3	4
		st.dev.	0.02	1.525	5.7	1.5	5.0	
		CV (%)	3.8	23.8	32.4	19.7	22.5	
	75	avg.	5.66	3.168	238.6	184.5	99.8	4
		st.dev.	0.35	0.596	66.3	48.2	10.1	
		CV (%)	6.2	18.8	27.8	26.1	10.2	
	100	avg.	12.06	2.036	707.7	596.0	140.4	10
		st.dev.	1.16	0.173	95.6	73.5	19.6	
		CV (%)	9.6	8.5	13.5	12.3	14.0	
0.5	50	avg.	0.71	2.240	51.9	32.4	10.4	9
		st.dev.	0.10	0.347	9.0	6.8	1.9	
		CV (%)	14.0	15.5	17.3	21.0	18.5	
	75	avg.	3.23	2.527	179.5	129.7	51.6	10
		st.dev.	0.32	0.384	27.7	16.6	11.3	
		CV (%)	9.8	15.2	15.4	12.8	21.8	
	100	avg.	6.87	2.414	381.8	287.9	92.2	10
		st.dev.	0.63	0.240	58.8	42.1	22.2	
		CV (%)	9.1	10.0	15.4	14.6	24.1	
0.6	50	avg.	0.54	2.909	28.3	19.3	10.3	9
		st.dev.	0.10	0.697	6.8	5.1	3.5	
		CV (%)	18.9	23.9	23.9	26.2	33.6	
	75	avg.	4.91	3.534	170.8	140.1	101.4	10
		st.dev.	0.41	0.364	13.4	18.2	16.0	
		CV (%)	8.3	10.3	7.8	13.0	15.7	
	100	avg.	1.93	4.159	65.9	47.1	58.4	10
		st.dev.	0.10	0.443	9.0	6.2	27.6	
		CV (%)	5.2	10.6	13.7	13.1	47.3	

A.3.6 Undivided fraction 2 (UND2)

Table A.14 - Average results of compression strength test of alkali-activated UND2 fines

l/s ratio	AS conc. (%)	Stat.	$\sigma_{c,max}$ (MPa)	$\varepsilon_c(\sigma_{c,max})$ (%)	$E_{T,c}$ (MPa)	$E_{S,c}$ (MPa)	T_c (kPa·mm/mm)	n. obs.
0.4	50	avg.	0.68	4.085	27.1	20.9	15.7	5
		st.dev.	0.04	0.293	1.6	1.4	3.2	
		CV (%)	6.4	7.2	5.8	6.6	20.1	
	75	avg.	2.95	3.327	155.8	122.2	49.1	5
		st.dev.	0.10	0.241	19.1	9.7	3.8	
		CV (%)	3.2	7.2	12.2	7.9	7.7	
	100	avg.	7.13	2.356	414.4	304.8	112.4	10
		st.dev.	0.35	0.200	28.7	32.6	26.8	
		CV (%)	5.0	8.5	6.9	10.7	23.8	
0.5	50	avg.	2.42	2.138	171.6	118.6	33.1	6
		st.dev.	0.22	0.491	47.3	30.4	9.9	
		CV (%)	8.9	23.0	27.6	25.7	30.1	
	75	avg.	8.13	2.799	391.9	296.9	139.1	10
		st.dev.	0.86	0.371	71.0	60.3	23.6	
		CV (%)	10.6	13.3	18.1	20.3	17.0	
	100	avg.	8.64	2.827	387.9	311.5	144.3	10
		st.dev.	0.86	0.437	38.1	48.0	29.7	
		CV (%)	9.9	15.5	9.8	15.4	20.6	
0.6	50	avg.	0.54	2.099	40.1	27.3	7.0	6
		st.dev.	0.07	0.661	10.8	6.7	3.2	
		CV (%)	12.4	31.5	27.0	24.7	45.6	
	75	avg.	3.19	2.706	173.6	121.7	54.0	10
		st.dev.	0.33	0.442	41.0	28.1	8.0	
		CV (%)	10.2	16.3	23.6	23.1	14.9	
	100	avg.	1.91	4.371	64.2	43.8	52.8	10
		st.dev.	0.09	0.344	8.0	2.8	6.4	
		CV (%)	4.5	7.9	12.5	6.4	12.0	

B. Exp. B1

B.1. Particle size distribution

Table B.1 - Results of sieve analysis of CDW samples collected at plant divided in 0÷25 mm and 0÷8 mm fractions

Opening size	Sample 0÷25 mm	Sample 0÷8 mm
[mm]	(%)	(%)
25	100.0	100.0
22.4	94.3	100.0
20	85.3	100.0
16	69.3	100.0
14	60.7	100.0
12.5	54.1	100.0
10	43.9	100.0
8	36.0	99.3
6.3	30.8	96.6
5	27.0	91.2
4	24.7	85.2
2	20.2	68.9
1	16.1	52.4
0.5	11.4	32.5
0.4	10.1	27.6
0.25	6.8	17.9
0.18	5.5	14.1
0.125	4.3	10.6
0.063	2.3	5.7

B.2. Resilient modulus results

Table B.2 - Values of RM (in MPa) of 7-day cured CDW specimens depending on AS concentration and water content

θ (kPa)	Water content (w_w)								
	6.6 %			8.6 %			10.6 %		
	AS conc.			AS conc.			AS conc.		
	0%	50%	100%	0%	50%	100%	0%	50%	100%
82.8	73.0	80.9	170.8	69.2	66.7	267.1	44.5	57.9	113.4
103.5	104.8	88.6	203.1	71.7	66.9	279.4	56.4	60.5	124.3
124.2	125.2	108.1	249.5	87.9	79.9	304.9	73.5	74.6	166.3
138.0	111.9	94.1	220.0	76.5	72.0	315.8	62.8	68.8	125.0
172.4	148.4	126.7	291.5	102.4	94.5	352.0	88.3	91.6	184.4
206.9	180.0	161.9	401.6	127.9	114.8	380.3	113.1	111.0	253.3
275.6	196.2	176.1	393.7	131.6	123.0	412.4	125.2	123.8	254.5
344.6	248.8	244.6	548.8	197.8	177.6	455.3	170.2	181.1	305.2
413.5	267.4	266.1	612.5	223.8	190.8	480.1	189.3	201.0	323.3
379.1	227.7	222.4	490.5	154.6	134.3	407.8	159.5	147.0	267.8
413.6	260.8	260.9	548.8	191.7	158.7	450.5	185.1	185.7	314.2
517.0	311.9	313.4	657.5	266.4	220.6	518.0	231.4	258.0	351.3
517.1	298.5	299.8	588.7	228.5	198.1	447.8	228.6	229.7	331.4
551.6	321.1	319.8	632.7	277.4	217.1	488.1	245.1	265.5	355.1
689.5	368.0	375.6	738.8	322.0	259.2	562.5	290.9	324.1	382.7

Table B.3 - Values of RM (in MPa) of 28-day cured CDW specimens depending on AS concentration and water content

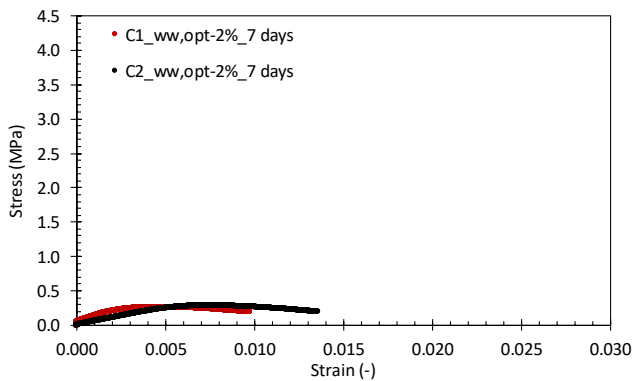
θ (kPa)	Water content (w_w)								
	6.6 %			8.6 %			10.6 %		
	AS conc.			AS conc.			AS conc.		
	0%	50%	100%	0%	50%	100%	0%	50%	100%
82.8	157.3	81.2	205.5	105.7	127.4	247.2	79.6	107.1	265.4
103.5	171.6	84.2	242.0	103.9	124.8	194.4	83.7	102.0	293.7
124.2	184.4	100.5	285.8	112.0	130.5	235.6	98.7	111.3	328.0
138.0	205.2	85.1	306.8	134.5	149.7	276.8	107.3	124.6	324.1
172.4	216.7	117.5	338.1	140.0	157.9	266.9	120.7	137.4	360.0
206.9	233.8	146.5	378.5	151.4	171.4	335.7	133.8	150.3	400.4
275.6	296.4	145.3	423.4	201.9	227.9	320.1	172.7	204.0	409.9
344.6	304.9	238.5	481.8	210.2	240.0	393.1	192.4	218.9	448.5
413.5	309.3	267.7	558.0	216.3	240.0	442.7	205.4	222.8	472.7
379.1	343.0	166.1	373.5	238.4	268.6	303.8	213.6	248.0	427.3
413.6	342.9	218.0	464.1	237.6	272.2	364.1	220.2	256.6	448.5
517.0	362.2	313.9	574.4	257.8	292.6	470.2	254.6	287.6	495.4
517.1	387.3	264.7	497.2	279.1	322.6	389.2	266.6	316.8	462.9
551.6	394.4	311.8	539.7	282.7	329.9	424.7	276.5	332.5	479.6
689.5	408.8	383.6	669.1	301.5	349.7	520.8	309.2	352.8	527.4

Table B.4 - Values of RM (in MPa) of 60-day cured CDW specimens depending on AS concentration and water content

θ (kPa)	Water content (w_w)								
	6.6 %			8.6 %			10.6 %		
	AS conc.			AS conc.			AS conc.		
	0%	50%	100%	0%	50%	100%	0%	50%	100%
82.8	187.5	155.8	290.4	115.6	111.0	281.2	55.3	82.2	281.9
103.5	180.3	160.4	371.9	113.5	108.4	328.9	63.1	76.8	334.3
124.2	184.1	172.0	412.0	121.3	115.3	365.4	79.5	85.1	367.9
138	205.9	194.1	412.2	143.1	132.1	372.4	84.8	98.1	359.6
172.4	208.7	204.1	406.5	149.1	141.6	418.9	97.1	107.9	404.5
206.9	220.7	223.5	461.6	161.2	155.4	464.1	113.9	118.7	442.4
275.6	272.4	284.6	550.3	215.7	202.0	493.8	153.3	167.6	472.2
344.6	283.6	306.1	624.1	225.5	216.5	555.8	171.6	178.4	528.4
413.5	287.9	308.1	657.4	233.5	220.7	601.3	186.4	183.5	554.5
379.1	316.0	334.3	593.2	261.0	240.5	559.2	193.2	210.8	503.0
413.6	315.7	337.3	632.7	261.8	241.5	589.9	198.5	211.7	535.9
517	336.0	362.6	707.9	284.4	268.7	649.1	233.1	238.2	592.3
517.1	360.5	389.4	680.3	312.5	289.2	624.7	249.1	267.1	568.6
551.6	369.4	397.7	705.6	316.0	298.2	650.5	256.3	277.2	593.8
689.5	387.4	417.4	773.9	337.5	323.7	704.2	287.4	297.4	647.2

B.3. Stress-strain curves of UCS test

B.3.1 *CDW-AS-0% mixtures*

**Figure B.1 - Stress-strain curves of CDW-AS-0% mixtures with $w_{w,opt-2\%}$ cured for 7 days**

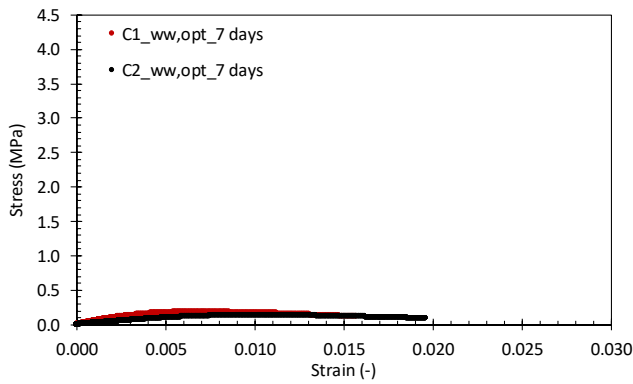


Figure B.2 - Stress-strain curves of CDW-AS-0% mixtures with $w_{w,opt}$ cured for 7 days

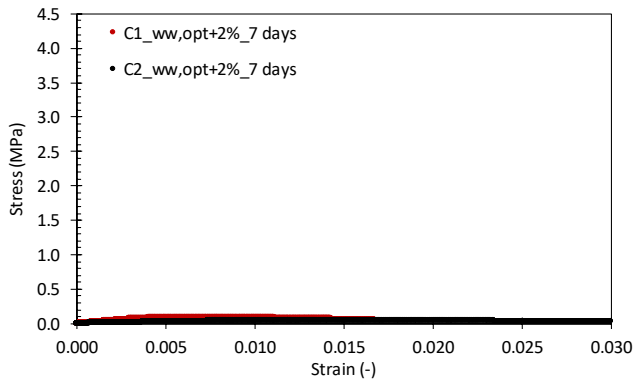


Figure B.3 - Stress-strain curves of CDW-AS-0% mixtures with $w_{w,opt}+2\%$ cured for 7 days

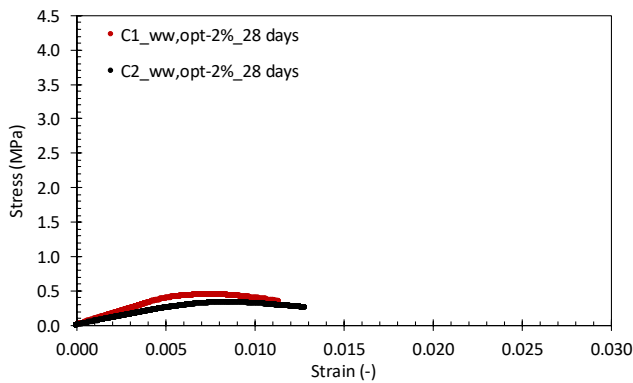


Figure B.4 - Stress-strain curves of CDW-AS-0% mixtures with $w_{w,opt}-2\%$ cured for 28 days

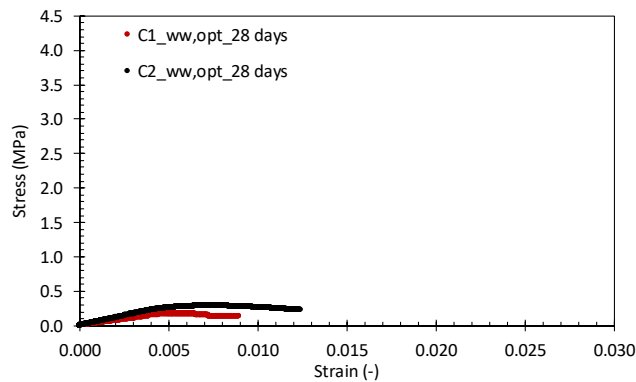


Figure B.5 - Stress-strain curves of CDW-AS-0% mixtures with $w_{w,opt}$ cured for 28 days

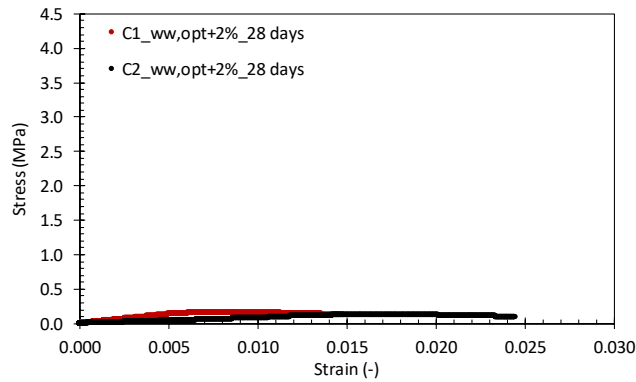


Figure B.6 - Stress-strain curves of CDW-AS-0% mixtures with $w_{w,opt} + 2\%$ cured for 28 days

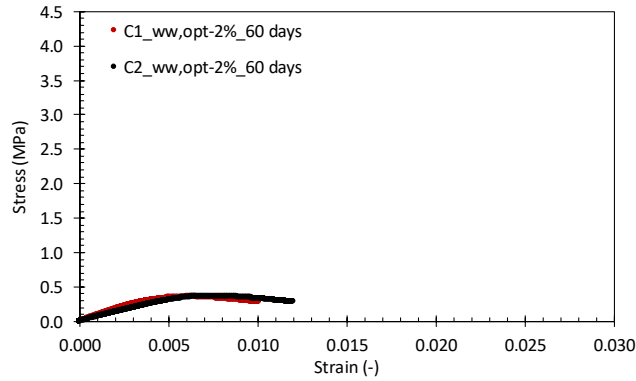


Figure B.7 - Stress-strain curves of CDW-AS-0% mixtures with $w_{w,opt} - 2\%$ cured for 60 days

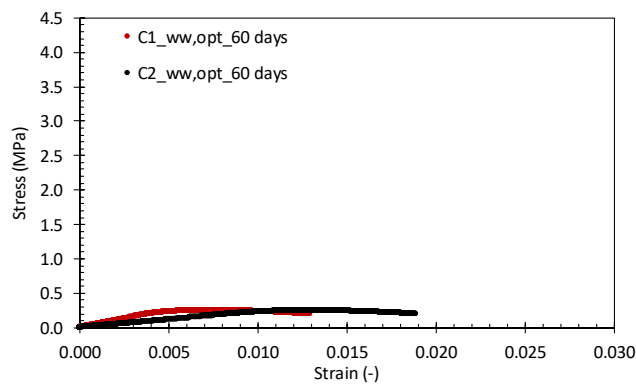


Figure B.8 - Stress-strain curves of CDW-AS-0% mixtures with $w_{w,opt}$ cured for 60 days

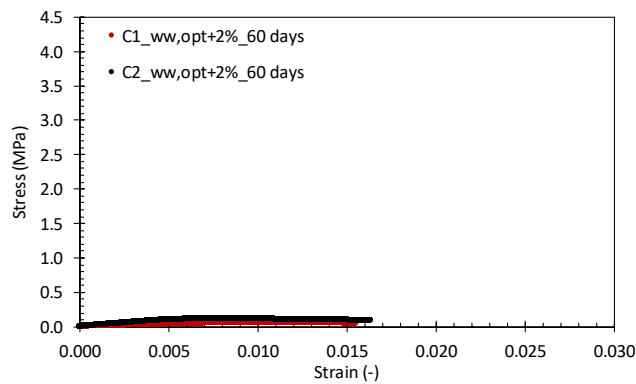


Figure B.9 - Stress-strain curves of CDW-AS-0% mixtures with $w_{w,opt} + 2\%$ cured for 60 days

B.3.2 CDW-AS-50% mixtures

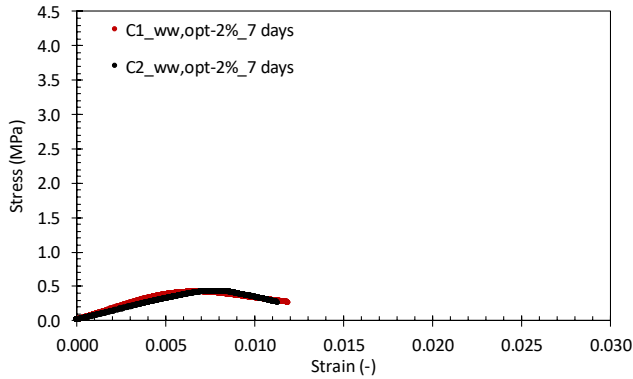


Figure B.10 - Stress-strain curves of CDW-AS-50% mixtures with $w_{w,opt}-2\%$ cured for 7 days

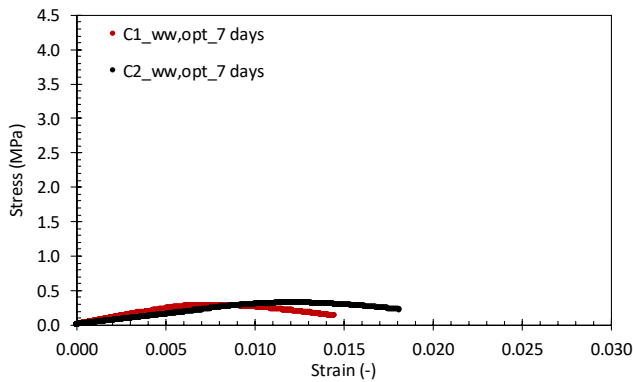


Figure B.11 - Stress-strain curves of CDW-AS-50% mixtures with $w_{w,opt}$ cured for 7 days

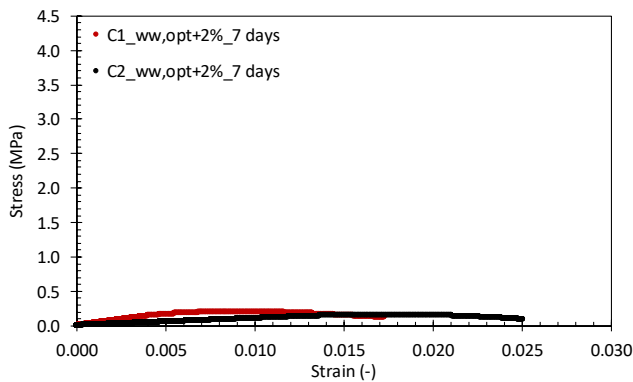


Figure B.12 - Stress-strain curves of CDW-AS-50% mixtures with $w_{w,opt}+2\%$ cured for 7 days

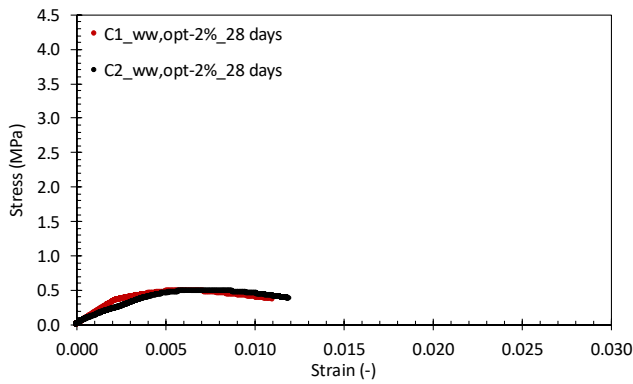


Figure B.13 - Stress-strain curves of CDW-AS-50% mixtures with $w_{w,opt}-2\%$ cured for 28 days

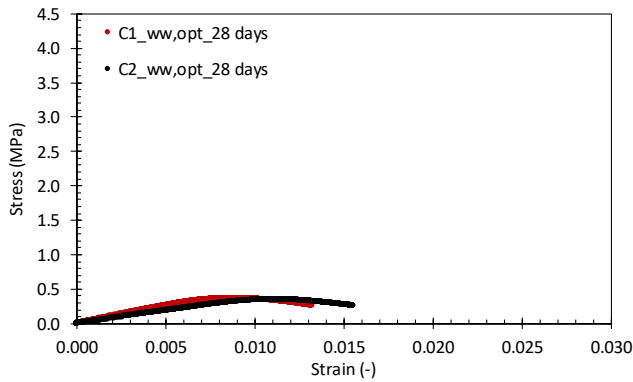


Figure B.14 - Stress-strain curves of CDW-AS-50% mixtures with $w_{w,opt}$ cured for 28 days

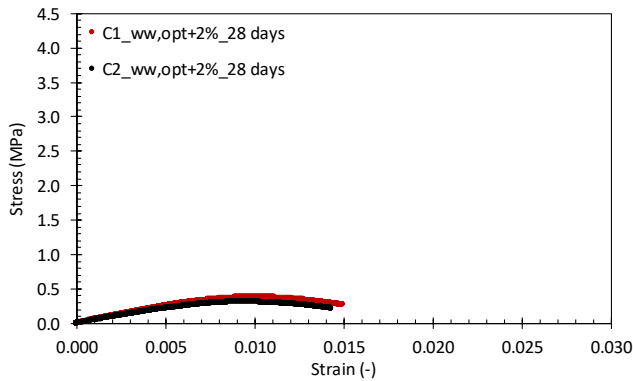


Figure B.15 - Stress-strain curves of CDW-AS-50% mixtures with $w_{w,opt}+2\%$ cured for 28 days

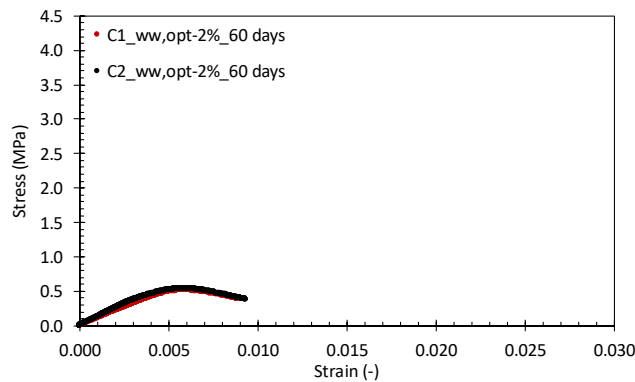


Figure B.16 - Stress-strain curves of CDW-AS-50% mixtures with $w_{w,opt}$ -2% cured for 60 days

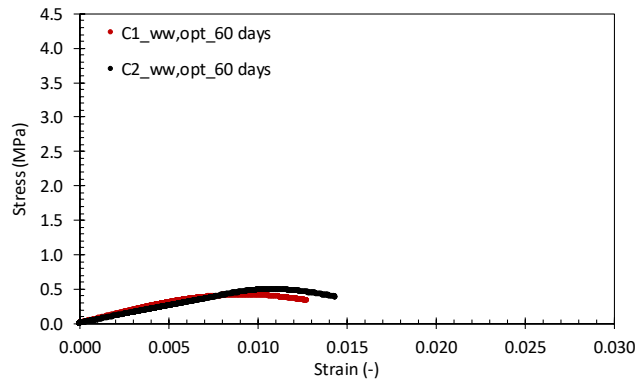


Figure B.17 - Stress-strain curves of CDW-AS-50% mixtures with $w_{w,opt}$ cured for 60 days

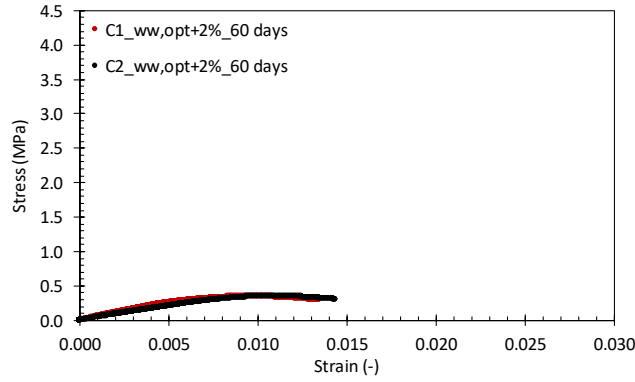


Figure B.18 - Stress-strain curves of CDW-AS-50% mixtures with $w_{w,opt}+2\%$ cured for 60 days

B.3.3 CDW-AS-100% mixtures

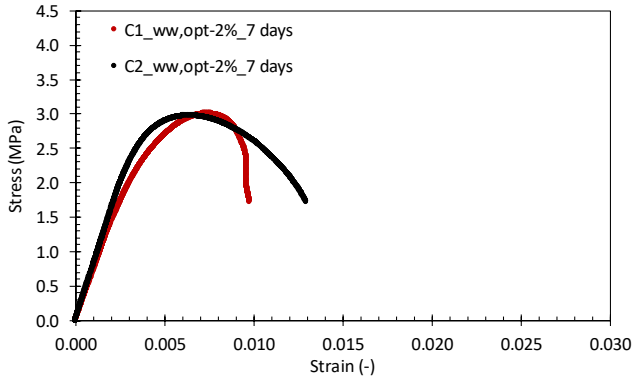


Figure B.19 - Stress-strain curves of CDW-AS-100% mixtures with $w_{w,opt}-2\%$ cured for 7 days

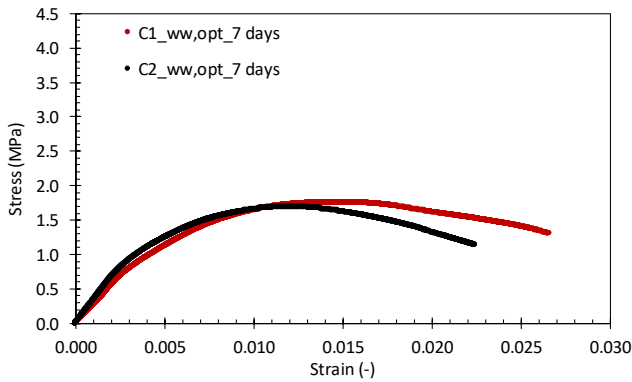


Figure B.20 - Stress-strain curves of CDW-AS-100% mixtures with $w_{w,opt}$ cured for 7 days

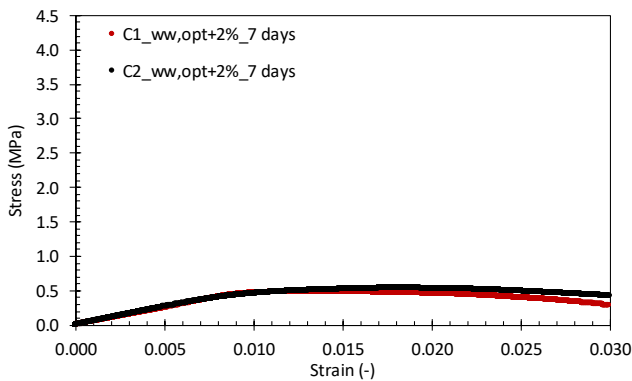


Figure B.21 - Stress-strain curves of CDW-AS-100% mixtures with $w_{w,opt}+2\%$ cured for 7 days

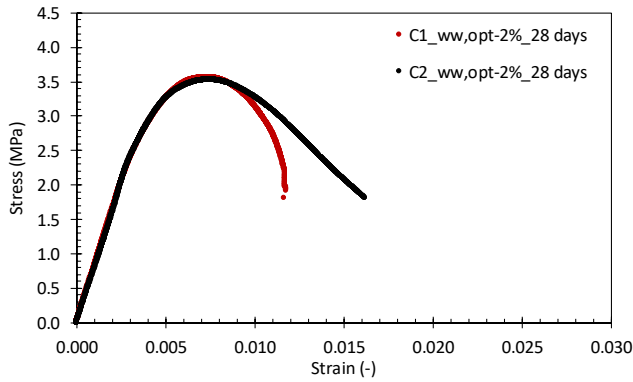


Figure B.22 - Stress-strain curves of CDW-AS-100% mixtures with $w_{w,opt}-2\%$ cured for 28 days

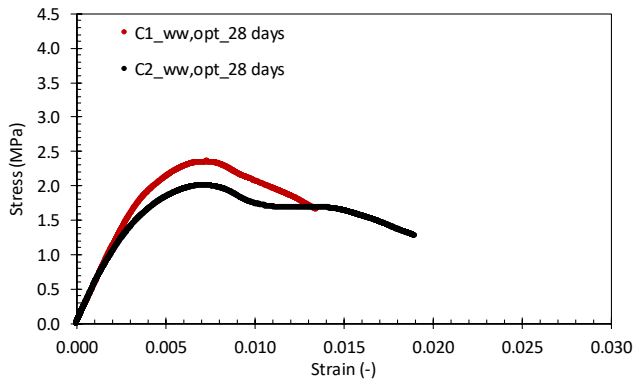


Figure B.23 - Stress-strain curves of CDW-AS-100% mixtures with $w_{w,opt}$ cured for 28 days

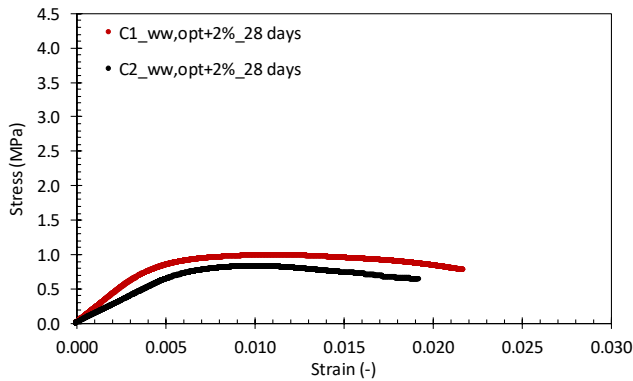


Figure B.24 - Stress-strain curves of CDW-AS-100% mixtures with $w_{w,opt}+2\%$ cured for 28 days

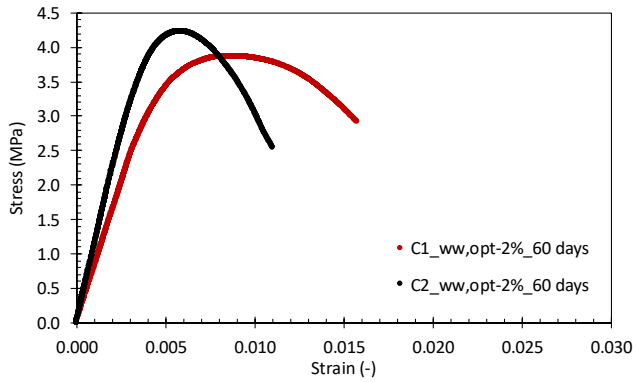


Figure B.25 - Stress-strain curves of CDW-AS-100% mixtures with $w_{w,opt}-2\%$ cured for 60 days

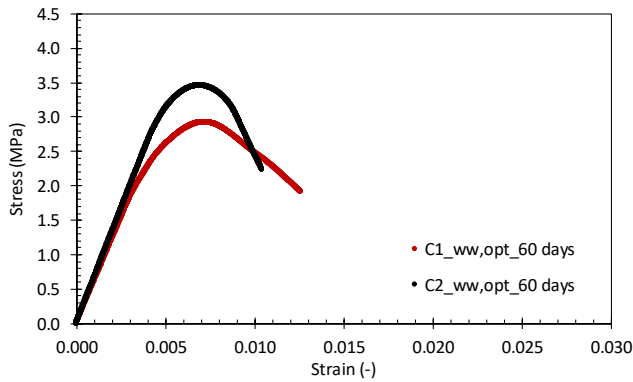


Figure B.26 - Stress-strain curves of CDW-AS-100% mixtures with $w_{w,opt}$ cured for 60 days

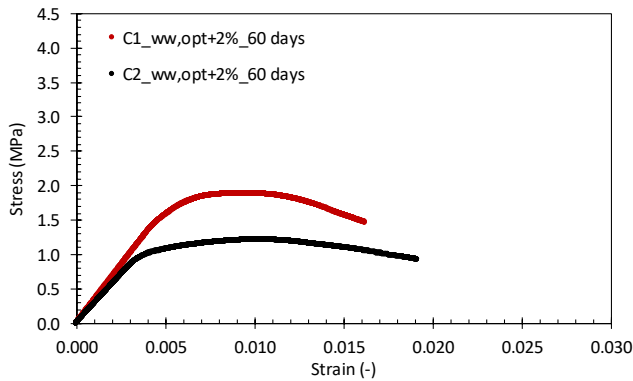


Figure B.27 - Stress-strain curves of CDW-AS-100% mixtures with $w_{w,opt}+2\%$ cured for 60 days

B.4. EDS analysis output

Sample 1 - Aggregate

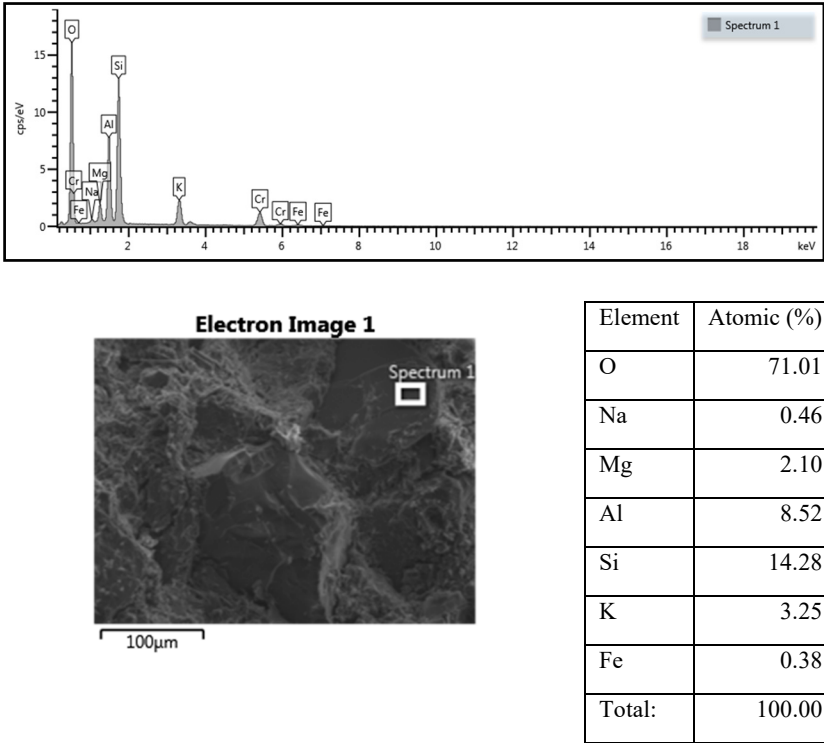


Figure B.28 - EDS analysis of aggregate zone of sample 1

Sample 1 - Binder

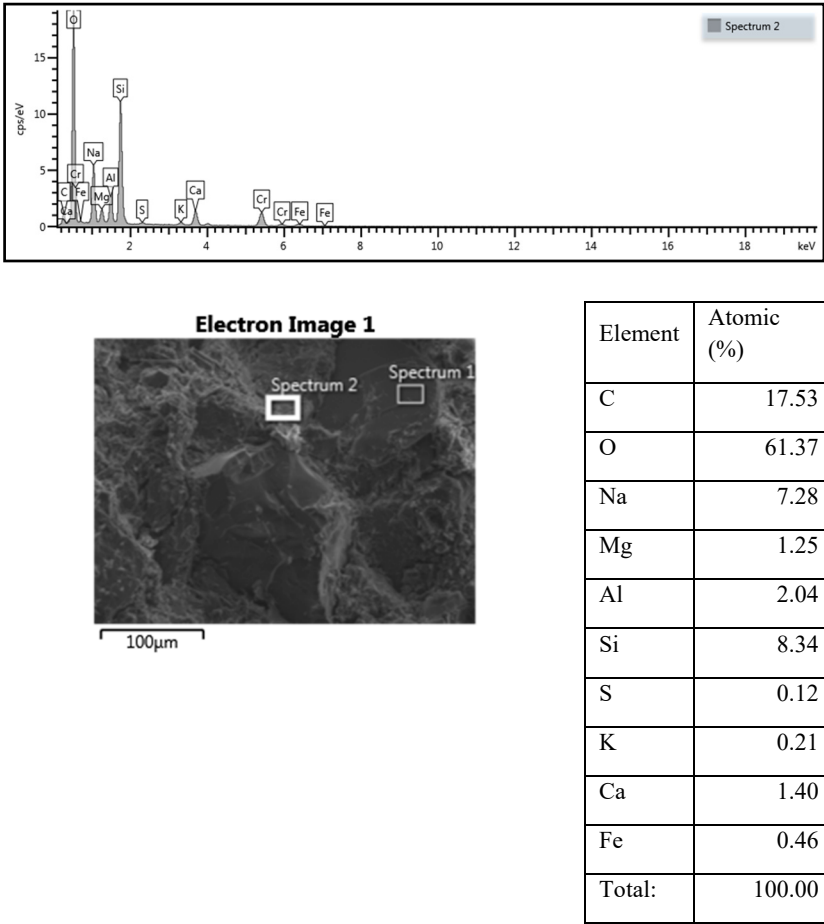


Figure B.29 - EDS analysis of binder zone of sample 1

Sample 2 - Aggregate

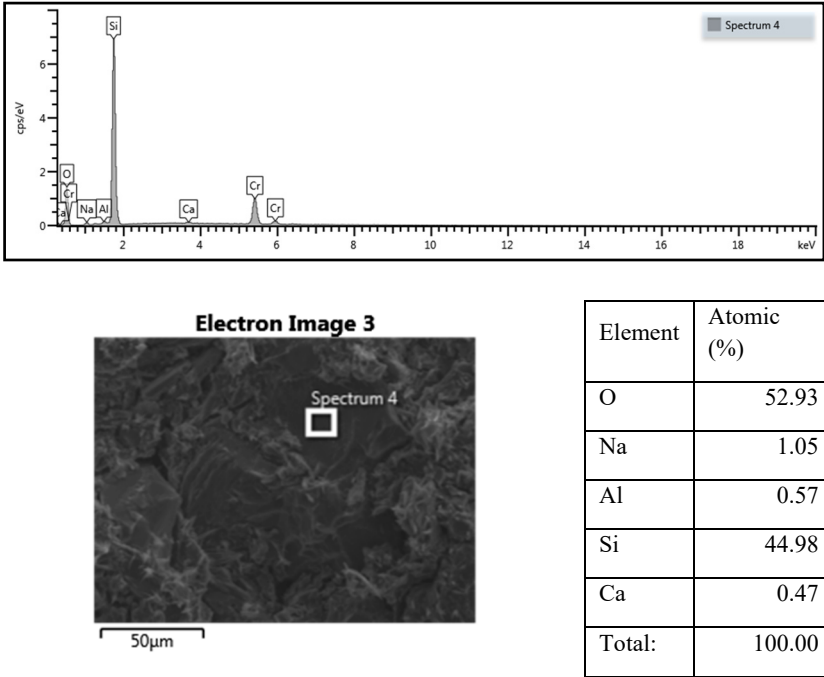
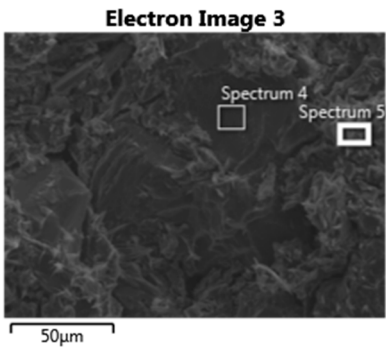
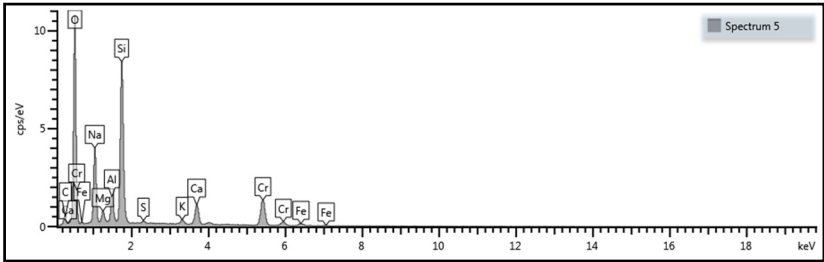


Figure B.30 - EDS analysis of aggregate zone of sample 2

Sample 2 - Binder



Element	Atomic (%)
C	11.67
O	61.60
Na	9.08
Mg	1.03
Al	1.98
Si	11.42
S	0.21
K	0.38
Ca	2.03
Fe	0.60
Total:	100.00

Figure B.31 - EDS analysis of binder zone of sample 2

Sample 3 - Aggregate

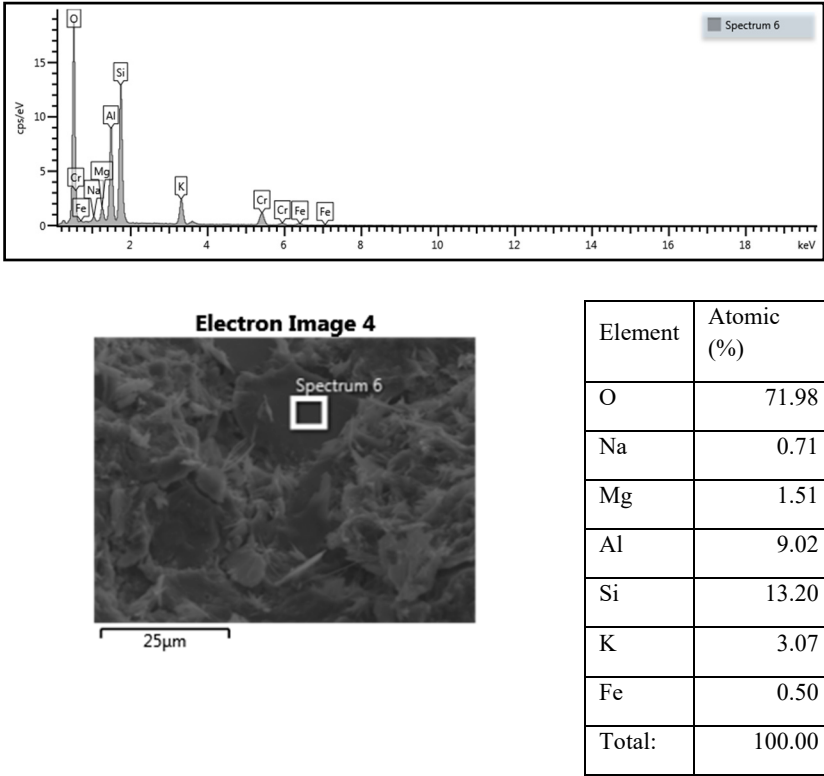
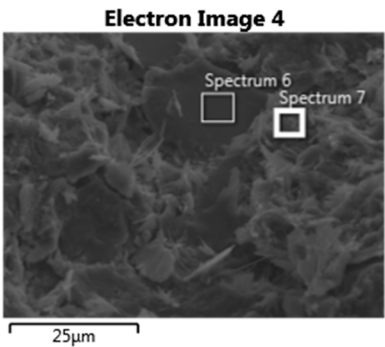
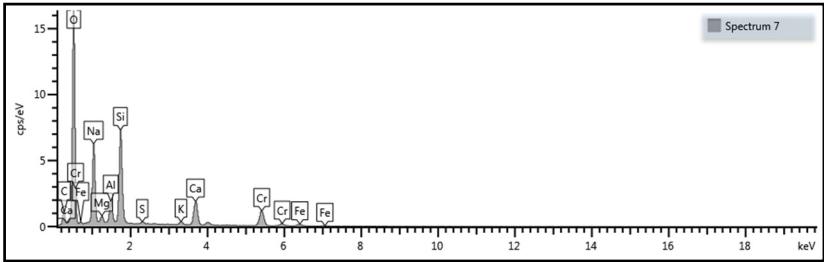


Figure B.32 - EDS analysis of aggregate zone of sample 3

Sample 3 - Binder



Element	Atomic (%)
C	16.82
O	62.26
Na	9.27
Mg	0.60
Al	1.62
Si	6.27
S	0.14
K	0.27
Ca	2.35
Fe	0.38
Total:	100.00

Figure B.33 - EDS analysis of binder zone of sample 3

Sample 4 - Aggregate

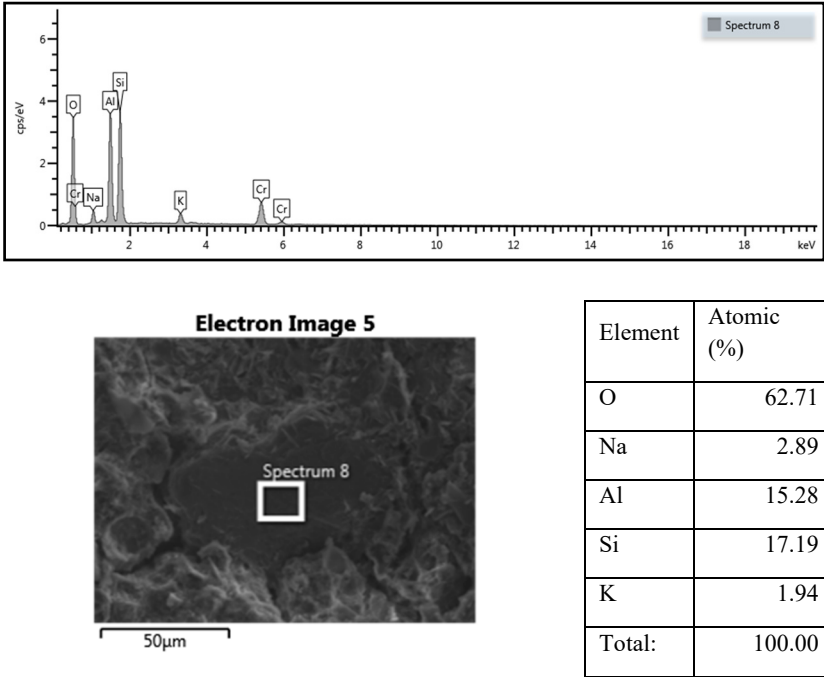
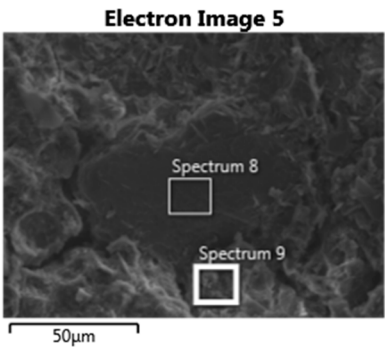
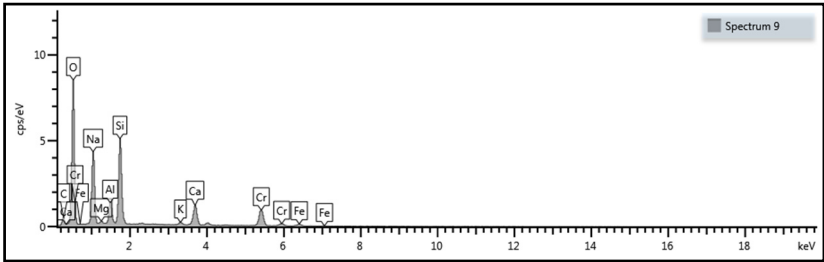


Figure B.34 - EDS analysis of aggregate zone of sample 4

Sample 4 - Binder



Element	Atomic (%)
C	14.21
O	59.41
Na	11.88
Mg	0.31
Al	2.26
Si	8.28
K	0.31
Ca	2.71
Fe	0.63
Total:	100.00

Figure B.35 - EDS analysis of binder zone of sample 4

C. Exp. B2

C.1. Resilient modulus results

C.1.1 CDW-AS-100% mixtures

Table C.1 - Values of RM (in MPa) of 7-day cured CDW-AS-100% mixtures exposed to F/T degradation

θ (kPa)	F/T cycles			
	0 F/T	4 F/T	8 F/T	12 F/T
82.8	307.0	135.0	168.6	164.5
103.5	353.4	143.0	190.9	173.8
124.2	411.5	160.6	211.0	188.5
138.0	374.4	165.6	225.1	203.9
172.4	465.9	194.2	249.9	225.2
206.9	531.6	216.8	270.1	244.2
275.6	537.7	254.3	319.0	298.1
344.6	627.8	290.3	343.3	318.4
413.5	675.5	309.6	355.2	324.7
379.1	565.5	297.2	358.1	339.3
413.6	613.8	322.7	376.0	357.4
517.0	709.1	360.8	400.6	381.3
517.1	645.9	358.1	415.2	405.5
551.6	681.5	381.0	427.6	419.7
689.5	752.5	415.1	448.2	436.6

Table C.2 - Values of RM (in MPa) of 28-day cured CDW-AS-100% mixtures exposed to F/T degradation

θ (kPa)	F/T cycles			
	0 F/T	4 F/T	8 F/T	12 F/T
82.8	199.0	186.3	155.2	165.5
103.5	259.0	198.2	162.4	172.6
124.2	324.4	248.1	207.2	199.0
138.0	240.2	201.3	167.8	192.4
172.4	369.6	276.7	238.9	223.4
206.9	434.8	324.8	287.6	257.0
275.6	445.8	334.8	284.5	275.1
344.6	554.9	404.8	366.2	325.4
413.5	617.9	438.9	406.5	352.6
379.1	474.2	356.4	305.6	300.3
413.6	538.5	402.4	367.2	338.8
517.0	659.3	476.3	449.0	397.3
517.1	574.2	426.7	398.2	381.4
551.6	625.1	461.2	437.1	406.6
689.5	736.3	527.7	509.2	459.3

Table C.3 - Values of RM (in MPa) of 45-day cured CDW-AS-100% mixtures exposed to F/T degradation

θ (kPa)	F/T cycles			
	0 F/T	4 F/T	8 F/T	12 F/T
82.8	289.5	230.6	146.9	133.6
103.5	329.1	277.0	170.1	157.9
124.2	371.7	344.4	196.5	186.5
138.0	369.6	291.2	191.3	175.7
172.4	428.0	388.3	229.1	216.5
206.9	478.9	477.8	265.6	246.6
275.6	475.6	451.4	288.9	269.7
344.6	563.2	589.7	336.6	308.6
413.5	607.8	647.2	368.1	332.3
379.1	499.9	469.5	311.1	297.1
413.6	554.9	543.5	341.5	320.9
517.0	638.4	690.0	408.2	369.1
517.1	582.1	569.0	369.5	343.5
551.6	614.1	622.8	395.6	365.6
689.5	687.7	787.8	457.0	412.4

Table C.4 - Values of RM (in MPa) of 60-day cured CDW-AS-100% mixtures exposed to F/T degradation

θ (kPa)	F/T cycles			
	0 F/T	4 F/T	8 F/T	12 F/T
82.8	335.6	250.1	159.3	173.9
103.5	375.5	281.0	198.5	193.7
124.2	464.5	319.9	243.9	229.1
138.0	385.1	326.6	208.5	228.4
172.4	518.9	390.1	273.9	262.2
206.9	630.2	440.0	325.3	293.1
275.6	573.2	497.5	335.3	316.4
344.6	760.1	561.0	416.5	363.4
413.5	863.2	591.1	443.7	391.6
379.1	589.8	540.5	369.4	338.6
413.6	690.4	581.5	422.0	377.1
517.0	913.6	645.8	487.9	435.3
517.1	737.5	614.5	452.3	403.3
551.6	821.2	643.9	488.9	431.6
689.5	989.0	697.7	538.7	492.5

C.1.2 NGM-OPC mixtures

Table C.5 - Values of RM (in MPa) of 7-day cured NGM-OPC mixtures exposed to F/T degradation

θ (kPa)	F/T cycles			
	0 F/T	4 F/T	8 F/T	12 F/T
82.8	222.3	258.2	169.3	253.0
103.5	241.6	287.4	221.5	285.2
124.2	304.1	338.3	277.8	357.3
138.0	233.3	307.6	224.1	307.1
172.4	331.9	394.8	304.5	412.7
206.9	424.7	467.0	384.4	499.5
275.6	385.2	490.9	352.2	523.2
344.6	539.2	604.7	488.5	654.4
413.5	634.4	657.5	597.5	711.6
379.1	382.2	511.1	377.7	552.8
413.6	477.8	590.0	437.7	648.6
517.0	664.0	708.2	619.8	765.4
517.1	515.2	618.7	462.0	670.9
551.6	588.3	677.4	515.4	736.0
689.5	754.0	783.3	724.5	835.2

Table C.6 - Values of RM (in MPa) of 28-day cured NGM-OPC mixtures exposed to F/T degradation

θ (kPa)	F/T cycles			
	0 F/T	4 F/T	8 F/T	12 F/T
82.8	306.8	203.3	200.2	240.6
103.5	345.9	228.5	222.8	291.2
124.2	401.4	291.0	282.6	359.5
138.0	389.4	240.3	238.8	305.8
172.4	473.4	356.8	339.2	413.9
206.9	547.4	439.3	432.8	491.2
275.6	568.8	483.0	426.1	501.1
344.6	682.0	610.3	574.1	632.4
413.5	744.1	676.1	661.8	700.7
379.1	534.8	509.4	446.9	535.7
413.6	625.9	599.5	528.4	612.2
517.0	774.9	728.5	695.6	752.6
517.1	634.5	640.1	558.4	649.1
551.6	695.0	692.5	627.3	707.9
689.5	845.2	810.1	792.6	836.1

C.2. Stress-strain curves of UCS test

C.2.1 CDW-AS-100%

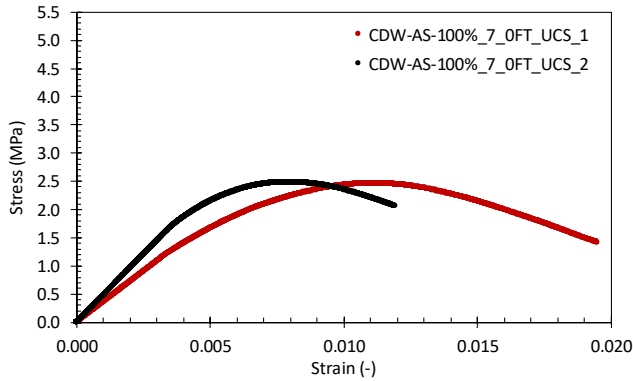


Figure C.1 - Stress-strain curves of CDW-AS-100% mixtures cured for 7 days (0 F/T)

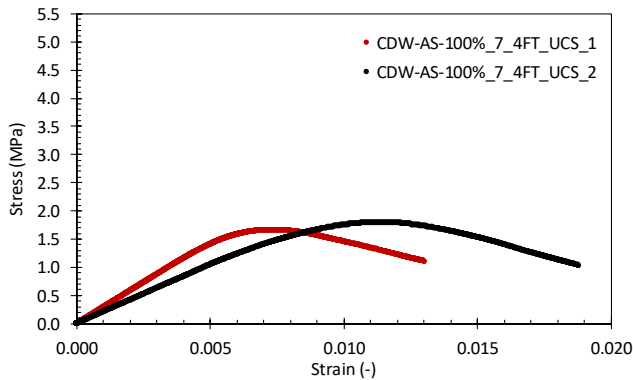


Figure C.2 - Stress-strain curves of CDW-AS-100% mixtures cured for 7 days and exposed to 4 F/T cycles

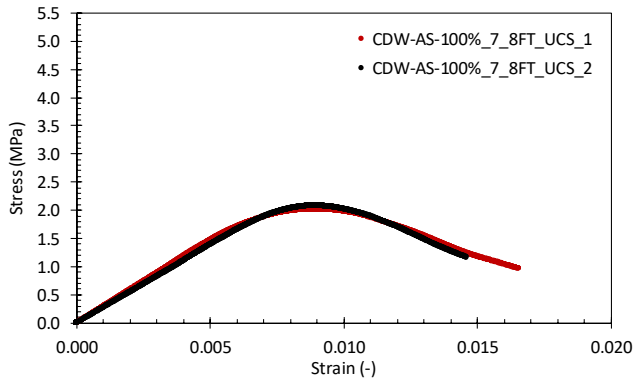


Figure C.3 - Stress-strain curves of CDW-AS-100% mixtures cured for 7 days and exposed to 8 F/T cycles

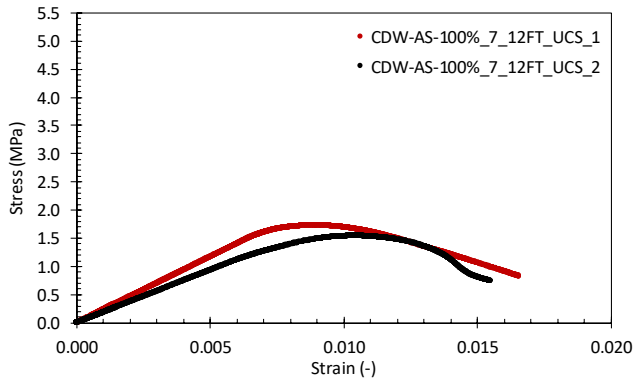


Figure C.4 - Stress-strain curves of CDW-AS-100% mixtures cured for 7 days and exposed to 12 F/T cycles

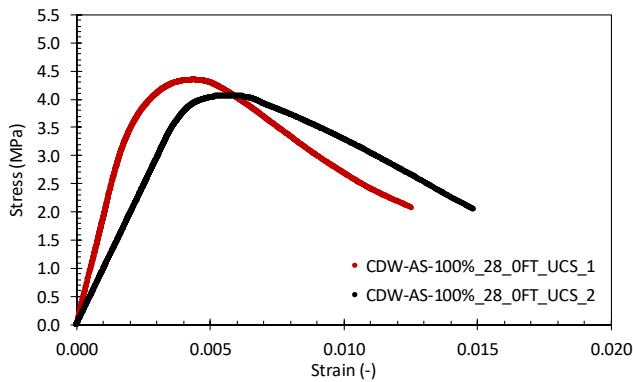


Figure C.5 - Stress-strain curves of CDW-AS-100% mixtures cured for 28 days (0 F/T)

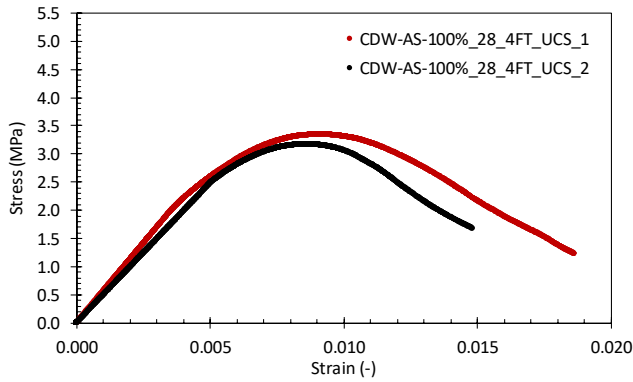


Figure C.6 - Stress-strain curves of CDW-AS-100% mixtures cured for 28 days and exposed to 4 F/T cycles

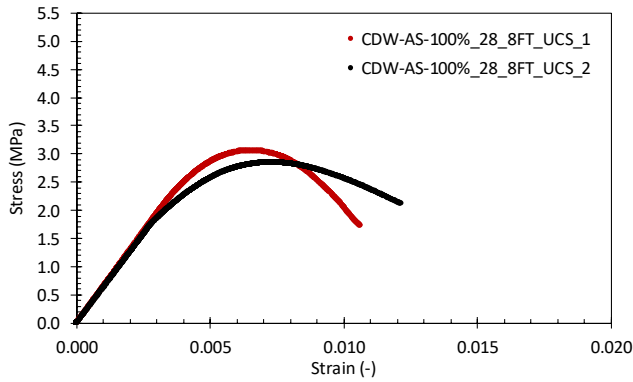


Figure C.7 - Stress-strain curves of CDW-AS-100% mixtures cured for 28 days and exposed to 8 F/T cycles

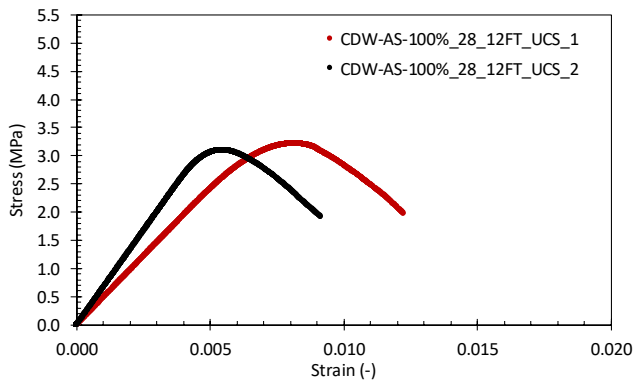


Figure C.8 - Stress-strain curves of CDW-AS-100% mixtures cured for 28 days and exposed to 12 F/T cycles

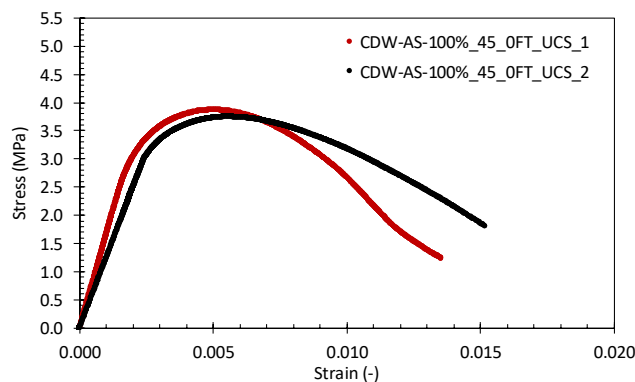


Figure C.9 - Stress-strain curves of CDW-AS-100% mixtures cured for 45 days (0 F/T)

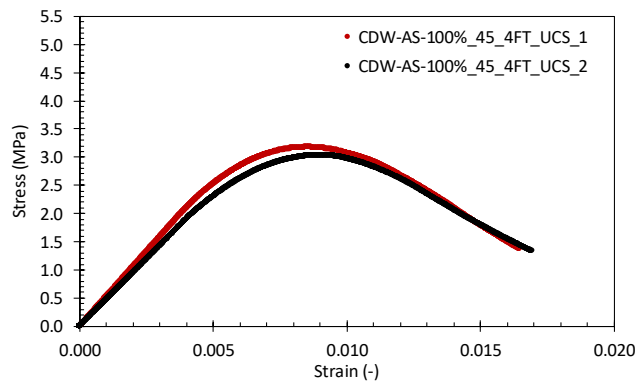


Figure C.10 - Stress-strain curves of CDW-AS-100% mixtures cured for 45 days and exposed to 4 F/T cycles

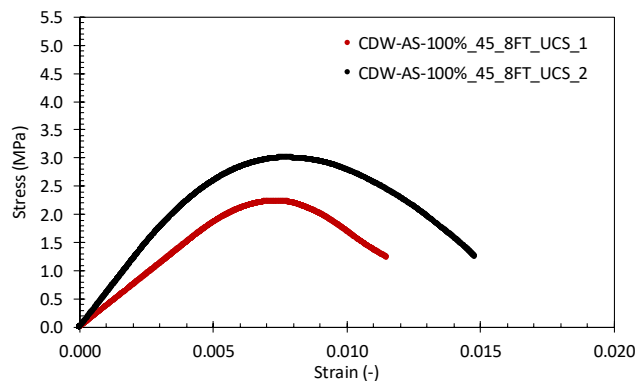


Figure C.11 - Stress-strain curves of CDW-AS-100% mixtures cured for 45 days and exposed to 8 F/T cycles

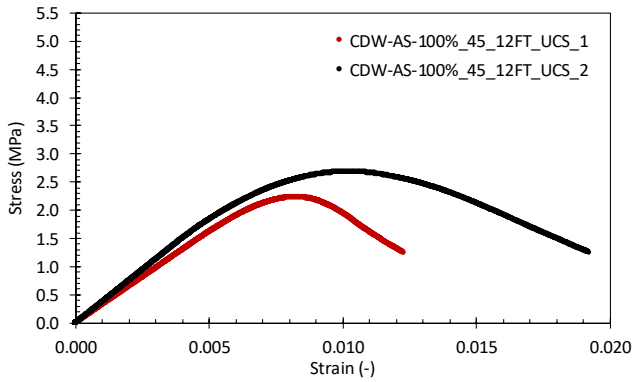


Figure C.12 - Stress-strain curves of CDW-AS-100% mixtures cured for 45 days and exposed to 12 F/T cycles

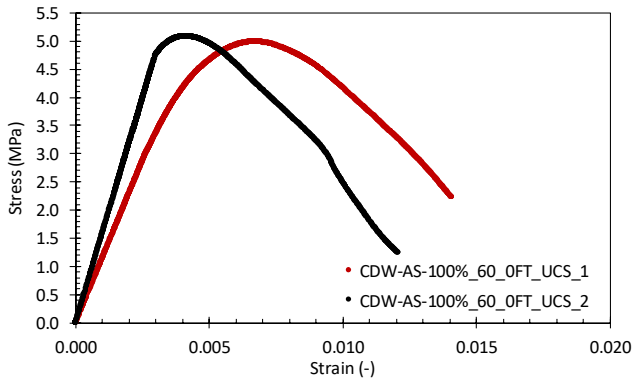


Figure C.13 - Stress-strain curves of CDW-AS-100% mixtures cured for 60 days (0 F/T)

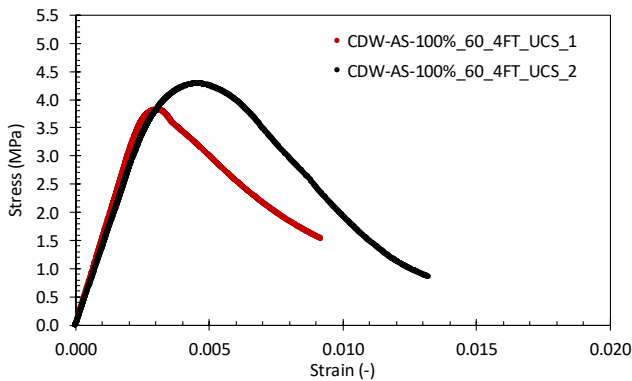


Figure C.14 - Stress-strain curves of CDW-AS-100% mixtures cured for 60 days and exposed to 4 F/T cycles

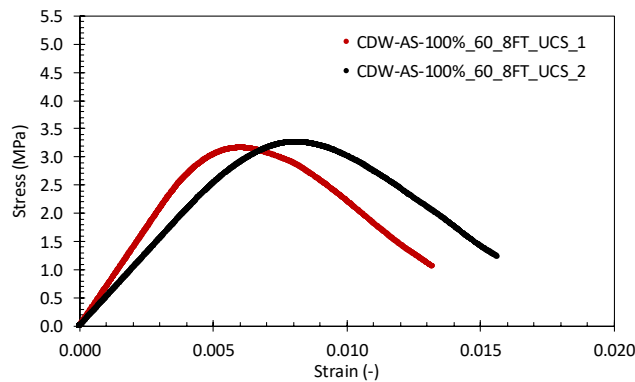


Figure C.15 - Stress-strain curves of CDW-AS-100% mixtures cured for 60 days and exposed to 8 F/T cycles

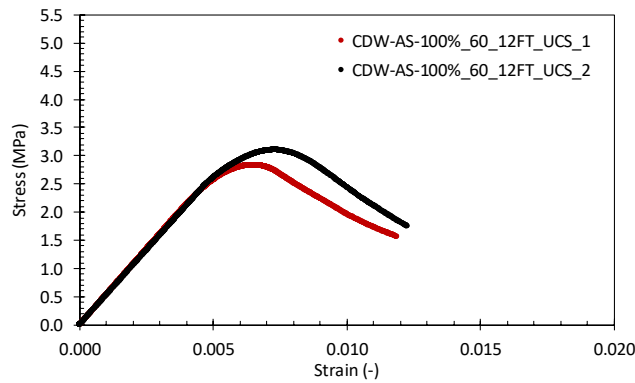


Figure C.16 - Stress-strain curves of CDW-AS-100% mixtures cured for 60 days and exposed to 12 F/T cycles

C.2.2 NGM-OPC mixtures

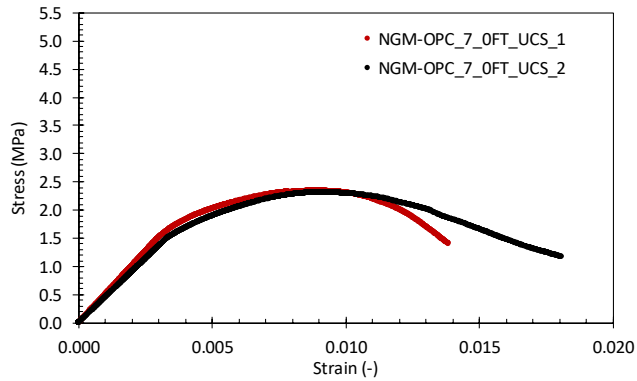


Figure C.17 - Stress-strain curves of NGM-OPC mixtures cured for 7 days (0 F/T)

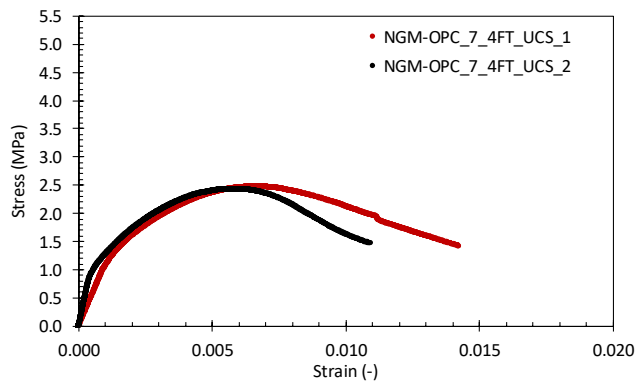


Figure C.18 - Stress-strain curves of NGM-OPC mixtures cured for 7 days and exposed to 4 F/T cycles

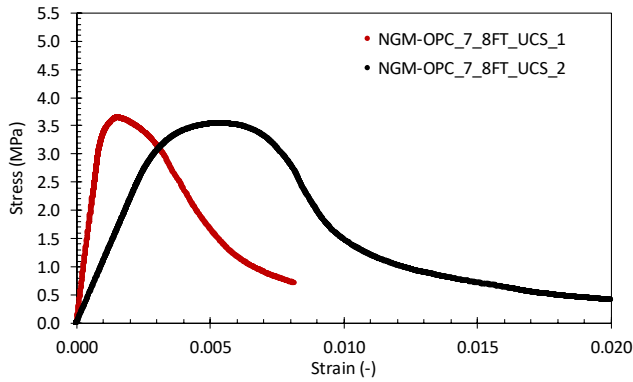


Figure C.19 - Stress-strain curves of NGM-OPC mixtures cured for 7 days and exposed to 8 F/T cycles

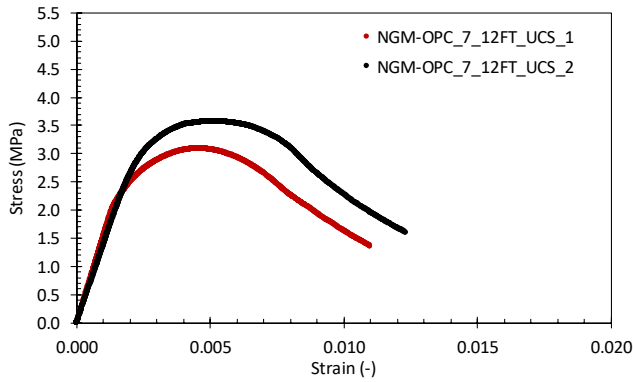


Figure C.20 - Stress-strain curves of NGM-OPC mixtures cured for 7 days and exposed to 12 F/T cycles

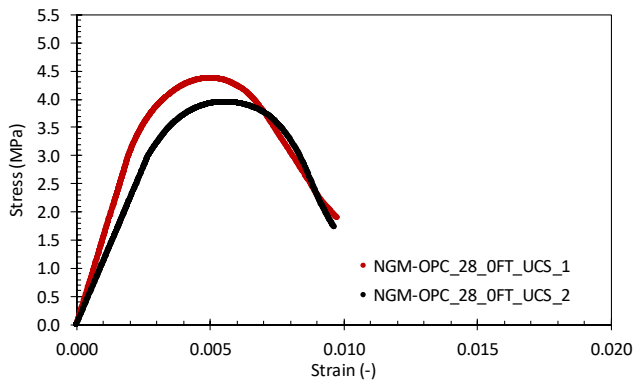


Figure C.21 - Stress-strain curves of NGM-OPC mixtures cured for 28 days (0 F/T)

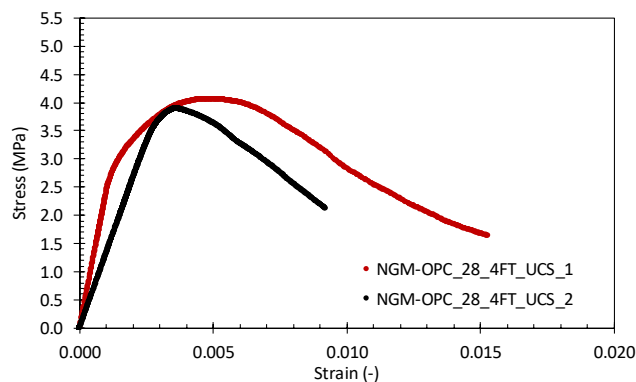


Figure C.22 - Stress-strain curves of NGM-OPC mixtures cured for 28 days and exposed to 4 F/T cycles

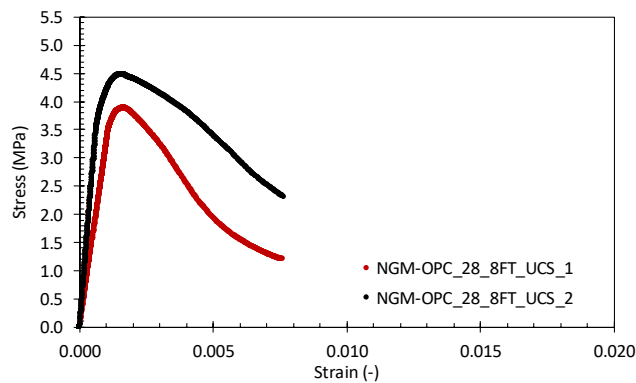


Figure C.23 - Stress-strain curves of NGM-OPC mixtures cured for 28 days and exposed to 8 F/T cycles

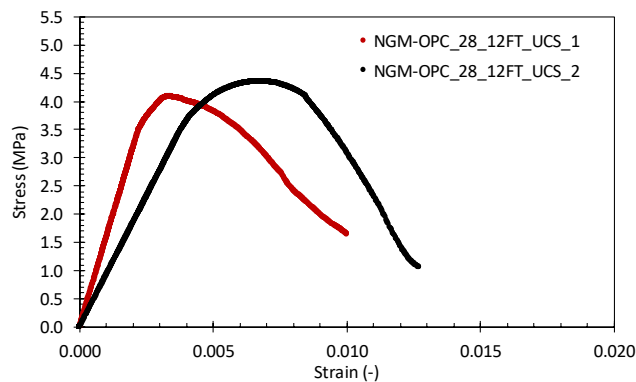


Figure C.24 - Stress-strain curves of NGM-OPC mixtures cured for 28 days and exposed to 12 F/T cycles



Luca Tefa is a Civil Engineer passionate about research and innovation in civil infrastructures. Between 2015 and 2018, he has been Ph.D. candidate at Politecnico di Torino (Italy) working in advanced mechanical characterization of recycled and sustainable materials for road pavements.

Politecnico di Torino
Department of Environment, Land
and Infrastructure Engineering
24, corso Duca degli Abruzzi
Torino (Italy)

Email: luca.tefa@polito.it
Mobile: +39 349 6033 772

Recycled aggregates from construction and demolition waste are a viable alternative to natural granular materials in the formation of unbound layers of low to medium trafficked roads. Several methods to improve the mechanical and durability properties of construction and demolition waste aggregates through stabilization techniques have been proposed. The recent use of alkali-activated binders in place of traditional ones has been attracting interest in the scientific community. With the aims of promoting the adoption of construction and demolition waste aggregates and avoiding the use of cementitious products, this research investigates the alkaline activation of fine particles of recycled aggregates as a new stabilization method for whole construction and demolition waste mixtures. The laboratory investigation adopted a multiscale approach. At the smallest scale, the alkali reactivity of fine particles ($d < 0.125\text{mm}$) was evaluated. The larger scale assessment aimed at verifying the mechanical and durability properties of construction and demolition waste aggregates in their typical particle size distribution stabilized as per the alkaline activation of their fines.

A preliminary chemical analysis of construction and demolition waste fines detected the presence of aluminosilicates needed for the alkaline activation process. The adequate compression and flexural strength values achieved by specimens made from alkali-activated fines and cured for 28 days at room temperature demonstrated the effective reactivity of these precursors.

At the larger scale, the mechanical properties of construction and demolition waste aggregates compacted with the undiluted alkaline solution were considerably higher than those of mixtures containing water only. The occurrence of alkaline activation apparently responsible for the formation of bonds between coarser grains was confirmed by microstructural observations.

The investigated stabilization technique is consistent with the most common practices in road constructions and promotes the use of construction and demolition waste aggregates also in applications with higher mechanical requirements (i.e. road bases and subbases). The reuse of waste materials otherwise destined for landfill sites and the exclusion of environmentally harmful binders meet the demand for sustainability increasingly pursued in civil infrastructures.